

MUTUAL POUNDING OF STRUCTURES DURING STRONG EARTHQUAKES

by

Mohammad S. Rohanimanesh

Dissertation submitted to the faculty of the
Virginia Polytechnic Institute and State University
in partial fulfillment of the requirements for the degree of

DOCTOR OF PHILOSOPHY

in

Engineering Mechanics

©Mohammad S. Rohanimanesh and VPI & SU 1994

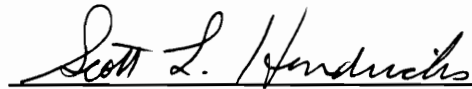
APPROVED:



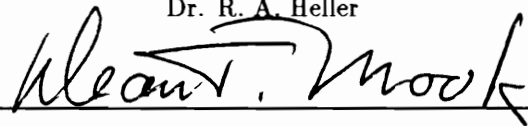
Dr. M. P. Singh, Chairman



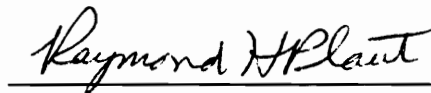
Dr. R. A. Heller



Dr. S. L. Hendricks



Dr. D. T. Mook



Dr. R. H. Plaut

April, 1994

Blacksburg, Virginia

C.2

LD
5655
V856
1994
R646
C.2

MUTUAL POUNDING OF STRUCTURES DURING STRONG EARTHQUAKES

by

Mohammad S. Rohanimanesh

Committee Chairman: Dr. M. P. Singh

Engineering Science and Mechanics

(ABSTRACT)

Structures built next to each other in congested cities are likely to pound on each other during strong ground shaking caused by earthquakes. The main objective of this study is to examine the problem of mutual structural pounding to identify its effect on structures and then propose solutions to mitigate its effects. Mutual pounding of structural systems with varying mass, stiffness, and seismic joint gaps, subjected to several different input motions are examined. To evaluate the effects of pounding, the numerical results with and without pounding have been considered. The resilience between two impacting masses is represented by linear springs and also nonlinear Hertz model contact stiffness. Pounding causes a large increase in the shear force in the stories higher than the top pounding story, a large increase in the accelerations of the pounding floors and also large overturning effects on both structures. The parametric study of pounding of structures in series showed that in most cases the corner structures are penalized more than the interior structures. The study of the effect of foundation flexibility on the structural pounding response showed that a proper consideration of this parameter must be included in the analysis.

To alleviate the pounding effects to avoid damage to structural elements and supported secondary equipment, it was found necessary to join the structures by rigid links and brace all the stories of at least the taller structure. Joining of the floors is required to reduce the excessive floor accelerations caused by impact, whereas the story bracings are required to reduce the excessive story shears or bending moments in the higher stories caused by pounding of the lower floors. It is observed that except for very soft soils, the proposed pounding mitigation scheme will increase the shear force transmitted to the foundation, thus requiring a strengthening of the foundation as well. Since the forces in the rigid links connecting the two structures were observed to be reasonable, the joining of the two

structures does not pose any special problem; it can be easily accomplished by using large-size steel rods hooked properly with both structures. In the case of column pounding where the floors of one structure pound on the columns of the other structure, the pounding mitigation strategy is to provide K-bracings on all pounding columns and diagonal bracing in the other stories to reduce high bending moment in the column, and to rigidly join them to avoid high pounding acceleration.

ACKNOWLEDGEMENTS

I would like to thank:

Dr. Mahandra P. Singh for his constant guidance, encouragement, and invaluable moral support throughout the duration of my research work and graduate studies at Virginia Tech not only as my advisor but also as a friend.

The members of my graduate committee, i.e., Dr. Robert A. heller, Dr. Scott L. Hendricks, Dr. Dean T. Mook and Dr. Raymond H. Plaut for serving on the committee.

All my teachers at the University of the District of Columbia and Virginia Tech.

Mr. Duane Taylor and Mr. Tim Tomlin, who run the ESM computer lab, for helping me out with the computers on which most of this work was done.

Dr. Mohammad H. Kadivar, visiting professor from Shiraz University (Shiraz, Iran), for his friendship and encouragement.

The National Science Foundation for financial support through Grant Number CES-8814319.

All my friends in Iran and the USA for their friendship and moral support, of them I name a few, Mr. Reza Karkehabadi, Mr. Abdolrahman Yarali, Mr. Majid Roghanizad, Dr. Madhu K. Sreedhar Dr. Naresh K. Chandiramani and Mr. Joseph Fritzsche.

And last but not the least, my parents, my wife and family for their constant support, understanding and encouragement without which this goal could never have been achieved.

TABLE OF CONTENTS

1	INTRODUCTION	1
1.1	Scope of This Work	5
2	POUNDING OF A FLEXIBLE STRUCTURE AGAINST AN OBSTRU- TION	6
2.1	Introduction	6
2.2	Equations of Motion	6
2.3	Problem Parameters for Numerical Analysis	9
2.4	Effect of Gap Size	10
2.5	Effect of Story Stiffness	12
2.6	Effect of Floor Mass	12
2.7	Effect of Pounding Stiffness	14
2.8	Effect of Change in the Pounding Level	14
2.9	Effect of Pounding on Floor Accelerations and Floor Response Spectra . . .	15
2.10	Effect of Structural Damping on the Response due to Pounding	16
2.11	Summary	17
3	POUNDING OF MDOF FLEXIBLE STRUCTURES	58
3.1	Introduction	58
3.2	Equations of Motion	58
3.3	Numerical Results	61
3.4	Effect of Gap Size	61
3.5	Effect of Story Stiffness of the Five-Story Structure	63
3.6	Effect of Story Stiffness of the Ten-Story Structure	64

CONTENTS

3.7	Effect of Floor Mass of the Five-Story Structure	64
3.8	Effect of Floor Mass of the Ten-Story Structure	65
3.9	Effect of Pounding Stiffness	66
3.10	Effect of Change in Height of s-Structure	66
3.11	Effect of Pounding on Floor Response Spectra	67
3.12	Pounding Response of Equal Fundamental Frequency Structures	68
3.13	Pounding Against a Flexible Versus Rigid Structure	68
3.14	Pounding with Hertz's Spring Model	69
3.14.1	Equations of motion with nonlinear model	70
3.14.2	Numerical results	72
3.15	Summary	73
4	POUNDING OF STRUCTURES IN SERIES	119
4.1	Introduction	119
4.2	Equations of Motion	119
4.3	Numerical Results	124
4.4	Summary	128
5	EFFECT OF SOIL-STRUCTURE INTERACTION ON THE STRUCTURAL POUNDING	136
5.1	Introduction	136
5.2	Model for Foundation Flexibility	136
5.3	Equations of Motion	137
5.4	Numerical Results	143
5.4.1	Force and acceleration responses	143
5.4.2	Forces in foundation media	146
5.4.3	Floor spectral response	146
5.5	Summary	147

CONTENTS

6	MITIGATION OF POUNDING PROBLEM	170
6.1	Introduction	170
6.2	Pounding on Soft Springs	171
6.3	Response of Rigidly Joined Structures	173
6.4	Pounding of Braced Structures - Analytical Formulation	174
6.5	Structures on Rigid Foundation	184
6.6	Structures on Flexible Foundations	187
6.6.1	Rigidly joined structures - equations of motion	187
6.6.2	Rigidly joined structures on flexible foundation - numerical results .	192
6.6.3	Braced structures on flexible foundation	192
6.6.4	Effect of bracing size	194
6.7	Foundation Shear	195
6.8	Forces in the Rigid Links Joining the Structures	197
6.9	Pounding of Structures at Unequal Levels - Column Pounding	198
6.10	Summary	199
7	SUMMARY AND CONCLUDING REMARKS	268
A	MATRICES	275

LIST OF FIGURES

2.1	Schematic of a 10-story deformable structure pounding against a 5-story rigid structure	21
2.2	Free body diagrams of a typical floor mass in the states of (a) pounding and (b) no-pounding	22
2.3	Acceleration time history of 1941 N-S El Centro earthquake used as an input in this study	23
2.4	Time history of shear force response in the 6th story for (a) pounding and (b) no-pounding cases	24
2.5	Time history of shear force response in the 10th story for (a) pounding and (b) no-pounding cases	25
2.6	Time history of overturning moment response at the base for (a) pounding and (b) no-pounding cases	26
2.7	Time history of absolute acceleration at floor 10 for (a) pounding and (b) no-pounding cases	27
2.8	Conventions for positive and negative response quantities	28
2.9	Graphs showing the effect of gap size on the maximum displacement, story shear and overturning moment responses at various floor levels of the 10-story structure — single level pounding	29
2.10	Graphs showing the effect of gap size on the maximum displacement, story shear and overturning moment responses at various floor levels of the 10-story structure — multiple level pounding	30
2.11	Ratio of multiple pounding to single level pounding responses for various gap sizes	31

LIST OF FIGURES

2.12 Ratio of multiple pounding to no-pounding responses for various gap sizes 32

2.13 Graphs showing the effect of changing the story stiffness on the maximum displacement, story shear and overturning moment responses in the single level pounding case — gap size = 0.0 33

2.14 Graphs showing the effect of changing the story stiffness on the maximum displacement, story shear and overturning moment responses in the multiple pounding case — gap size = 0.0 34

2.15 Ratio of multiple pounding to single level pounding responses for various story stiffnesses 35

2.16 Ratio of multiple pounding to no-pounding responses for various story stiffnesses 36

2.17 Graphs showing the effect of changing the floor mass on the maximum displacement, story shear and overturning moment responses — single level pounding case, gap size = 0.0 37

2.18 Graphs showing the effect of changing the floor mass on the maximum displacement, story shear and overturning moment responses — multiple pounding case, gap size = 0.0 38

2.19 Ratio of multiple pounding to single level pounding responses for various floor masses 39

2.20 Ratio of multiple pounding to no-pounding responses for various floor masses 40

2.21 Graphs showing the effect of fundamental frequency of the structure on the multiple pounding to no-pounding responses 41

2.22 Graphs showing the effect of the impact stiffness coefficient on the ratio of multiple pounding to single level pounding responses 42

2.23 Graphs showing the effect of impact stiffness coefficient on the ratio of multiple pounding to no-pounding responses 43

2.24 Graphs showing the effect of the height of the rigid structure on the multiple pounding responses - (rigid structure heights 1, 2, 3, 4 and 5 stories) 44

LIST OF FIGURES

2.25 Graphs showing the effect of the height of the rigid structure on the multiple pounding responses - (rigid structure heights 6, 7, 8, 9 and 10 stories) . . . 45

2.26 Graphs showing the effect of the height of the rigid structure on the ratio of multiple pounding to no-pounding responses - (rigid structure heights 1, 2, 3, 4 and 5 stories) 46

2.27 Graphs showing the effect of the height of the rigid structure on the ratio of multiple pounding to no-pounding responses - (rigid structure heights 6, 7, 8, 9 and 10 stories) 47

2.28 Absolute acceleration and acceleration response ratio at various floor levels in multiple pounding case against a 5-story rigid structure 48

2.29 Floor acceleration response spectra of various floors in pounding and no-pounding cases - (multiple pounding against 5-story rigid structure) 49

2.30 Floor acceleration response spectra of various floors in pounding and no-pounding cases - (multiple pounding against 5-story rigid structure) 50

2.31 Pounding to no-pounding floor response spectrum ratios (multiple pounding against 5-story structure) 51

2.32 Ratio of multiple pounding to no-pounding responses for various gap sizes (2% structural damping) 52

2.33 Ratio of multiple pounding to no-pounding responses for various story stiffnesses (2% structural damping) 53

2.34 Ratio of multiple pounding to no-pounding responses for various floor masses (2% structural damping) 54

2.35 Graphs showing the effect of fundamental frequency of the structure on the multiple pounding to no-pounding responses (2% structural damping) . . . 55

2.36 Graphs showing the effect of the impact stiffness coefficient on the ratio of multiple pounding to no-pounding responses (2% structural damping) . . . 56

2.37 Pounding to no-pounding floor response spectrum ratios (multiple pounding against a 5-story rigid structure) — 2% structural damping 57

LIST OF FIGURES

3.1	Schematic of a 10-story deformable structure pounding against a 5-story deformable structure	75
3.2	Free body diagram of two typical floor masses of the p and s-structure in state of pounding	76
3.3	Ratio of multiple pounding to no-pounding responses for various gap sizes (10-story structure)	77
3.4	Ratio of multiple pounding to no-pounding responses for various gap sizes (5-story structure)	78
3.5	The variation of the story shear ratio versus the gap ratio for various stories of the 10-story structure	79
3.6	The story shear versus the gap size for various stories of the 10-story structure	80
3.7	The maximum absolute acceleration versus the gap size for various pounding floors of the 10-story structure	81
3.8	The maximum absolute acceleration ratio versus the gap ratio for various pounding floors of the 10-story structure	82
3.9	Ratio of multiple pounding to no-pounding responses of the 10-story structure for various story stiffnesses of the 5-story structure	83
3.10	Ratio of multiple pounding to no-pounding responses of the 5-story structure for various story stiffnesses of the 5-story structure	84
3.11	Ratio of multiple pounding to no-pounding responses of the 10-story structure for various story stiffnesses of the 10-story structure	85
3.12	Ratio of multiple pounding to no-pounding responses of the 5-story structure for various story stiffnesses of the 10-story structure	86
3.13	Ratio of multiple pounding to no-pounding responses of the 10-story structure for various floor masses of the 5-story structure	87
3.14	Ratio of multiple pounding to no-pounding responses of the 5-story structure for various floor masses of the 5-story structure	88

LIST OF FIGURES

3.15 Ratio of multiple pounding to no-pounding responses of the 10-story structure for various floor masses of the 10-story structure 89

3.16 Ratio of multiple pounding to no-pounding responses of the 5-story structure for various floor masses of the 10-story structure 90

3.17 Ratio of multiple pounding to no-pounding responses of the 10-story structure for various impact stiffness coefficients 91

3.18 Ratio of multiple pounding to no-pounding responses of the 5-story structure for various impact stiffness coefficients 92

3.19 The effect of changing the height of the s-structure on the ratio of multiple pounding to no-pounding responses of the p-structure (s-structure heights: 1, 2, 3, 4 and 5 stories) 93

3.20 The effect of changing the height of the s-structure on the ratio of multiple pounding to no-pounding responses of the p-structure (s-structure heights: 6, 7, 8 and 9 stories) 94

3.21 The effect of changing the height of the s-structure on the ratio of multiple pounding to no-pounding responses of the s-structure (s-structure heights: 1, 2, 3, 4 and 5 stories) 95

3.22 The effect of changing the height of the s-structure on the ratio of multiple pounding to no-pounding responses of the s-structure (s-structure heights: 6, 7, 8 and 9 stories) 96

3.23 Floor acceleration response spectra of various floors in pounding and no-pounding cases for 10-story structure (multiple pounding against 5-story structure) 97

3.24 Floor acceleration response spectra of various floors in pounding and no-pounding cases for 10-story structure (multiple pounding against 5-story structure) 98

3.25 Floor acceleration response spectra of various floors in pounding and no-pounding cases for 5-story structure 99

LIST OF FIGURES

3.26 Pounding to no-pounding floor response spectrum ratios for 10-story structure 100

3.27 Pounding to no-pounding floor response spectrum ratios for 5-story structure 101

3.28 Pounding response of equal fundamental frequency structures: response ratios for the 10-story structure 102

3.29 Pounding response of equal fundamental frequency structures: response ratios for the 5-story structure 103

3.30 The ratio of responses obtained in pounding against a flexible and a rigid 5-story structure for various gap sizes 104

3.31 The ratio of responses obtained in pounding against a flexible and a rigid 5-story structure for various story stiffnesses of the 10-story structure . . . 105

3.32 The ratio of responses obtained in pounding against a flexible and a rigid 5-story structure for various floor masses of the 10-story structure 106

3.33 The ratio of responses obtained in pounding against a flexible and a rigid 5-story structure for various impact stiffness coefficients 107

3.34 The effect of linear and nonlinear modeling of the contact springs on the response of the 10-story structure 108

3.35 The effect of linear and nonlinear modeling of the contact springs on the response of the 5-story structure 109

3.36 The ratio of nonlinear to linear pounding responses of the 10-story structure 110

3.37 The ratio of nonlinear to linear pounding responses of the 5-story structure 111

3.38 Floor acceleration response spectra of various floors of the 10-story structure obtained with linear and nonlinear impact spring model 112

3.39 Floor acceleration response spectra of various floors of the 10-story structure obtained with linear and nonlinear impact spring model 113

3.40 Floor acceleration response spectra of various floors of the 5-story structure obtained with linear and nonlinear impact spring model 114

3.41 Nonlinear to linear pounding floor response spectrum ratios for the 10-story structure 115

LIST OF FIGURES

3.42 Nonlinear to linear pounding floor response spectrum ratios for the 5-story structure 116

3.43 Nonlinear to no-pounding floor response spectrum ratios for the 10-story structure 117

3.44 Nonlinear to no-pounding floor response spectrum ratios for the 5-story structure 118

4.1 Schematic of adjacent structures in series undergoing the pounding 129

4.2 Free body diagram of a typical floor mass of the interior structure undergoing the two-sided pounding 130

4.3 Free body diagram of a typical floor mass of the exterior structure undergoing the one-sided pounding 131

4.4 Pounding to no-pounding response ratios of the observed structure (exterior or interior) for different fundamental frequencies of its neighboring building 132

4.5 Pounding to no-pounding response ratios of the observed structure (exterior or interior) for different floor masses of its neighboring building 133

4.6 Pounding to no-pounding response ratios of the observed structure (exterior or interior) for different gap sizes 134

4.7 Pounding to no-pounding response ratios of the observed structure (exterior or interior) for different impact element stiffnesses 135

5.1 Schematic of pounding structures supported on the flexible foundation . . . 150

5.2 The average input ground acceleration spectra 151

5.3 The effect of foundation stiffness on the pounding responses of the 10-story structure 152

5.4 The effect of foundation stiffness on the pounding responses of the 5-story structure 153

LIST OF FIGURES

5.5 Comparison of the pounding and no-pounding responses of the 10-story structure obtained for different flexible foundations with the corresponding responses obtained for the rigid foundation model 154

5.6 Comparison of the pounding and no-pounding responses of the 5-story structure obtained for different flexible foundations with the corresponding responses obtained for the rigid foundation model 155

5.7 The effect of pounding on the force and moment responses of the translational and rotational foundation springs for the 10-story structure 156

5.8 The effect of pounding on the force and moment responses of the translational and rotational foundation springs for the 5-story structure 157

5.9 Pounding to no-pounding foundation springs force and moment ratios for the 5- and 10-story structures 158

5.10 The effect of foundation shear wave velocity on the floor acceleration response spectra of various floors of the 10-story structure – floors 1 through 5 159

5.11 The effect of foundation shear wave velocity on the floor acceleration response spectra of various floors of the 10-story structure – floors 6 through 10 160

5.12 The effect of foundation shear wave velocity on the floor acceleration response spectra of floor 1 of the 10-story structure in enlarged form 161

5.13 The effect of foundation shear wave velocity on the floor acceleration response spectra of floor 5 of the 10-story structure in enlarged form 162

5.14 The effect of foundation shear wave velocity on the floor acceleration response spectra of floor 10 of the 10-story structure in enlarged form 163

5.15 The effect of the foundation shear wave velocity on the floor acceleration response spectra of various floors of the 5-story structure 164

5.16 The effect of foundation shear wave velocity on the floor acceleration response spectra of floor 1 of the 5-story structure in enlarged form 165

5.17 The effect of foundation shear wave velocity on the floor acceleration response spectra of floor 5 of the 5-story structure in enlarged form 166

LIST OF FIGURES

5.18 Floor acceleration response spectra of various floors in pounding and no-pounding cases for 10-story structure supported on the flexible foundation – floors 1 through 5 167

5.19 Floor acceleration response spectra of various floors in pounding and no-pounding cases for 10-story structure supported on the flexible foundation – floors 6 through 10 168

5.20 Floor acceleration response spectra of various floors in pounding and no-pounding cases for 5-story structure supported on the flexible foundation . 169

6.1 Response of structures with springs of varying stiffness coefficients provided at the pounding interfaces 201

6.2 Response of structures with springs of varying stiffness coefficients provided at the pounding interfaces 202

6.3 Variation of story shears of various stories versus impact spring stiffness coefficients 203

6.4 Variation of absolute accelerations of various impacting floors versus impact spring stiffness coefficients 204

6.5 Maximum deformations versus stiffness coefficient of springs provided at different pounding interfaces 205

6.6 Effect of increasing the interface damping coefficient on the story shear response 206

6.7 Effect of increasing the interface damping coefficient on the floor acceleration response 207

6.8 Schematic of rigidly joined structures supported on the rigid foundation . . 208

6.9 Comparison of the column bending moment and absolute floor acceleration responses of rigidly joined structures with the corresponding responses obtained for the no-pounding and free-pounding cases (rigid foundation model, El-Centro time history) 209

LIST OF FIGURES

6.10 Comparison of the column bending moment and absolute floor acceleration responses of rigidly joined structures with the corresponding responses obtained for the no-pounding and free-pounding cases (rigid foundation model, 1 synthetic time history) 210

6.11 Comparison of the column bending moment and absolute floor acceleration responses of rigidly joined structures with the corresponding responses obtained for the no-pounding and free-pounding cases (rigid foundation model, 50 synthetic time histories) 211

6.12 Schematic of pounding structures supported on the flexible foundation . . . 212

6.13 Comparison of responses obtained with bracing, without bracing and no-pounding cases (rigid foundation model, El-Centro time history) 213

6.14 Comparison of responses obtained with bracing, without bracing and no-pounding cases (rigid foundation model, 1 synthetic time history) 214

6.15 Comparison of responses obtained with bracing, without bracing and no-pounding cases (rigid foundation model, 50 synthetic time histories) 215

6.16 Comparison of responses obtained for different configurations of bracings with the responses obtained for unbraced and no-pounding cases (rigid foundation model, El-Centro time history) 216

6.17 Comparison of responses obtained for different configurations of bracings with the responses obtained for unbraced and no-pounding cases (rigid foundation model, 1 synthetic time history) 217

6.18 Comparison of responses obtained for different configurations of bracings with the responses obtained for unbraced and no-pounding cases (rigid foundation model, 50 synthetic time histories) 218

6.19 Comparison of the bending moment response obtained for joined structures with different bracing configurations with the response obtained for unbraced joined and unbraced disjoined freely pounding structures (rigid foundation model, El-Centro time history) 219

LIST OF FIGURES

6.20 Comparison of the bending moment response obtained for joined structures with different bracing configurations with the response obtained for unbraced joined and unbraced disjoined freely pounding structures (rigid foundation model, 1 synthetic time history) 220

6.21 Comparison of the bending moment response obtained for joined structures with different bracing configurations with the response obtained for unbraced joined and unbraced disjoined freely pounding structures (rigid foundation model, 50 synthetic time histories) 221

6.22 Comparison of the acceleration response obtained for joined structures with different bracing configurations with the response obtained for unbraced joined and unbraced disjoined freely pounding structures (rigid foundation model, El-Centro time history) 222

6.23 Comparison of the acceleration response obtained for joined structures with different bracing configurations with the response obtained for unbraced joined and unbraced disjoined freely pounding structures (rigid foundation model, 1 synthetic time history) 223

6.24 Comparison of the acceleration response obtained for joined structures with different bracing configurations with the response obtained for unbraced joined and unbraced disjoined freely pounding structures (rigid foundation model, 50 synthetic time histories) 224

6.25 Comparison of responses obtained for joined and completely braced 10-story structure with the responses of the disjoined and completely braced 10-story structure (rigid foundation model, El-Centro time history) 225

6.26 Comparison of responses obtained for joined and completely braced 10-story structure with the responses of the disjoined and completely braced 10-story structure (rigid foundation model, 1 synthetic time history) 226

LIST OF FIGURES

6.27 Comparison of responses obtained for joined and completely braced 10-story structure with the responses of the disjoined and completely braced 10-story structure (rigid foundation model, 50 synthetic time histories) 227

6.28 Comparison of responses obtained for different bracing sizes with the responses obtained for unbraced and no-pounding cases (rigid foundation model) 228

6.29 The effect of bracing sizes on the bracing force and stress responses in various bracings of the 10-story structure for pounding structures (rigid foundation model) 229

6.30 The effect of bracing sizes on the bracing force and stress pounding responses in various bracings of the 10-story structure (rigid foundation model) 230

6.31 Comparison of responses obtained for joined and completely braced 10-story structure, with different bracing sizes, with the responses of unbraced joined and no-pounding cases (rigid foundation model) 231

6.32 The effect of bracing sizes on the bracing force and stress responses in various bracings of the 10-story structure for joined structures (rigid foundation model) 232

6.33 Schematic of rigidly joined structures supported on the flexible foundation . 233

6.34 Comparison of the column bending moment and absolute floor acceleration responses of rigidly joined structures with the corresponding responses obtained for the no-pounding and free-pounding cases (flexible foundation model, El-Centro time history) 234

6.35 Comparison of the column bending moment and absolute floor acceleration responses of rigidly joined structures with the corresponding responses obtained for the no-pounding and free-pounding cases (flexible foundation model, 1 synthetic time history) 235

6.36 Comparison of the column bending moment and absolute floor acceleration responses of rigidly joined structures with the corresponding responses obtained for the no-pounding and free-pounding cases (flexible foundation model, 50 synthetic time histories) 236

LIST OF FIGURES

6.37 Comparison of responses obtained with bracing, without bracing and no-pounding cases (flexible foundation model, El-Centro time history) 237

6.38 Comparison of responses obtained with bracing, without bracing and no-pounding cases (flexible foundation model, 1 synthetic time history) 238

6.39 Comparison of responses obtained with bracing, without bracing and no-pounding cases (flexible foundation model, 50 synthetic time histories) 239

6.40 Comparison of responses obtained for different configurations of bracings with the responses obtained for unbraced and no-pounding cases (flexible foundation model, El-Centro time history) 240

6.41 Comparison of responses obtained for different configurations of bracings with the responses obtained for unbraced and no-pounding cases (flexible foundation model, 1 synthetic time history) 241

6.42 Comparison of responses obtained for different configurations of bracings with the responses obtained for unbraced and no-pounding cases (flexible foundation model, 50 synthetic time histories) 242

6.43 Comparison of the bending moment response obtained for joined structures with different bracing configurations with the response obtained for unbraced joined and unbraced disjoined freely pounding structures (flexible foundation model, El-Centro time history) 243

6.44 Comparison of the bending moment response obtained for joined structures with different bracing configurations with the response obtained for unbraced joined and unbraced disjoined freely pounding structures (flexible foundation model, 1 synthetic time history) 244

6.45 Comparison of the bending moment response obtained for joined structures with different bracing configurations with the response obtained for unbraced joined and unbraced disjoined freely pounding structures (flexible foundation model, 50 synthetic time histories) 245

LIST OF FIGURES

6.46 Comparison of the acceleration response obtained for joined structures with different bracing configurations with the response obtained for unbraced joined and unbraced disjointed freely pounding structures (flexible foundation model, El-Centro time history) 246

6.47 Comparison of the acceleration response obtained for joined structures with different bracing configurations with the response obtained for unbraced joined and unbraced disjointed freely pounding structures (flexible foundation model, 1 synthetic time history) 247

6.48 Comparison of the acceleration response obtained for joined structures with different bracing configurations with the response obtained for unbraced joined and unbraced disjointed freely pounding structures (flexible foundation model, 50 synthetic time histories) 248

6.49 Comparison of responses obtained for different bracing sizes with the responses obtained for unbraced and no-pounding cases (flexible foundation model) 249

6.50 The effect of bracing sizes on the bracing force and stress responses in various bracings of the 10-story structure for pounding structures (flexible foundation model) 250

6.51 The effect of bracing sizes on the bracing force and stress pounding responses in various bracings of the 10-story structure (flexible foundation model) 251

6.52 Comparison of responses obtained for joined and completely braced 10-story structure, with different bracing sizes, with the responses of unbraced joined and no-pounding cases (flexible foundation model) 252

6.53 The effect of bracing sizes on the bracing force and stress responses in various bracings of the 10-story structure for joined structures (flexible foundation model) 253

6.54 Forces in the rigid links for various configurations of bracings 254

6.55 Forces in the rigid links for different bracing sizes of the 10-story structure 255

LIST OF FIGURES

6.56 Forces in the rigid links for different shear wave velocities of the foundation media 256

6.57 Schematic of column pounding structures 257

6.58 Schematic of K-braced column pounding structures 258

6.59 Comparison of the bending moment and acceleration responses obtained for braced pounding and unbraced no-pounding structures with different bracing configurations with the response obtained for braced joined structures (bracing size $W530 \times 66$, El-Centro time history) 259

6.60 Comparison of the bending moment and acceleration responses obtained for braced pounding and unbraced no-pounding structures with different bracing configurations with the response obtained for braced joined structures (bracing size $W530 \times 66$, 50 synthetic time histories) 260

6.61 Comparison of the bending moment and acceleration responses obtained for braced pounding and unbraced no-pounding structures with different bracing configurations with the response obtained for braced joined structures (bracing size $W310 \times 23.8$, El-Centro time history) 261

6.62 Comparison of the bending moment and acceleration responses obtained for braced pounding and unbraced no-pounding structures with different bracing configurations with the response obtained for braced joined structures (bracing size $W310 \times 23.8$, 50 synthetic time histories) 262

6.63 Comparison of the bending moment and acceleration responses obtained for braced pounding and unbraced no-pounding structures with different bracing configurations with the response obtained for braced joined structures (bracing size $W150 \times 13.5$, El-Centro time history) 263

6.64 Comparison of the bending moment and acceleration responses obtained for braced pounding and unbraced no-pounding structures with different bracing configurations with the response obtained for braced joined structures (bracing size $W150 \times 13.5$, 50 synthetic time histories) 264

LIST OF TABLES

2.1	Natural frequencies and maximum positive displacements of the basic configuration	20
5.1	Properties of the ten and five-story pounding structures including the impact element and the foundation medium properties.	149
6.1	The forces in the foundation springs of the 5- and 10-story structures for no-pounding, pounding and joined without bracing and with different bracing configurations	265
6.2	The forces in the foundation springs of the 5- and 10-story structures for pounding and joined structures with different bracing sizes of the 10-story structure	266
6.3	The forces in the foundation springs of the 5- and 10-story structures for unbraced no-pounding, braced pounding and joined structures with different shear wave velocities of the foundation media	267

Chapter 1

INTRODUCTION

Because of pressure on land, buildings in large cities are often constructed next to each other with no or small clearance between them. When the dynamic characteristics of such closely spaced buildings are different, their motions during an earthquake will usually not be in phase. If the clearance between such buildings is not adequate, they are likely to collide during an earthquake. Such collisions are commonly referred to as “mutual pounding”. Indeed, such mutual poundings have been reported in several past earthquakes [3, 4, 5, 27, 37, 38].

The pounding can cause local as well as overall failure of pounding structures. The post-earthquake analytical investigation of the failure of a stair tower, warehouse and other structures at Olive View Hospital [23] confirmed that pounding during the San Fernando Earthquake did, indeed, contribute to damage and failure of these structures. Although no other confirmatory analytical studies have been reported, several other damages observed in past earthquakes have been attributed to pounding. Widespread occurrences of mutual poundings, causing severe building damages and even collapses, have been reported in the 1985 Mexico City Earthquake [5, 14] and in the more recent 1989 Loma Prieta Earthquake [3].

The structural pounding is a vibro-impact problem. This problem is commonly encountered in machines and mechanical equipment and as such it has been of significant interest to mechanical engineers for some time now. The literature [9, 10, 12, 13, 22, 30, 31, 34, 39, 40, 44] on this subject which includes books [11, 21] is fairly rich. In the study of mechanical vibro-impact problems, the primary interest is in reducing the wear and tear and noise level, whereas in structural engineering the motivation to study seismic pounding problem is to

lessen its local and overall damaging effects on civil structures.

The easiest approach to eliminate pounding is to provide enough clearance between the pounding structures. However, for existing structures, it is not possible to change the clearance. In such cases, it is of interest to study this problem to understand and ascertain the effect of impact and propose impact mitigating schemes. This is the main objective of this study.

The fact that pounding can indeed occur has prompted a few investigators to study the behavior of single-degree-of-freedom impacting structures subjected to base motions. Miller [28] has investigated the problem of vibro-impact of two single-degree-of-freedom structures subjected to harmonic base motion with single-impact-per-cycle oscillations. The impact effects and loss of energy were included through the coefficient of restitution. For the case of a harmonic input and single-impact-per-cycle, the exact solution of the equations of motion was obtained. Parametric studies were conducted to examine the effect of the excitation frequency and amplitude, gap size and coefficient of restitution. The results indicate that if the coefficient of restitution between the impacting bodies is small, a beneficial energy dissipation can occur, thereby leading to a reduction in the overall response. This however, need not be the case all the time, as reported in another investigation [45, 46].

A significant study on this topic was conducted by Wolf and Skrikerud in 1979 [45] and reported in a rather extensive form in 1980 [46]. This study examined a single-degree-of-freedom system impacting stiff boundaries on one and both sides (asymmetrical and symmetrical impacts), subjected to harmonic as well as transient base motion. The impacting surfaces were modeled by stiff springs acting in parallel with the oscillator spring. Thus the entire system was assumed to have a hardening bilinear spring. The energy dissipation during impact was included by providing viscous dashpots with damping factors related to the coefficient of restitution through an exponential relationship, well-known in vibro-impact studies [13]. The study identified subharmonic and hyperharmonic response characteristics along with the “break even” frequency below which the response of impacting system is lower than that of the nonimpacting system. An analysis of the impact between

the multi-degree-of-freedom reactor building and adjacent auxiliary building, modeled as a single-degree-of-freedom mass-spring system, was also conducted to ascertain the forces induced by a possible impact. For this specific problem it was concluded that impact was not a problem with regard to the safety of the reactor building, and it only caused local effects. The analyses were also carried out to see what effect a spring placed between the two impacting structures would have on the response. It was observed that the use of a precompressed spring between the structures reduced the high-frequency response as well as the acceleration induced in the structures.

In a study by Davis [8], pounding was modeled by a single-degree-of-freedom oscillator which may impact against either a stationary or moving neighboring barrier and subjected to harmonic excitation. Non-linear Hertzian contact law is incorporated to present the impact stiffness. The spectra of impact velocity versus excitation period for a range of model parameters show a strong peak near a period equal to one-half the natural period of a similar non-impacting oscillator. Bands of response in which periodic multiple impacts and non-periodic or chaotic impacts occur are found.

Another study which has considered impact in the collapse of buildings is by Wada et al. [41]. Simple single-degree-of-freedom models of impacting buildings with stiffnesses characterized by elasto-plastic rotational springs at the base were considered to investigate the effect of gravity on collapse. For this assumed model, the study showed that gravity effects can, indeed, aggravate the situation leading to a collapse, indicated by very large displacement response of the masses in the analysis.

In another study, Anagnostopoulos [1] considered a series of single-degree-of-freedom oscillators representing a set of buildings in a city block. The numerical results have been reported for four such oscillators impacting with each other. The bilinear force deformation relationship was used to characterize the stiffness of the structures as well as the impacting bodies. The parametric studies were conducted in which the clearances between the masses, yield levels of bilinear stiffness elements and the ratios of the stiffnesses of the outside and inside oscillators were varied. One conclusion of the study was that the outside or corner

structures in a row of buildings would experience higher levels of deformation than the inside structures. They are, thus, particularly vulnerable to pounding effects and are more likely to get damaged than the inside structures. This has also been reported to be the case in some past earthquakes [37, 38]. In a more recent study [2], Anagnostopoulos basically did the same parametric investigation [1] but for MDOF structures with the bases supported on translational and rocking spring-dashpots.

In a rather different context, there have also been studies where impact has been considered with the primary purpose of reducing the response of structures and equipment by providing constraints [26]. Such devices have been called impact dampers. In another related study, Iwan [15] has developed an interesting response spectrum procedure to predict seismic response of equipment with motion-limiting constraints. The possibility of extending this approach to predict the response of multi-degree-of-freedom systems with motion limiting constraints by means of equivalent linear modal analysis has also been briefly mentioned [15].

A study of the pounding problem involving MDOF buildings has been reported by Maison and Kasai [24, 25] and Kasai et al. [19, 20]. In these studies, the pounding responses of MDOF structures colliding at a fixed level against a rigid obstruction as well as a flexible structure have been examined. The effect of various problem parameters on the pounding response has also been reported. Jeng et al. [16] presented a spectral difference method based on random vibration theory with the assumption of fixed level pounding to estimate the minimum building separation necessary to avoid seismic pounding.

The problem of multilevel structural pounding between a MDOF structure pounding against a rigid as well as a MDOF flexible structure has been reported by the writers for the first time [35].

Jing and Young [17, 18] have studied the random response of vibro-impact systems subjected to white-noise input. The Hertz's contact law is used to model the contact or pounding stiffness. The Fokker-Planck equation is solved for the stationary transition density function of the response.

On the alleviation of the pounding effects, the work by Westermo [42] is significant. In that study, the pounding structures are connected by a link and beam system which transmits the connection forces to the floors of the structures. It is shown that for structures with closely similar properties the linkage prevents the two from oscillating out of phase while transmitting a relatively small force through the connection.

1.1 Scope of This Work

In the present study, we examine the pounding response of a multi-degree-of-freedom structure pounding at several levels against a rigid as well as a multi-degree-of-freedom deformable structure. To understand and evaluate the pounding effects, the displacements, story shears, overturning moments, floor accelerations and floor spectrum responses have been obtained with and without pounding.

In Chapter 2, the simpler problem of a multi-degree-of-freedom structure colliding against a rigid obstruction of different heights has been examined. This is followed by the study of pounding of two deformable multi-degree-of-freedom structures in Chapter 3. Extensive parametric studies have been conducted to understand the characteristics of the pounding response. As a part of the parametric study, the nonlinear Hertz's model for the contact stiffness at the pounding interface has been considered. The problem of pounding of structures in series is examined in Chapter 4. As structural foundation may not be completely rigid, in Chapter 5 the effect of foundation flexibility on the structural pounding response is investigated. In Chapter 6, several methods to alleviate the pounding problem are investigated and pounding mitigation strategies are proposed. Finally, the study and its main findings are summarized in Chapter 7.

Chapter 2

POUNDING OF A FLEXIBLE STRUCTURE AGAINST AN OBSTRUCTION

2.1 Introduction

As a simplification to study pounding, in this chapter we consider the case of a multi-degree-of-freedom flexible structure pounding at its floor levels against a rigid obstruction (Figure 2.1). A parametric study is conducted, where the parameters of the pounding structure are changed to study their effect on the pounding response. In the following, we first describe the equations of motion and then present the numerical results.

2.2 Equations of Motion

We will model the vibrating structure as a p degrees-of-freedom shear building, being pounded at its first s lower floors by a rigid obstruction. To develop the equations of motion, consider the free body diagram of a typical mass m_i as shown in Figure 2.2 for the two cases of pounding and no-pounding. Using Newton's law, the equation of motion for the no-pounding case can be written as:

$$m_i \ddot{x}_i - k_i x_{i-1} + (k_i + k_{i+1}) x_i - k_{i+1} x_{i+1} = -m_i \ddot{x}_g(t) \quad (2.1)$$

where m_i is the i th floor mass; k_i = stiffness of the i th story; $\ddot{x}_g(t)$ = ground acceleration; x_i = displacement of mass m_i relative to the ground.

When the free displacement of the mass exceeds the gap between the mass and adjacent obstruction, the collision will occur. In such a case, the free body diagram is as shown in

Figure 2.2(a). Using Newton's law in this case, the equation of motion for this mass can be written as:

$$m_i \ddot{x}_i - k_i x_{i-1} + (k_i + k_{i+1}) x_i - k_{i+1} x_{i+1} + d_i \dot{x}_i + s_i (x_i - g_i) = -m_i \ddot{x}_g(t) \quad (2.2)$$

where g_i is the size of the gap at the level of mass m_i and s_i is the coefficient of the contact stiffness during pounding. Here it is assumed that this stiffness is linear. A nonlinear contact stiffness will be considered later.

Equations for different masses can be collected and written in matrix form for the no-pounding case as:

$$[M]\{\ddot{X}\} + [C]\{\dot{X}\} + [K]\{X\} = -[M]\{r\}\ddot{x}_g(t) \quad (2.3)$$

and for the pounding case as:

$$[M]\{\ddot{X}\} + [C + D]\{\dot{X}\} + [K + S]\{X\} = -[M]\{r\}\ddot{x}_g(t) + [S]\{g\} \quad (2.4)$$

where $[M]$ = mass matrix; $[K]$ = stiffness matrix; $\{r\}$ = influence coefficient vector; $\{g\}$ = the vector of clearances (gaps); and $[S]$ is the supplemental stiffness matrix provided by the contact springs whenever pounding occurs. In equations 2.3 and 2.4, we have now added the system damping matrix $[C]$ to include the energy dissipation effects. This matrix is defined in terms of the modal damping ratio and eigenproperties of the structure using standard procedures [5]. This structural damping matrix is supplemented by the damping matrix coming from the dashpots provided at the pounding surfaces. These dashpots are provided to include the loss of energy which occurs during any pounding.

In equations 2.3 and 2.4, the mass matrix is diagonal. The stiffness matrices $[K]$ and $[S]$, supplemental damping matrix $[D]$ and vector $\{g\}$ are defined as:

$$[K] = \begin{bmatrix} k_1 + k_2 & -k_2 & 0 & \dots & 0 & 0 \\ -k_2 & k_2 + k_3 & -k_3 & \dots & 0 & 0 \\ 0 & -k_3 & k_3 + k_4 & \dots & 0 & 0 \\ \vdots & \vdots & \vdots & \ddots & \vdots & \vdots \\ 0 & 0 & 0 & \dots & k_{p-1} + k_p & -k_p \\ 0 & 0 & 0 & \dots & -k_p & k_p \end{bmatrix} \quad (2.5)$$

$$[D] = \begin{bmatrix} d_1 & 0 & \dots & 0 \\ 0 & d_2 & \dots & 0 \\ \vdots & \vdots & \ddots & \vdots \\ 0 & 0 & \dots & d_s \end{bmatrix} \quad (2.6)$$

$$[S] = \begin{bmatrix} s_1 & 0 & \dots & 0 \\ 0 & s_2 & \dots & 0 \\ \vdots & \vdots & \ddots & \vdots \\ 0 & 0 & \dots & s_s \end{bmatrix} \quad (2.7)$$

$$\{g\}^T = (g_1 \quad g_2 \quad \dots \quad g_s \quad 0 \quad \dots \quad 0) \quad (2.8)$$

The elements s_i and d_i are zero for the floors which do not pound. Also if only s number of the floors are likely to pound, then the vector $\{g\}$ contains only s nonzero elements.

The equations of motion 2.3 and 2.4, with and without pounding, are both linear. Thus, if desired, they can be solved by the modal analysis approach. However, since $[D]$ and $[S]$ matrices constantly change because of the pounding and no-pounding situations, the problem is essentially nonlinear. It was, therefore, found to be best to solve it by a step-by-step integration approach. Here the Newmark- β [5] approach as well as Runge-Kutta [6] approach have been used. The time steps of the integration were kept very small to capture the everchanging ‘‘pounding’’ and ‘‘no-pounding’’ states as the motion proceeded.

2.3 Problem Parameters for Numerical Analysis

Numerical results have been obtained for several configurations of two pounding structures. The assumed basic configuration is a ten-story structure pounding against a five-story rigid structure as shown in Figure 2.1. Some results of pounding against a rigid structure of varying height have also been obtained. In the basic configuration the structural parameters are: the floor mass $= 6.02E + 5 \text{ Kg}$, story stiffness $= 1.81E + 9 \text{ N/m}$ and the stiffness of the impact spring $= 8.76E + 9 \text{ N/m}$. The damping ratio of 0.05 has been assumed in each mode. Also a dashpot with coefficient $d_i = 2.04E + 7 \text{ Kg/sec}$ has been added at each pounding interface to include some loss of energy due to pounding in the analysis. Each of these problem parameters has also been varied to examine its effect on the pounding response. Another parameter which has been considered is the clearance between pounding floors. Also the cases of pounding at a fixed level as well as possible pounding at all lower level floors have been considered. It is assumed that pounding occurs only at the floor levels. The case of a floor mass pounding in the middle of a column will be considered elsewhere.

The seismic base motion used to obtain the numerical results is the 1941 N-S El Centro component with maximum ground acceleration level of $0.2 G$. The plot of the acceleration time history for this input motion is shown in Figure 2.3. For this input, the response time histories have been obtained for the floor displacements, story shears and overturning moments at all floor levels. Figures 2.4 and 2.5 show the time histories with and without pounding of the shear forces in the 6th and 10th stories, respectively. Similarly, Figures 2.6(a) and (b) show with and without pounding time histories for the overturning moments at the base. As the maximum response values are of design interest, these values have been obtained from the calculated response time histories and compared with each other to evaluate the pounding effect. These maximum values usually occur at the instant of pounding, as shown by the spikes in the response time histories for the pounding cases shown in Figures 2.4(b), 2.5(b) and 2.6(b).

To evaluate the effect of pounding on supported equipment, the floor acceleration time

histories have also been obtained. Figure 2.7 shows the acceleration time histories with and without pounding at floor 10. The presence of acceleration spikes is noted in these time histories. Also the presence of high frequency components can be clearly noticed in the acceleration and other response time histories obtained in the pounding cases. The floor acceleration time histories obtained in the pounding cases have been utilized to generate floor response spectra to examine the changes in the frequency content caused by the pounding of structures.

The fundamental frequency for the basic configuration is 1.304 cps; the remaining frequencies are shown in Table 2.1. In the table are also shown the maximum displacement of each floor for the ground motion under consideration. These displacements also define the minimum clearance required at the top of the adjacent building for no pounding between the floors.

The following set of figures shows the maximum positive and negative values of the floor displacements, story shears and overturning moments. The positive and negative values are defined according to the convention shown in Figure 2.8. Although the shear in a story remains constant over the story height, in the figure presented herein it is shown at the top floor level of the story. These shear values are then joined by straight lines. The effect of changing various parameters on the pounding response will now be discussed.

2.4 Effect of Gap Size

Figure 2.9 shows the effect of changing the clearance or gap size on the response when the pounding is permitted only at the top of the adjacent rigid building, that is, at the fifth floor level. Such a pounding will be referred to as single level pounding. The case when the pounding occurs at all possible levels is referred to as multiple pounding. The results for the multiple pounding are shown in Figure 2.10. The results are also shown for the no-pounding case when the gap size at the fifth floor is larger than the displacement shown in Table 2.1 for the fifth floor (that is, the gap > 0.0545 m). Also shown are the results

for gap sizes of about 90%, 50% and 0% (that is, no clearance) of the minimum gap for the no-pounding case.

The results in Figure 2.9(a) show that the displacements on the pounding side are reduced because of the obstruction due to the adjacent structure. The displacements on the opposite side are also seen to decrease slightly, especially for larger gaps; for the no-gap case, they increase slightly for the lower floors and decrease for the higher floors. The most dramatic effect of pounding is, however, felt in the story shears and overturning moments. The positive story shears increase dramatically for floors above the pounding floor whereas the negative shear forces are seen to increase as well as decrease depending upon the case. The magnitudes of the negative overturning moments increase but more significantly at the ground level. Similar observations can be made from the results in Figure 2.10 shown for the multiple pounding case; in fact, the results of the two cases are almost identical. This is more clearly seen from the results shown in Figure 2.11 where the ratios of the response values in the multiple pounding case to the values in the single pounding case are plotted. In most cases this ratio is about one, except for the positive displacements and shear force values below the pounding level where this ratio is less than 1, thus indicating that the response in the multiple pounding case is less than the response in the single pounding case.

To show the effect of pounding vis-a-vis no-pounding more clearly, in Figure 2.12 we plot the ratios of the multiple pounding responses to the no-pounding responses. As seen from the figure, the positive displacements are, of course, reduced because of the obstruction due to the adjacent structure. Also reduced are the positive shear force values in the stories below the pounding levels, but this has little design implication as the shear forces on the negative side for these levels are essentially unchanged. A dramatic increase in the shear force and overturning moment in the top stories, compared to their values in the no-pounding case, has, of course, definite design implications. The top floors are seen to be affected the most by pounding. Also, the case with no gap is most severe and, as we would expect, increasing the gap size reduces the overall pounding effect.

2.5 Effect of Story Stiffness

The next set of four figures shows the effect of changing the story stiffness of the ten-story structure on the pounding response. Two additional story stiffnesses, with $\frac{1}{4}$ and $\frac{1}{16}$ of the original story stiffness, have been considered. All other structural parameters are the same as in the basic configuration. Also, the gap between the pounding structures is assumed to be zero.

Figure 2.13 is for the single level pounding case whereas the next figure (Figure 2.14) is for the multiple pounding case. A decrease in the story stiffness causes the pounding displacement response to increase and the shear and moment responses to decrease. Similar observations also apply to the multiple pounding case (Figure 2.14), although a slight increase in the overturning moment at the base for the case of a flexible structure is also noted. Comparison of the responses in the multiple and single pounding cases is again best shown by their ratios which are plotted in Figure 2.15. In general, below the pounding level, the multiple pounding seems to cause lower displacement and shear responses than the single pounding case. The overturning moment response, on the other hand, is seen to be higher in the multiple pounding case at the lower levels of the softer structures.

In Figure 2.16, we compare the multiple pounding to no-pounding responses for structures with different stiffnesses by plotting the ratios of the two responses. It is seen that decreasing the stiffness does not necessarily decrease the pounding effect of increased shear above the pounding level as the curve for the stiffest structure is in between the curves of the two softer structures. The overturning moment due to pounding, however, increases at the lower levels when the structure becomes softer.

2.6 Effect of Floor Mass

The next four figures show the effect of changing the floor mass and keeping all other parameters the same as in the basic case. Again the gap size is taken as zero. The response results for the structures with $\frac{1}{2}$ and $\frac{1}{4}$ of the original mass have been compared with

the response for the basic case. The lower the mass, the higher the fundamental frequency. Figures 2.17 and 2.18 show the results for the single and multiple pounding case. The larger mass structure is seen to experience a higher level of response in pounding. Comparison of the responses in the multiple and single pounding cases is shown by plotting the ratio of the two responses in Figure 2.19 for different mass parameters. It is noted that changing the mass does not seem to change the ratio of the multiple to single pounding responses except in the vicinity of the top floor and the pounding floor in the case of shear response and near the base in the case of the overturning moment response. As in the previous case, the displacement and shear force responses are in general less in the multiple pounding case with some exceptions near the fifth floor in the shear response and near the base in the moment response.

In Figure 2.20 we compare the responses obtained in the multiple pounding case with the responses in the no-pounding case. The figures for all three responses show that the pounding effect is most severe in the case of the structure with the largest mass, except near the top in the shear and moment responses where the structure with the lowest mass seems to be more severely affected by the pounding than the heavier structure.

In Figure 2.21 we put together the results of Figures 2.16 and 2.20 to compare the effect of the fundamental frequency of the structure on its pounding susceptibility. The fundamental frequencies ranged between 0.326 and 2.604 cps. Comparing the results for various frequencies we observe that there is no particular correlation between the fundamental frequency of the structure and pounding severity measured by the increase in the response caused by pounding. Pounding, being an impact phenomenon, probably interacts with the higher frequency modes the most and not with the lower fundamental frequency of the structure. The fundamental frequency of a structure, thus, does not seem to be a significant parameter in predicting the pounding effects.

2.7 Effect of Pounding Stiffness

Next we examine the sensitivity of the results with respect to the assumed value of the stiffness coefficient of the pounding spring ($8.76E + 10 \text{ N/m}$), a parameter which is hard to predict. We consider three values of the stiffness coefficient which are 1, 2 and 4 times the stiffness used in the previous figures. In Figure 2.22 we plot the ratio of the multiple pounding to the single pounding case. We observe that the shear response ratio near the top pounding floor is reduced by an increase in the stiffness. Thus with stiffer pounding spring, neglecting the multiple pounding can overestimate the response. At the same time, however, neglecting the possibility of multiple pounding can also lead to underestimation of the overturning moment effect, especially near the base.

In Figure 2.23 we plot the ratio of the response with pounding to the response without pounding for structures with three different pounding stiffnesses. For the range of stiffness variation considered here, the displacement and shear responses are not changed very much with a change in the pounding stiffness. The overturning moment effect at the bottom level is increased with an increase in the pounding stiffness. That is, a stiffer spring tends to cause a higher overturning moment response at the lower levels of the structure due to pounding than a softer spring.

2.8 Effect of Change in the Pounding Level

Here we compare the response results obtained when the height of the rigid structure is changed. We consider pounding with rigid structures of 1 to 10 story heights. The response values for the displacement, story shear and overturning moments obtained in the multiple pounding cases are shown in Figures 2.24 and 2.25. We observe that the displacements on the pounding side become smaller as the number of floors involved in pounding increases. The displacements on the other side do not necessarily increase with the number of pounding floors; they seem to be reaching their maximum values when about five or six floors are involved. For higher level poundings, these displacements seem to become less, as is seen

from Figure 2.25. As noted before, the shear decreases below the top pounding floor, but increases dramatically above this floor. It is always the next higher story which experiences the highest shear force. The maximum shear force values attained in all cases are about the same (see Figure 2.24), except for the pounding higher than level six the maximum shear becomes small (see Figure 2.25). It seems that for the ten-story structure considered here, the pounding against a five or six story rigid structure would seem to cause the highest deformation and maximum story shear responses. The negative shears, however, do not seem to have any particular trend with a change in the height of the rigid structure, but pounding against a five or six story structure again causes the largest response.

The overturning moment response has a definite trend: as the height of the adjacent rigid structure is increased, the overturning moment is also increased. A very large increase in the overturning moment is noted for the case when all floors impact (see Figure 2.26).

Figures 2.26 and 2.27 show the ratio of the pounding to no-pounding responses for different numbers of floors involved in the impact. It is noted that as more floors are engaged, the effect of impact as measured by the increase in the positive shear force above the pounding level is increased. The increase in the negative shear caused by pounding, however, does not have any particular trend. The increase in the overturning moment due to pounding with an increasing number of floors is quite obvious: when the top floor is also engaged, the overturning moment on the negative side can increase dramatically due to pounding. This is primarily due to large impacting forces applied at the top with large lever arms.

2.9 Effect of Pounding on Floor Accelerations and Floor Response Spectra

In Figure 2.28 we plot the maximum accelerations of various floors caused by pounding of the basic configuration ten-story structure against a five-story rigid structure. Also shown are the accelerations obtained with no pounding. A large increase in the acceleration due to

pounding is noted at all floor levels. The acceleration of the highest floor of pounding (fifth floor) is, of course, the highest. In Figure 2.28(b) we also plot the ratio of the maximum accelerations obtained with and without pounding. It is seen that in this case the pounding accelerations are up to about 7 times the no-pounding accelerations.

In the next two figures (Figures 2.29 and 2.30) we also plot the acceleration floor response spectra of all floors. These spectra give a more complete picture about the frequency content of the floor acceleration time histories. In these figures are also plotted the floor spectra without any pounding. It is seen that floor spectra are greatly amplified in the high frequency range, indicating that pounding introduces high-frequency components in the response.

In Figure 2.31 we plot the ratio of the floor response spectrum values obtained with and without pounding. It is noted that this ratio is more than 1.0 for almost all frequencies higher than 1.5 cps. For frequencies higher than 10 cps there is a large increase in the floor response spectrum values due to pounding. Also, it is noted that there are two distinct groups of amplifications. The pounding floors are seen to experience a much larger increase in the spectrum values (as high as 14 times the no-pounding spectrum values) than the non-pounding floors, although the non-pounding floors also experience a significant increase (as high as 7 times the no-pounding response spectrum values). The lowest floor experiences the highest amplification in the response spectrum values. Thus pounding can severely affect equipment which has high-frequency characteristics, especially those supported on the lower floors.

2.10 Effect of Structural Damping on the Response due to Pounding

To examine the effect of structural damping on the pounding response characteristics, all the results described above for 5% structural damping were also repeated for 2% and 0% structural damping ratios. Qualitatively all the response characteristics of the 2% and 0% structure were very much similar to the response characteristics of the 5% damping

structure. We will therefore not present all the results, but for 2% damping, we will give the results of the ratios of the pounding to no-pounding responses for various parameters considered before.

Figure 2.32 showing the effect of the clearance on the pounding response should be compared with Figure 2.12 showing similar results for 5% damping. The appearance of the figures is very similar, but the numbers are slightly different. The structure with smaller damping seems to experience a larger pounding effect.

The results in Figure 2.33 showing the effect of changing the structural stiffness parameter for the 2%-damping structure should be compared with their counterparts in Figure 2.16 drawn for the 5%-damping structure. Similarly, Figures 2.34, 2.35 and 2.36, drawn for 2% must be compared with the corresponding Figures 2.20, 2.21 and 2.23 drawn for a 5% damping ratio. Although there are some differences in the relative positions of various curves and numerical values, qualitatively the two sets of results are similar. Comparison of Figures 2.37 and 2.31, plotting the floor response spectra ratios of various floors, shows that there is a larger amplification of the spectral response due to pounding in the 2%-damping structure.

In general, it is observed that a structure with a smaller damping value will invite a higher level of response due to pounding than a structure with higher damping. This conclusion is also attested by the numerical results obtained for a structure with 0% damping, although these results have not been reported here.

2.11 Summary

In this chapter, the effect of pounding of a 10-story structure against a rigid obstruction was examined. A parametric study involving the following structural parameters has been conducted: (1) clearance between the structure and adjacent obstruction, (2) stiffness, mass and frequency of the structure, (3) pounding stiffness coefficient, (4) height of rigid obstruction and (5) damping ratio of the structure. The numerical results for the displacement,

story shear, overturning moment and floor acceleration responses have been obtained. The pounding responses were compared with the no-pounding responses to ascertain the effect of pounding. The main observations of this study are:

1. The pounding causes a severe increase in the shear force in the stories above the pounding stories, with the largest relative increase occurring in the top story. The supporting columns in the higher stories will, therefore, experience a large increase in their bending moments and are likely to be damaged first by pounding.
2. The overturning moment at different story levels and at the base level is also increased significantly. This increase may affect the stability of individual columns of the lower stories and also the entire structure.
3. Pounding causes a large increase in the floor accelerations, especially of the floors involved in pounding. Also floor acceleration response spectrum values are amplified many times in the high frequency range. Thus, the high-frequency equipment supported on the lower floors is most vulnerable to structural pounding.

The conclusions of the parametric study are:

1. The pounding effects are most severe when there is no clearance between the structure and the adjacent obstruction.
2. The stiffness, mass and fundamental frequency of the vibrating structure are important parameters affecting the pounding response. However, no special trend in the response change with respect to these parameters could be identified.
3. For the range of pounding stiffness coefficient values considered in the analysis, the pounding response was not found to be very sensitive.
4. For the 10-story example problem considered herein, the increase in the story shear was observed to be most severe when the adjacent obstruction was about five to six

stories high. The overturning moment at the base increased with the height of the obstruction.

5. The structures with smaller damping are likely to be affected more severely by pounding.

Table 2.1: Natural frequencies and maximum positive displacements of the basic configuration

Frequency No.	Frequency (cps)	Floor No.	Maximum Floor Displacement (m)
1	1.304	1	0.0124
2	3.884	2	0.0243
3	6.377	3	0.0355
4	8.727	4	0.0457
5	10.882	5	0.0545
6	12.795	6	0.0622
7	14.421	7	0.0686
8	15.725	8	0.0738
9	16.678	9	0.0775
10	17.259	10	0.0794

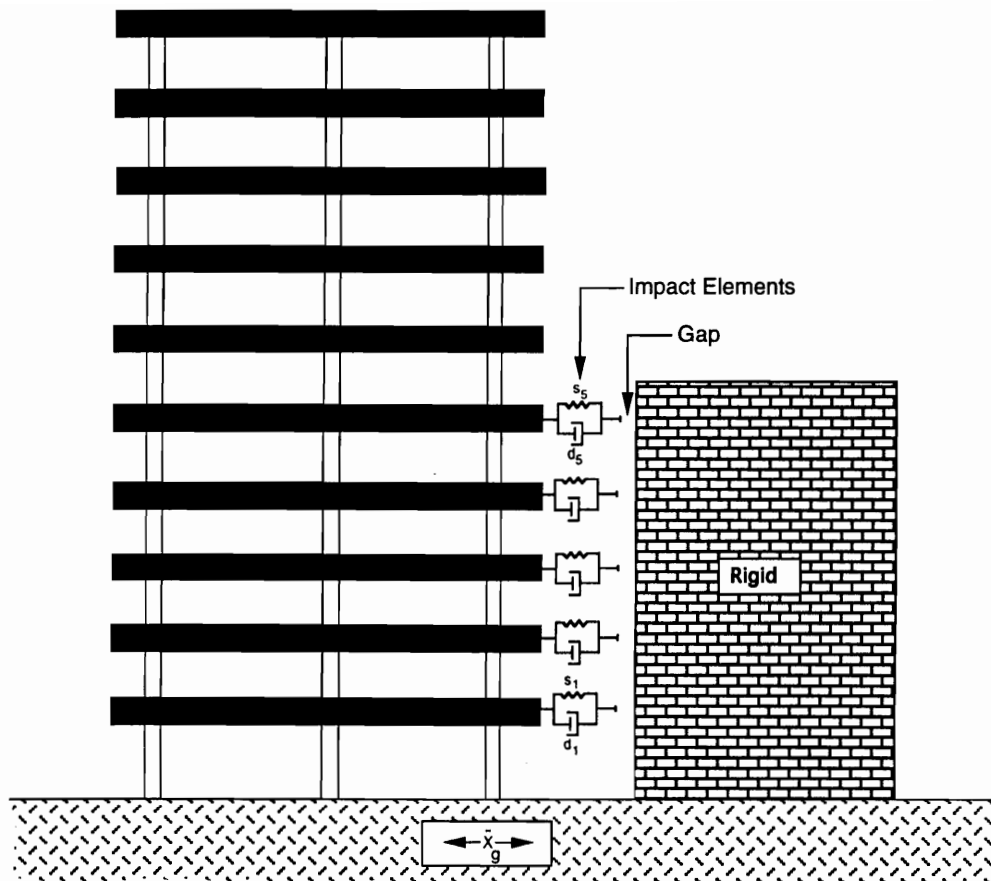


Figure 2.1: Schematic of a 10-story deformable structure pouncing against a 5-story rigid structure

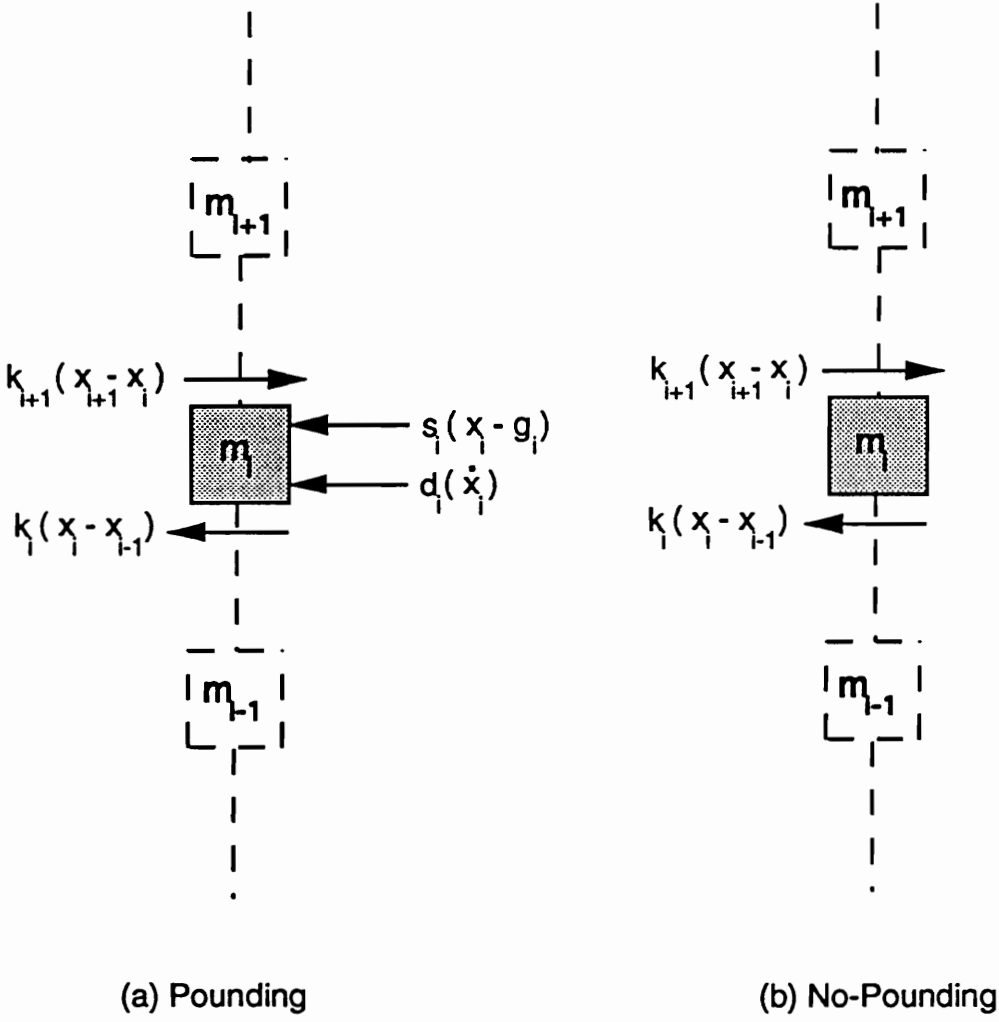


Figure 2.2: Free body diagrams of a typical floor mass in the states of (a) pouncing and (b) no-pouncing

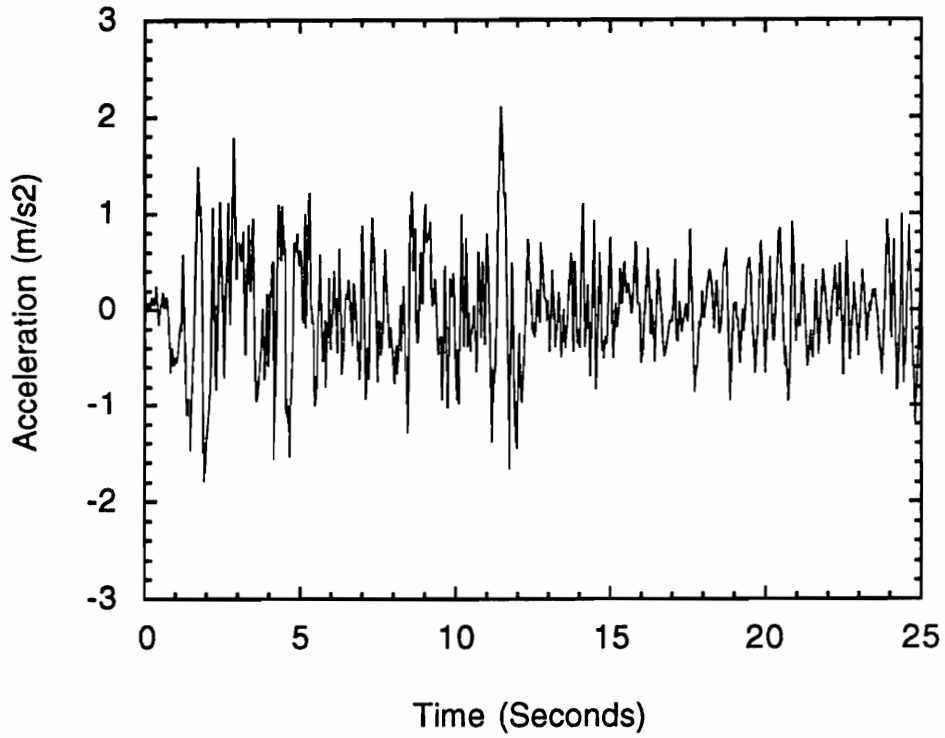
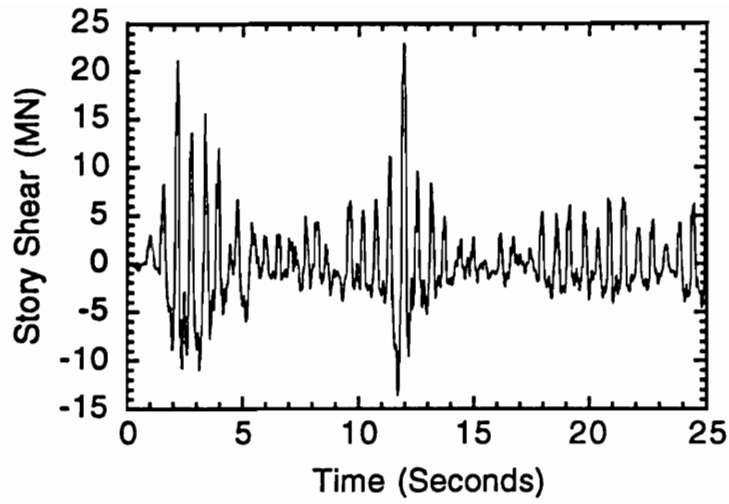
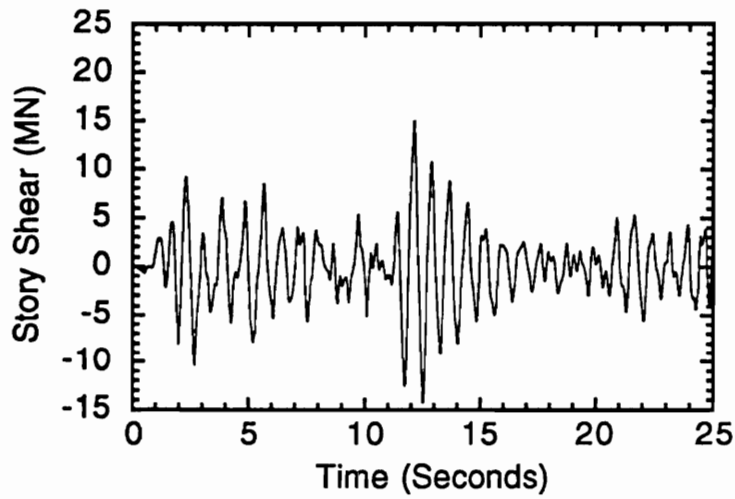


Figure 2.3: Acceleration time history of 1941 N-S El Centro earthquake used as an input in this study

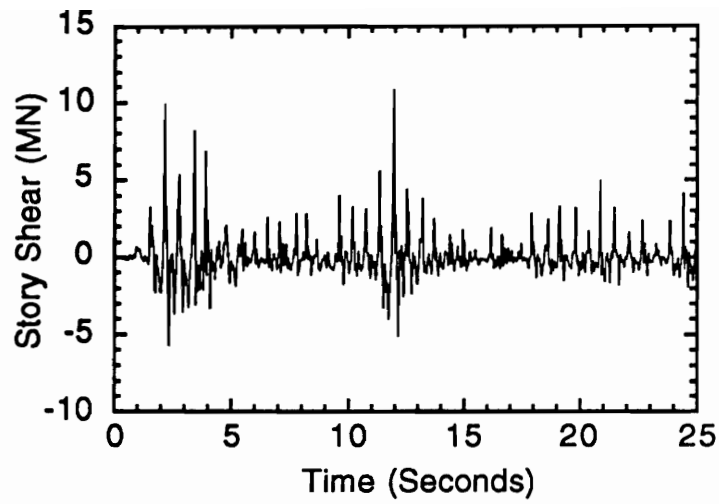


(a) Pounding

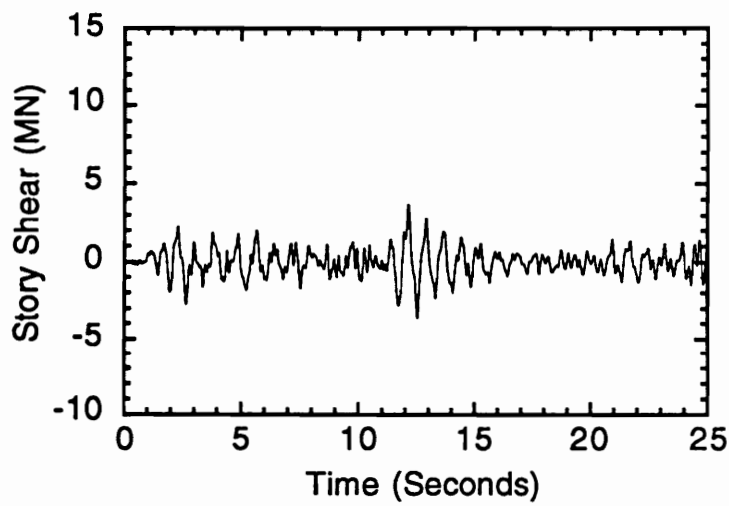


(b) No-Pounding

Figure 2.4: Time history of shear force response in the 6th story for (a) pouncing and (b) no-pounding cases

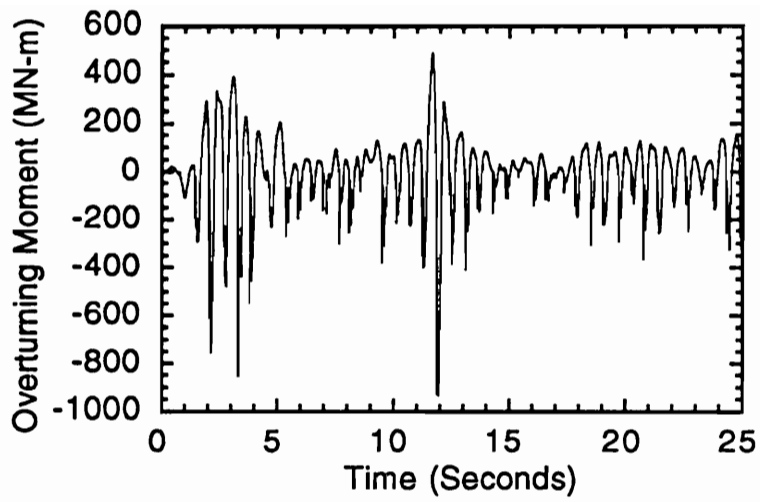


(a) Pounding

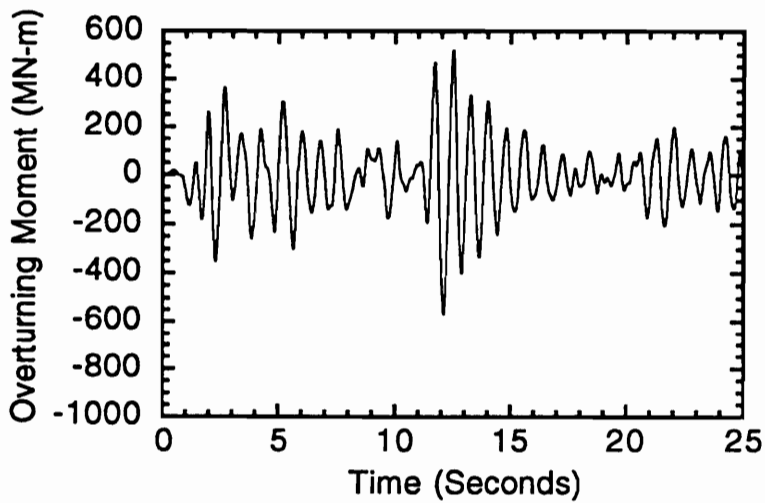


(b) No-Pounding

Figure 2.5: Time history of shear force response in the 10th story for (a) pounding and (b) no-pounding cases

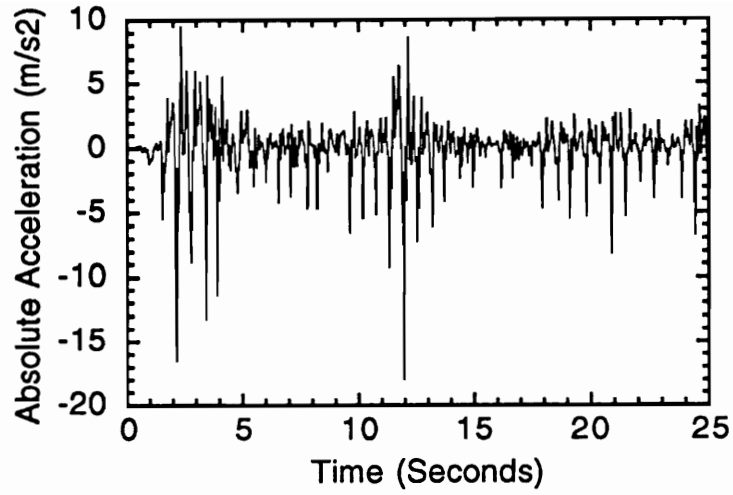


(a) Pounding

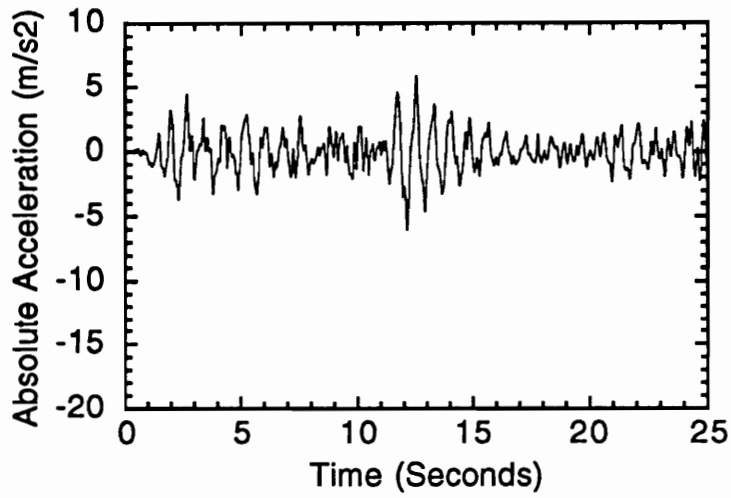


(b) No-Pounding

Figure 2.6: Time history of overturning moment response at the base for (a) pounding and (b) no-pounding cases

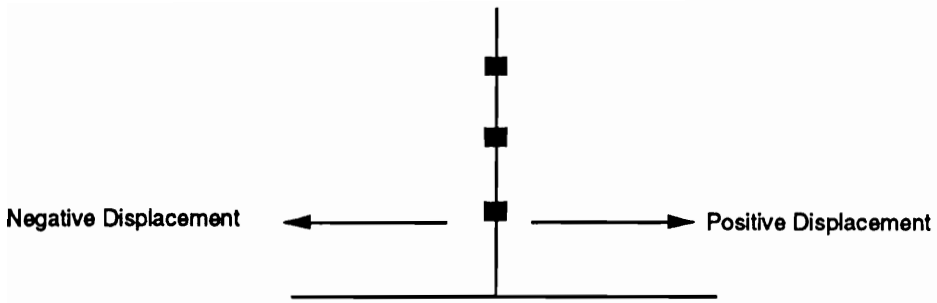


(a) Pounding

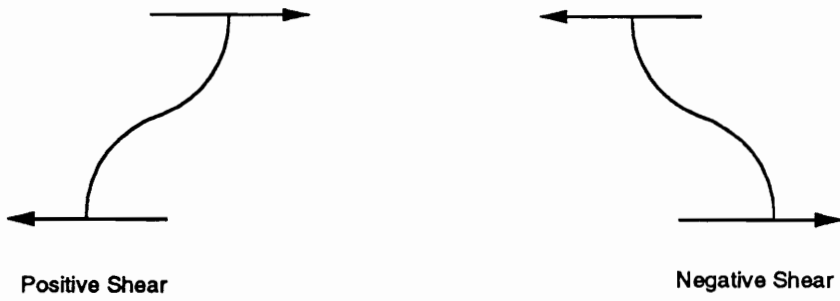


(b) No-Pounding

Figure 2.7: Time history of absolute acceleration at floor 10 for (a) pounding and (b) no-pounding cases



(a) Displacements

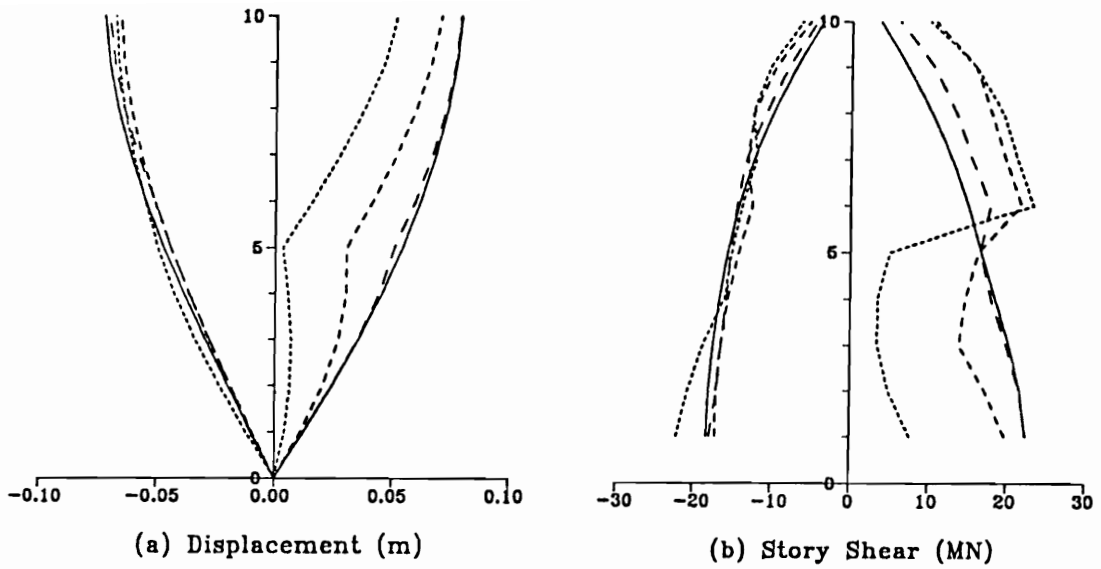


(b) Story Shears



(c) Overturning Moments

Figure 2.8: Conventions for positive and negative response quantities



- - - - $g=0.0$
 - - - - $g=0.0275$ m
 - - - - $g=0.0498$ m
 ———— No Pounding

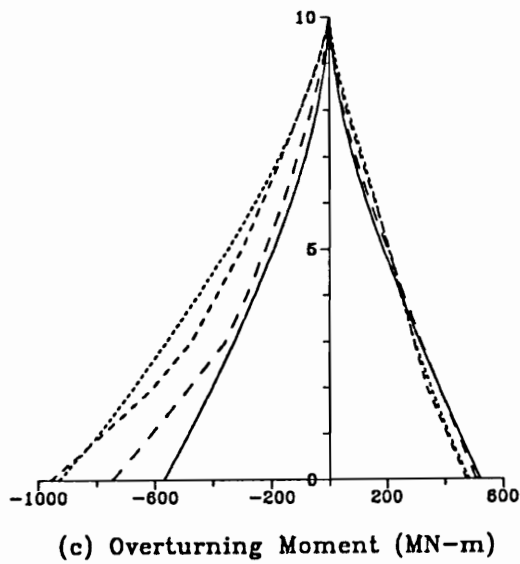
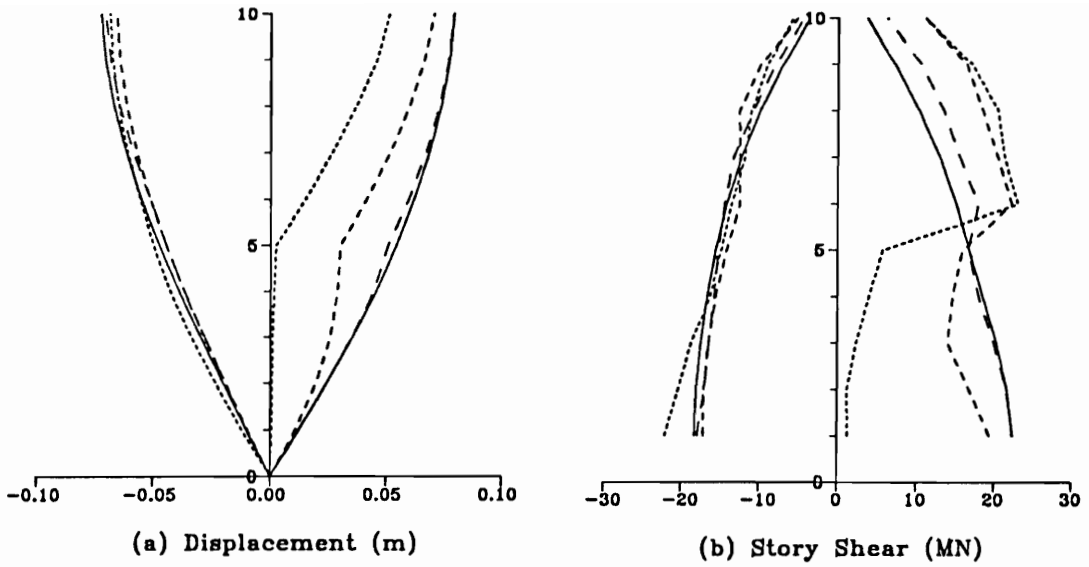


Figure 2.9: Graphs showing the effect of gap size on the maximum displacement, story shear and overturning moment responses at various floor levels of the 10-story structure — single level pounding



- - - - $g=0.0$
 - - - - $g=0.0275$ m
 - - - - $g=0.0498$ m
 ———— No Pounding

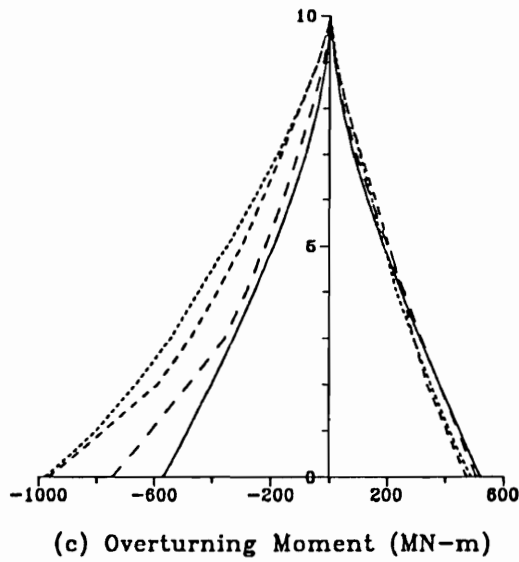
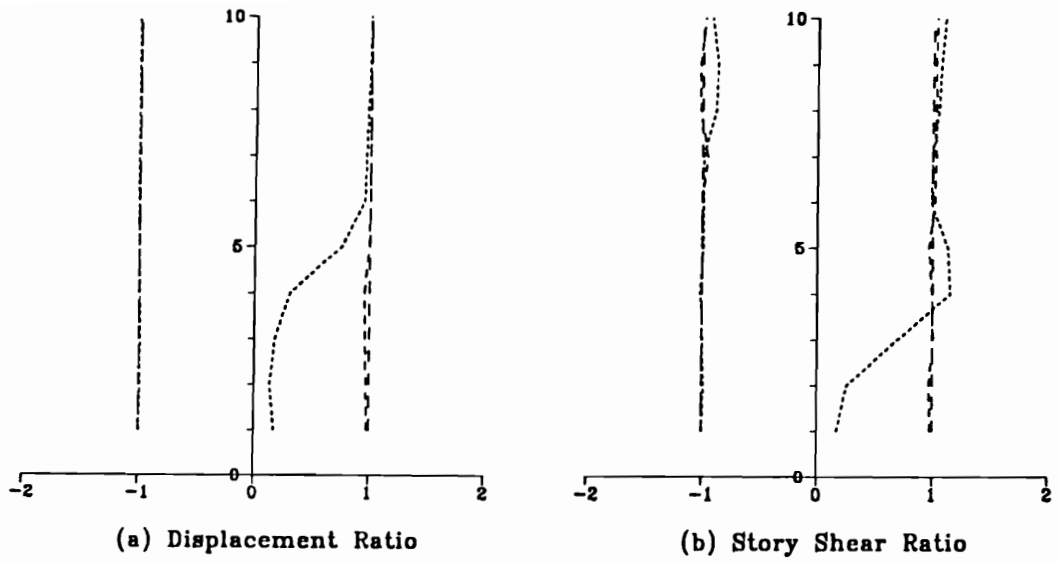


Figure 2.10: Graphs showing the effect of gap size on the maximum displacement, story shear and overturning moment responses at various floor levels of the 10-story structure — multiple level pounding



..... $g=0.0$
 - - - - $g=0.0275$ m
 - - - - $g=0.0496$ m

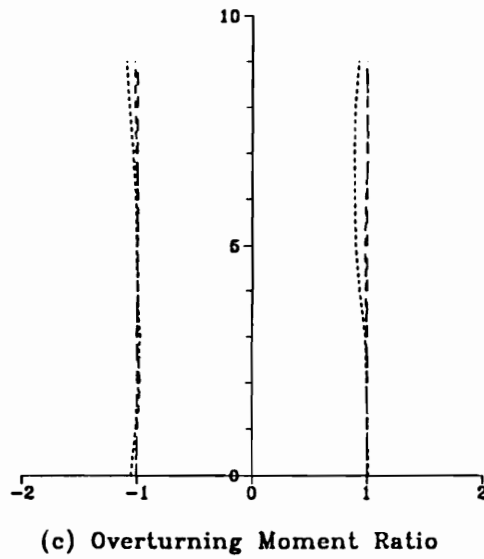
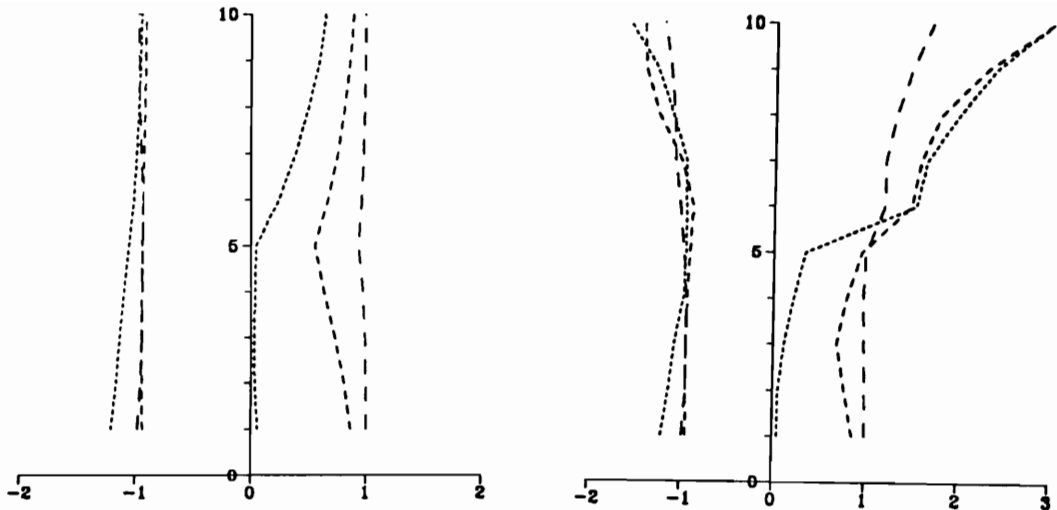


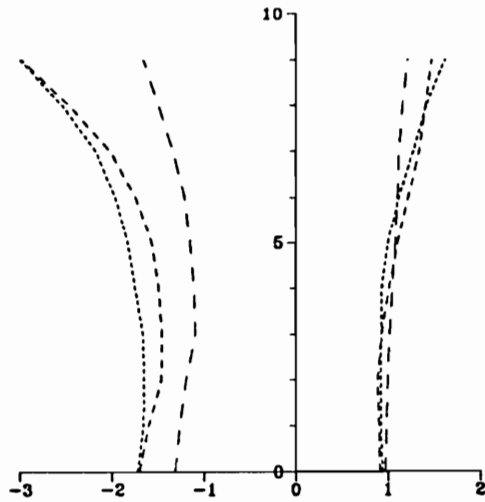
Figure 2.11: Ratio of multiple pounding to single level pounding responses for various gap sizes



(a) Displacement Ratio

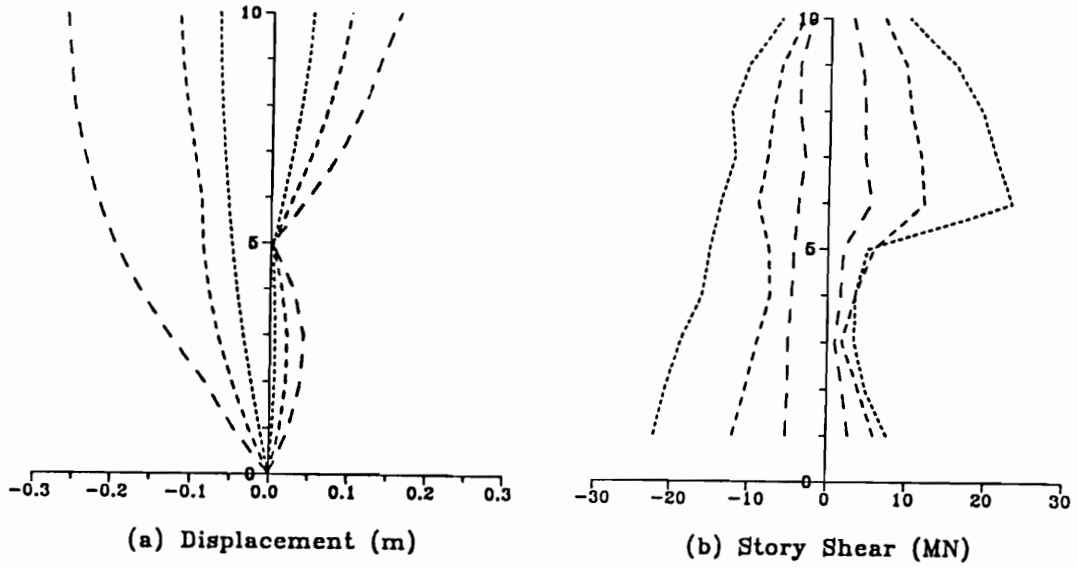
(b) Story Shear Ratio

..... $g=0.0$
 ----- $g=0.0275$ m
 - . - . $g=0.0498$ m



(c) Overturning Moment Ratio

Figure 2.12: Ratio of multiple pounding to no-pounding responses for various gap sizes



..... $k=1.81E+09$ N/m
 - - - $k=4.53E+08$ N/m
 - . - $k=1.13E+08$ N/m

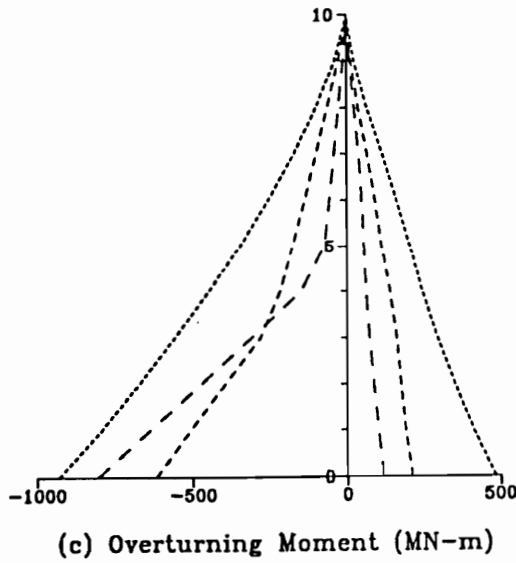


Figure 2.13: Graphs showing the effect of changing the story stiffness on the maximum displacement, story shear and overturning moment responses in the single level pounding case — gap size = 0.0

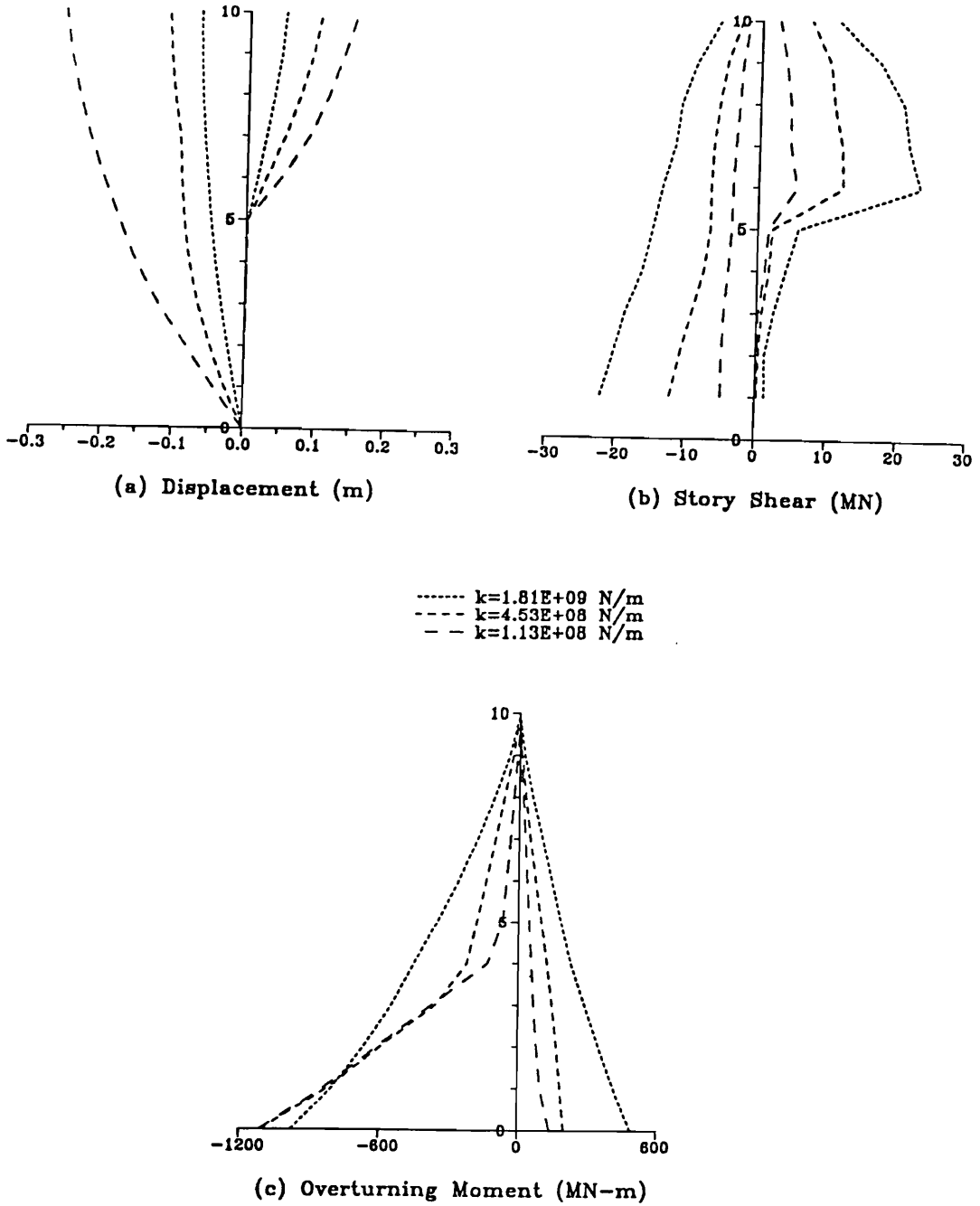
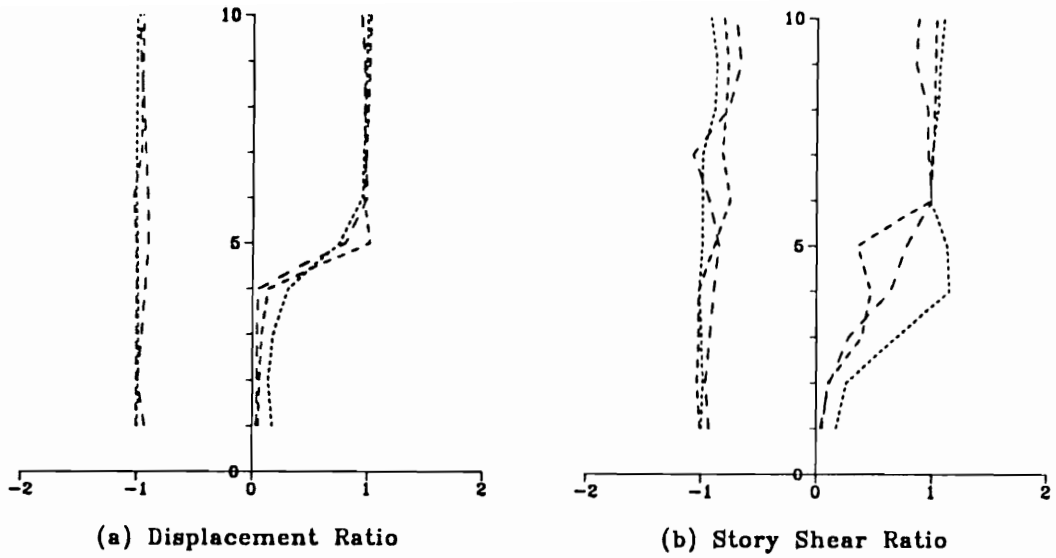


Figure 2.14: Graphs showing the effect of changing the story stiffness on the maximum displacement, story shear and overturning moment responses in the multiple pounding case — gap size = 0.0



..... $k=1.81E+09$ N/m
 - - - - $k=4.53E+08$ N/m
 - · - · $k=1.13E+08$ N/m

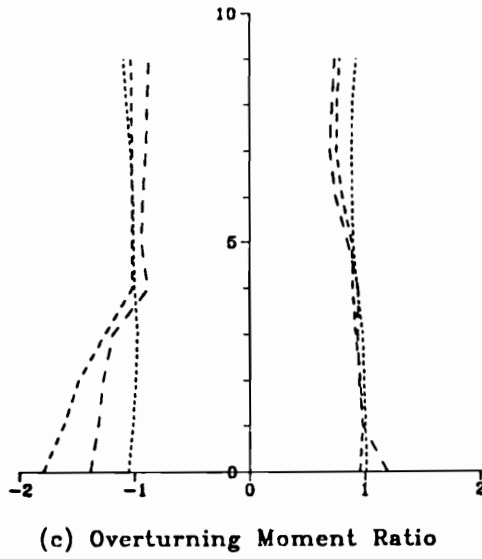
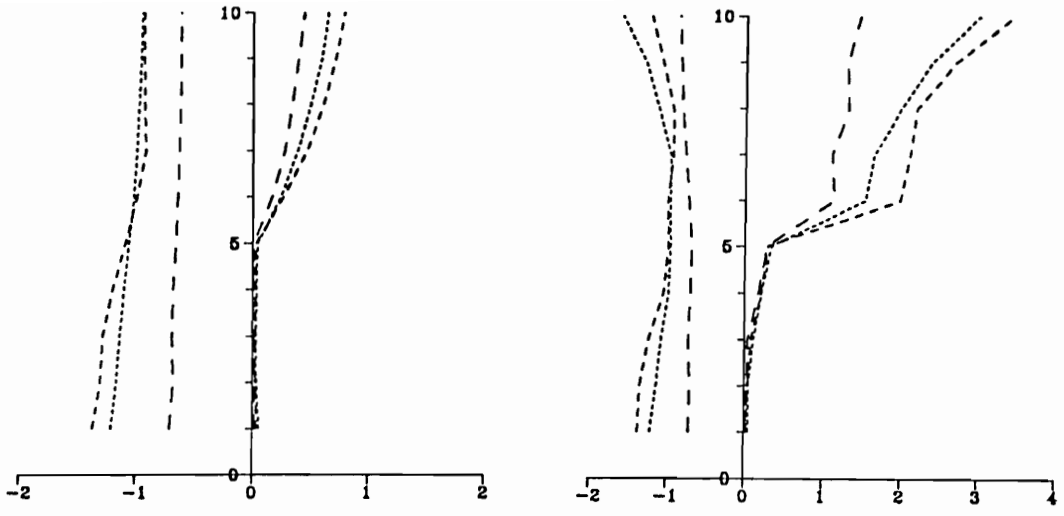


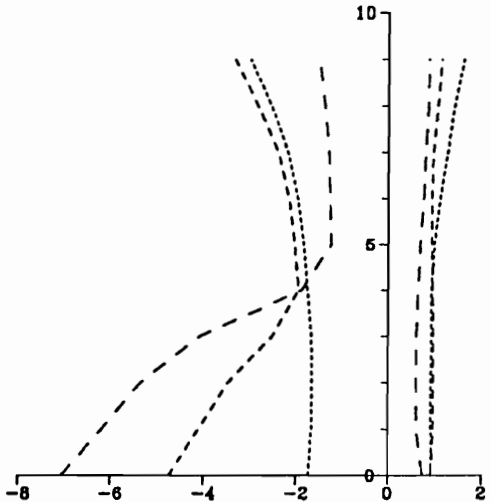
Figure 2.15: Ratio of multiple pounding to single level pounding responses for various story stiffnesses



(a) Displacement Ratio

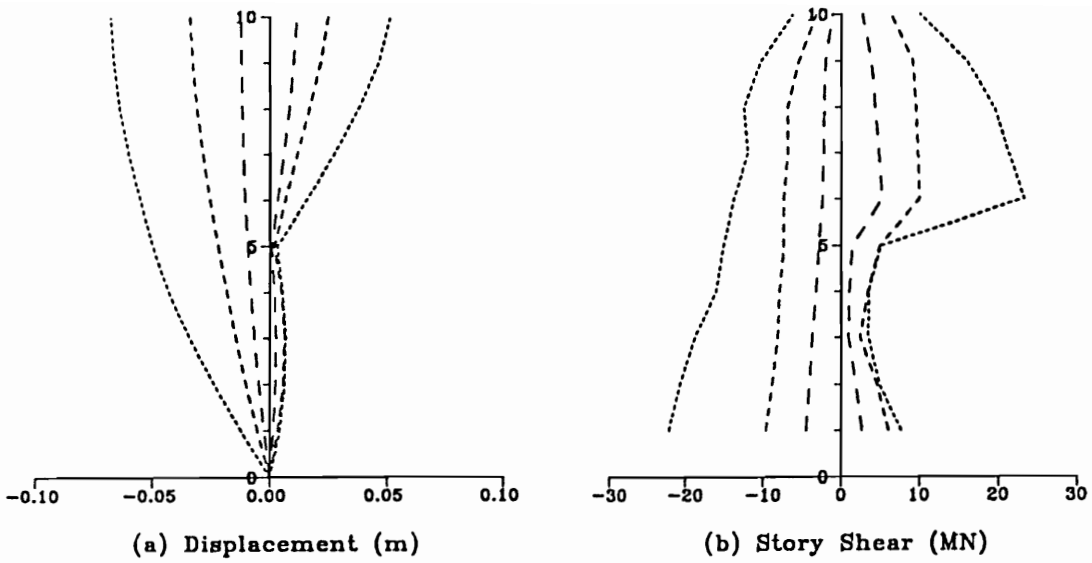
(b) Story Shear Ratio

..... $k=1.81E+09$ N/m
 - - - - $k=4.53E+08$ N/m
 - · - · $k=1.13E+08$ N/m



(c) overturning moment ratio

Figure 2.16: Ratio of multiple pounding to no-pounding responses for various story stiffnesses



..... $m=8.02E+05$ Kg
 - - - - $m=3.01E+05$ Kg
 - - - - $m=1.51E+05$ Kg

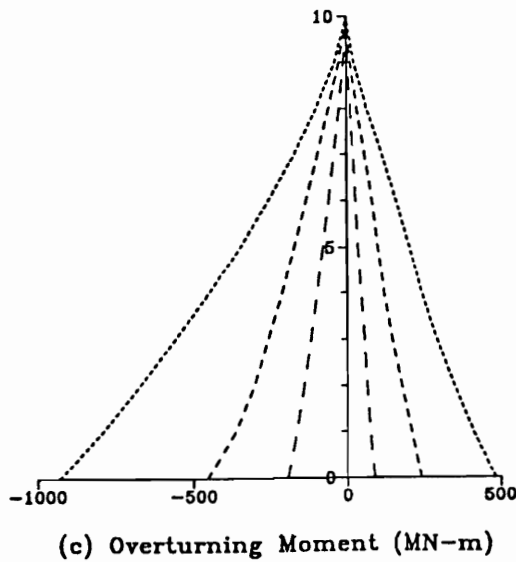


Figure 2.17: Graphs showing the effect of changing the floor mass on the maximum displacement, story shear and overturning moment responses — single level pounding case, gap size = 0.0

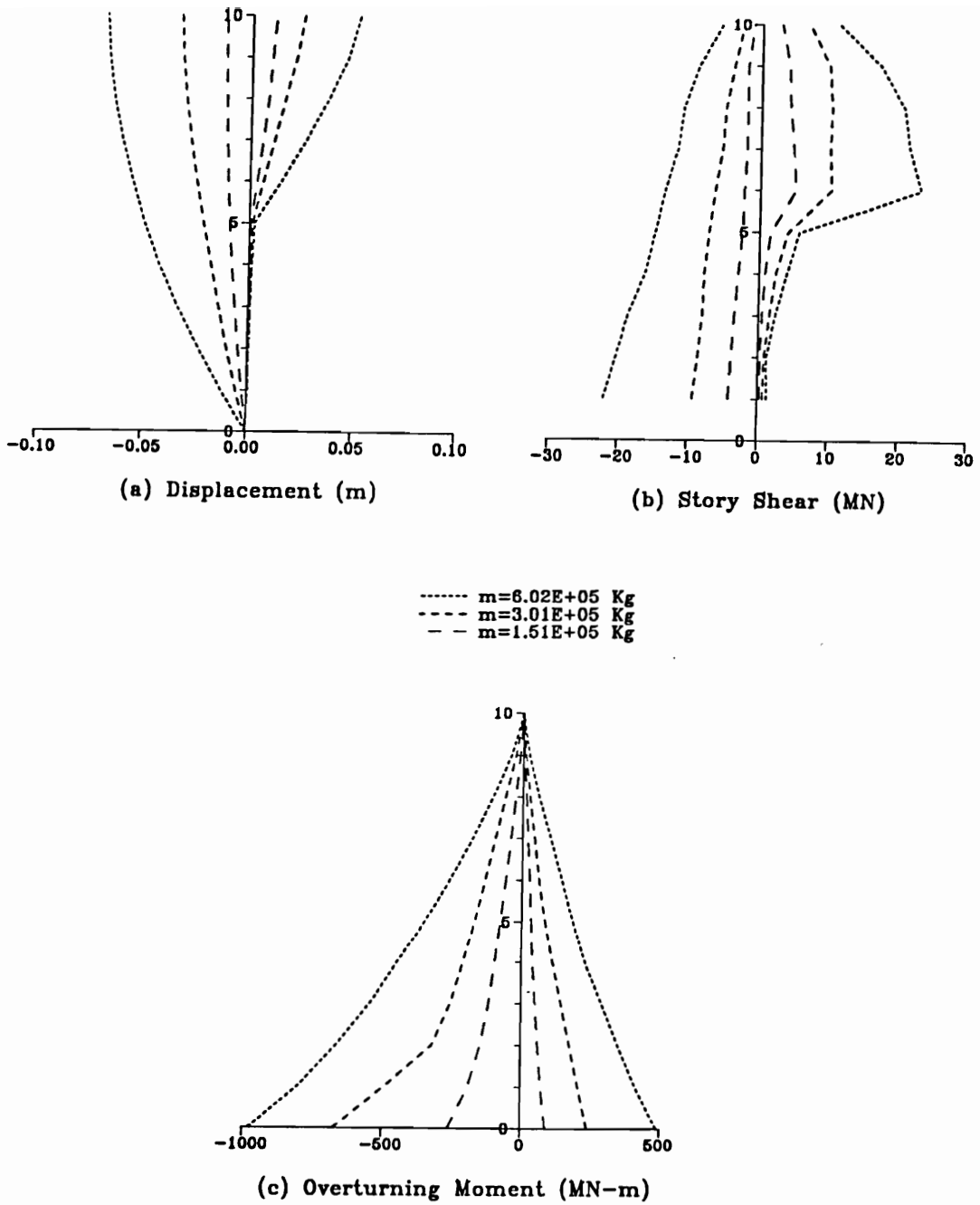
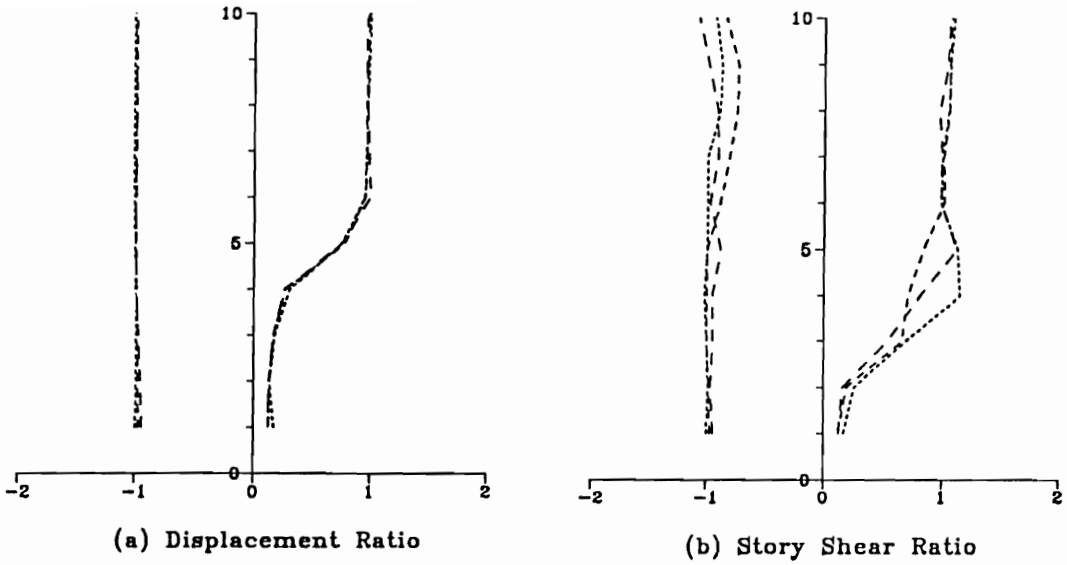


Figure 2.18: Graphs showing the effect of changing the floor mass on the maximum displacement, story shear and overturning moment responses — multiple pounding case, gap size = 0.0



..... $m=6.02E+05$ Kg
 ----- $m=3.01E+05$ Kg
 - . - . - $m=1.51E+06$ Kg

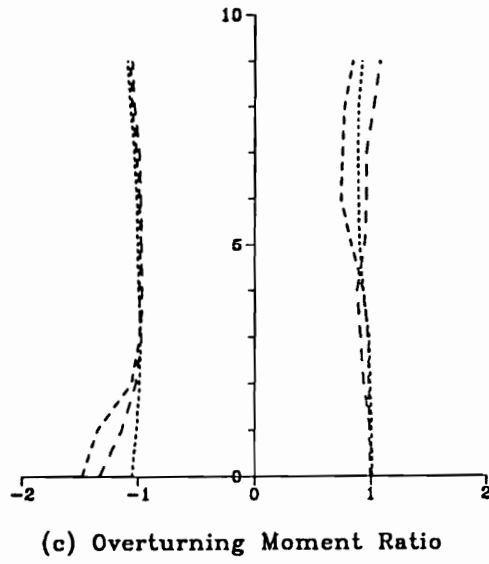
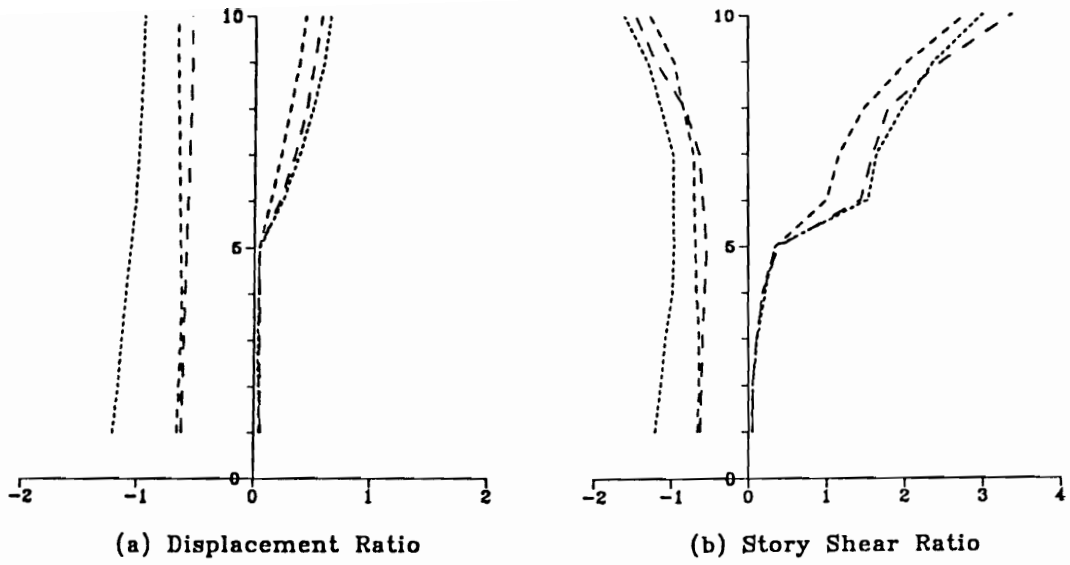


Figure 2.19: Ratio of multiple pounding to single level pounding responses for various floor masses



..... $m=6.02E+05$ Kg
 ----- $m=3.01E+05$ Kg
 - . - . $m=1.51E+05$ Kg

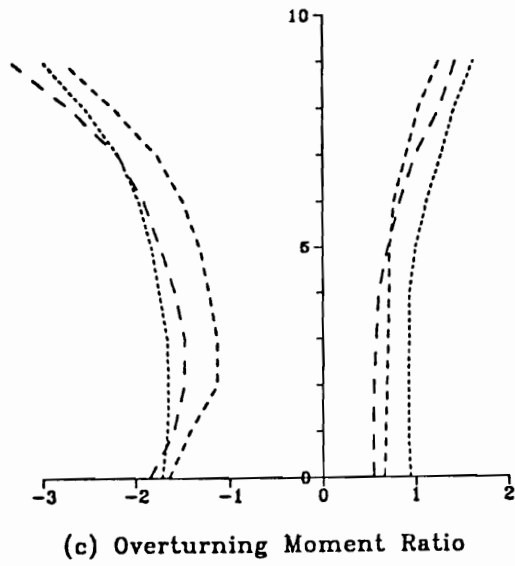
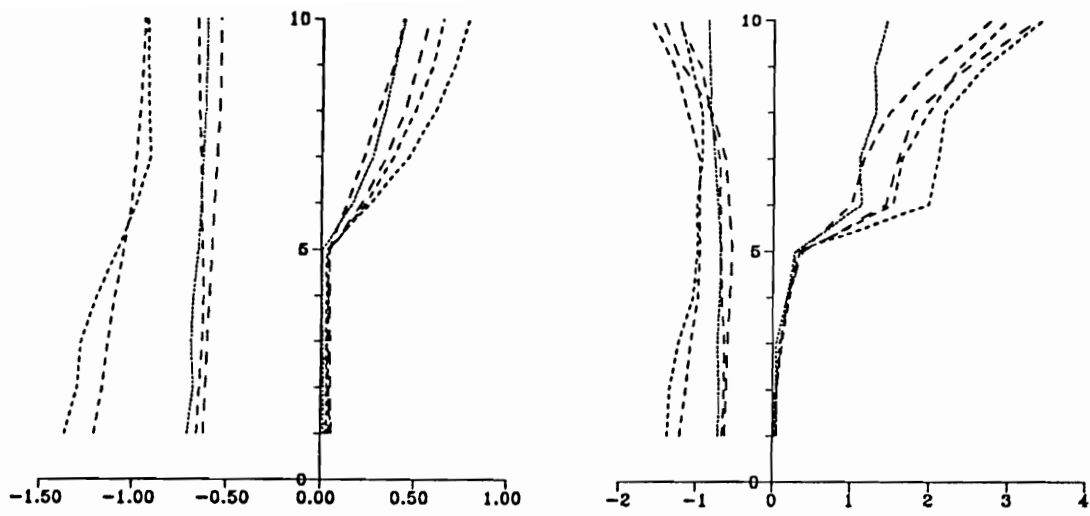


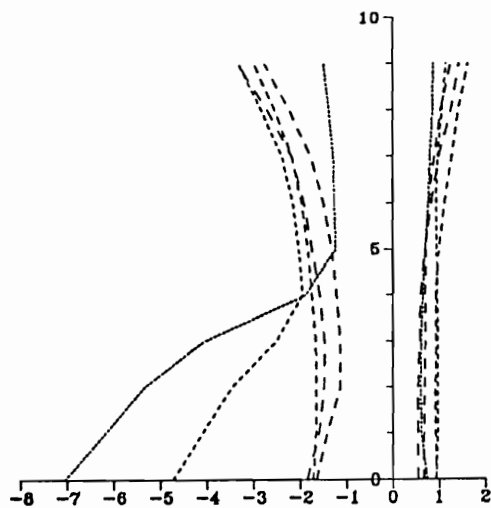
Figure 2.20: Ratio of multiple pounding to no-pounding responses for various floor masses



(a) Displacement Ratio

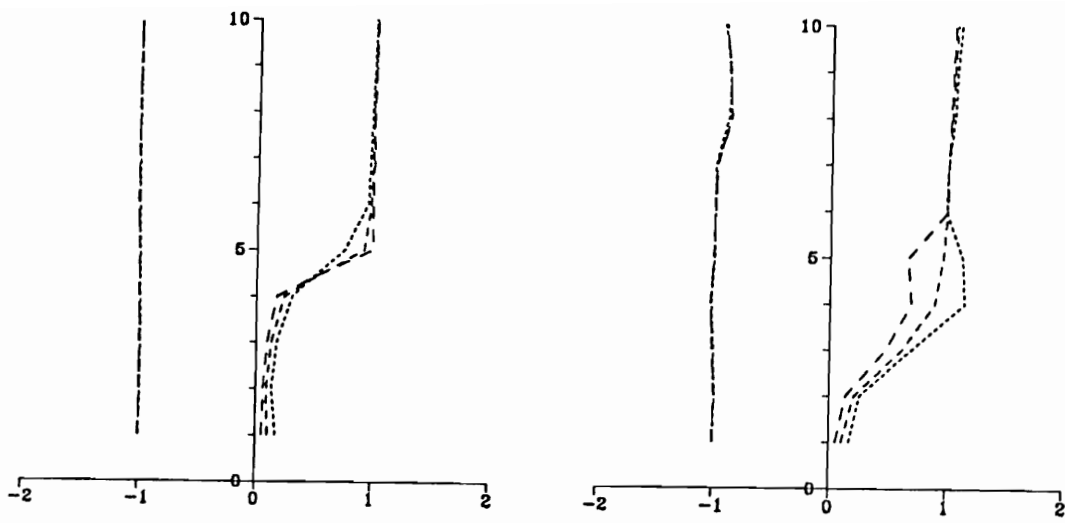
(b) Story Shear Ratio

— $f=0.326$ cps
 - - - $f=0.653$ cps
 - - - $f=1.304$ cps
 - - - $f=1.845$ cps
 - - - $f=2.604$ cps



(c) Overturning Moment Ratio

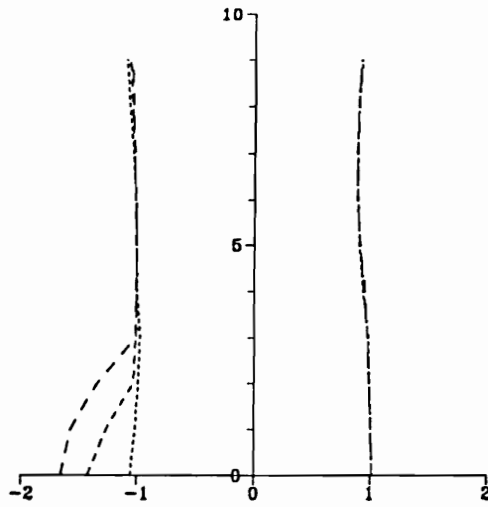
Figure 2.21: Graphs showing the effect of fundamental frequency of the structure on the multiple pounding to no-pounding responses



(a) Displacement Ratio

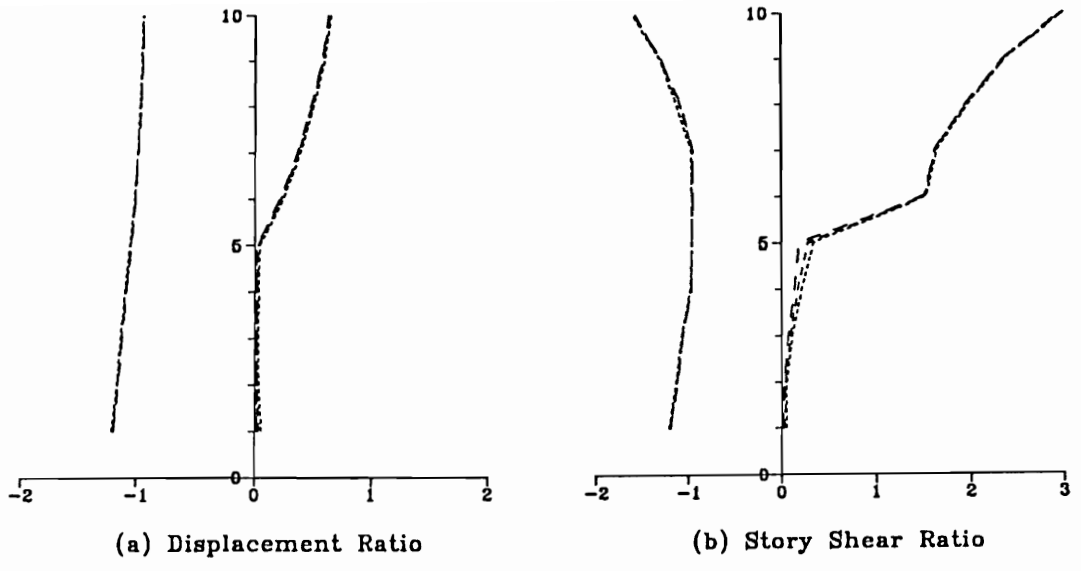
(b) Story Shear Ratio

..... $\alpha = 8.76 \times 10^9$ N/m
 ----- $\alpha = 1.75 \times 10^{10}$ N/m
 - . - . $\alpha = 3.50 \times 10^{10}$ N/m



(c) Overturning Moment Ratio

Figure 2.22: Graphs showing the effect of the impact stiffness coefficient on the ratio of multiple pounding to single level pounding responses



..... $s=8.76E+09$ N/m
 - - - $s=1.75E+10$ N/m
 - - - $s=3.50E+10$ N/m

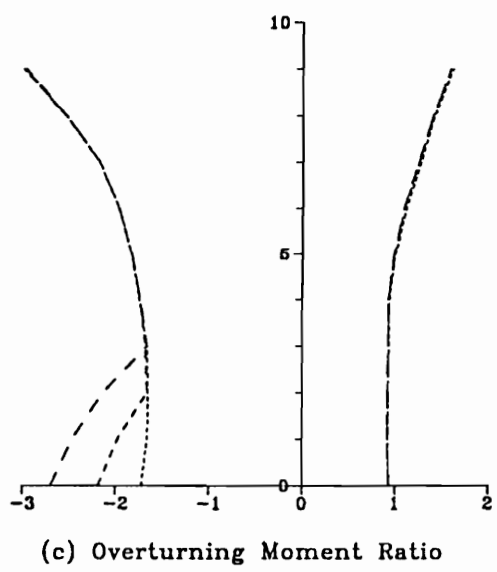
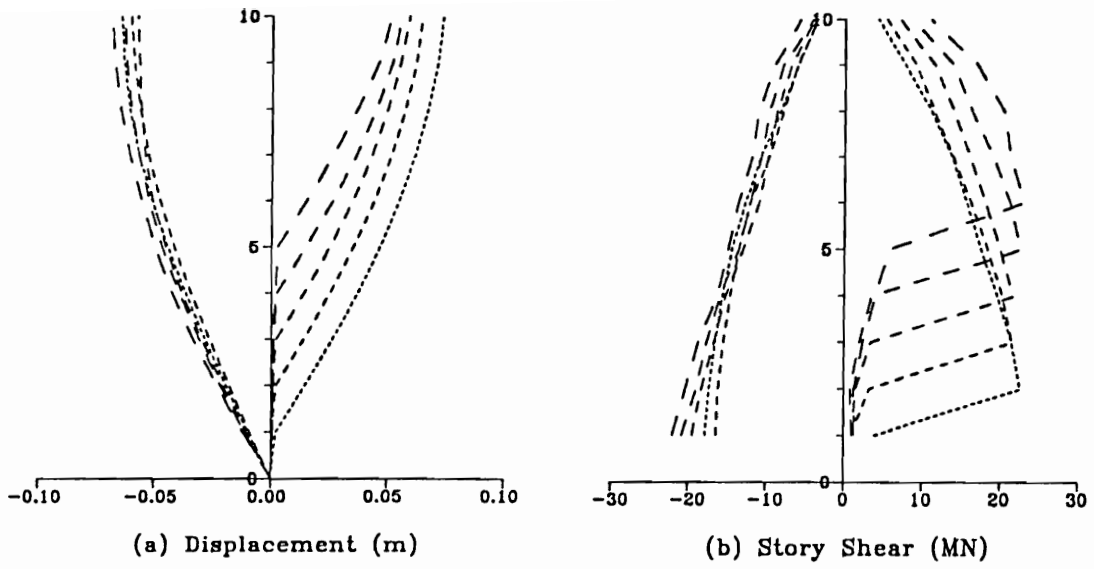


Figure 2.23: Graphs showing the effect of impact stiffness coefficient on the ratio of multiple pounding to no-pounding responses



- 1 LEVEL POUNDING
- 2 LEVELS POUNDING
- 3 LEVELS POUNDING
- 4 LEVELS POUNDING
- 5 LEVELS POUNDING

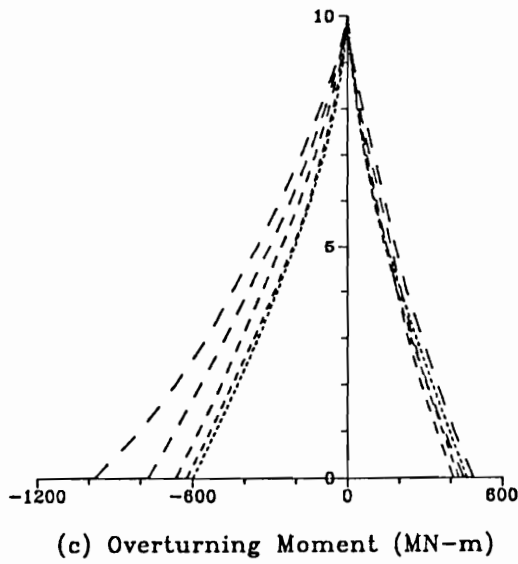
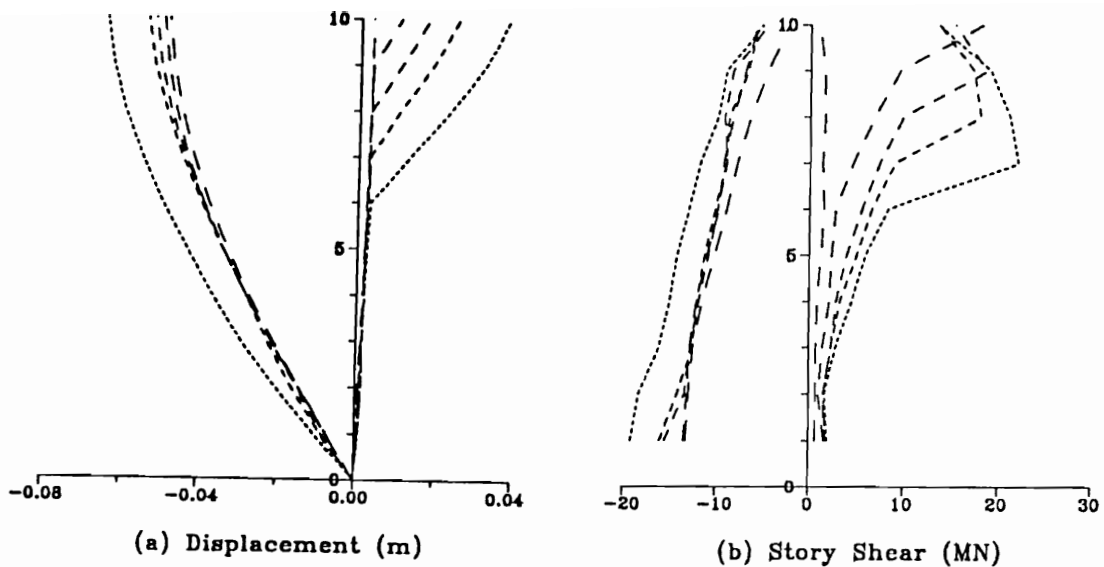


Figure 2.24: Graphs showing the effect of the height of the rigid structure on the multiple pounding responses - (rigid structure heights 1, 2, 3, 4 and 5 stories)



----- 6 LEVELS POUNDING
 - - - - - 7 LEVELS POUNDING
 - - - - - 8 LEVELS POUNDING
 - - - - - 9 LEVELS POUNDING
 - - - - - 10 LEVELS POUNDING

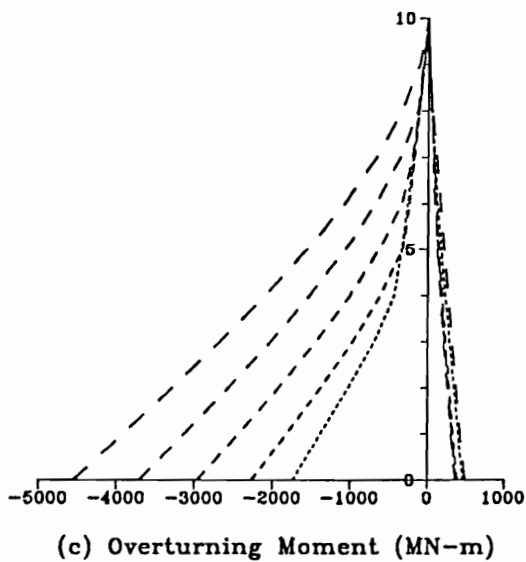
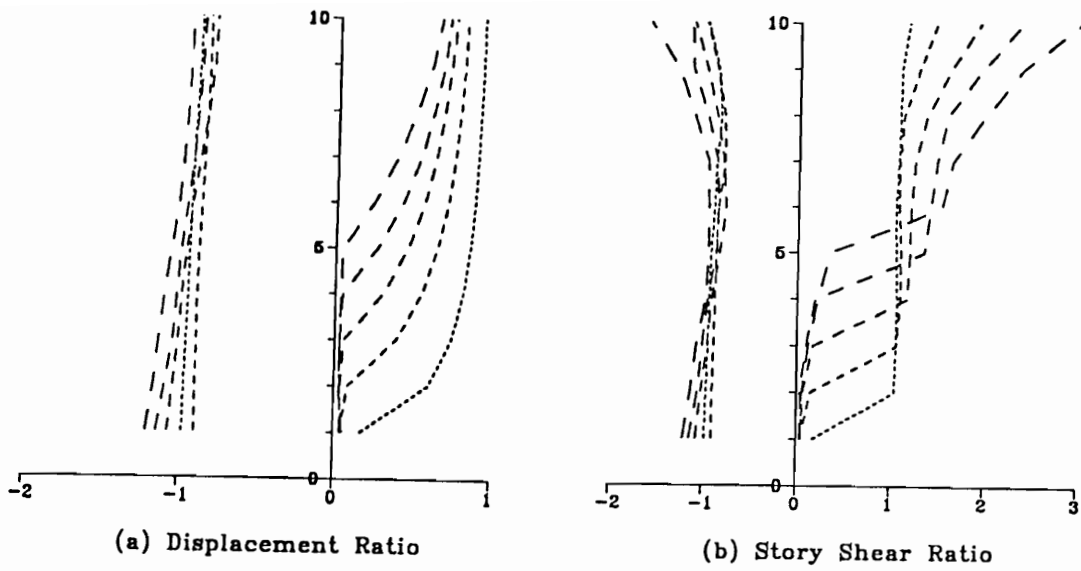


Figure 2.25: Graphs showing the effect of the height of the rigid structure on the multiple pounding responses - (rigid structure heights 6, 7, 8, 9 and 10 stories)



- 1 LEVEL POUNDING
- - - - 2 LEVELS POUNDING
- - - - 3 LEVELS POUNDING
- - - - 4 LEVELS POUNDING
- - - - 5 LEVELS POUNDING

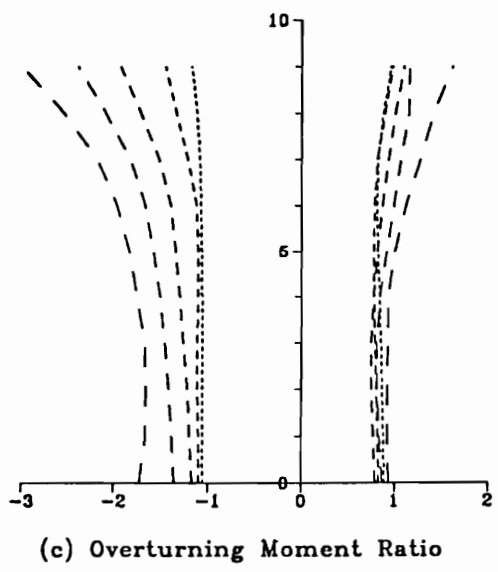
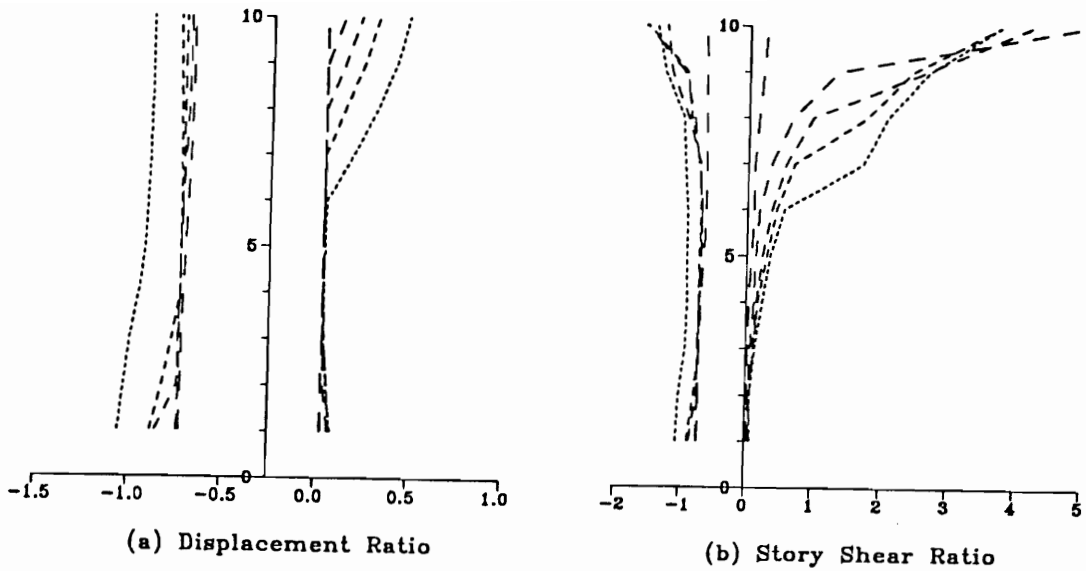


Figure 2.26: Graphs showing the effect of the height of the rigid structure on the ratio of multiple pounding to no-pounding responses - (rigid structure heights 1, 2, 3, 4 and 5 stories)



- - - - 6 LEVELS POUNDING
 - - - - 7 LEVELS POUNDING
 - - - - 8 LEVELS POUNDING
 - - - - 9 LEVELS POUNDING
 - - - - 10 LEVELS POUNDING

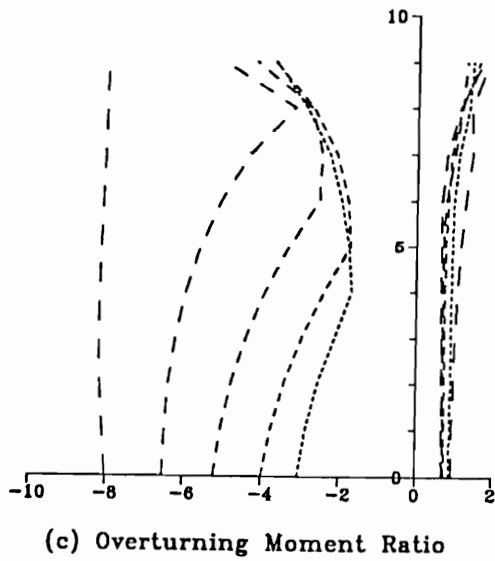


Figure 2.27: Graphs showing the effect of the height of the rigid structure on the ratio of multiple pounding to no-pounding responses - (rigid structure heights 6, 7, 8, 9 and 10 stories)

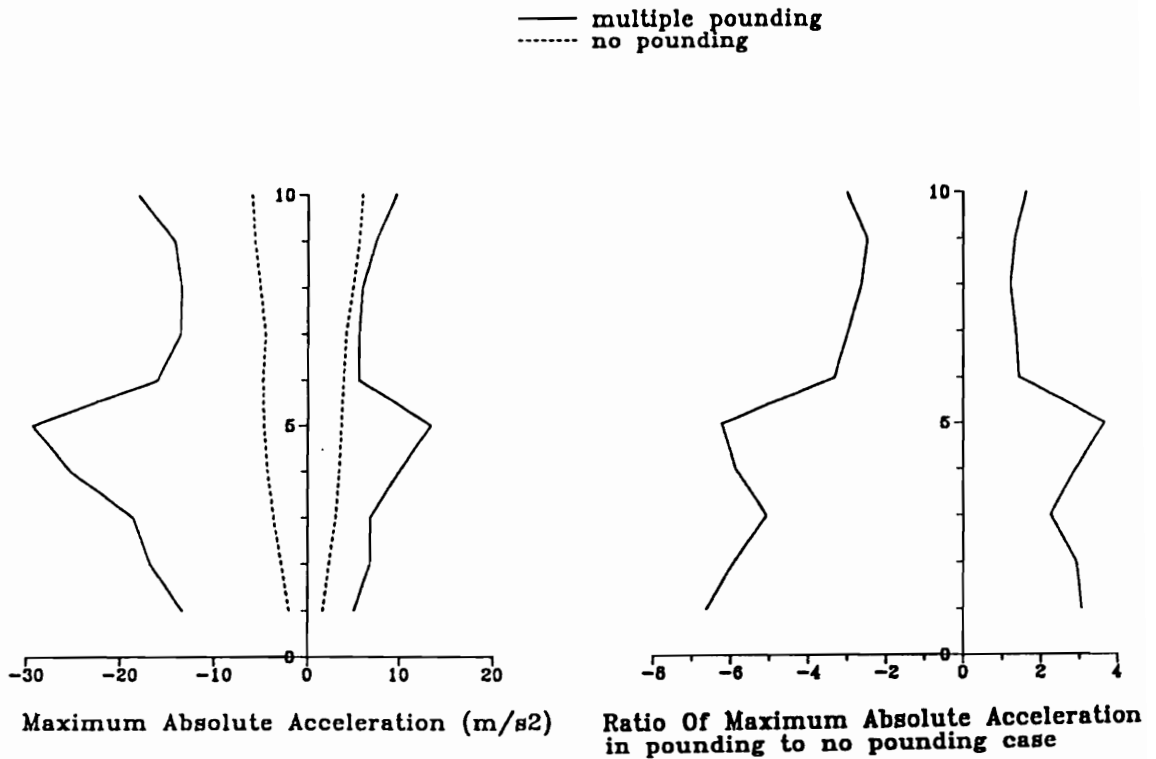


Figure 2.28: Absolute acceleration and acceleration response ratio at various floor levels in multiple pounding case against a 5-story rigid structure

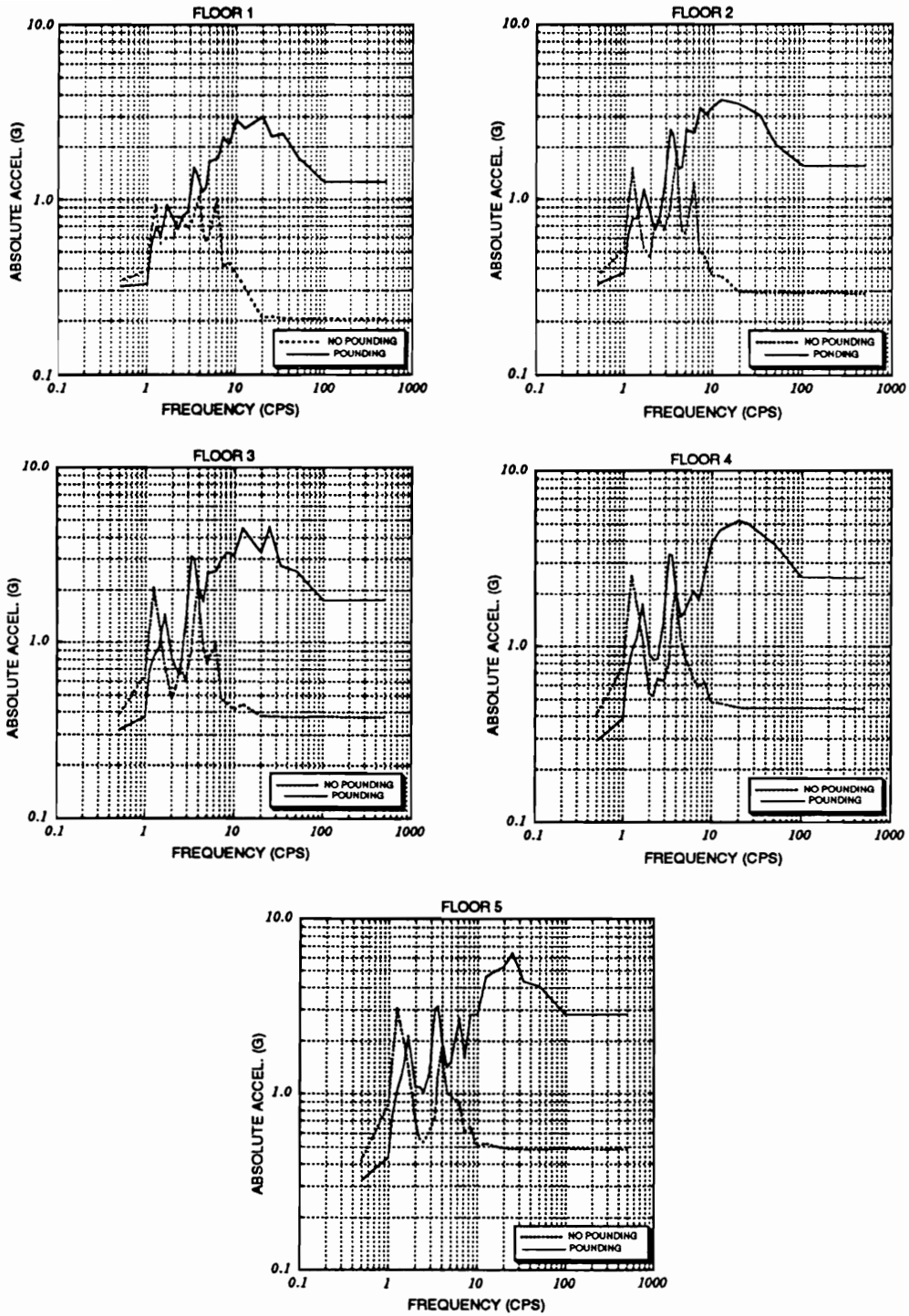


Figure 2.29: Floor acceleration response spectra of various floors in pounding and no-pounding cases - (multiple pounding against 5-story rigid structure)

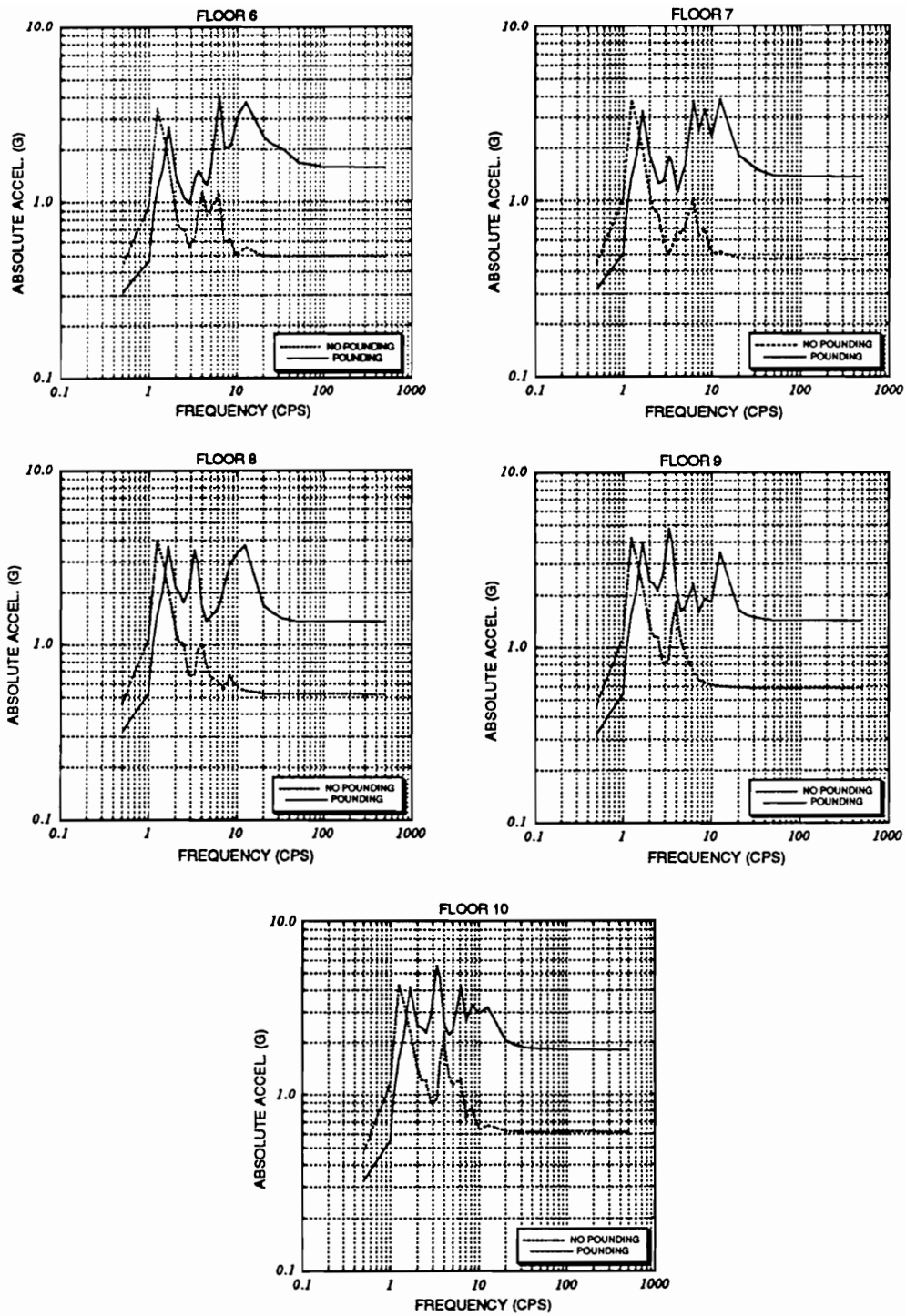


Figure 2.30: Floor acceleration response spectra of various floors in pounding and no-pounding cases - (multiple pounding against 5-story rigid structure)

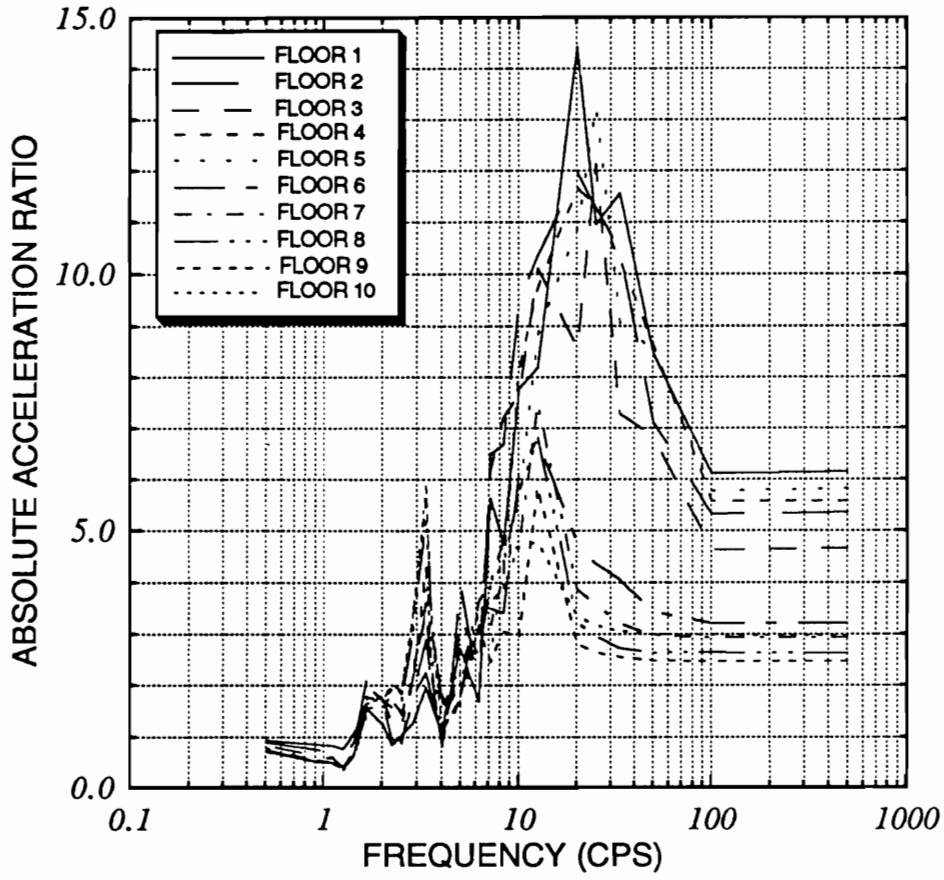
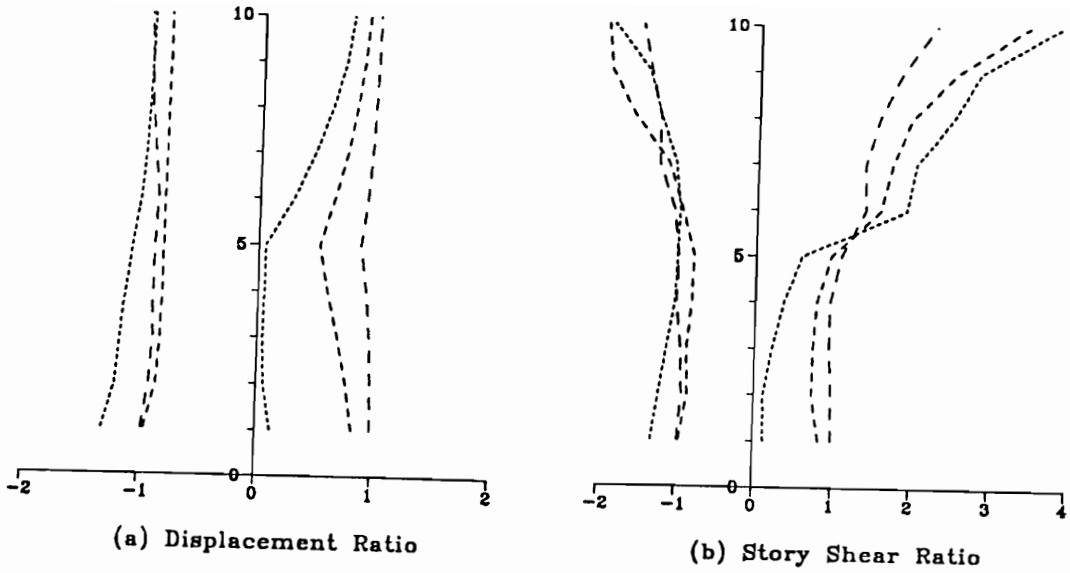


Figure 2.31: Pounding to no-pounding floor response spectrum ratios (multiple pounding against 5-story structure)



..... $g=0.0$
 - - - - $g=0.0275$ m
 - - - - $g=0.0496$ m

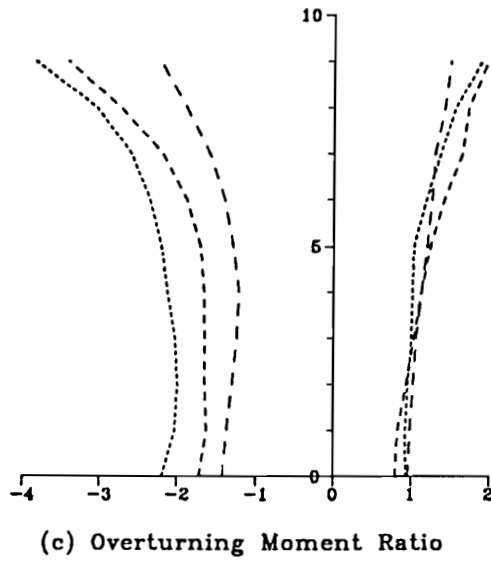
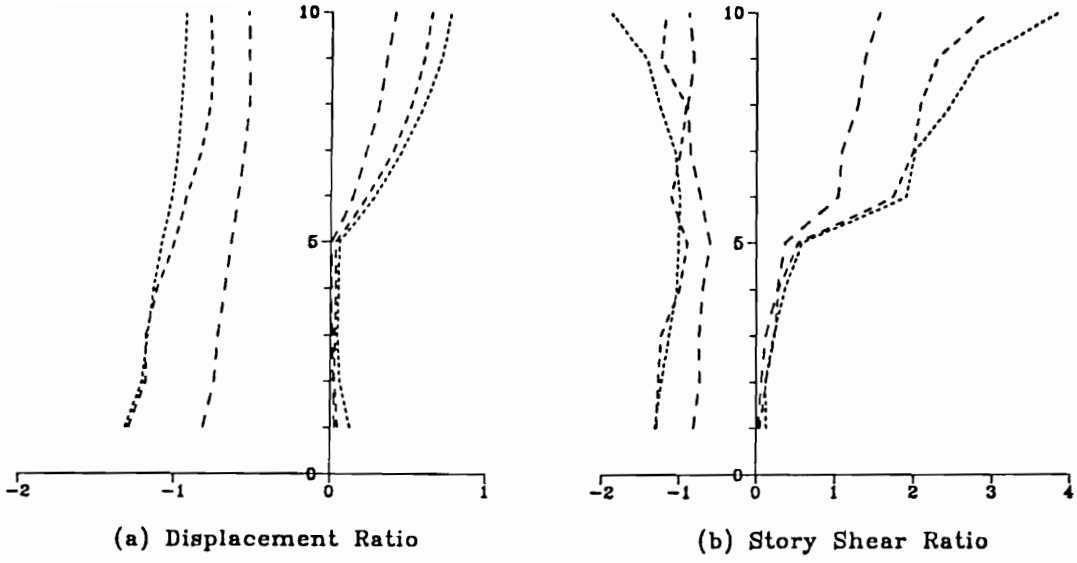


Figure 2.32: Ratio of multiple pounding to no-pounding responses for various gap sizes (2% structural damping)



..... $k=1.81E+09$ N/m
 ----- $k=4.53E+08$ N/m
 - · - · - $k=1.13E+08$ N/m

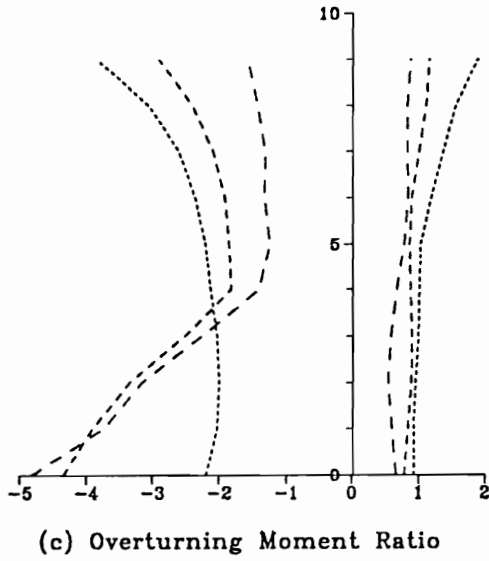
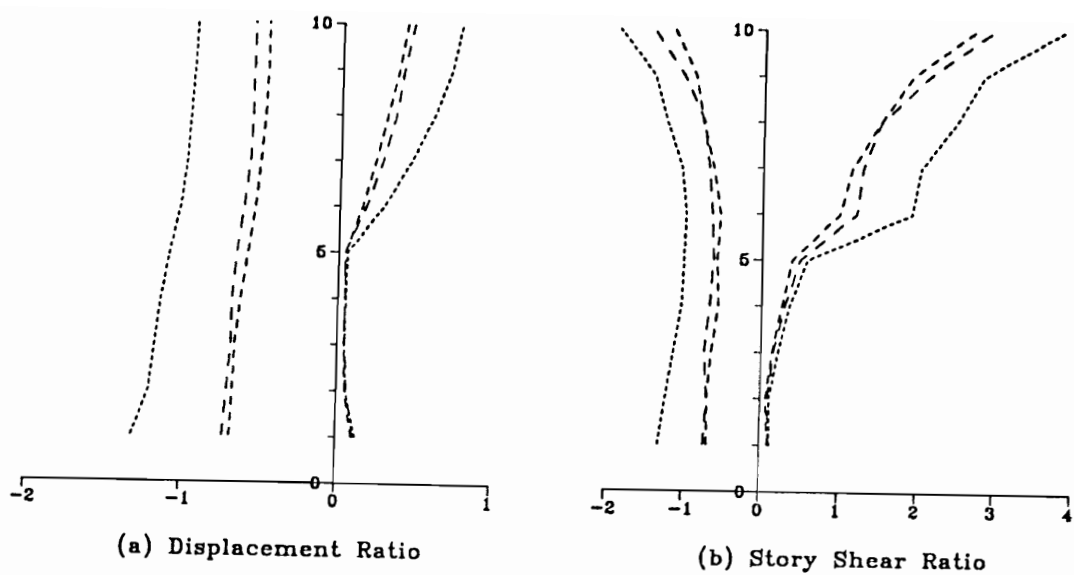


Figure 2.33: Ratio of multiple pounding to no-pounding responses for various story stiffnesses (2% structural damping)



..... $m=6.02E+05$ Kg
 - - - - $m=3.01E+05$ Kg
 - · - · $m=1.51E+05$ Kg

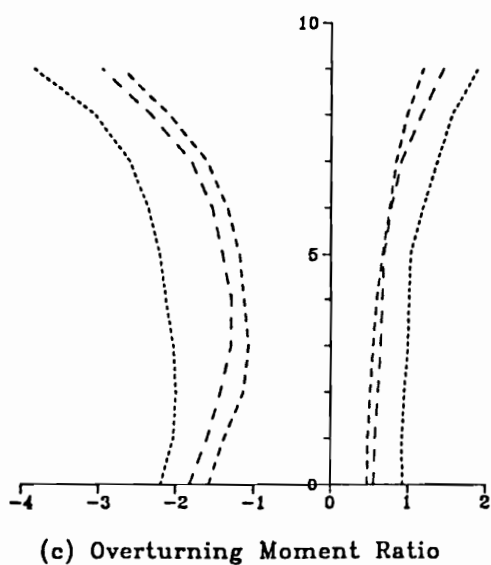


Figure 2.34: Ratio of multiple pounding to no-pounding responses for various floor masses (2% structural damping)

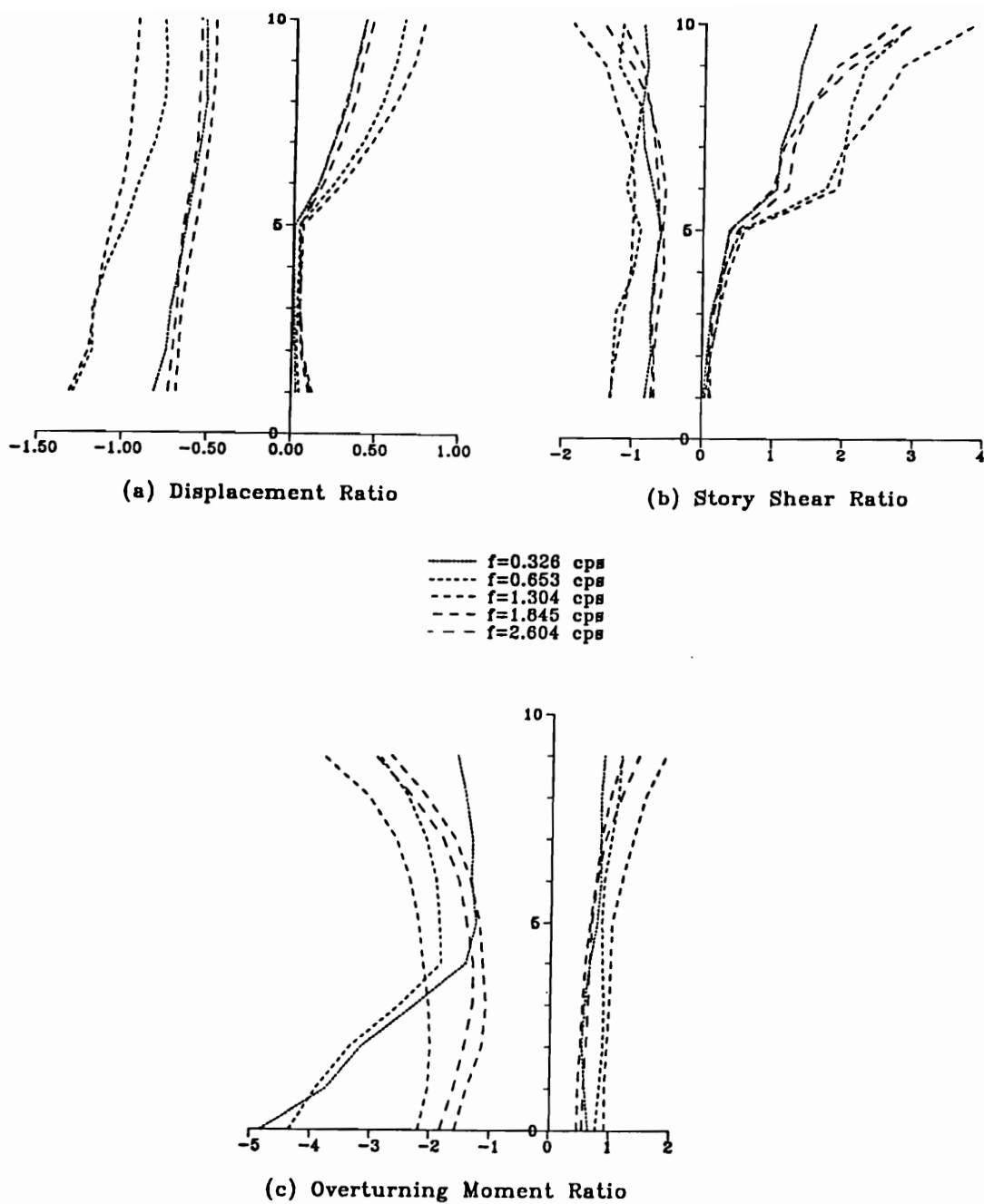
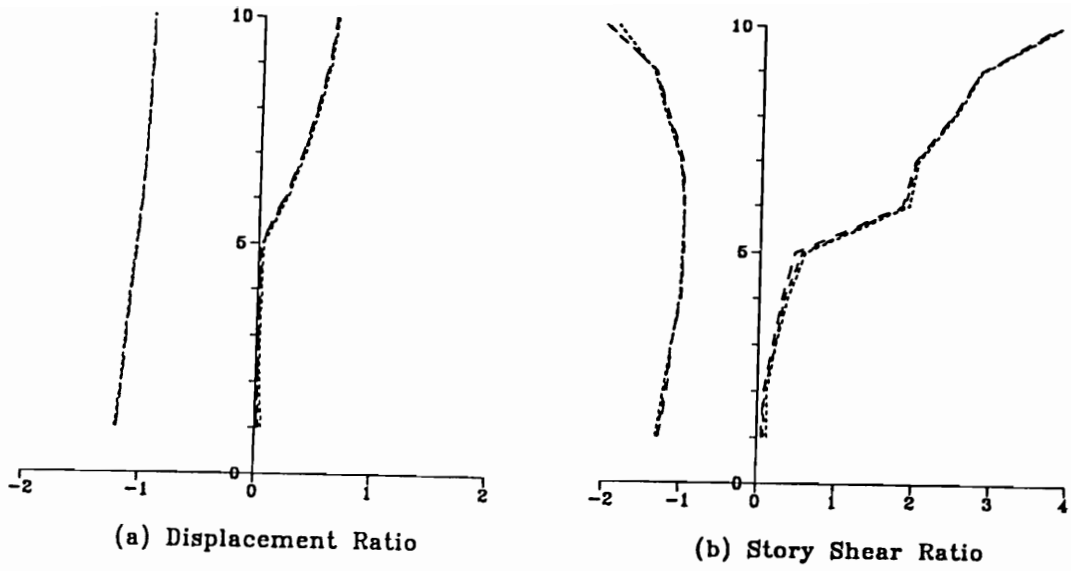


Figure 2.35: Graphs showing the effect of fundamental frequency of the structure on the multiple pounding to no-pounding responses (2% structural damping)



..... $s=8.76E+09$ N/m
 - - - - $s=1.75E+10$ N/m
 - - - - $s=3.50E+10$ N/m

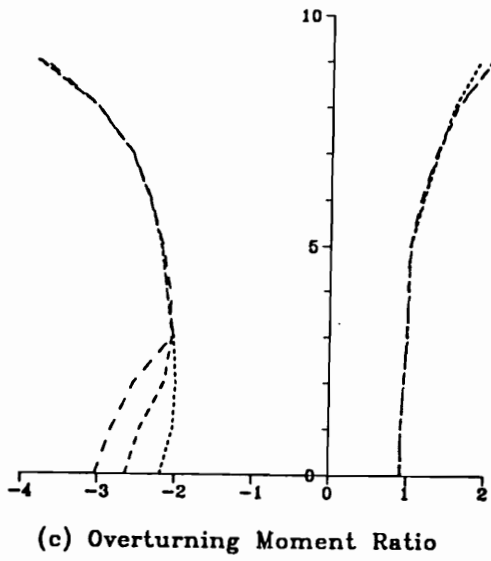


Figure 2.36: Graphs showing the effect of the impact stiffness coefficient on the ratio of multiple pounding to no-pounding responses (2% structural damping)

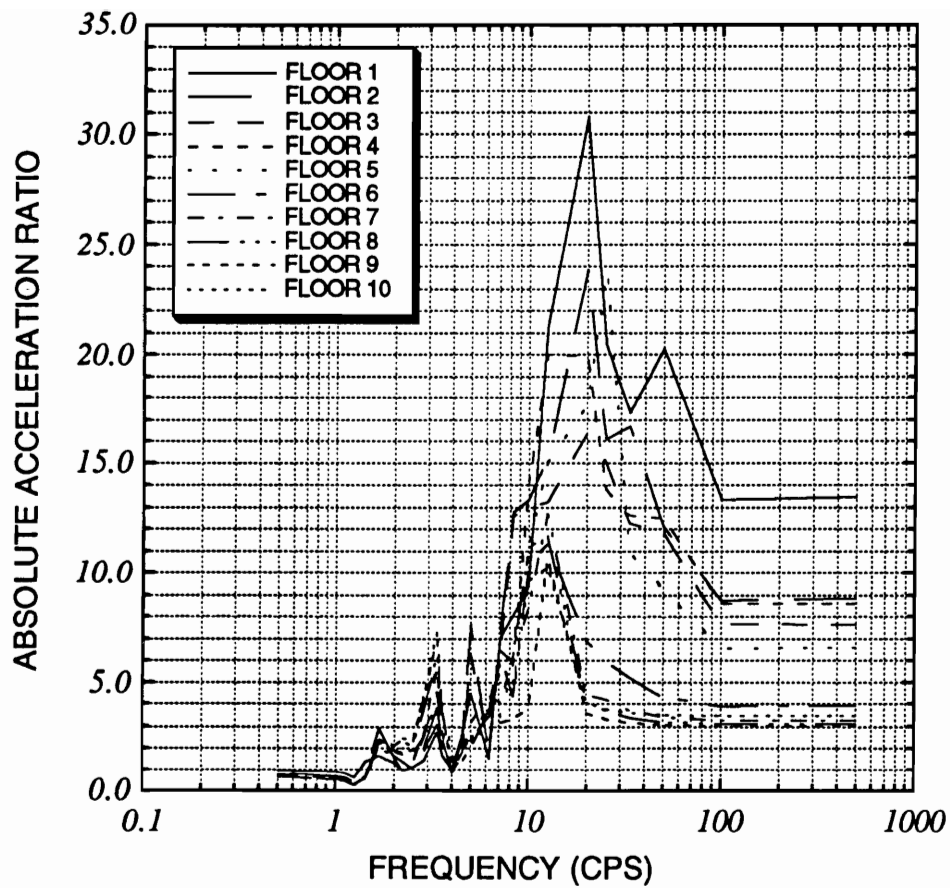


Figure 2.37: Pounding to no-pounding floor response spectrum ratios (multiple pounding against a 5-story rigid structure) — 2% structural damping

Chapter 3

POUNDING OF MDOF FLEXIBLE STRUCTURES

3.1 Introduction

In chapter 2, we examined the pounding of a multi-story structure against a rigid obstruction. In this section we will consider both pounding structures to be flexible. In the following section we develop the equations of motion. The numerical results parallel to those presented in chapter 2 are also obtained for this case. They are discussed and compared with the results for the rigid case in the subsequent section. Also considered is the nonlinear Hertz model for pounding stiffness. The numerical results for the nonlinear and linear pounding stiffness models are also compared.

3.2 Equations of Motion

Two multi-story flexible shear buildings are considered and identified as p and s-structures. The properties associated with these structures will be identified by subscripts p and s, respectively.

Let the p-structure be modeled as a p degrees of freedom [DOF] system described by stiffness matrix $[K_p]$, damping matrix $[C_p]$, and mass matrix $[M_p]$. Similarly, the s-structure be modeled as an s DOF system with stiffness matrix $[K_s]$, damping matrix $[C_s]$ and mass matrix $[M_s]$. It is assumed that $p \geq s$.

It is assumed that the floor heights of both structures are the same and, therefore the pounding will occur only at their floor levels. A schematic of the two structures is shown in Figure 3.1. As assumed before, the impact is modeled by a linear spring and dashpot

element introduced between the colliding floor masses of the two structures.

Figure 3.2 shows the free body diagram of the colliding masses of the two structures. Using Newton's law, the equation of motion for the two masses can be written as:

$$\begin{aligned}
 m_{ip}\ddot{x}_{ip}(t) + (k_{ip} + k_{ip+1} + s_i)x_{ip}(t) - k_{ip}x_{ip-1}(t) - k_{ip+1}x_{ip+1}(t) \\
 + d_i\dot{x}_{ip}(t) - d_i\dot{x}_{is}(t) - s_ix_{is}(t) - s_ig_i = -m_{ip}\ddot{x}_g(t)
 \end{aligned} \tag{3.1}$$

$$\begin{aligned}
 m_{is}\ddot{x}_{is}(t) + (k_{is} + k_{is+1} + s_i)x_{is}(t) - k_{is}x_{is-1}(t) - k_{is+1}x_{is+1}(t) \\
 + d_i\dot{x}_{is}(t) - d_i\dot{x}_{ip}(t) - s_ix_{ip}(t) + s_ig_i = -m_{is}\ddot{x}_g(t)
 \end{aligned} \tag{3.2}$$

where x_{ip} , m_{ip} and k_{ip} , respectively, are the relative displacement, mass and the combined column stiffness of the i th story of the p-structure. Similar quantities with subscript s pertain the s-structure. The stiffness and damping coefficient of the impact element are s_i and d_i . The gap between the two colliding masses is denoted by g_i .

It is noted that when $\delta_i = x_{ip} - x_{is} - g_i < 0$, there will be no pounding. In that case the terms containing s_i and d_i in equations 3.1 and 3.2 are set equal to zero.

Collecting equations for all masses, the combined equations of motion of the two pounding systems can be written as:

$$[M]\{\ddot{X}\} + [C]\{\dot{X}\} + [K]\{X\} + \{F\} = -[M]\{r\}\ddot{x}_g(t) \tag{3.3}$$

where

$$[M] = \begin{bmatrix} [M_p] & 0 \\ 0 & [M_s] \end{bmatrix} \tag{3.4}$$

$$[C] = \begin{bmatrix} [C_p] & 0 \\ 0 & [C_s] \end{bmatrix} + [D] \quad (3.5)$$

$$[K] = \begin{bmatrix} [K_p] & 0 \\ 0 & [K_s] \end{bmatrix} + [S] \quad (3.6)$$

$$[S] = \begin{bmatrix} \overbrace{s_1 \ 0 \ \dots \ 0}^s & \overbrace{0 \ \dots \ 0}^{p-s} & \overbrace{-s_1 \ 0 \ \dots \ 0}^s \\ s_2 \ \dots \ 0 & 0 \ \dots \ 0 & 0 \ -s_2 \ \dots \ 0 \\ \vdots \ \vdots \ \vdots & \vdots \ \vdots \ \vdots & \vdots \ \vdots \ \vdots \\ \dots & s_s \ 0 \ \dots \ 0 & 0 \ 0 \ \dots \ -s_s \\ \dots & 0 \ \dots \ 0 & 0 \ 0 \ \dots \ 0 \\ \dots & \vdots \ \vdots \ \vdots & \vdots \ \vdots \ \vdots \\ \dots & 0 \ 0 \ 0 \ \dots \ 0 & \dots \ 0 \\ \dots & \dots & s_1 \ 0 \ \dots \ 0 \\ \dots & \dots & s_2 \ \dots \ 0 \\ \dots & \dots & \vdots \ \vdots \\ \dots & \dots & s_s \end{bmatrix} \quad (3.7)$$

SYM.

$$\{F\} = -[S] \begin{Bmatrix} g_1 \\ g_2 \\ \vdots \\ g_s \\ 0 \\ \vdots \\ 0 \end{Bmatrix} \quad (3.8)$$

where $[M_p]$, $[C_p]$ and $[K_p]$ are the mass, damping and stiffness matrices of the p-structure. They are the same as those defined in chapter 2. The matrices associated with subscript s

belong to the s-structure. The matrix $[D]$ in equation 3.5 is of the same form as matrix $[S]$, except that s_i in equation 3.7 are replaced by d_i to obtain $[D]$. The sizes of submatrices in $[S]$, and similarly in $[D]$ are shown in equation 3.7.

The system of equations 3.3 is solved by the Newmark- β approach to obtain numerical results for the parametric study, the results of which are presented in the following section.

3.3 Numerical Results

Numerical results have been obtained for several configurations of two pounding structures. The assumed basic configuration consists of a ten-story flexible structure pounding against a five-story flexible structure, as shown in Figure 3.1. In the basic configuration the structural parameters for both structures are: the floor mass $=6.02E + 5 \text{ Kg}$, story stiffness $=1.81E + 9 \text{ N/m}$ and the stiffness of the impact spring $=8.76E + 9 \text{ N/m}$. The damping ratio of 0.05 has been assumed in each mode. Also a dashpot with coefficient $d_i = 2.04E + 7 \text{ Kg/sec}$ has been added at each pounding interface to include some loss of energy due to pounding in the analysis. A parametric study parallel to the study presented in chapter 2 has been conducted here to examine the effect of changing various parameters of the two systems.

The seismic base motion considered to obtain the numerical results is the 1941 N-S El Centro component with maximum ground acceleration of $0.2 G$.

3.4 Effect of Gap Size

To evaluate the effect of pounding, the ratios of multiple pounding to no-pounding responses for different gap sizes are shown in Figure 3.3 for the ten-story structure and in Figure 3.4 for the five-story structure. The results in Figure 3.3 show that on the pounding side the displacement ratio is less than 1.0 for the gap size of zero, and converges to 1.0 as the gap size increases. The story shear above the top pounding level increases, and this increase becomes less as we widen the gap between the two structures. In the case of

overturning moment, pounding causes a large increase in the negative overturning moment, especially at the base and top stories. Again these increments become small and approach the no-pounding case as the gap size is increased. The negative displacements, negative story shears and positive overturning moments remain essentially unchanged.

For the five-story building, the displacements on the pounding side (that is, the negative displacements) are reduced because of the obstruction from the adjacent structure, as seen in Figure 3.4. Also reduced are the negative story shears. The positive displacements, positive story shears, and positive and negative overturning moments, however, increase due to pounding. These increases are more noticeable at the top story of the structure. The most severe effect of pounding is felt in the story shears and overturning moments. The positive overturning moments increase dramatically with decreasing gap size. Increasing the gap size causes the responses to approach those for the no-pounding case.

Figure 3.5 shows the plot of the story shear ratio versus the gap ratio. The gap ratio is defined as the ratio of the clearance between the structures to the unobstructed maximum displacement of the taller structure at the highest pounding floor. It is seen that, like a whiplash effect, the largest relative increase in the shear occurs in the highest floor, as is indicated by the shear ratio of story 10; for zero gap, the pounding has caused the shear force to increase by about 140% in this particular story. Thus if the higher floors are designed with a tight safety margin they are likely to fail first due to this relatively large increase in the shear force caused by pounding. However, as expected, the effect of pounding is reduced as the gap size is increased. For a gap ratio of slightly higher than 1.0, the shear ratio also approaches a value of 1.0, indicating no pounding of the structures. Figure 3.6 shows results similar to those shown in the previous figure but not in ratio form. It is seen that although the relative increase in the shear force due to pounding is larger in the higher stories, the magnitude of the shear force is actually larger in the lower stories. Thus lower stories may still be required to be designed for higher shear forces.

In Figure 3.7 is shown the variation of the absolute accelerations of various floors versus the gap. Similar information is shown in Figure 3.8 in the ratio form where the ratio of

pounding acceleration to the no-pounding acceleration is plotted against the gap ratio. From these figures it is seen that all pounding floors experience a rather large increase in their accelerations due to pounding (about 8 to 9 times the no-pounding accelerations). This effect is reduced (more so for the lower floors) as the gap ratio is increased. Later on it is shown that the corresponding floor acceleration spectra are also increased significantly by pounding. This is of direct relevance in the design of supported secondary systems.

3.5 Effect of Story Stiffness of the Five-Story Structure

In this section the effect of changing the story stiffness of the five-story structure on the pounding response is investigated. Two additional story stiffnesses, with $\frac{1}{4}$ and $\frac{1}{16}$ of the original story stiffness, have been considered. All other structural parameters of the two pounding structures are the same as in the basic configuration. Also the gap between the pounding structures is assumed to be zero.

Figure 3.9 is for the ten-story structure whereas Figure 3.10 is for the five-story structure. In these figures we compare the multiple pounding to no-pounding responses for structures with different stiffnesses by plotting the ratios of the two responses.

In Figure 3.9 it is seen that decreasing the stiffness of the five-story structure does not necessarily decrease the pounding effect of increased shear above the top pounding level, as the positive shear ratio for the highest and lowest stiffnesses are about equal and they are larger than the ratio for the medium stiffness. A similar observation can also be made for the negative overturning moments at the lower levels. In fact, it is interesting to note that the ratio of pounding to no-pounding response is about 1.0 at all floor levels for the case when the stiffness of the shorter structure is reduced to $4.53E+8$ N/m. For this particular stiffness value of the shorter structure, the fundamental frequencies of the two structures are nearly equal. This causes them to vibrate in phase with each other, with minimum collision and pounding effect.

Figure 3.10 shows that the negative displacement responses of the five-story structure

due to pounding decrease when the structure becomes softer. It is also seen that the story shear responses are highest for the stiffest structure. Also the overturning moment increases dramatically for the softest structure. Again for the case when the two structures have equal fundamental frequencies, the response ratios are nearly equal to unity as the two structures vibrate in phase with each other with a minimum number of collisions.

3.6 Effect of Story Stiffness of the Ten-Story Structure

The effects of changing the story stiffness of the ten-story structure on the pounding responses of the two structures are shown in Figures 3.11 and 3.12. As in the previous section, two additional story stiffnesses, with $\frac{1}{4}$ and $\frac{1}{16}$ of the original story stiffness, have been considered. All other structural parameters of the two buildings are the same as in the basic configuration.

Figure 3.11 shows that the positive displacement responses at the lower levels decrease when the structure becomes softer. Also, decreasing the stiffness does not necessarily decrease the pounding effect of increased shear above the pounding level, as the curve for the stiffest configuration is in between the curves of the two softer structures. The overturning moment due to pounding, however, increases at the lower levels when the structure becomes softer.

Figure 3.12 shows the pounding to no-pounding response ratios for the five-story structure. As the ten-story structure becomes softer, the negative pounding displacement and story shear responses increase. For the story shear this increase is highest at the top story. A large increase in pounding overturning moment response occurs for the softest structure.

3.7 Effect of Floor Mass of the Five-Story Structure

The next two figures show the effect of changing the floor mass of the five-story structure and keeping all other parameters of the two pounding structures the same as in the basic configuration. The pounding to no-pounding response ratios for the structures with $\frac{1}{2}$ and

$\frac{1}{4}$ of the original floor mass are shown for the ten- and five-story structures in Figures 3.13 and 3.14, respectively. As shown in Figure 3.13, for the largest mass of the five-story structure, the pounding response is largest for the ten-story structure. On the other hand, Figure 3.14 shows that, for the largest mass of the five-story structure, the pounding response is the lowest one. Generally as the mass decreases, the pounding response increases. This increase is more severe for the story shear (especially at the top story) and overturning moment.

3.8 Effect of Floor Mass of the Ten-Story Structure

Next we examine the effect of changing the mass of the ten-story structure by keeping all other parameters of the two pounding structures the same as in the basic configuration. The pounding to no-pounding response ratio for the structures with $\frac{1}{2}$ and $\frac{1}{4}$ of the original mass are shown for ten- and five-story structures in Figures 3.15 and 3.16, respectively.

Figure 3.15 shows that as the mass of the ten-story structure decreases, the positive pounding displacement response increases. The same kind of behavior can be seen in the positive story shear for the pounding floors. The positive shear for the top floors and negative overturning moments are higher for the heavier ten-story structure. Again as the fundamental frequencies of the two structures become closer, the ratio of pounding to no-pounding response is nearly equal to 1.0 for all stories due to the fact that the motions of the two structures are in phase with minimal collision and pounding effect.

The effect of increase in the mass of the ten-story structure on the response of the five-story structure is seen in Figure 3.16. The positive displacements, shears and moments are larger for the heavier ten-story structure. Again when the fundamental frequencies of the two structures become closer, a uniform *decrease* in the pounding response of the five-story structure is observed in the figures. That is, whatever pounding occurs in this case, it only reduces and not increases the story shear and overturning moment.

3.9 Effect of Pounding Stiffness

To examine the sensitivity of the pounding responses with respect to the assumed value of the stiffness of the pounding springs, we consider three values of the stiffness coefficient which are 1, 2 and 4 times the stiffness used in the basic configuration.

In Figure 3.17 we plot the ratio of pounding to no-pounding responses with three different pounding stiffnesses. For the range of stiffness variation considered here, the displacement and shear responses are almost unchanged with a change in the pounding stiffness. The overturning moment effect at the lower pounding levels is, however, increased with an increase in the pounding stiffness. That is, a stiffer spring tends to cause a higher overturning moment response at the lower levels of the ten-story structure due to pounding than a softer spring.

In Figure 3.18 we plot the ratio of pounding to no-pounding responses for the five-story structure. The displacement and shear responses are not changed much with a change in the pounding stiffness. The overturning moment pounding response increases with an increase in the pounding stiffness.

3.10 Effect of Change in Height of s-Structure

In this section we consider the pounding of the p-structure against the s-structure with different heights. The height of the s-structure is changed from one story to nine stories. The properties of the two structures are the same as in the basic configuration. The gap between the structures is assumed to be zero. The results are again presented in the form of ratios of the pounding to no-pounding responses. Figures 3.19 and 3.20 are for the taller structure and 3.21 and 3.22 are for the shorter structure. Figures 3.19 and 3.21 show the results for the s-structure heights of 1, 2, 3, 4 and 5 stories, whereas Figures 3.20 and 3.22 show similar results as Figures 3.19 and 3.21 but for the s-structure heights of 6, 7, 8 and 9 stories.

From Figures 3.19 and 3.20, it is noted that below the highest pounding level in the taller

structure, the positive displacements and story shears decrease slightly whereas the overturning moment and floor accelerations increase dramatically. Above the highest pounding floor level, the story shear and overturning moments also increase significantly. Also the most severe pounding effect is observed when the s-structure is 5 or 6-stories high, that is, when it is about half as tall as the taller structure.

The effect on the s-structure is shown in Figure 3.21 and 3.22. A very short structure shows higher displacement and story shear ratios and lower overturning moment and acceleration ratios. As the height of the s-structure is increased, the shear ratio is seen to decrease. The overturning moment and acceleration ratios on the other hand increase with an increase in the height up to 5 stories and then decrease thereafter. That is, a medium-height s-structure experiences the maximum overturning effect and floor acceleration due to pounding.

3.11 Effect of Pounding on Floor Response Spectra

As was done in chapter 2, here also we plot the floor response spectra of various floors for the pounding and no-pounding cases. The floor spectra for the ten-story building are shown in Figures 3.23 and 3.24, and for the five-story structure in Figure 3.25. In all these cases, it is seen that floor response spectra with pounding are very high compared to the spectra with no pounding, especially in the high-frequency range. To show the relative increase, in Figures 3.26 and 3.27 we plot the ratio of pounding to no-pounding floor spectra at various frequencies for the ten-story and five-story structures, respectively. First we note that due to pounding the floor spectrum values of the pounding floors are amplified much more than the spectrum values of the higher (no-pounding) floors. A similar observation was also made when we discussed Figure 2.32 in chapter 2. However, a comparison of the amplification values obtained in Figure 3.26 with those in Figure 2.32 also shows that the pounding floors of the ten-story structure are more severely affected, especially in the high-frequency range when the adjacent structure is considered flexible. Also a comparison of the ratios for the

pounding floors in Figure 3.26 for the ten-story structure with the ratio shown in Figure 3.27 for the five-story structure shows that the floor spectrum values of the ten-story structure floors are more severely affected by pounding than those of the five-story structure.

3.12 Pounding Response of Equal Fundamental Frequency Structures

While discussing Figures 3.9 and 3.15, it was observed that when the fundamental frequencies of the two structures were the same, the pounding effect was somewhat lessened. To examine this effect further, we considered three sets of pounding structures with fundamental frequencies of 0.653 cps, 1.304 cps and 2.484 cps. We show the pounding to no-pounding response for displacement, story shear, overturning moment and absolute acceleration ratio for the ten-story structure in Figure 3.28 and for the five-story structure in Figure 3.29. It is noted that for the ten-story structure the displacement, story shear and positive overturning moment ratios are near 1.0, indicating that there is not much pounding effect. The negative overturning moment and floor acceleration values for the flexible case show the same pounding effect. Similar observations are also applicable to the five-story structure (Figure 3.29) as well, except that in this case now the overturning moment and acceleration values which are affected by pounding are on the opposite side from those of the ten-story structure.

3.13 Pounding Against a Flexible Versus Rigid Structure

In chapter 2, the s-structure was assumed to be rigid, whereas in this chapter it is assumed to be flexible with the same mass and stiffness parameters as the first structure. To show the effect of the s-structure flexibility in the pounding analysis, in Figures 3.30 through 3.33 we plot the ratios of the flexible to rigid responses for various parametric variations from results shown in Figures 3.3, 3.11, 3.15 and 3.17. The s-structure properties are taken the same as in the basic configuration. Thus we plot the ratios of flexible to rigid responses obtained for different gap sizes in Figure 3.30, for different stiffness and

mass parameters of the ten-story structure in Figures 3.31 and 3.32, respectively, and for different contact stiffness coefficients in Figure 3.33. In all cases, ratios greater than 4, which occur for the positive displacements and shears for the pounding floors, are not shown as these two responses are not critical or significant. In all other response quantities, it is noted that this ratio is not exactly equal to 1.0 but does fluctuate around the value of 1.0 for various cases. These fluctuations are quite large in the floor acceleration response. This implies that, for calculating the response, it will not be accurate to consider the smaller structure rigid when it is not. The inclusion of s-structure flexibility might complicate the analysis somewhat, but for evaluating the pounding effects it is necessary that flexibility of the smaller structure is also reflected in the analysis.

3.14 Pounding with Hertz's Spring Model

A study of structural pounding involves several parameters. We do have a better handle on most of these parameters except the parameter of stiffness and coefficient of damping of the contact element at the pounding interface. In the numerical study in the previous section and in chapter 2, it was assumed that the pounding stiffness was linear. However in pounding studies, the Hertz contact model has also been adopted to represent the pounding stiffness. In fact it has been claimed to be more realistic [14,15], as it has been derived on the basis of elastic behavior during contact of two bodies. Without going into the details of the merits or validity of this model, it is considered appropriate to include this model as well in the parametric study presented herein. In this section, therefore, we now assume that the contact stiffness is such that the contact force is given by the following nonlinear relationship:

$$F_i = s_i(x_{ip} - x_{is} - g_i)^{\frac{3}{2}} \quad (3.9)$$

Since no damping model is available in the literature to represent the energy loss, here we have assumed the same model as the one used in the previous numerical study.

The numerical responses have been obtained for pounding between two flexible structures. Since the primary purpose of these results is to see what effect this nonlinear model will have on the response compared to the previously used linear model, here we present the numerical results only for the standard configuration (that is, the taller building is ten-stories high and shorter building is five-stories high). The stiffness and mass parameters are the same as described at the beginning of this chapter.

3.14.1 Equations of motion with nonlinear model

The free body diagram in this case remains the same as shown in Figure 3.2, except that the interface force between the colliding masses, instead of being $s_i(x_{ip} - x_{is} - g_i)$, is now replaced by $s_i(x_{ip} - x_{is} - g_i)^{\frac{3}{2}}$. This changes the form of the combined equations of motion to the following:

$$[M]\{\ddot{X}\} + [C]\{\dot{X}\} + [K']\{X\} + \{F'\} = -[M]\{r\}\ddot{x}_g(t) \quad (3.10)$$

where $[M]$ and $[C]$ are the same as in equations 3.4 and 3.5. The new stiffness matrix $[K']$ and vector $\{F'\}$ are, however, defined differently as:

$$[K'] = \begin{bmatrix} [K_p] & 0 \\ 0 & [K_s] \end{bmatrix} \quad (3.11)$$

$$\{F'\} = [S] \left\{ \begin{array}{c} (x_1 - x_{p+1} - g_1)^{\frac{3}{2}} \\ (x_2 - x_{p+2} - g_2)^{\frac{3}{2}} \\ \vdots \\ (x_p - x_{p+s} - g_s)^{\frac{3}{2}} \\ 0 \\ \vdots \\ 0 \end{array} \right\} \quad (3.12)$$

It is noted that because of the nonlinear terms, these equations of motion are of different form than equations 3.3 - 3.8.

To solve these equations, the fourth order Runge-Kutta method was used. The details of the method are quite standard and are available in texts on numerical methods [6]. Here, however, only the basic information needed to implement this method is provided for completeness sake.

The $(p + s)$ second order system of differential equations in 3.10 can be transformed into $2(p + s)$ first order differential equations as:

$$\{\dot{Y}\} = \begin{bmatrix} [0] & [I] \\ -[M]^{-1}[K'] & -[M]^{-1}[C] \end{bmatrix} \{Y\} + \begin{Bmatrix} \{0\} \\ -[M]\{F'\} - \{r\}\ddot{x}_g(t) \end{Bmatrix} \quad (3.13)$$

where

$$\{Y\} = \begin{Bmatrix} x_1 \\ x_2 \\ \vdots \\ x_{p+s} \\ \dot{x}_1 \\ \dot{x}_2 \\ \vdots \\ \dot{x}_{p+s} \end{Bmatrix} \quad (3.14)$$

The fourth-order Runge-Kutta method is applied to equation 3.13 directly to compute the solution across the i th interval according to the following equation:

$$x_{j,i+1} = x_{ji} + \frac{1}{6}\Delta t(k_{j1} + 2k_{j2} + 2k_{j3} + k_{j4})$$

where

$$\begin{aligned}
k_{j1} &= f_j(t_i, x_{1i}, x_{2i}, \dots, x_{2(p+s),i}) \\
x_{ji}^* &= x_{ji} + \frac{1}{2}\Delta t k_{j1} \\
k_{j2} &= f_j(t_i + \frac{1}{2}\Delta t, x_{1i}^*, x_{2i}^*, \dots, x_{2(p+s),i}^*) \\
\bar{x}_{ji} &= x_{ji} + \frac{1}{2}\Delta t k_{j2} \\
k_{j3} &= f_j(t_i + \frac{1}{2}\Delta t, \bar{x}_{1i}, \bar{x}_{2i}, \dots, \bar{x}_{2(p+s),i}) \\
\bar{x}_{ji}^* &= x_{ji} + \Delta t k_{j3} \\
k_{j4} &= f_j(t_i + \Delta t, \bar{x}_{1i}^*, \bar{x}_{2i}^*, \dots, \bar{x}_{2(p+s),i}^*)
\end{aligned}$$

$$j = 1, 2, \dots, 2(p + s) \quad (3.15)$$

3.14.2 Numerical results

In Figure 3.34, we show the displacement, story shear force, overturning moment and floor acceleration responses for the taller (p-structure) obtained with linear and nonlinear models of the contact spring. It is interesting to note that the displacement and shear force responses are nearly the same for the two cases, but the negative overturning moment and floor acceleration of the colliding floors are quite different. The nonlinear model is associated with the lower values of these response quantities. In Figure 3.35, we compare the ratio of the nonlinear to linear responses. As observed before, this ratio is nearly equal to 1.0, except for the overturning moment and floor acceleration responses where it is less than 1.0.

Results similar to those in Figures 3.34 and 3.35 are also presented in Figures 3.36 and 3.37 for the smaller (s-structure). Here again we observe that the differences in the displacements and story shears are not large but the overturning moments and acceleration values for the impacting floors are significantly different. Again, these values are smaller for the nonlinear case.

Thus we conclude that in general the nonlinear model will lead to a prediction of smaller response values than the values predicted by the linear model.

The next set of figures shows the effect of nonlinear models on the floor response spectra. Figures 3.38 and 3.39 are for the taller structure and Figure 3.40 is for the smaller structure. Again we observe that the nonlinear case gives lower floor response spectrum values than the values given by the linear case. This is more clearly shown in Figures 3.41 and 3.42 where we plot the ratio of the nonlinear to linear spectra for the ten-story and five-story structures, respectively. Except in the low-frequency range, this ratio is less than 1.0, indicating a smaller impacting effect if the impacting spring behaves according to Hertz's model.

To compare the effect of pounding on the floor spectrum response in the nonlinear case, we have plotted the ratio of pounding to no-pounding floor response spectrum values for the taller structure in Figure 3.43 and for the smaller structure in Figure 3.44. We observe that the floor response is affected by pounding. This effect is specially large for the pounding floors. However, when we compare these figures with Figures 3.26 and 3.27, we observe that the impacting effect is significantly reduced if the impact springs are nonlinear.

3.15 Summary

In this chapter, the pounding response of two flexible structures was examined. The parametric variation study involving the parameters of gap size, masses and stiffness of the two structures, stiffness coefficient of the pounding springs and the height of the smaller structure has been conducted. The response quantities calculated are displacement, story shear force, overturning moment, floor acceleration and acceleration response spectra. Also considered is the pounding of structures with equal fundamental frequencies as well as pounding of structures with pounding springs modeled according to Hertz's contact law.

The main conclusions drawn from this parametric study are that:

1. The shear forces in the higher stories not involved in pounding are significantly increased.

2. Accelerations and high-frequency acceleration spectrum values of the floors involved in pounding are greatly increased.
3. Overturning moments at the levels of the lower floors and the foundation are also increased.
4. It is important to consider the flexibility of the shorter structure to assess the effect of pounding more accurately. That is, inaccurate conclusions can result in the study of a pounding problem if the shorter structure is considered perfectly rigid.

Other conclusions of the parametric variation study are:

1. The closer the structure, the more serious the pounding effects.
2. The pounding effects depend upon the relative velocity as well as the relative magnitude of the colliding floor masses. The relative velocity depends upon the dynamic characteristics of the two structures such as frequency, damping and modal response characteristics, and not how the masses or stiffness of these structures change individually. Therefore, any two simple shear structures with equal fundamental frequencies will experience minimal pounding as they are likely to move in phase with respect to each other during an earthquake.
3. For the range of values considered for the impact spring stiffness, the pounding response was generally insensitive to this parameter.
4. The consideration of nonlinearity in the impact stiffness according to the Hertz's model mainly affected the magnitudes of the overturning moments and floor accelerations.

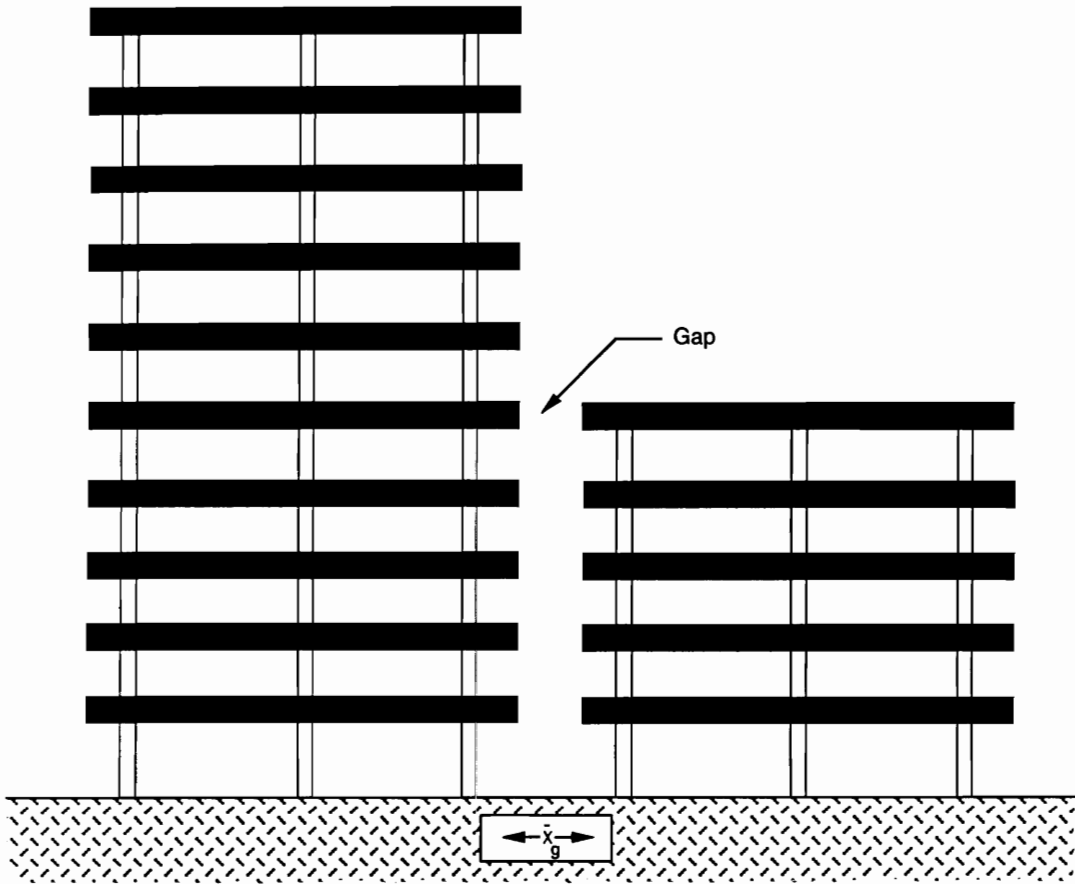


Figure 3.1: Schematic of a 10-story deformable structure pounding against a 5-story deformable structure

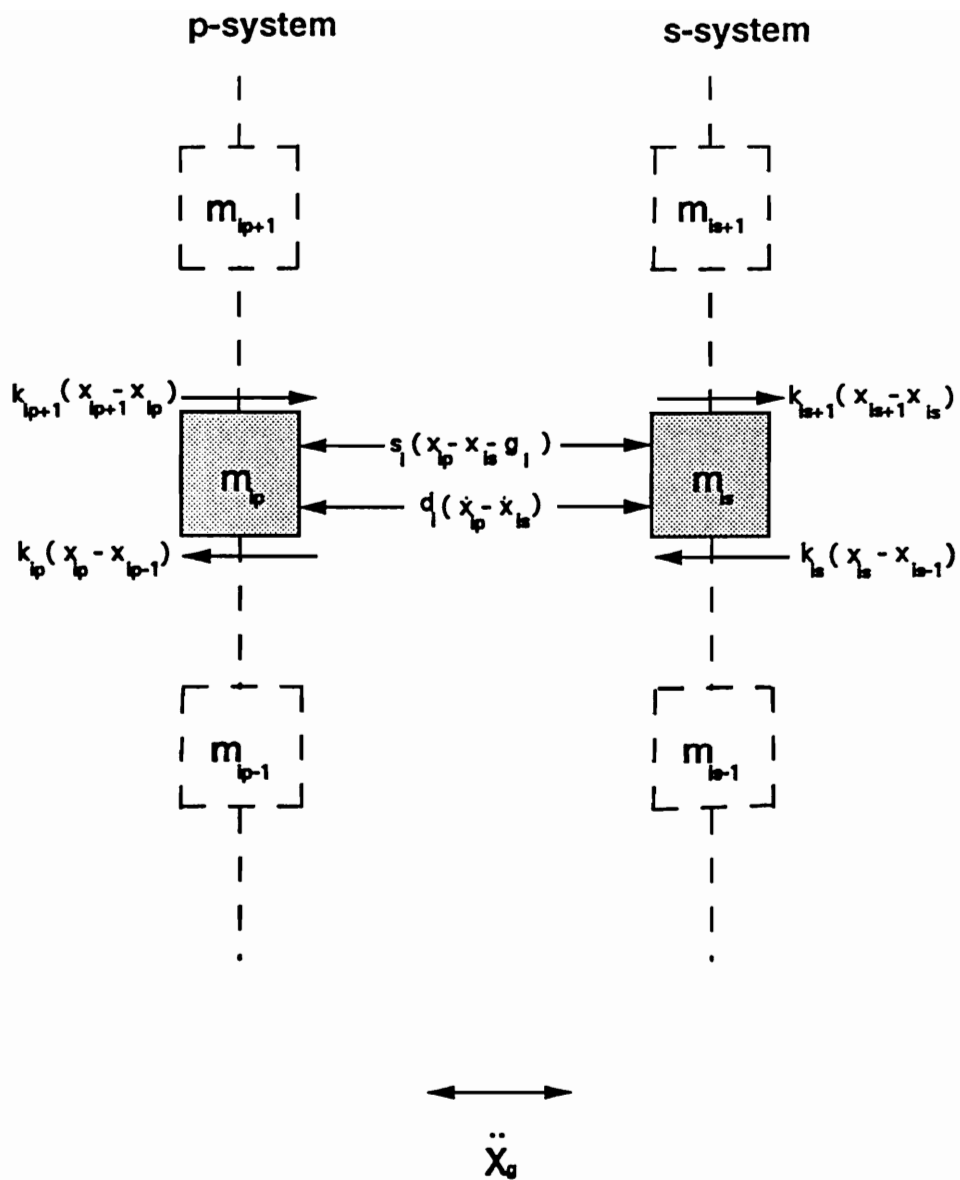
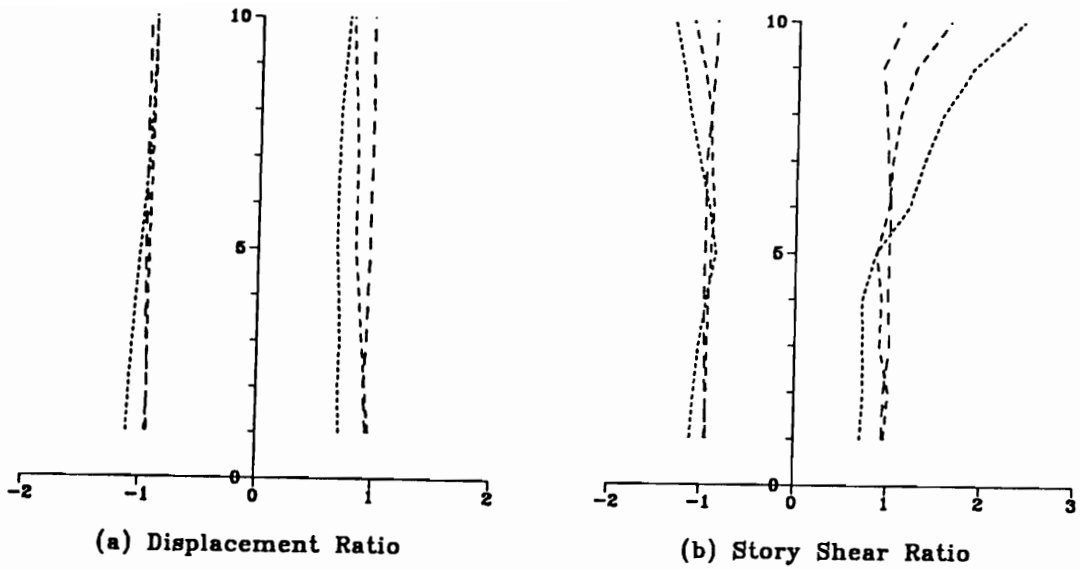


Figure 3.2: Free body diagram of two typical floor masses of the p and s-structure in state of pounding



..... $g=0.0$ m
 - - - - $g=0.0275$ m
 - - - - $g=0.0496$ m

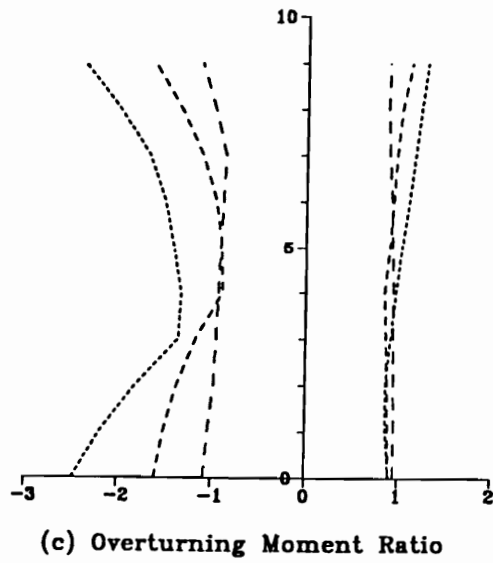
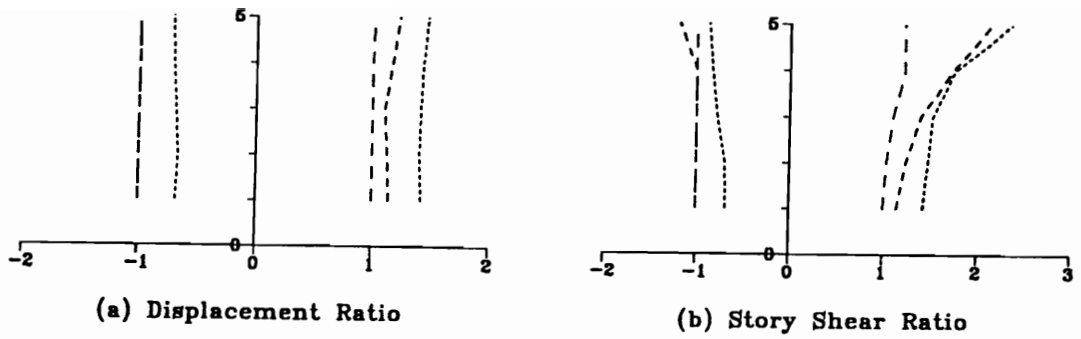


Figure 3.3: Ratio of multiple pounding to no-pounding responses for various gap sizes (10-story structure)



..... $g=0.0$ m
 - - - - $g=0.0275$ m
 - - - - $g=0.0496$ m

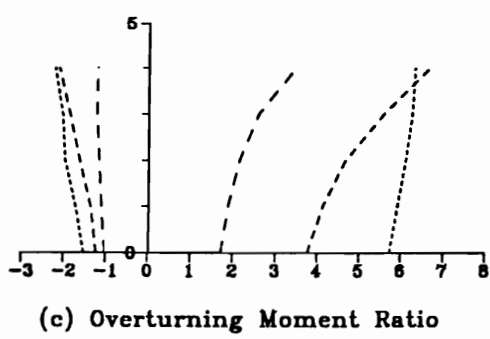


Figure 3.4: Ratio of multiple pounding to no-pounding responses for various gap sizes (5-story structure)

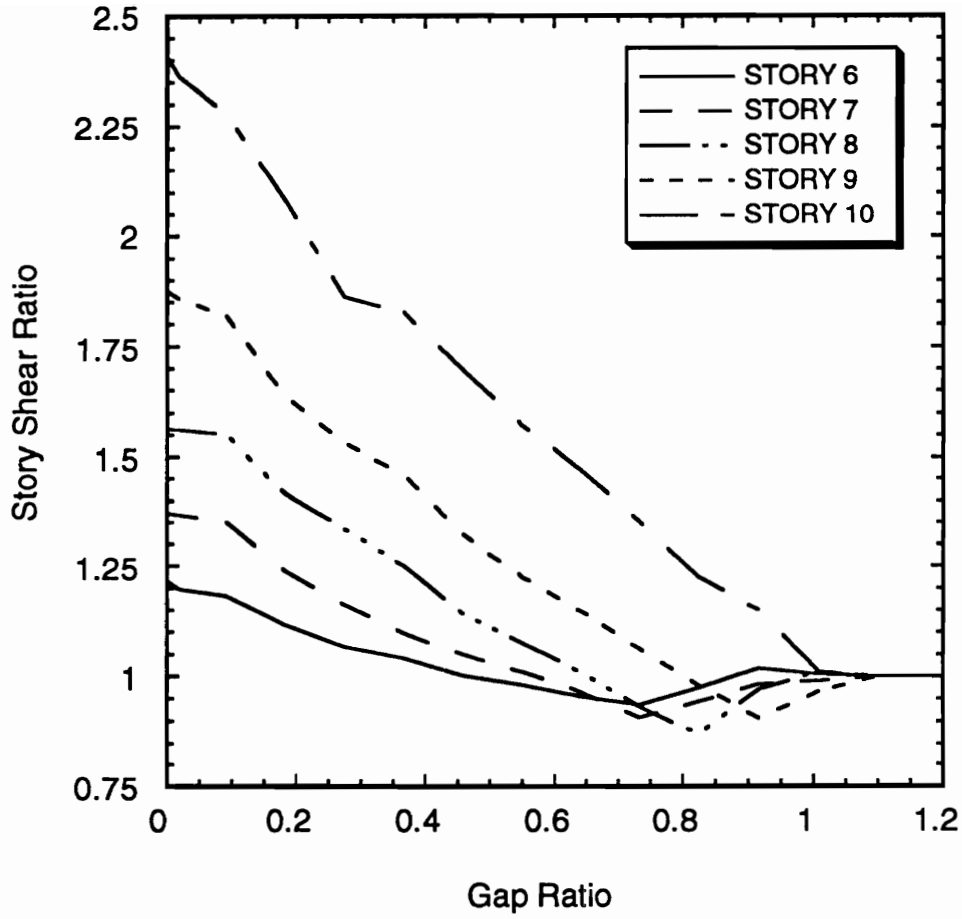


Figure 3.5: The variation of the story shear ratio versus the gap ratio for various stories of the 10-story structure

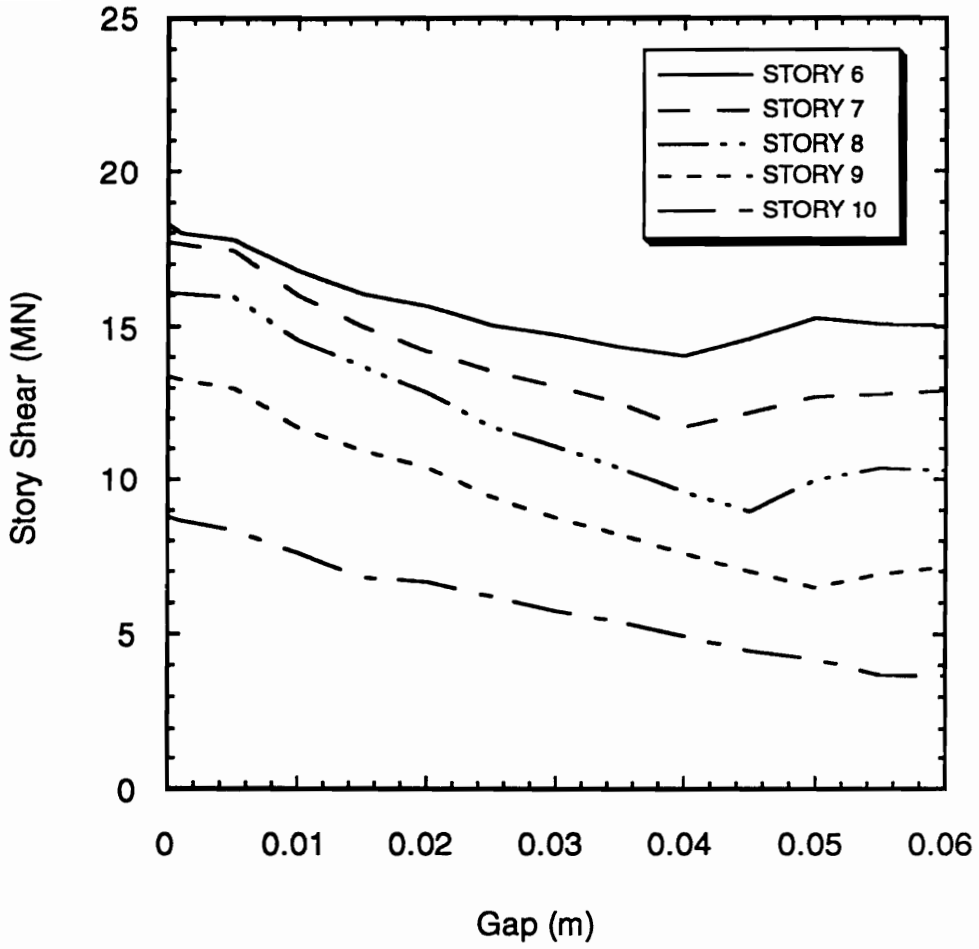


Figure 3.6: The story shear versus the gap size for various stories of the 10-story structure

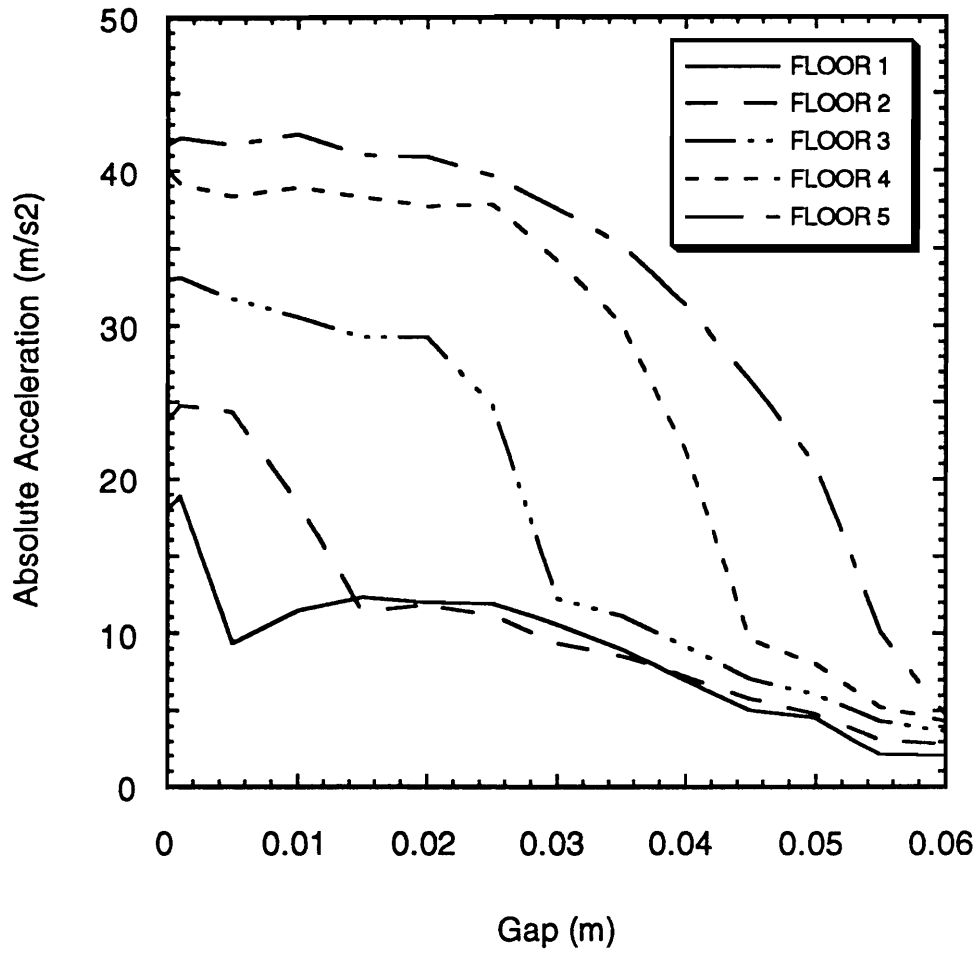


Figure 3.7: The maximum absolute acceleration versus the gap size for various pounding floors of the 10-story structure

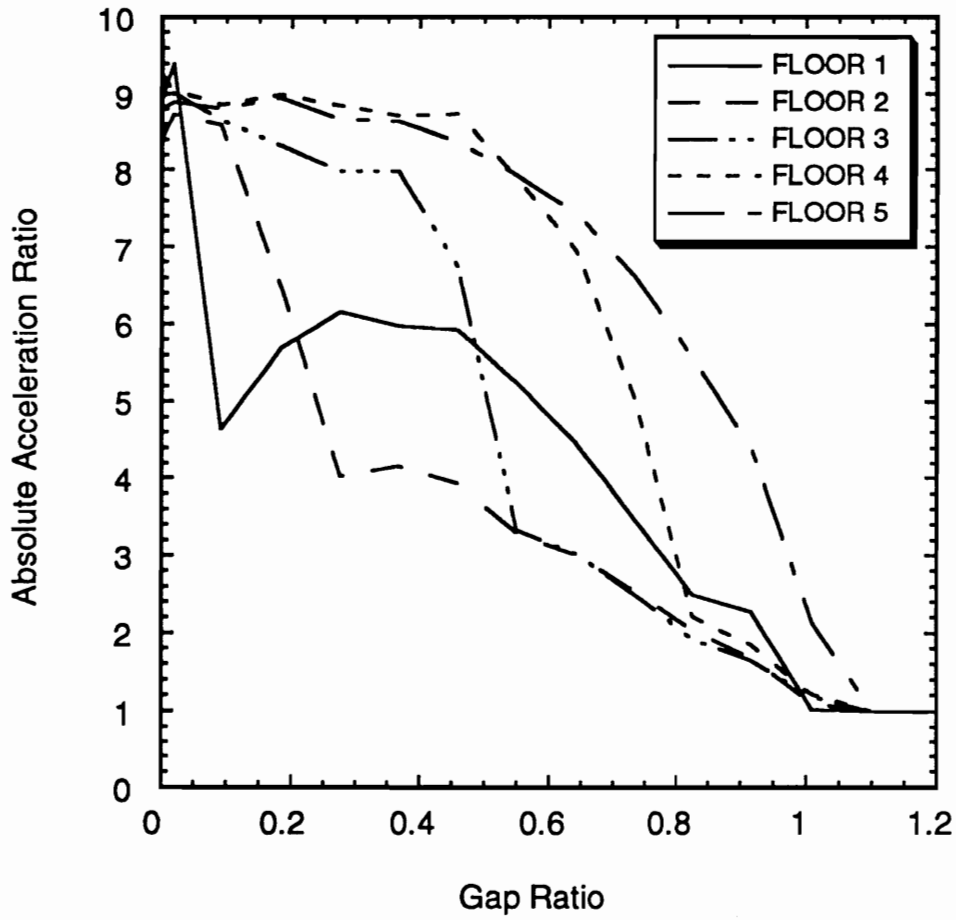
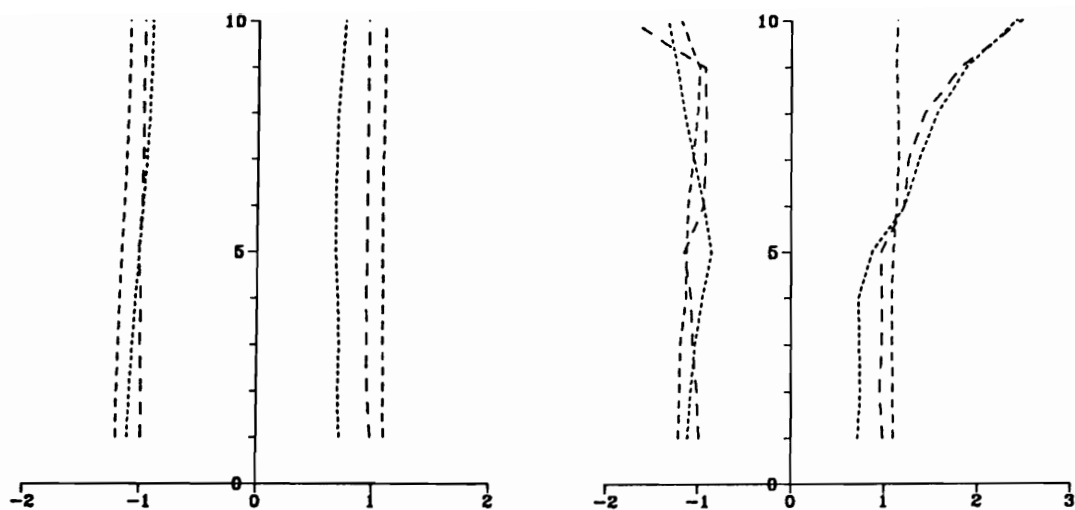


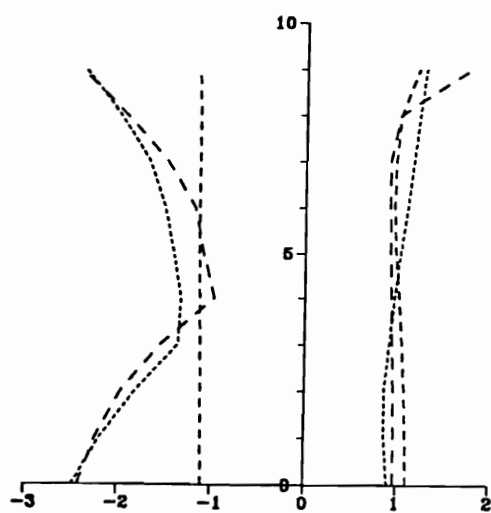
Figure 3.8: The maximum absolute acceleration ratio versus the gap ratio for various pounding floors of the 10-story structure



(a) Displacement Ratio

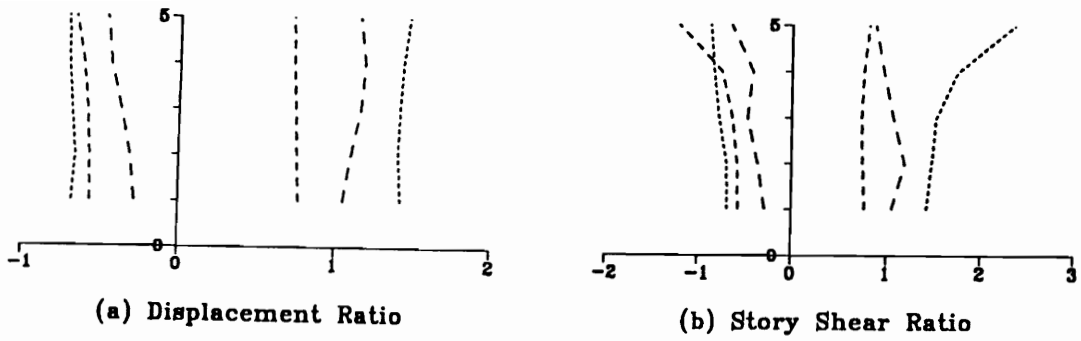
(b) Story Shear Ratio

..... $k=1.81E+09$ N/m
 ----- $k=4.53E+08$ N/m
 - . - . $k=1.13E+08$ N/m



(c) Overturning Moment Ratio

Figure 3.9: Ratio of multiple pounding to no-pounding responses of the 10-story structure for various story stiffnesses of the 5-story structure



..... $k=1.81E+09$ N/m
 ----- $k=4.53E+08$ N/m
 - . - . $k=1.13E+08$ N/m

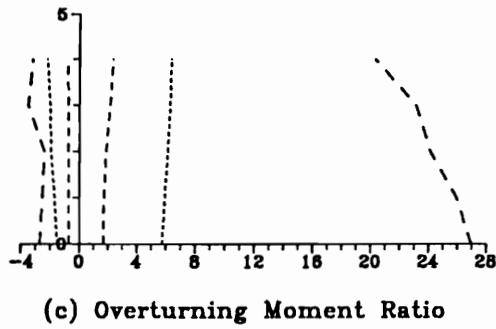
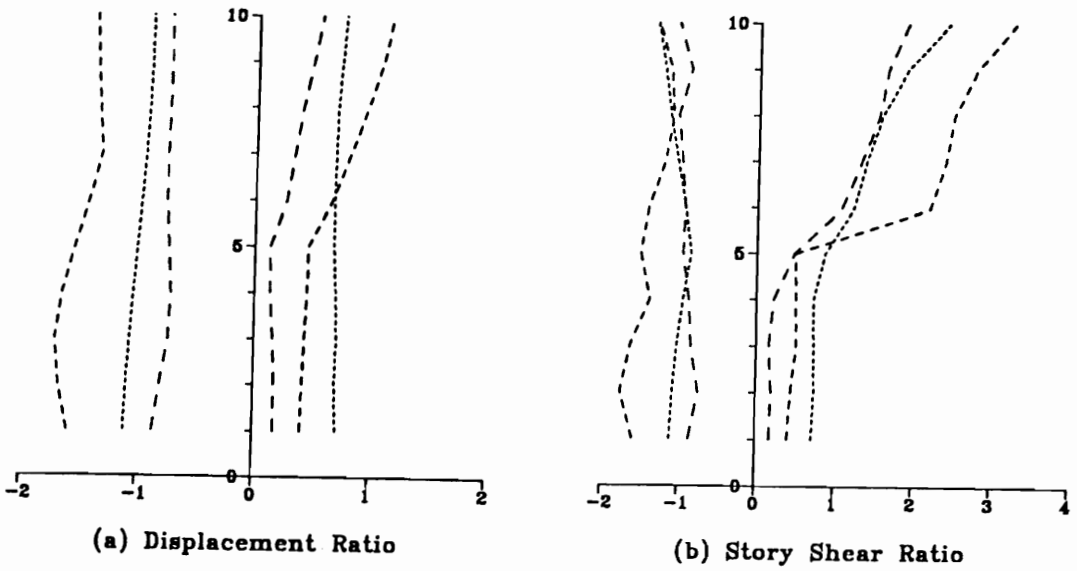


Figure 3.10: Ratio of multiple pounding to no-pounding responses of the 5-story structure for various story stiffnesses of the 5-story structure



..... $K=1.81E+09$ N/m
 ----- $K=4.53E+08$ N/m
 - · - · - $K=1.13E+08$ N/m

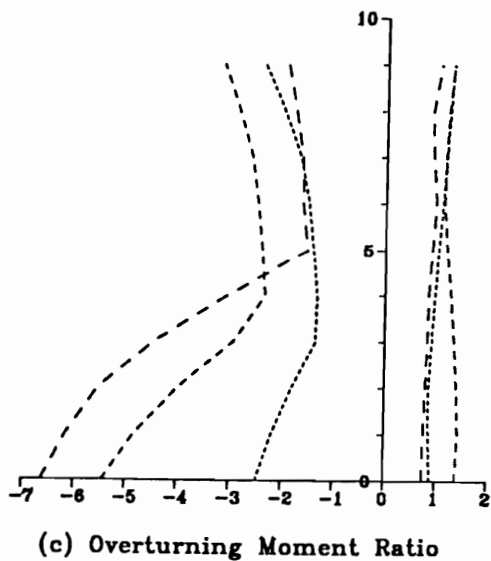
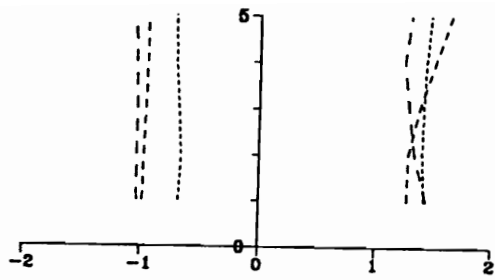
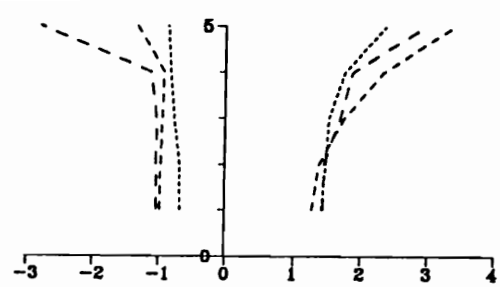


Figure 3.11: Ratio of multiple pounding to no-pounding responses of the 10-story structure for various story stiffnesses of the 10-story structure

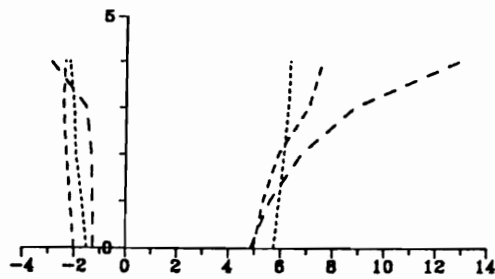


(a) Displacement Ratio



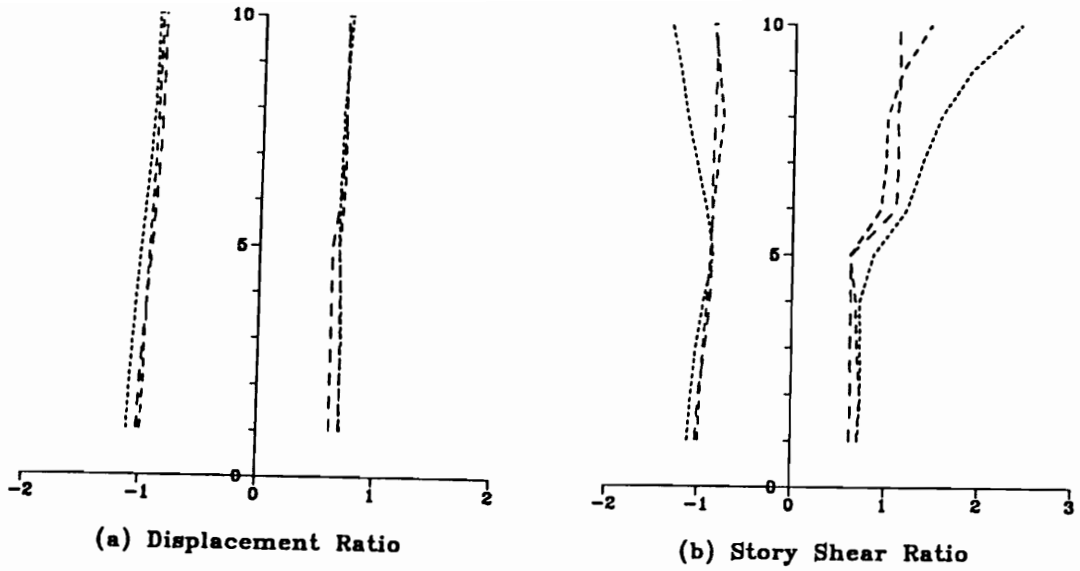
(b) Story Shear Ratio

..... $K=1.81E+09$ N/m
 ----- $K=4.53E+08$ N/m
 - . - . $K=1.13E+08$ N/m



(c) Overturning Moment Ratio

Figure 3.12: Ratio of multiple pounding to no-pounding responses of the 5-story structure for various story stiffnesses of the 10-story structure



..... $m=6.02E+05$ Kg
 ----- $m=3.01E+05$ Kg
 - . - . $m=1.51E+05$ Kg

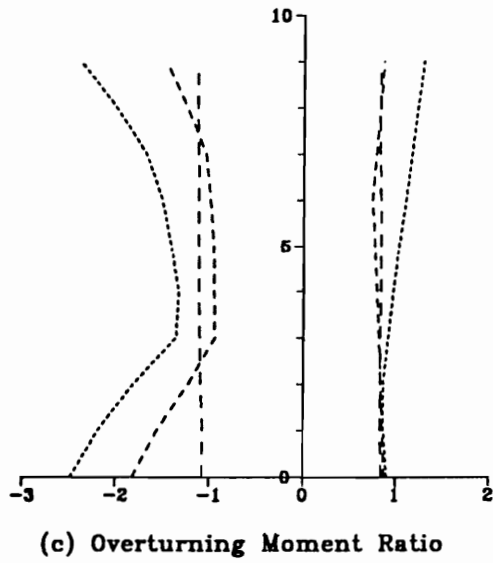
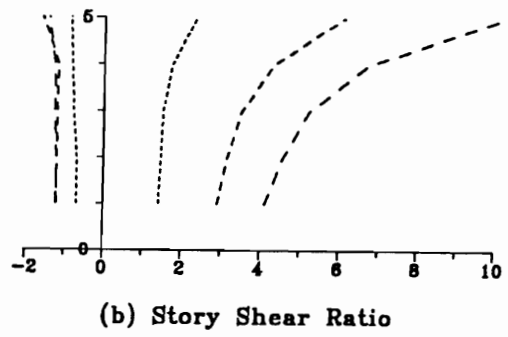
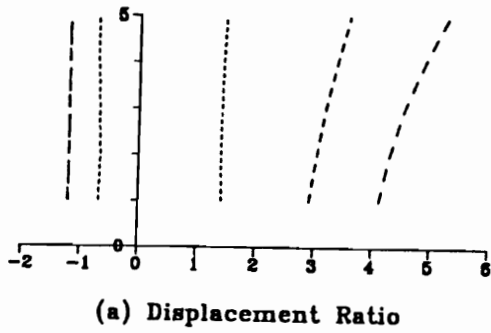


Figure 3.13: Ratio of multiple pounding to no-pounding responses of the 10-story structure for various floor masses of the 5-story structure



..... $m=6.02E+05$ Kg
 - - - - $m=3.01E+05$ Kg
 - · - · $m=1.51E+05$ Kg

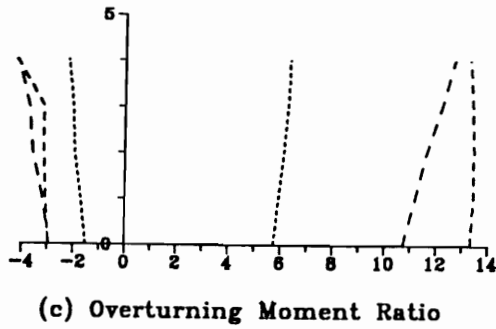
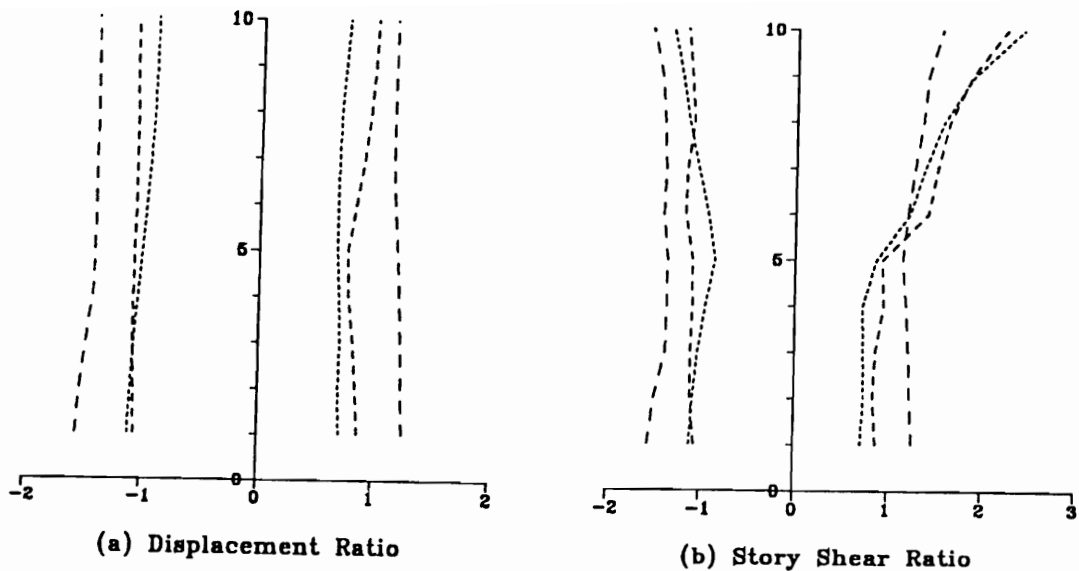


Figure 3.14: Ratio of multiple pounding to no-pounding responses of the 5-story structure for various floor masses of the 5-story structure



..... $M=6.02E+05$ Kg
 ----- $M=3.01E+05$ Kg
 - . - . - $M=1.51E+05$ Kg

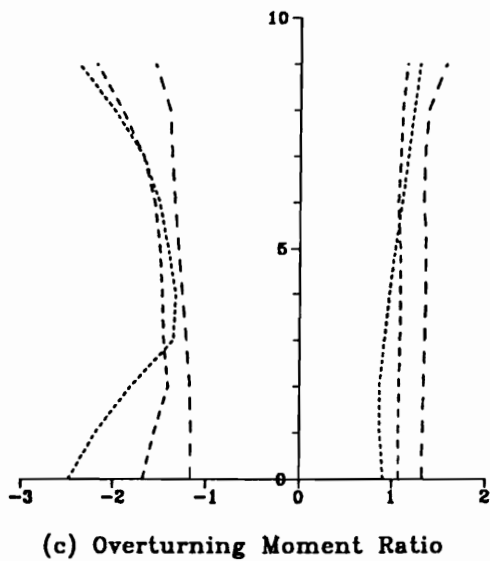
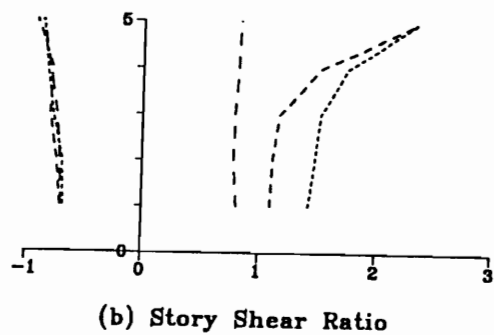
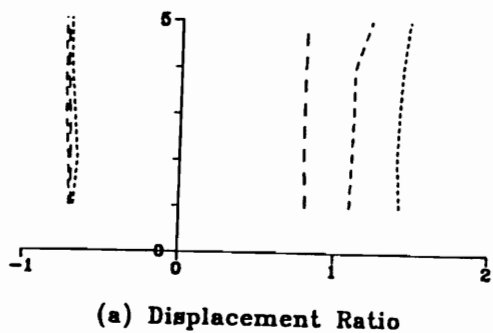


Figure 3.15: Ratio of multiple pounding to no-pounding responses of the 10-story structure for various floor masses of the 10-story structure



..... $M=6.02E+05$ Kg
 ----- $M=3.01E+05$ Kg
 - . - . $M=1.51E+05$ Kg

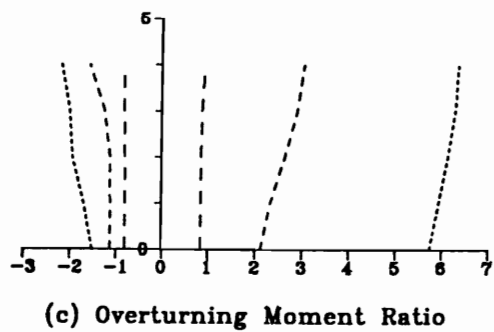
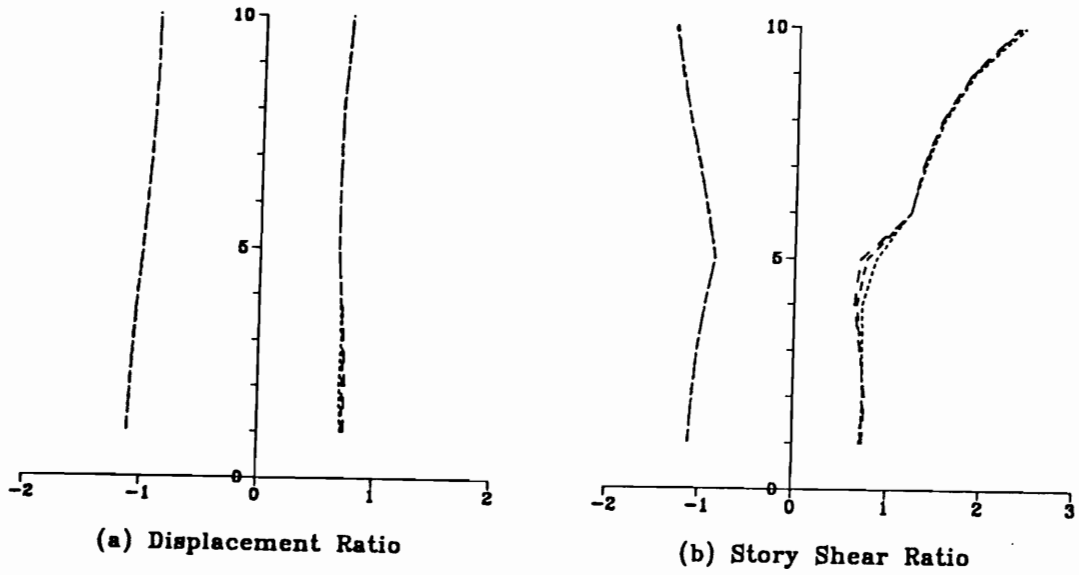


Figure 3.16: Ratio of multiple pounding to no-pounding responses of the 5-story structure for various floor masses of the 10-story structure



..... $\# = 8.76E+09 \text{ N/m}$
 ----- $\# = 1.75E+10 \text{ N/m}$
 - . - . - $\# = 3.50E+10 \text{ N/m}$

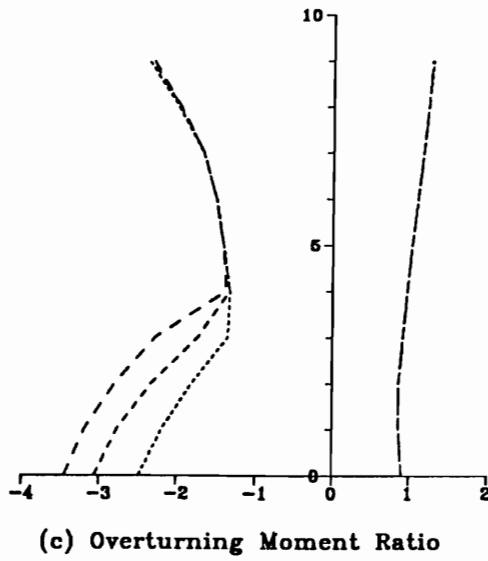


Figure 3.17: Ratio of multiple pounding to no-pounding responses of the 10-story structure for various impact stiffness coefficients

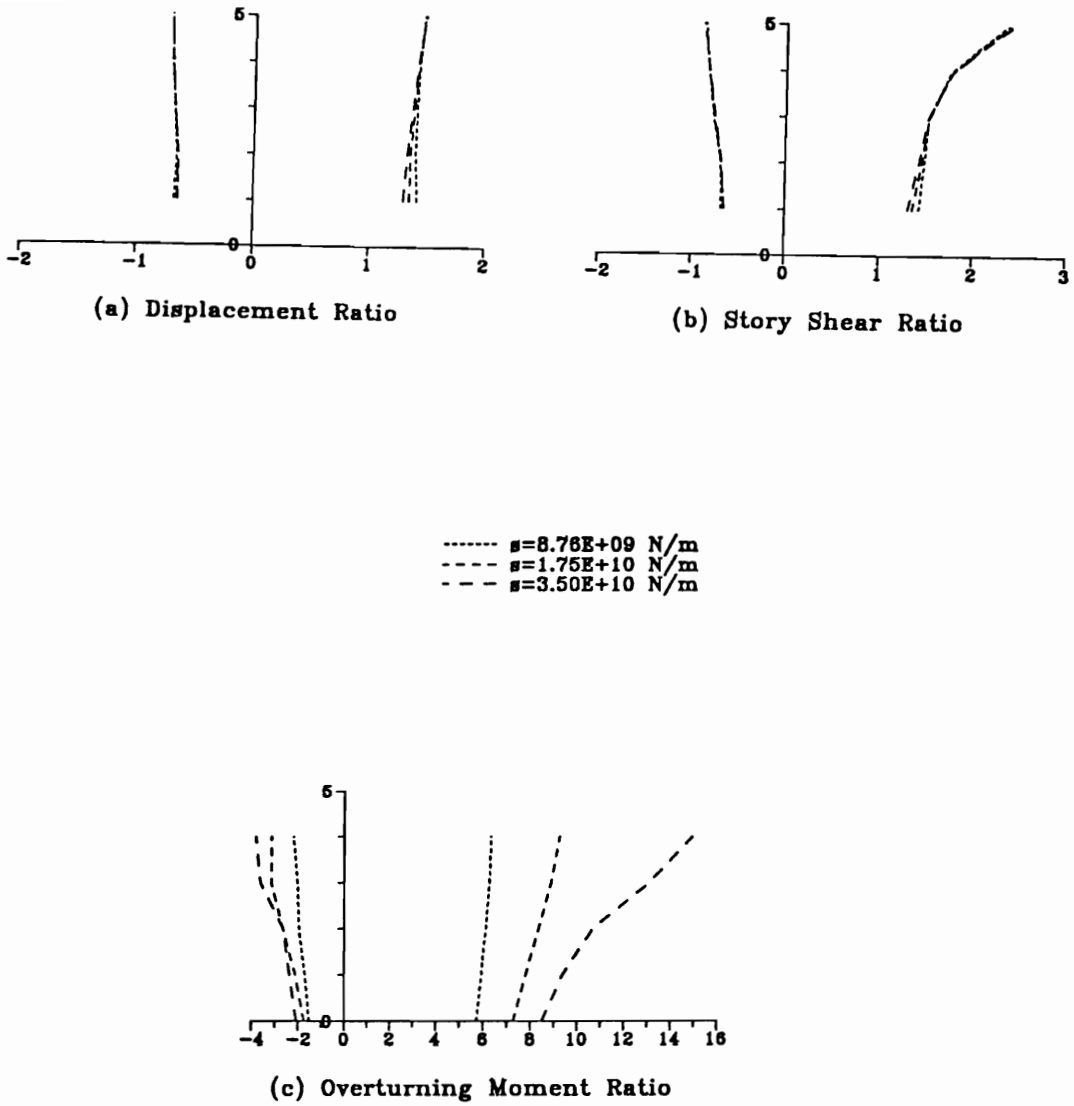
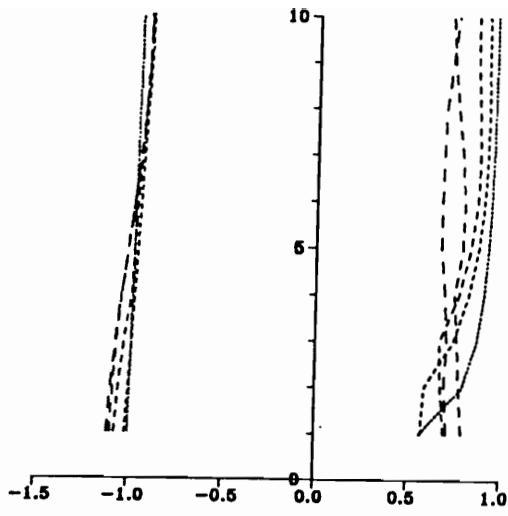
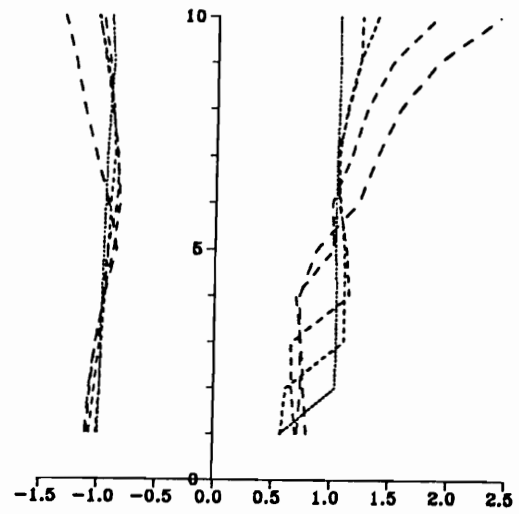


Figure 3.18: Ratio of multiple pounding to no-pounding responses of the 5-story structure for various impact stiffness coefficients

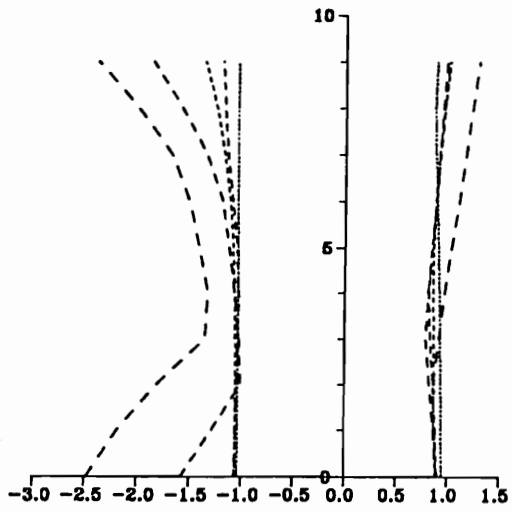


(a) Displacement Ratio

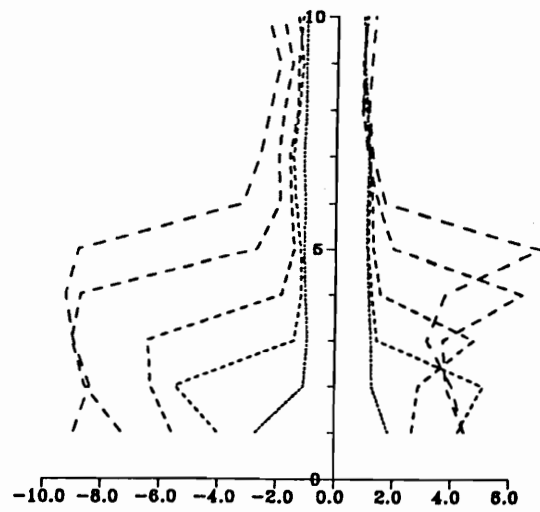


(b) Story Shear Ratio

- 1 story s-structure
- - - 2 stories s-structure
- - - 3 stories s-structure
- - - 4 stories s-structure
- - - 5 stories s-structure

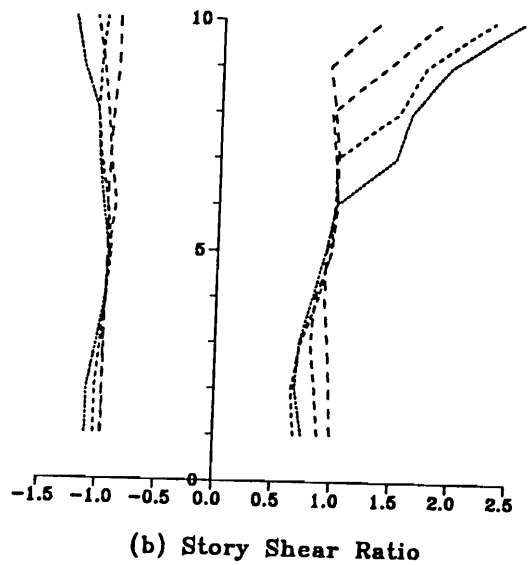
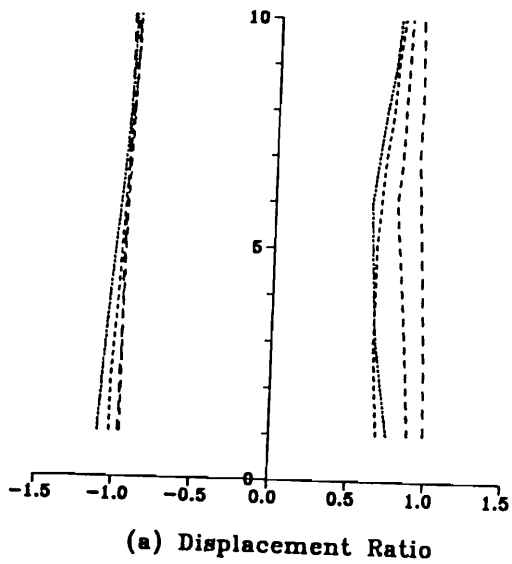


(c) Overturning Moment Ratio



(d) Absolute Acceleration Ratio

Figure 3.19: The effect of changing the height of the s-structure on the ratio of multiple pounding to no-pounding responses of the p-structure (s-structure heights: 1, 2, 3, 4 and 5 stories)



— 6 stories s-structure
 - - - 7 stories s-structure
 - - - 8 stories s-structure
 - - - 9 stories s-structure

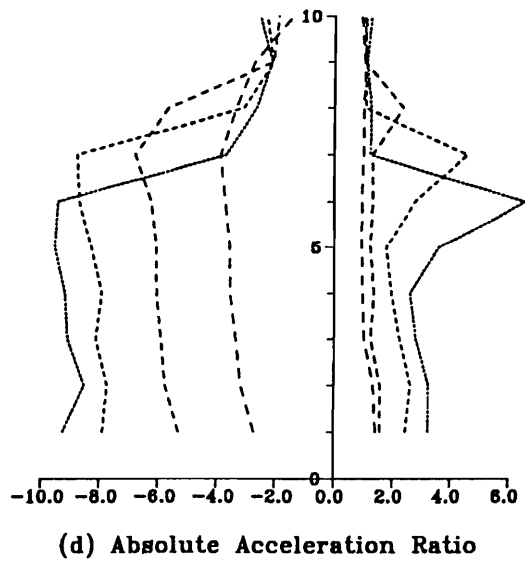
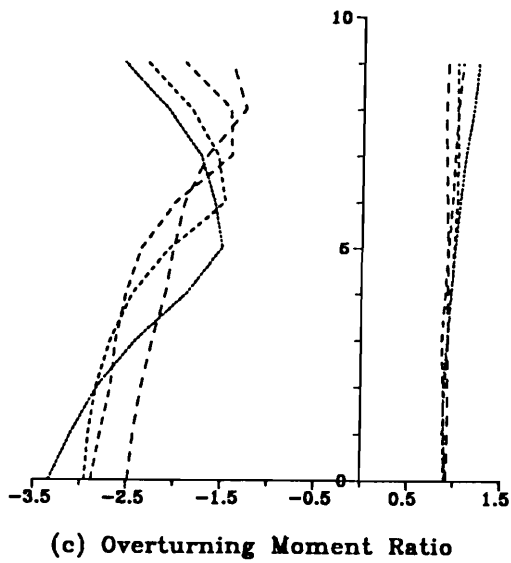
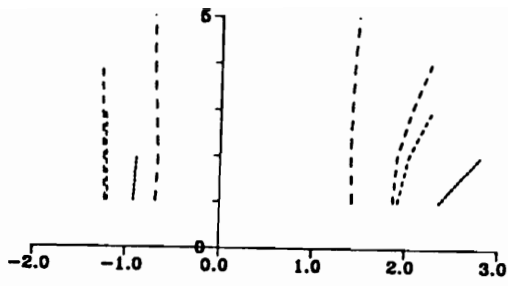
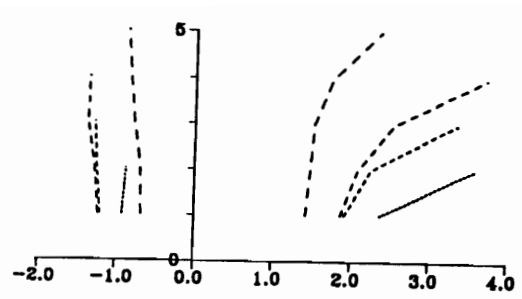


Figure 3.20: The effect of changing the height of the s-structure on the ratio of multiple pounding to no-pounding responses of the p-structure (s-structure heights: 6, 7, 8 and 9 stories)

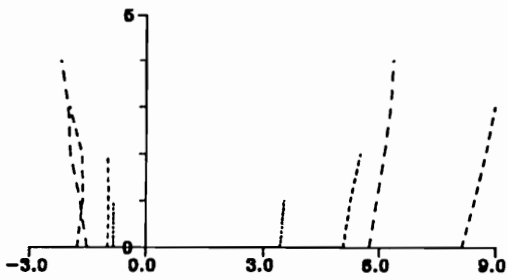


(a) Displacement Ratio

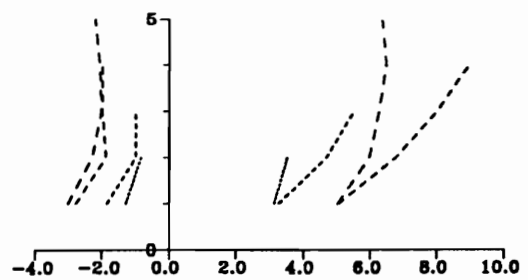


(a) Story Shear Ratio

— 2 stories s-structure
 - - - 3 stories s-structure
 - · - 4 stories s-structure
 · · · 5 stories s-structure

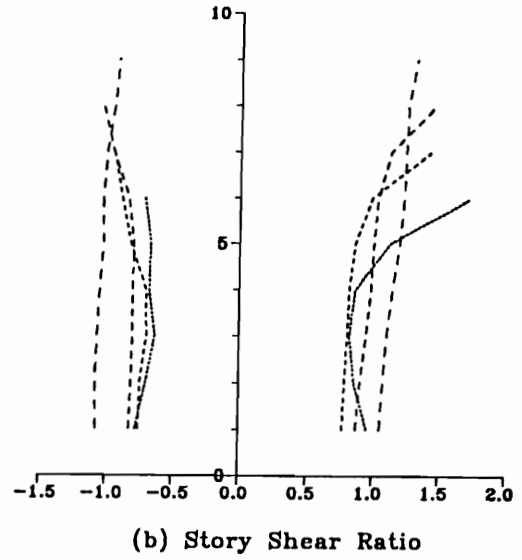
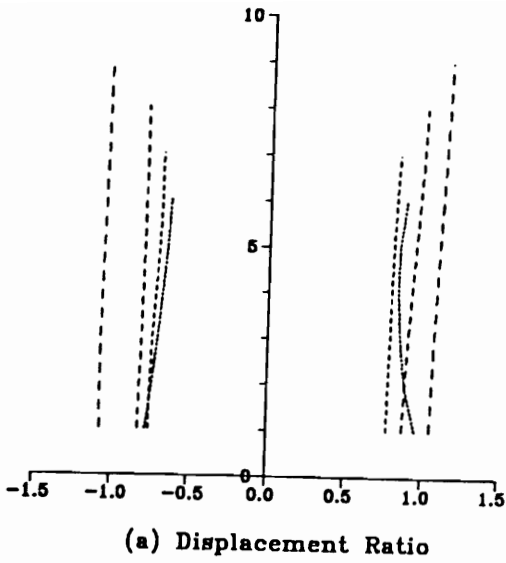


(c) Overturning Moment Ratio



(d) Absolute Acceleration Ratio

Figure 3.21: The effect of changing the height of the s-structure on the ratio of multiple pounding to no-pounding responses of the s-structure (s-structure heights: 1, 2, 3, 4 and 5 stories)



— 6 stories s-structure
 ··· 7 stories s-structure
 - - - 8 stories s-structure
 - · - 9 stories s-structure

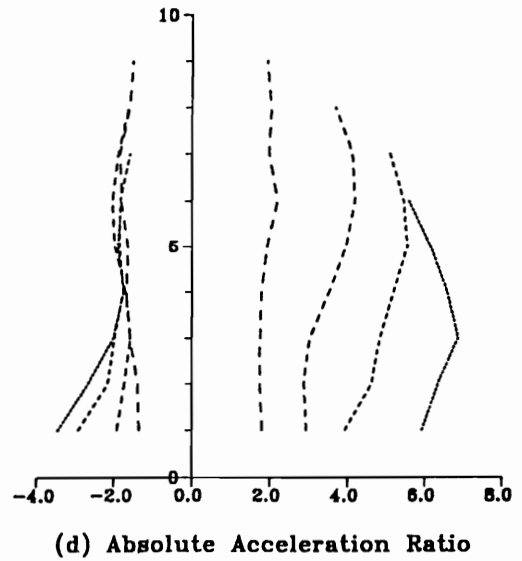
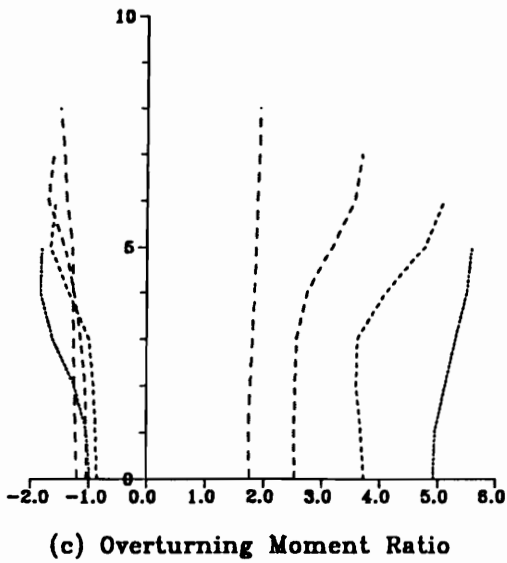


Figure 3.22: The effect of changing the height of the s-structure on the ratio of multiple pounding to no-pounding responses of the s-structure (s-structure heights: 6, 7, 8 and 9 stories)

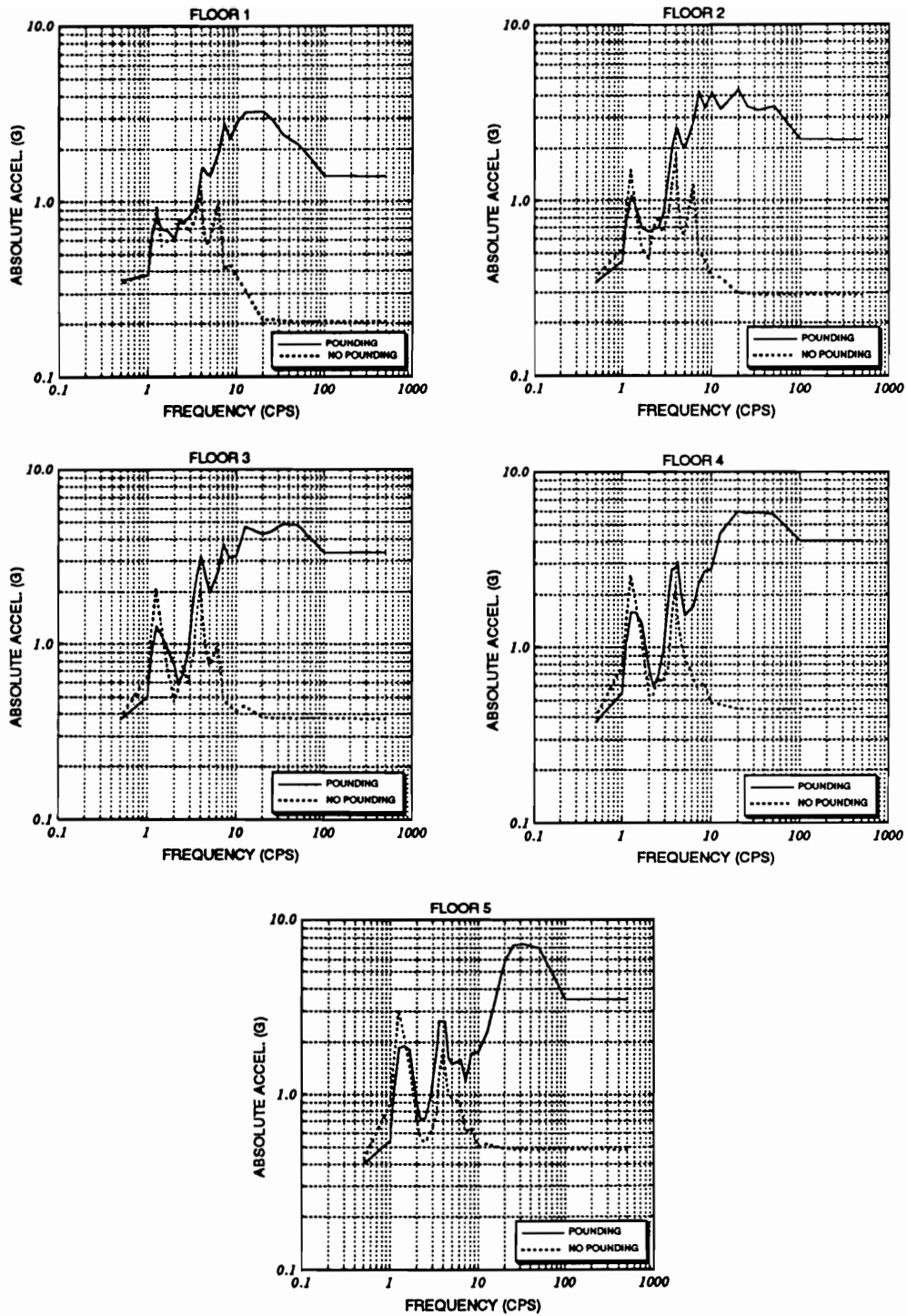


Figure 3.23: Floor acceleration response spectra of various floors in pounding and no-pounding cases for 10-story structure (multiple pounding against 5-story structure)

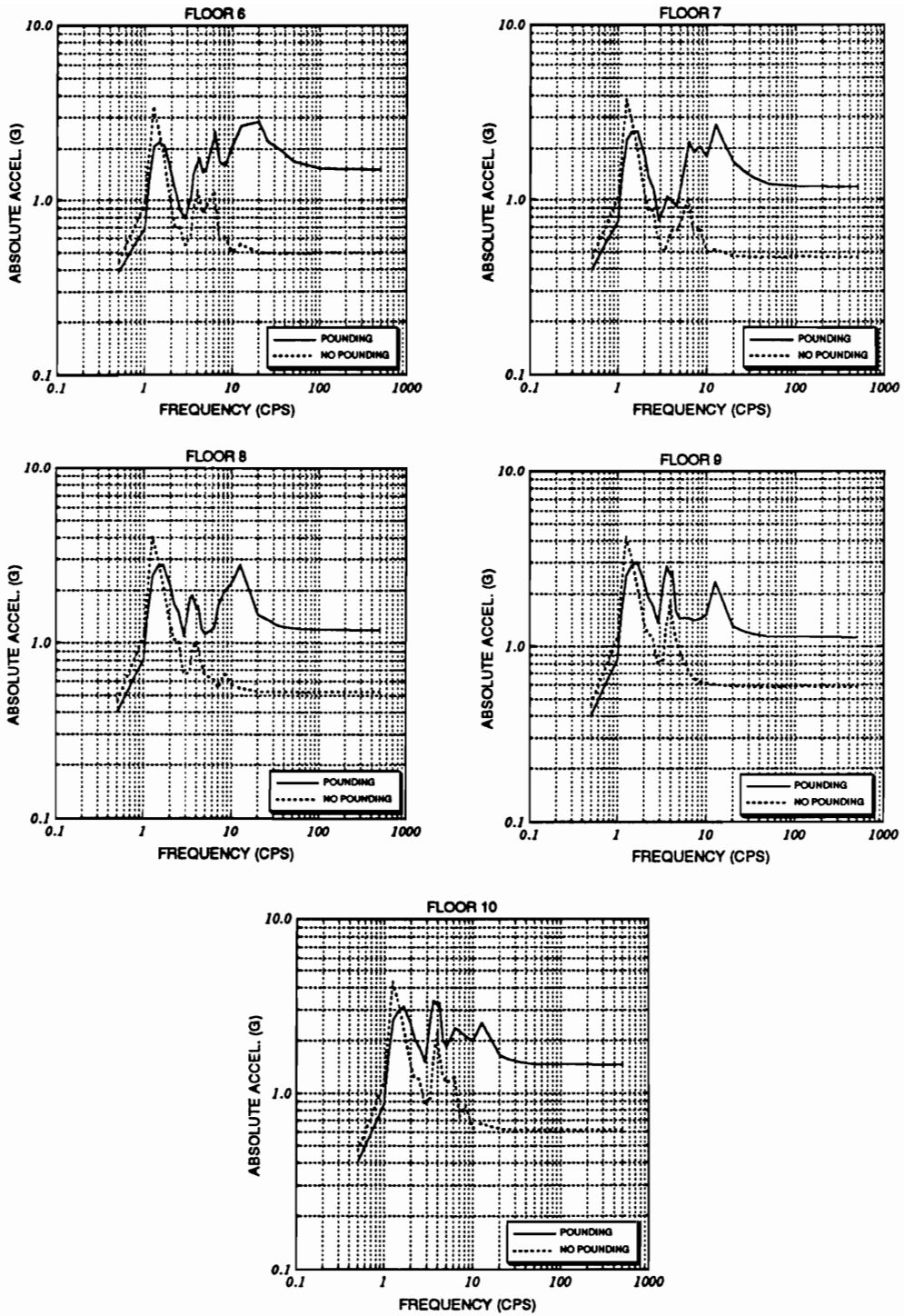


Figure 3.24: Floor acceleration response spectra of various floors in pounding and no-pounding cases for 10-story structure (multiple pounding against 5-story structure)

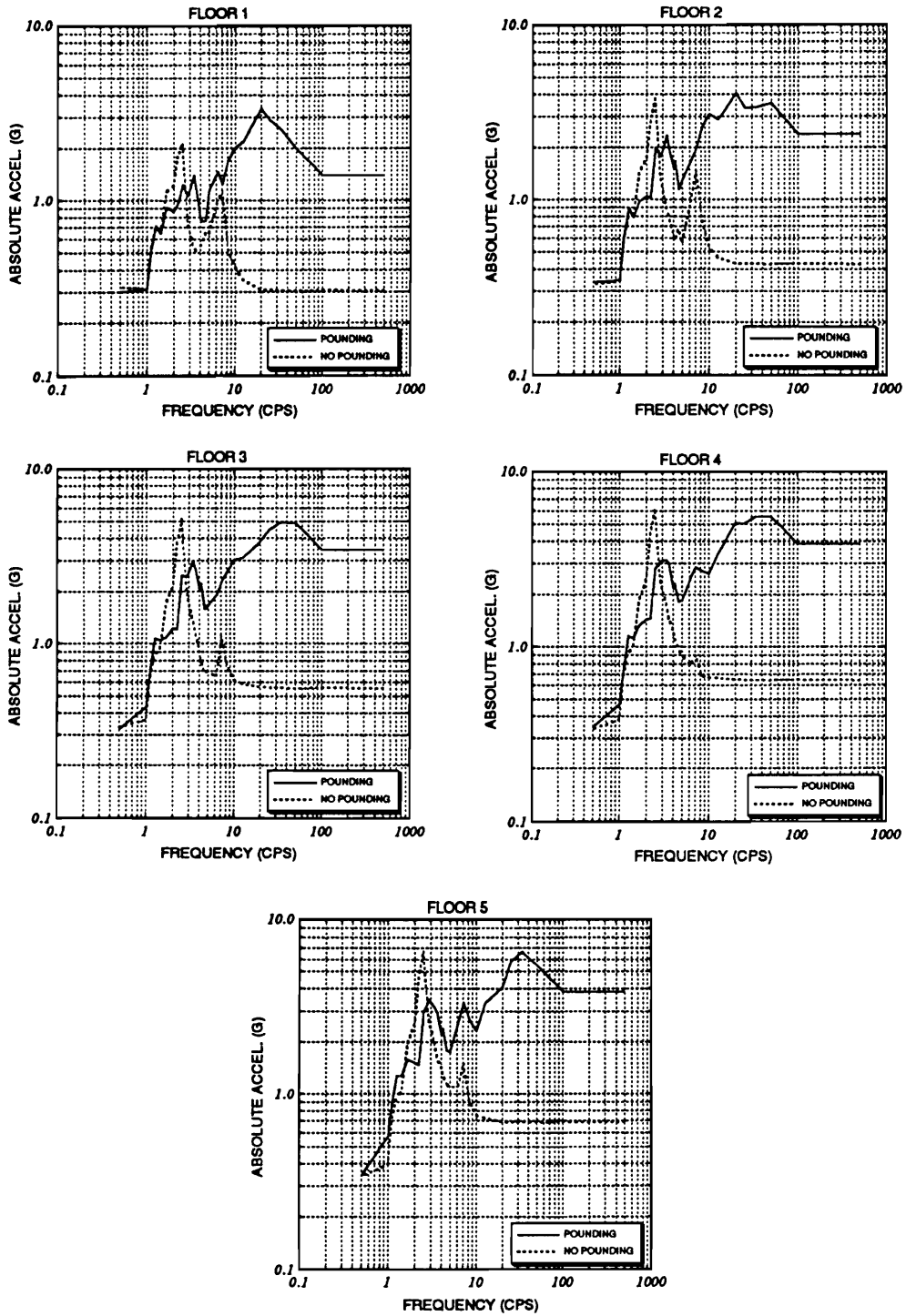


Figure 3.25: Floor acceleration response spectra of various floors in pounding and no-pounding cases for 5-story structure

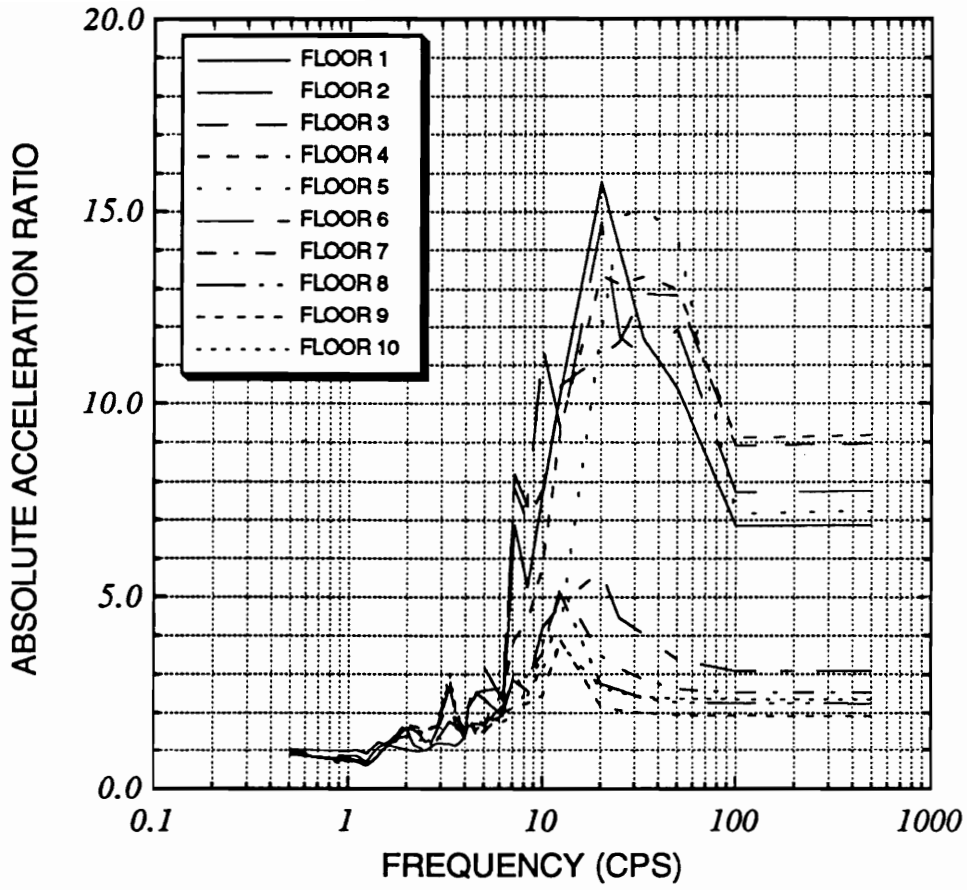


Figure 3.26: Pounding to no-pounding floor response spectrum ratios for 10-story structure

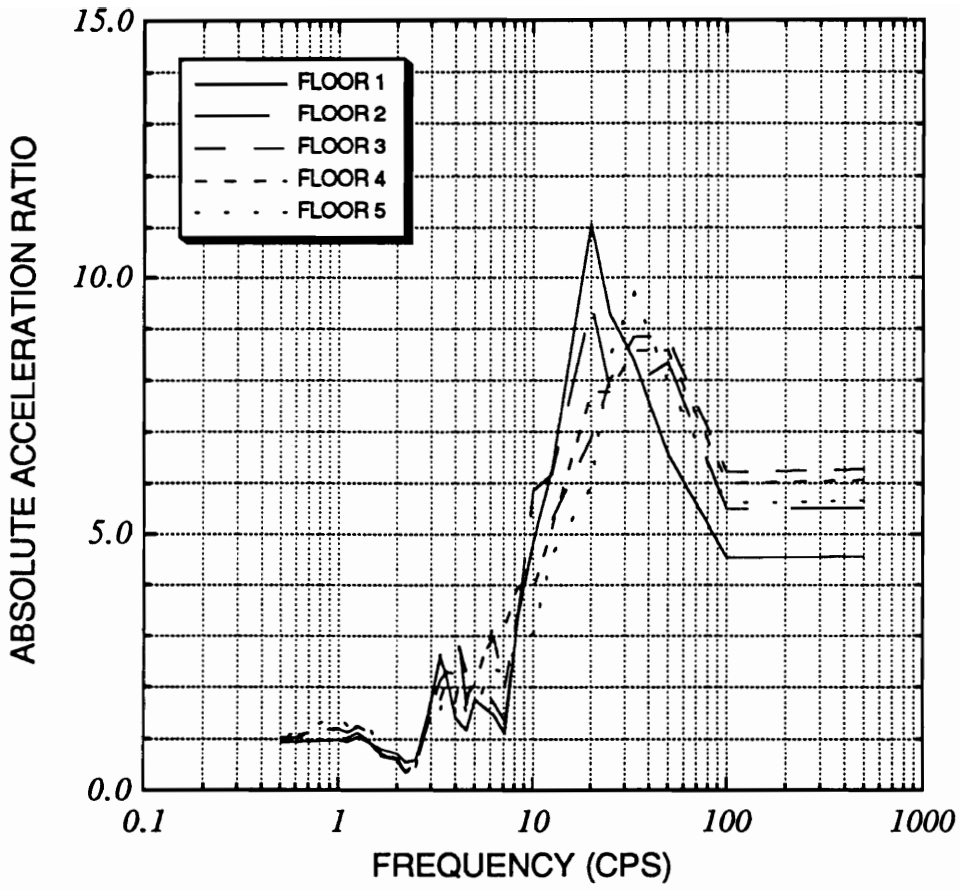
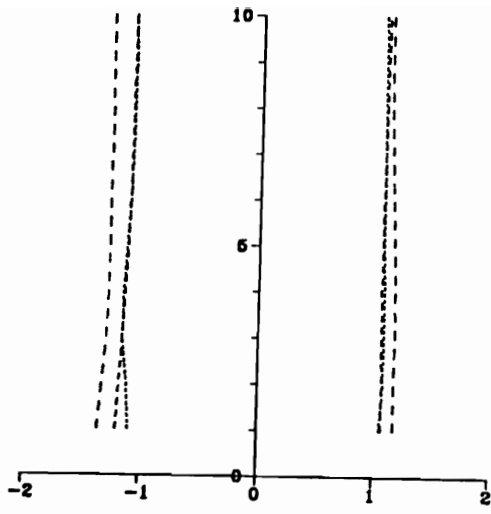
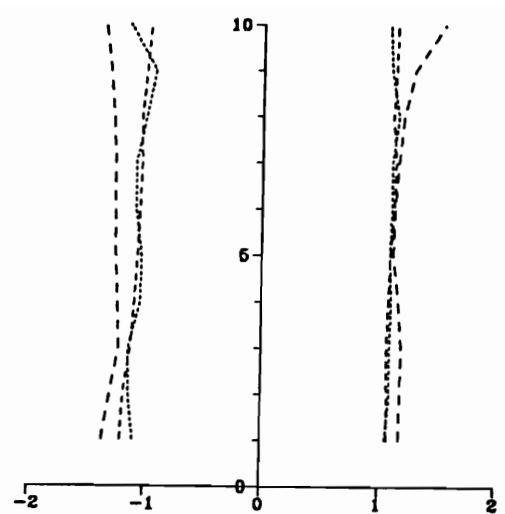


Figure 3.27: Pounding to no-pounding floor response spectrum ratios for 5-story structure

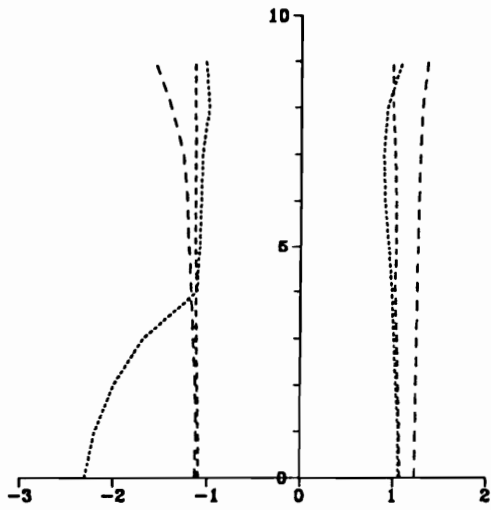


(a) Displacement Ratio

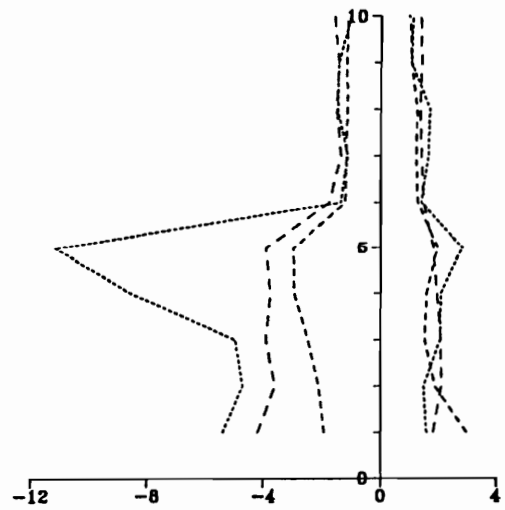


(b) Story Shear Ratio

- - - - $f_1=f_2=0.853$ cps
 - · - · $f_1=f_2=1.304$ cps
 - - - - $f_1=f_2=2.484$ cps

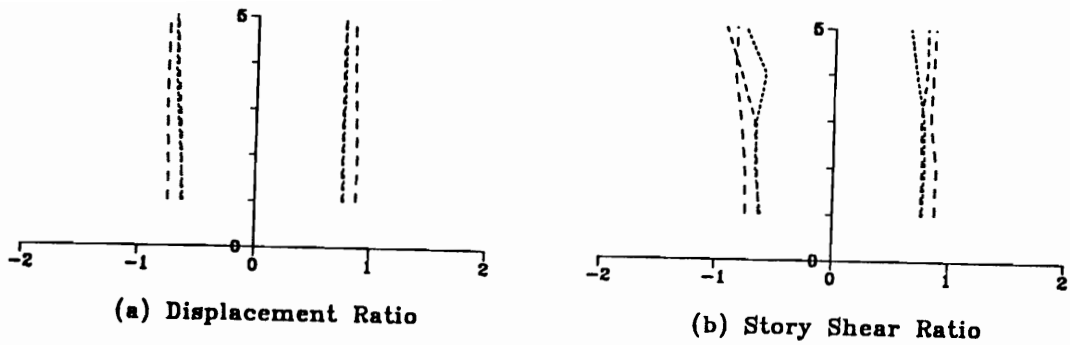


(c) Overturning Moment Ratio



(d) Absolute Acceleration Ratio

Figure 3.28: Pounding response of equal fundamental frequency structures: response ratios for the 10-story structure



- - - - $f_1=f_2=0.653$ cps
 - - - - $f_1=f_2=1.304$ cps
 - - - - $f_1=f_2=2.484$ cps

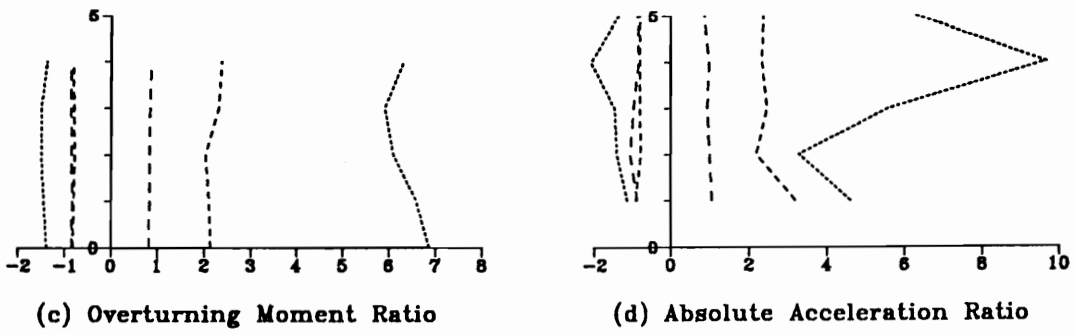
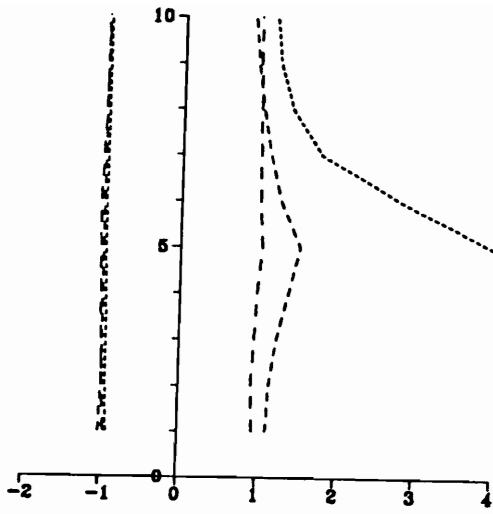
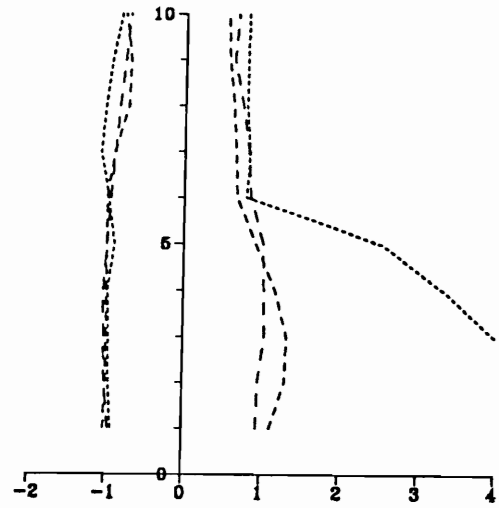


Figure 3.29: Pounding response of equal fundamental frequency structures: response ratios for the 5-story structure

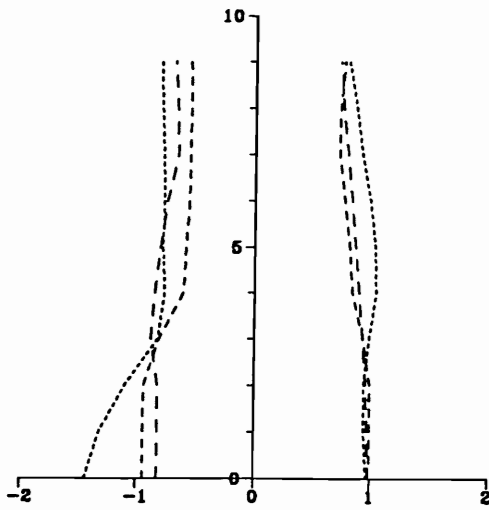


(a) Displacement Ratio

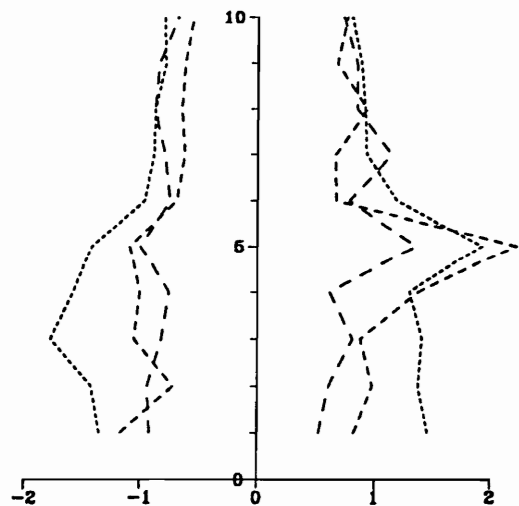


(b) Story Shear Ratio

- - - - $g=0.00$
 - - - - $g=0.0275$ m
 - - - - $g=0.0496$ m



(c) Overturning Moment Ratio



(d) Absolute acceleration Ratio

Figure 3.30: The ratio of responses obtained in pounding against a flexible and a rigid 5-story structure for various gap sizes

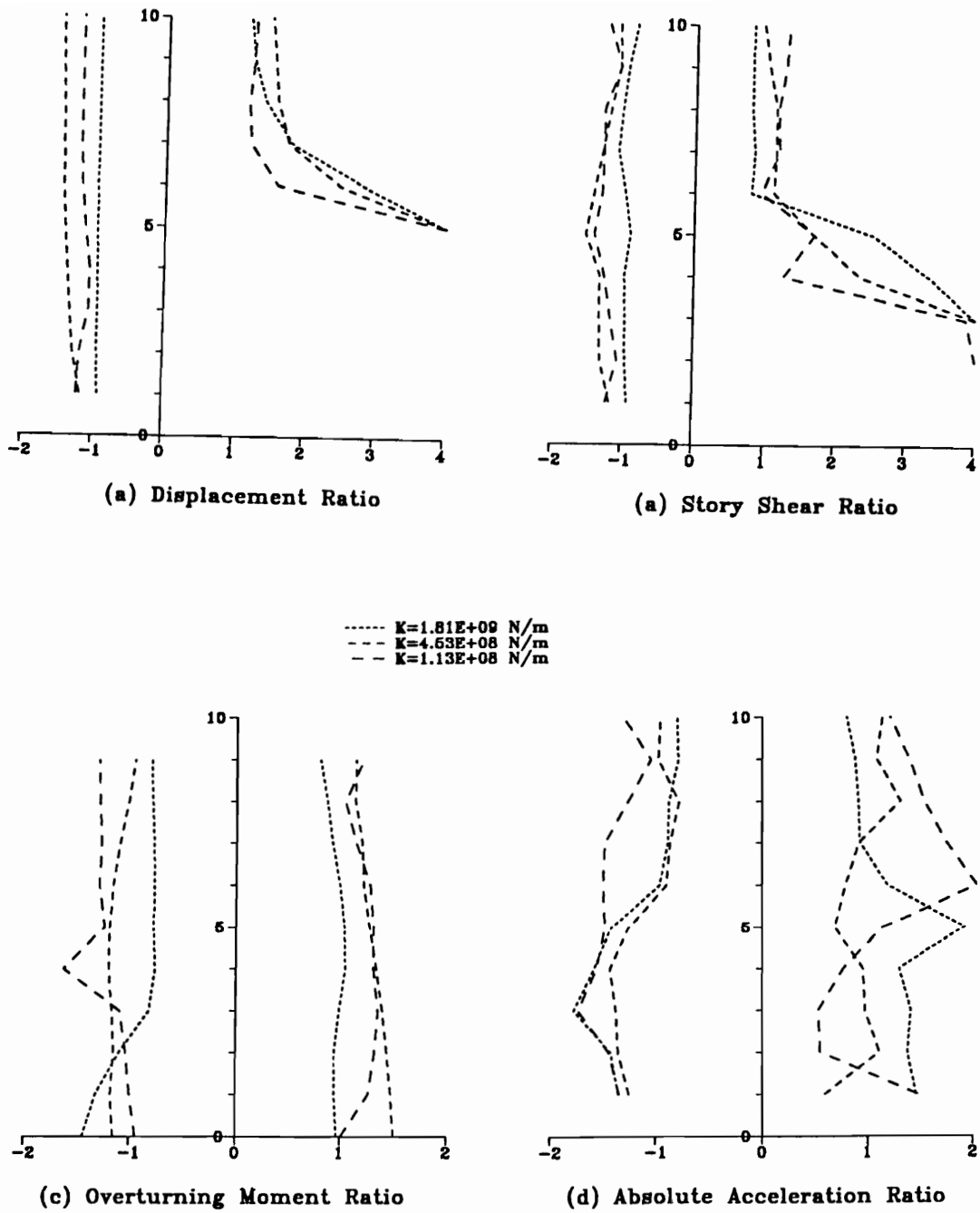


Figure 3.31: The ratio of responses obtained in pounding against a flexible and a rigid 5-story structure for various story stiffnesses of the 10-story structure

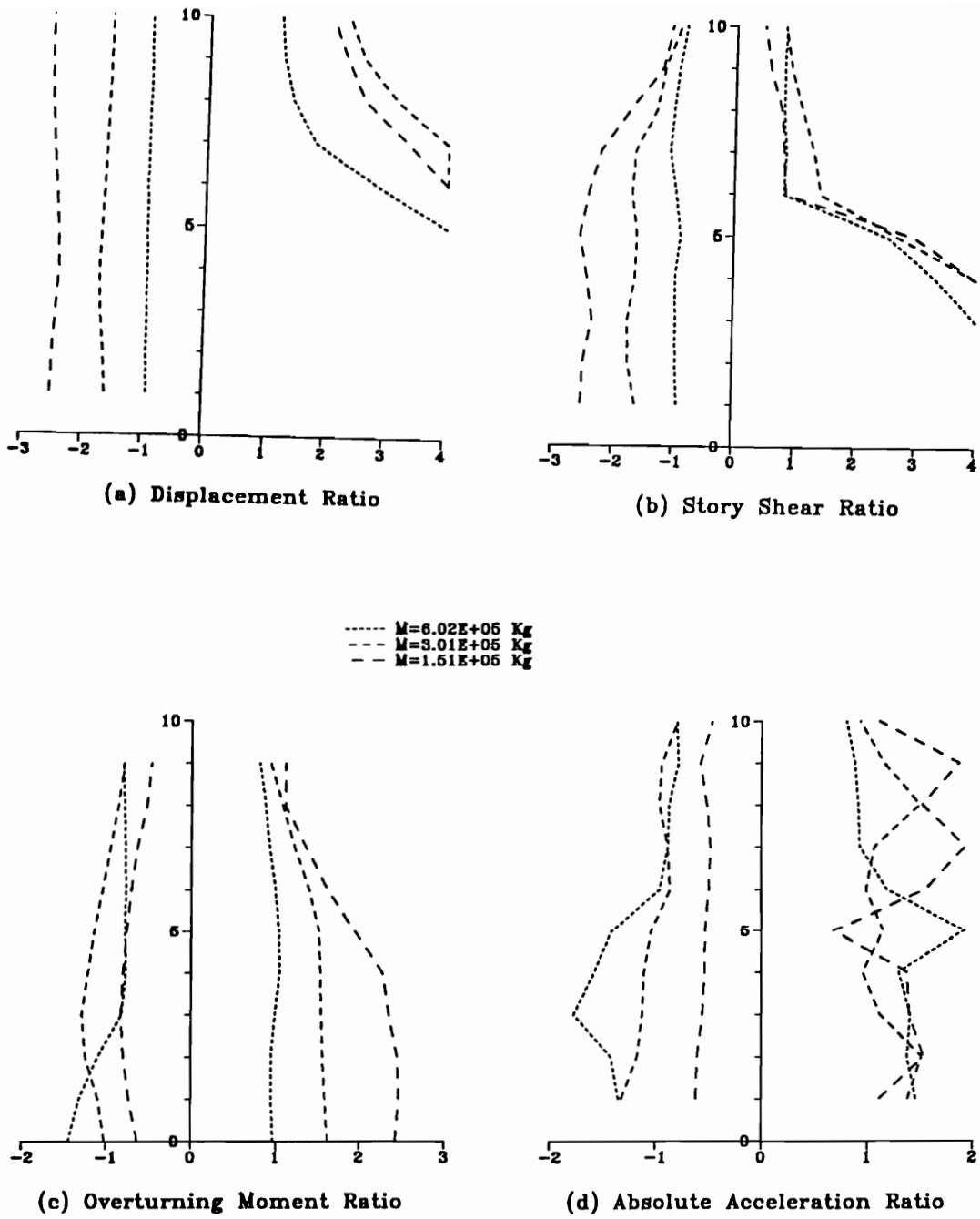
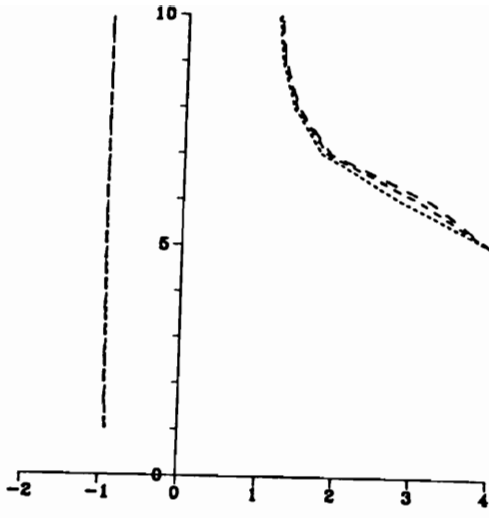
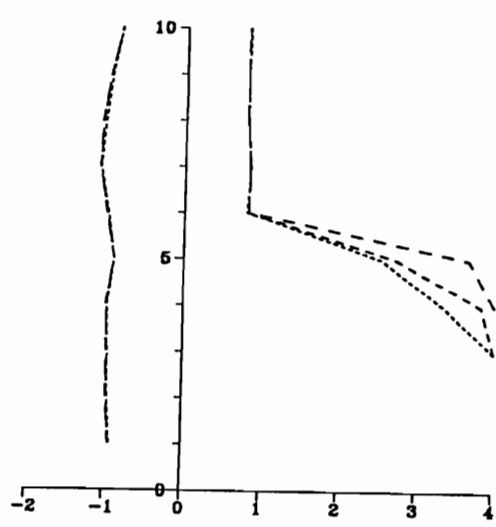


Figure 3.32: The ratio of responses obtained in pounding against a flexible and a rigid 5-story structure for various floor masses of the 10-story structure

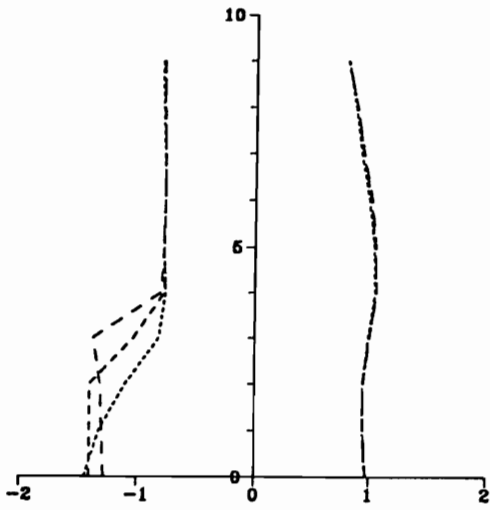


(a) Displacement Ratio

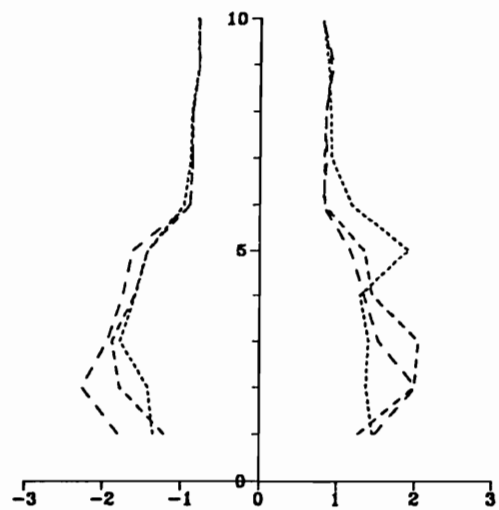


(b) Story Shear Ratio

..... $\mu=8.76E+09$ N/m
 - - - $\mu=1.75E+10$ N/m
 - . - $\mu=3.50E+10$ N/m



(c) Overturning Moment Ratio



(d) Absolute Acceleration Ratio

Figure 3.33: The ratio of responses obtained in pounding against a flexible and a rigid 5-story structure for various impact stiffness coefficients

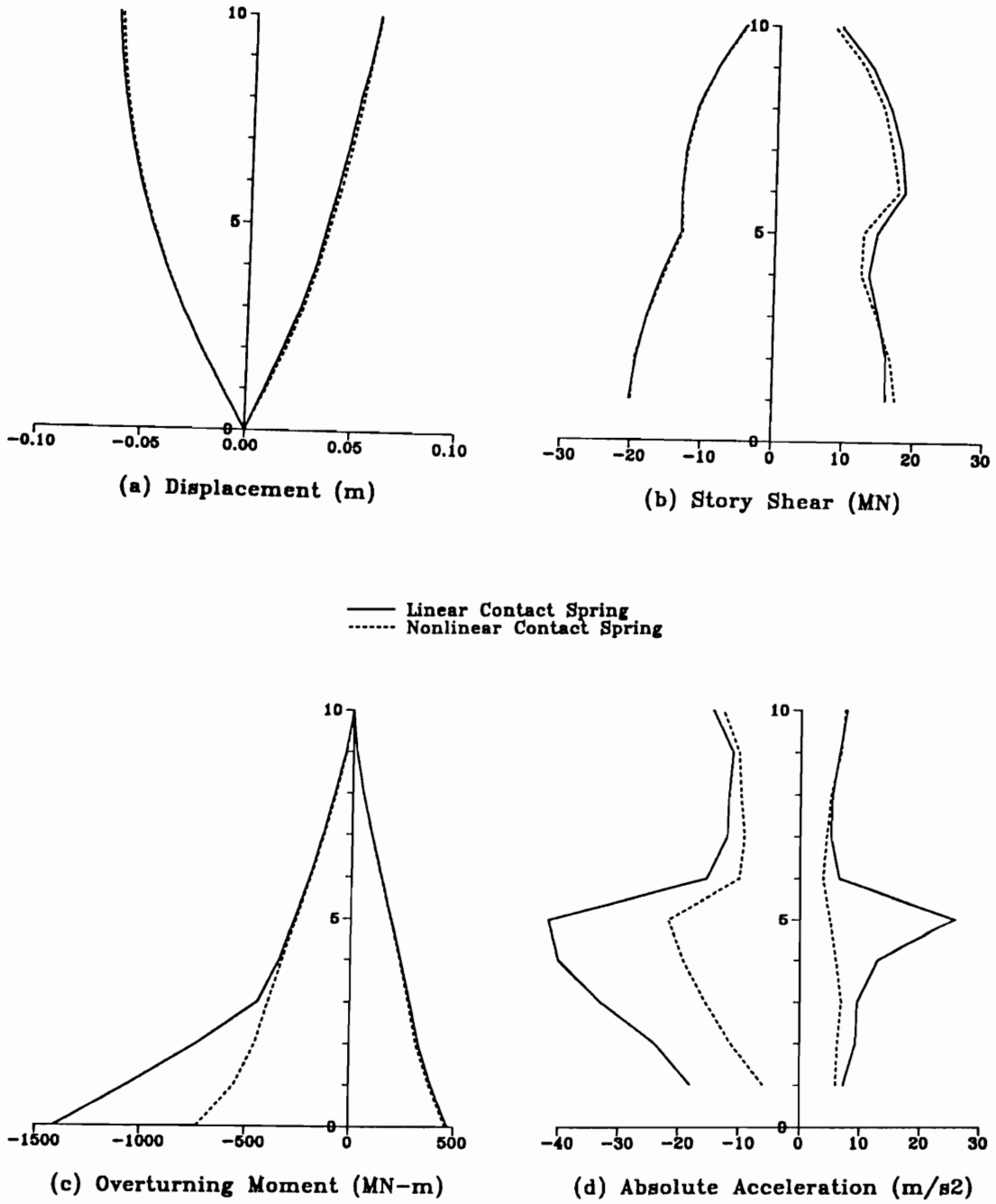
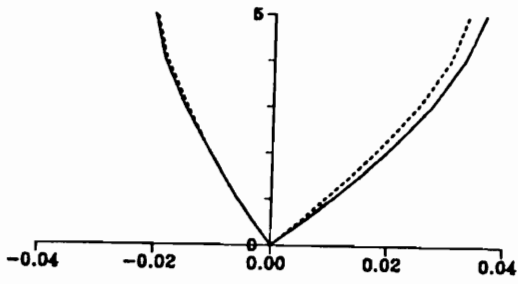
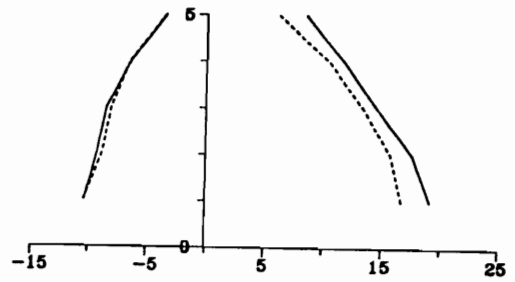


Figure 3.34: The effect of linear and nonlinear modeling of the contact springs on the response of the 10-story structure

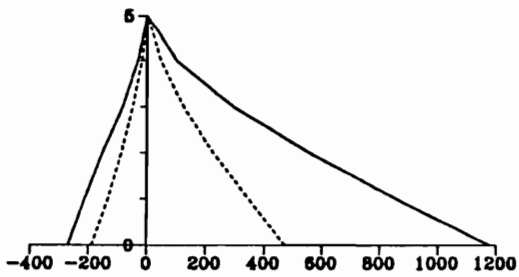


(a) Displacement (m)

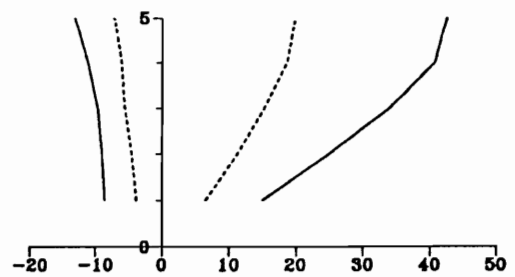


(b) Story Shear (MN)

— Linear Contact Spring
 - - - Nonlinear Contact Spring

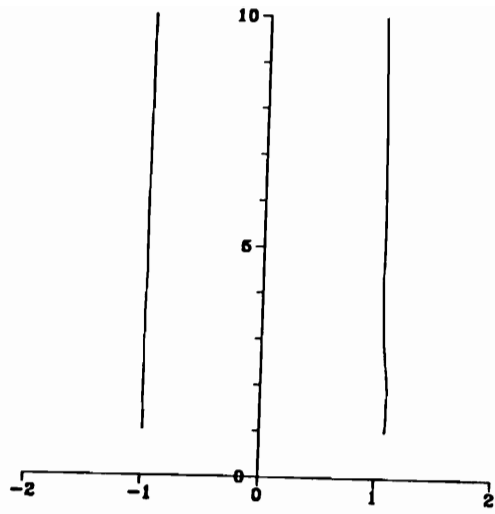


(c) Overturning Moment (MN-m)

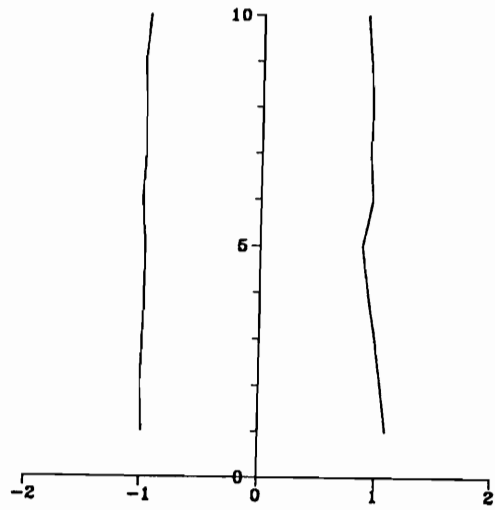


(d) Absolute Acceleration (m/s²)

Figure 3.35: The effect of linear and nonlinear modeling of the contact springs on the response of the 5-story structure

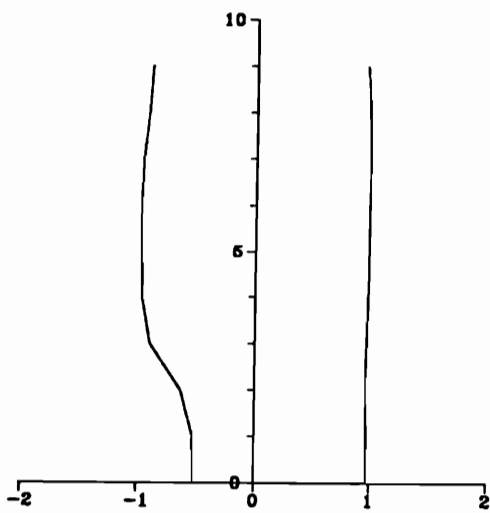


(a) Displacement Ratio

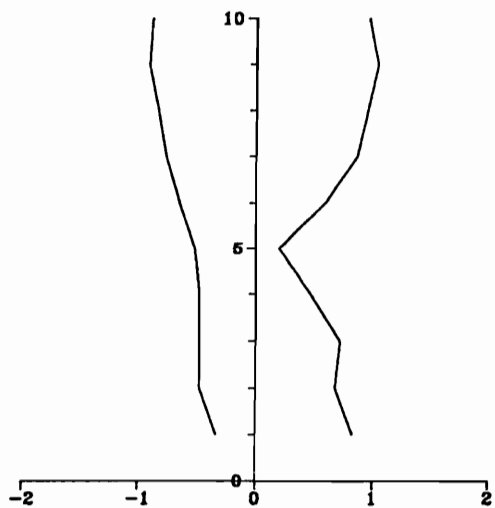


(b) Story Shear Ratio

— Nonlinear / Linear Contact Spring

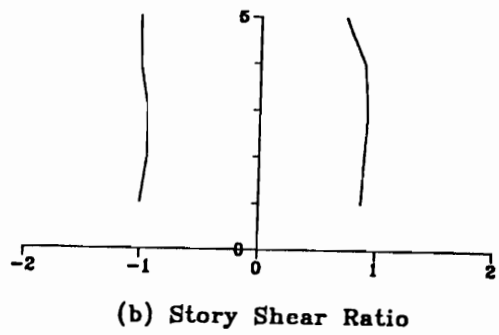
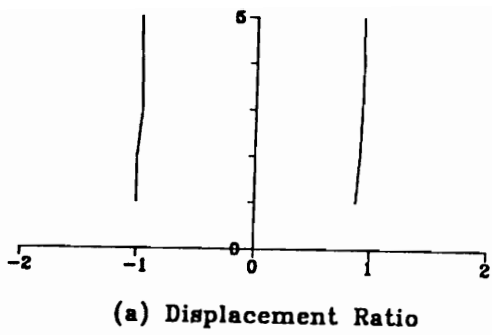


(c) Overturning Moment Ratio



(d) Absolute Acceleration Ratio

Figure 3.36: The ratio of nonlinear to linear pounding responses of the 10-story structure



— Nonlinear / Linear Contact Spring

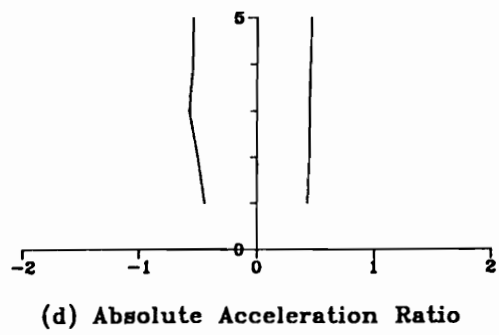
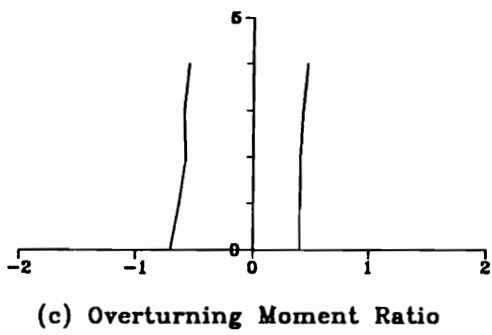


Figure 3.37: The ratio of nonlinear to linear pounding responses of the 5-story structure

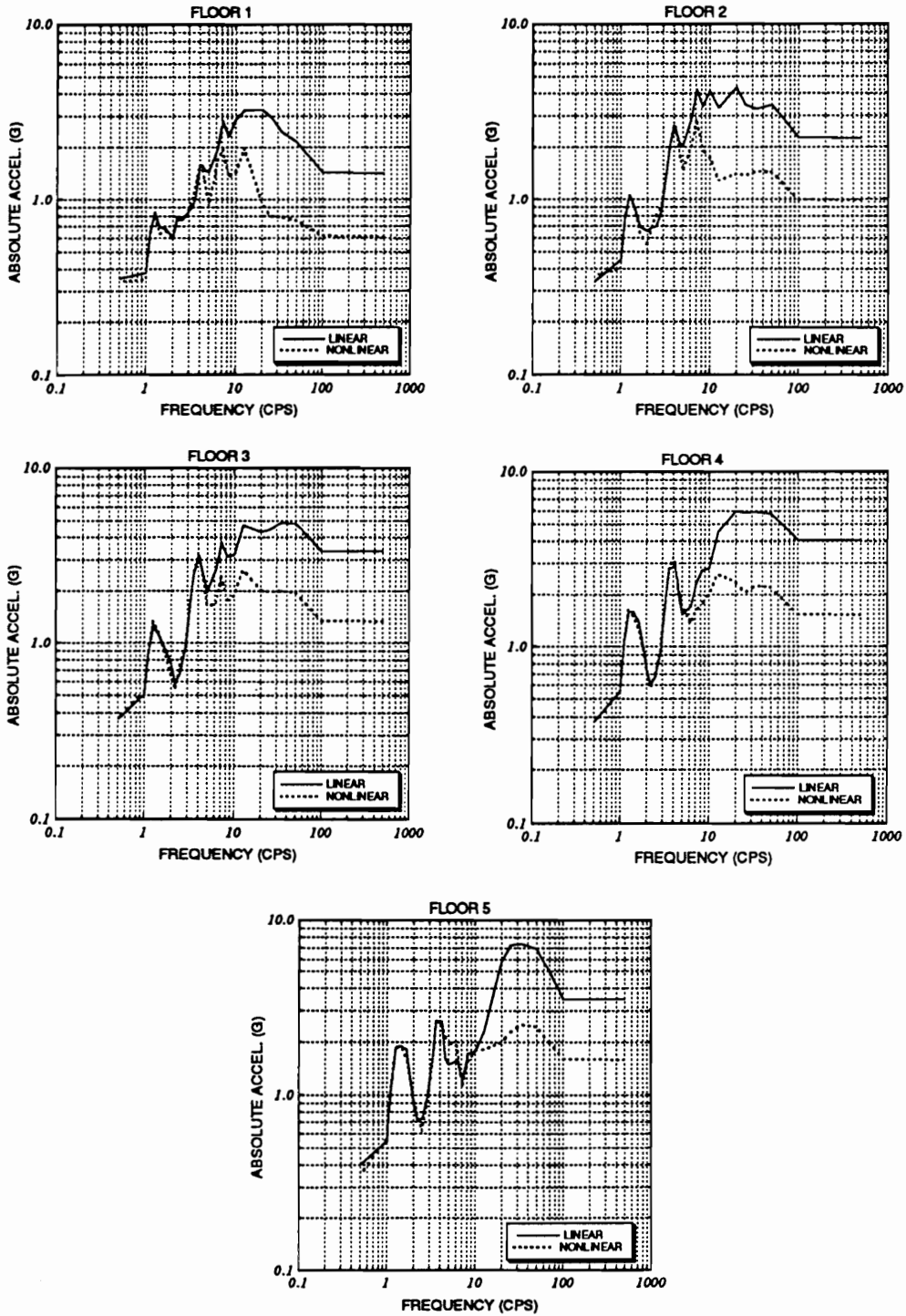


Figure 3.38: Floor acceleration response spectra of various floors of the 10-story structure obtained with linear and nonlinear impact spring model

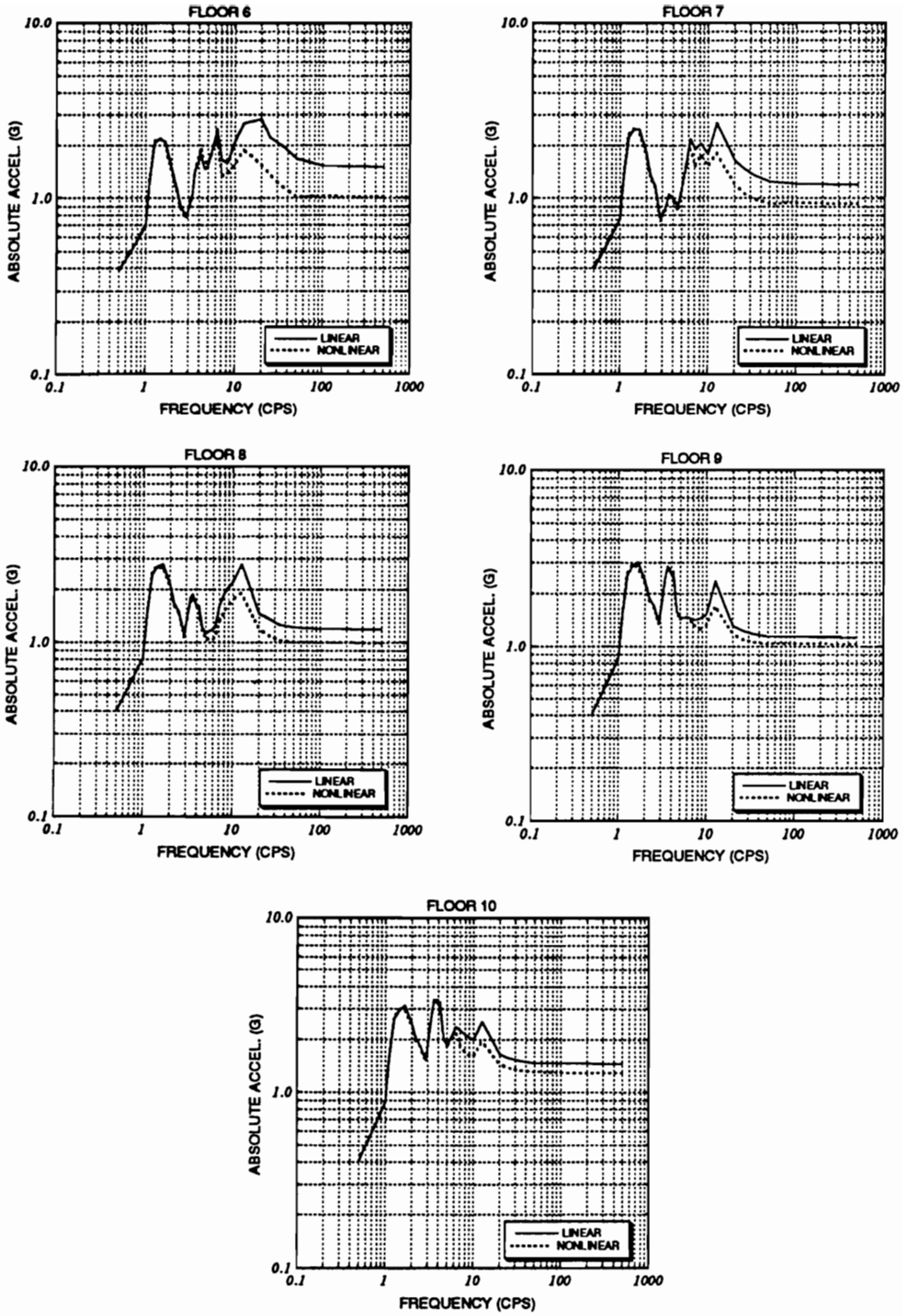


Figure 3.39: Floor acceleration response spectra of various floors of the 10-story structure obtained with linear and nonlinear impact spring model

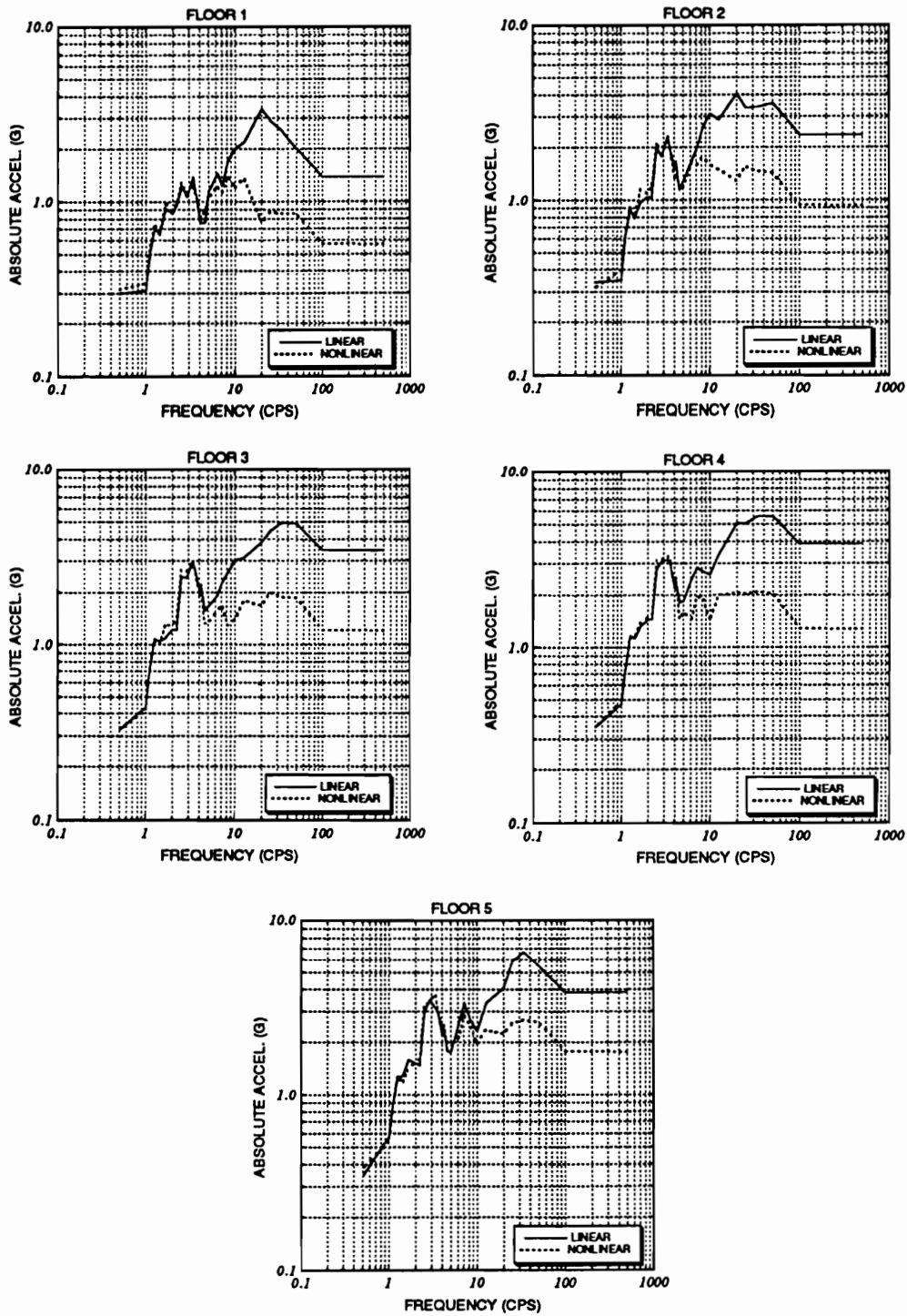


Figure 3.40: Floor acceleration response spectra of various floors of the 5-story structure obtained with linear and nonlinear impact spring model

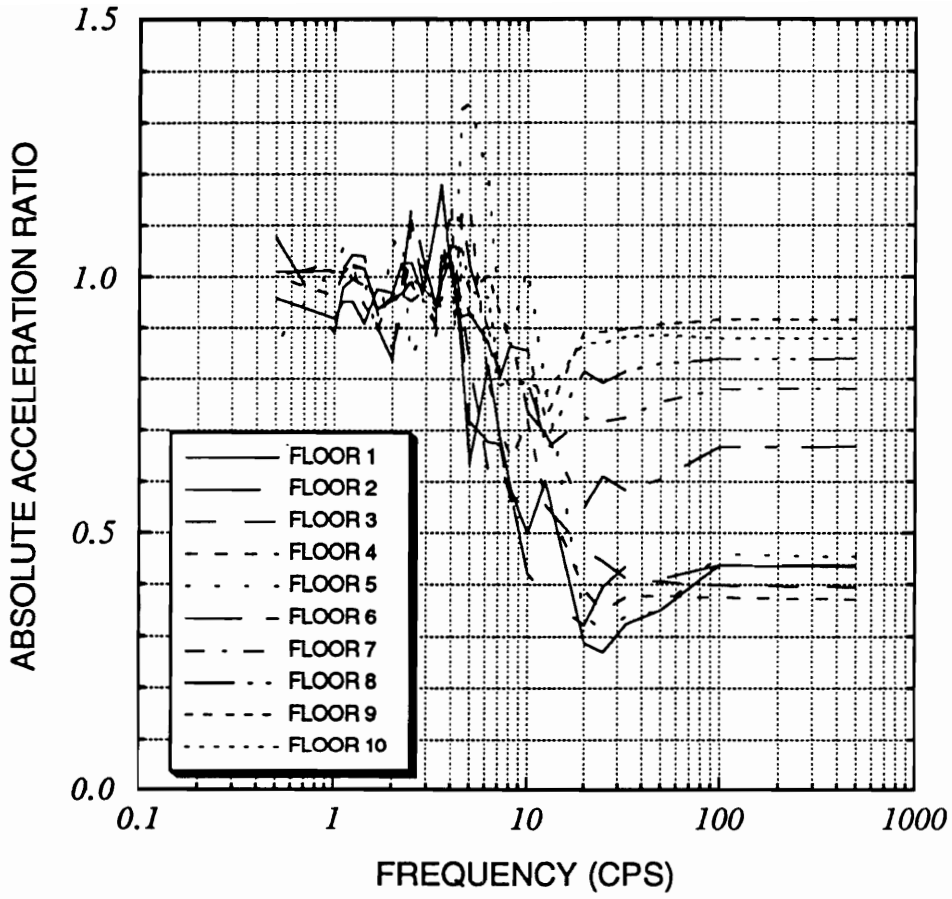


Figure 3.41: Nonlinear to linear pounding floor response spectrum ratios for the 10-story structure

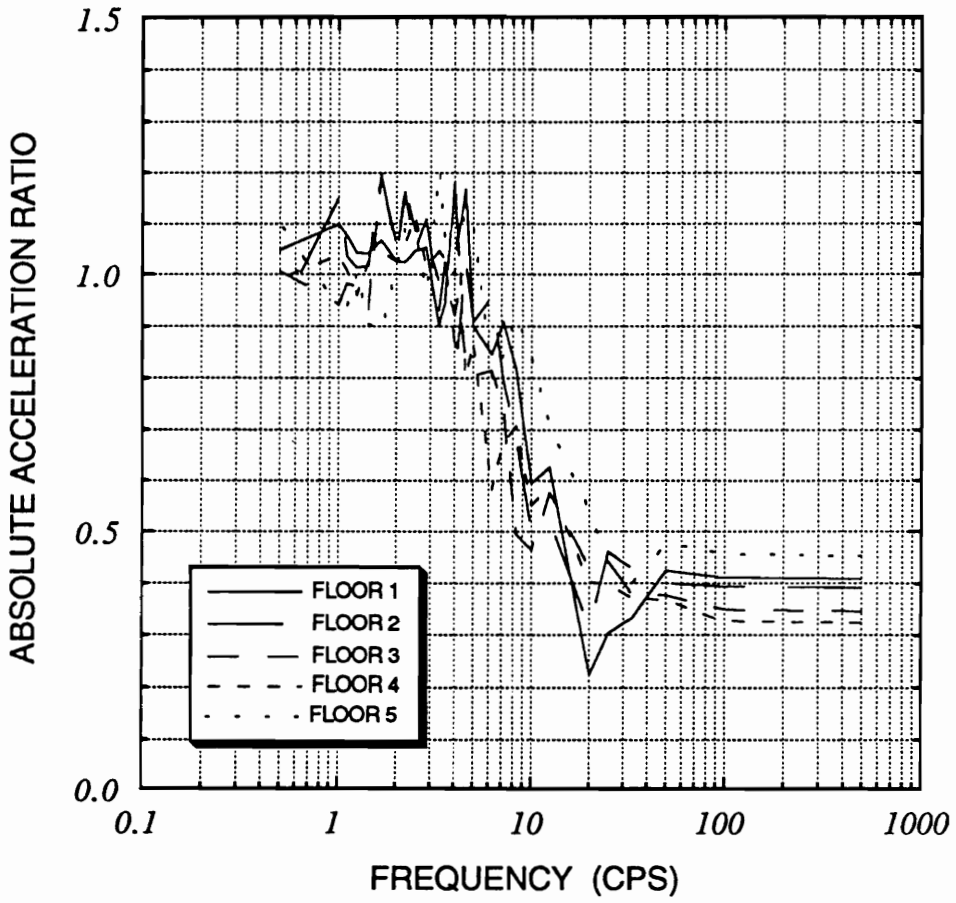


Figure 3.42: Nonlinear to linear pounding floor response spectrum ratios for the 5-story structure

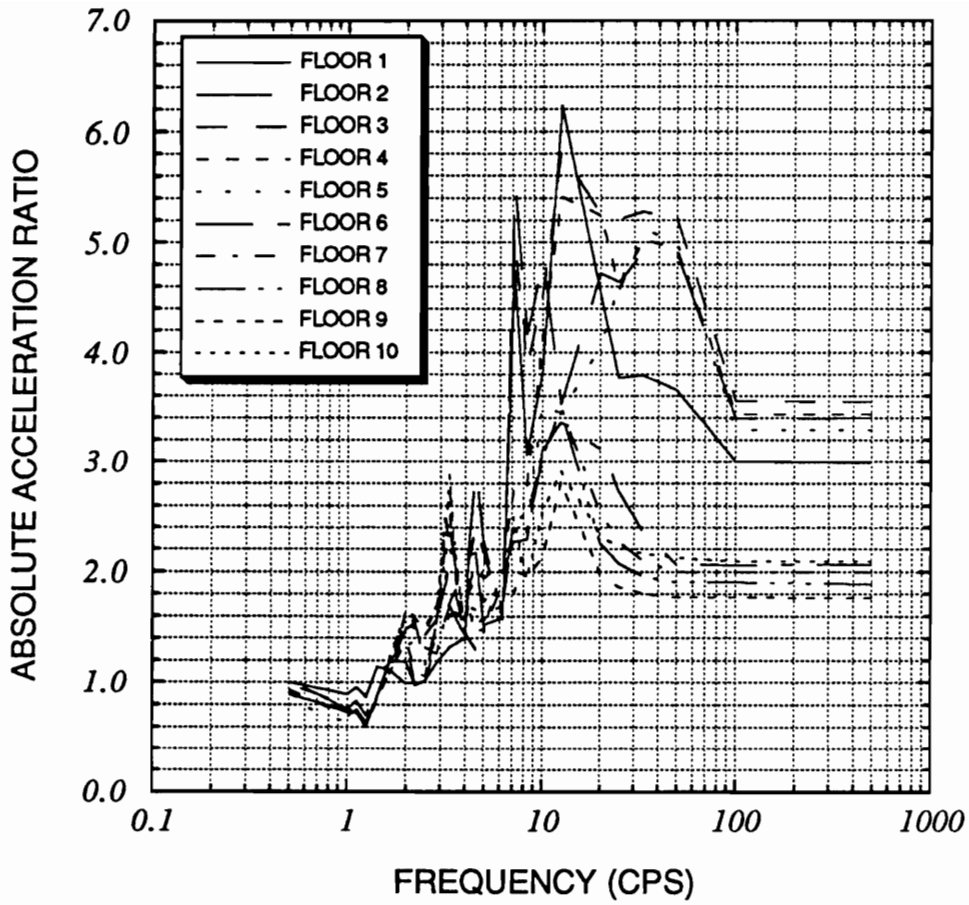


Figure 3.43: Nonlinear to no-pounding floor response spectrum ratios for the 10-story structure

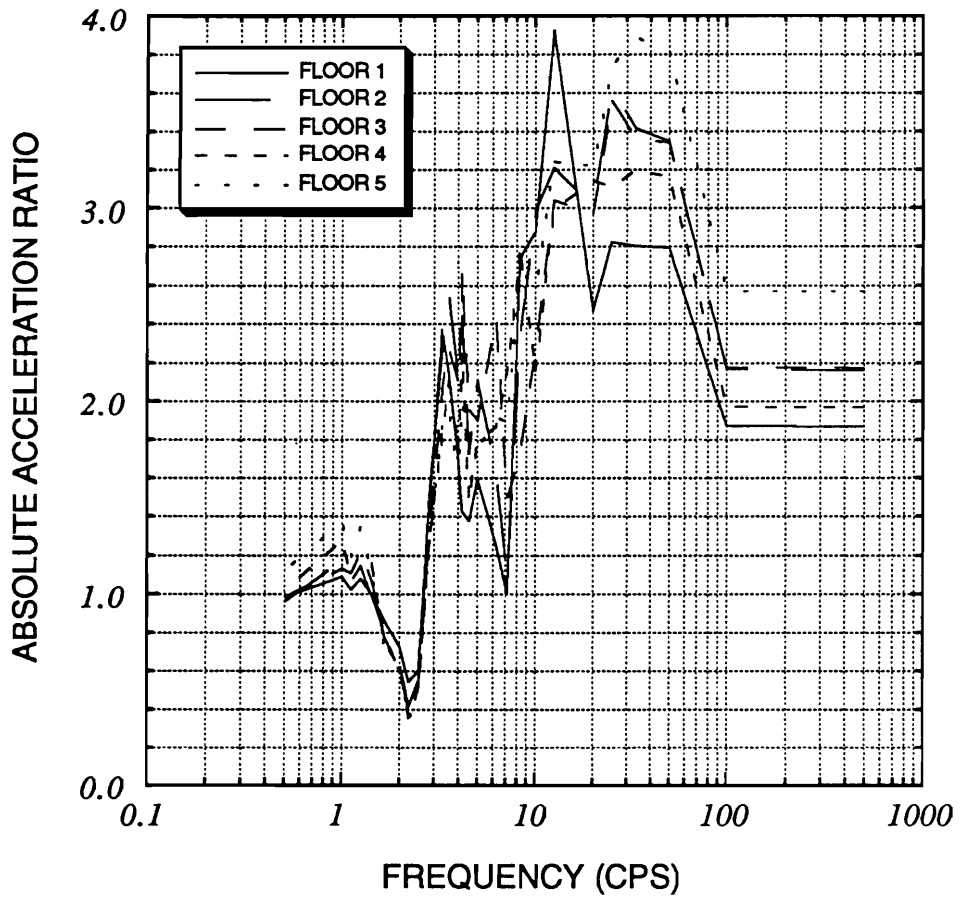


Figure 3.44: Nonlinear to no-pounding floor response spectrum ratios for the 5-story structure

Chapter 4

POUNDING OF STRUCTURES IN SERIES

4.1 Introduction

In chapters 2 and 3 the effects of pounding on the response of two adjacent structures were investigated. In many cities, however, several buildings in a row are commonly put next to each other. During an earthquake they can pound against each other. The end buildings will be subjected to one-sided pounding whereas a building in middle will be subjected to pounding on both sides. In this chapter, therefore, the problem of earthquake-induced pounding of multi-degree-of-freedom adjacent structures in a row will be examined. There can be many different possible arrangements of buildings in a row. Here, however, the numerical results for a simpler case of three buildings of the same height in a row are obtained. The effect of pounding on the response of the interior building subjected to two-sided impact, and the response of the exterior structures, subjected to one-sided impact, are investigated.

4.2 Equations of Motion

Let there be q adjacent buildings in a block, each modeled as a p degrees-of-freedom shear building. It is assumed that the floor heights of the structures are the same, and therefore the pounding will occur only at their floor levels. A schematic of such pounding structures in series is shown in Figure 4.1. As before, the impact is modeled by a linear spring and dashpot elements introduced between the pounding floor masses.

To develop the equations of motion, consider the free body diagram of a typical mass m_i of the interior and exterior buildings in a state of pounding shown in Figures 4.2 and 4.3

respectively. Using Newton's law, the equations of motion for the masses of the interior and exterior buildings can be written as:

Interior Building:

$$\begin{aligned}
m_{i,j}\ddot{x}_{i,j}(t) &+ (k_{i,j} + k_{i+1,j} + s_{j-1} + s_j)x_{i,j}(t) - k_{i,j}x_{i-1,j}(t) \\
&- k_{i+1,j}x_{i+1,j}(t) + (d_{j-1} + d_j)\dot{x}_{i,j}(t) - d_{j-1}\dot{x}_{i,j-1}(t) \\
&- d_j\dot{x}_{i,j+1}(t) - s_{j-1}x_{i,j-1}(t) - s_jx_{i,j+1}(t) \\
&+ s_{j-1}g_{j-1} - s_jg_j = -m_{i,j}\ddot{x}_g(t)
\end{aligned} \tag{4.1}$$

Exterior Building:

$$\begin{aligned}
m_{i,1}\ddot{x}_{i,1}(t) &+ (k_{i,1} + k_{i+1,1} + s_1)x_{i,1}(t) - k_{i,1}x_{i-1,1}(t) \\
&- k_{i+1,1}x_{i+1,1}(t) + d_1\dot{x}_{i,1}(t) - d_1\dot{x}_{i,2}(t) \\
&- s_1x_i(t) - s_1g_1 = -m_{i,1}\ddot{x}_g(t)
\end{aligned} \tag{4.2}$$

where $x_{i,j}$, $m_{i,j}$ and $k_{i,j}$, respectively, are the relative displacement, mass and the combined column stiffness of the i -th story of the j -th structure. The stiffness and damping coefficients of the impact element introduced between colliding masses, $m_{i,j}$ and $m_{i,j+1}$, are s_j and d_j , respectively. The gap between these masses is denoted by g_j and $\ddot{x}_g(t)$ is the ground acceleration.

Equation 4.1 is the general equation of motion of the mass m_i for either interior building which undergoes the two-sided impact or the exterior building which is pounded on one side only. It is noted that equation 4.2 can also be derived from equation 4.1 by setting $j = 1$ and letting the terms containing s_{j-1} and d_{j-1} become zero. Also in the case of no-pounding when:

$$\begin{aligned}
\delta_{i1} &= x_{i,j-1} - x_{i,j} - g_{j-1} < 0 \\
\delta_{i2} &= x_{i,j} - x_{i,j+1} - g_j < 0
\end{aligned} \tag{4.3}$$

then the terms containing s_{j-1} , s_j , d_{j-1} and d_j in equation 4.1 are set equal to zero.

Collecting equations for all masses, the combined equations of motion of the q pounding buildings can be written as:

$$[M]\{\ddot{X}\} + [C]\{\dot{X}\} + [K]\{X\} + \{F\} = -[M]\{r\}\ddot{x}_g(t) \quad (4.4)$$

where

$$[M] = \begin{bmatrix} [M_1] & 0 & \dots & 0 \\ & [M_2] & \dots & 0 \\ SYM. & & \ddots & \vdots \\ & & & [M_q] \end{bmatrix} \quad (4.5)$$

$$[C] = \begin{bmatrix} [C_1] & 0 & \dots & 0 \\ & [C_2] & \dots & 0 \\ SYM. & & \ddots & \vdots \\ & & & [C_q] \end{bmatrix} + [D] \quad (4.6)$$

$$\left[K \right] = \begin{bmatrix} [K_1] & 0 & \cdots & 0 \\ & [K_2] & \cdots & 0 \\ SYM. & & \ddots & \vdots \\ & & & [K_q] \end{bmatrix} + \left[S \right] \quad (4.7)$$

$$\left[S \right] = \begin{bmatrix} [S_1] & -[S_1] & 0 & \cdots & 0 \\ & [S_1] + [S_2] & -[S_2] & \cdots & 0 \\ & & \ddots & \ddots & \vdots \\ SYM. & & & [S_{q-2}] + [S_{q-1}] & -[S_{q-1}] \\ & & & & [S_{q-1}] \end{bmatrix} \quad (4.8)$$

where

$$\left[S_i \right] = \begin{bmatrix} s_i & 0 & \cdots & 0 \\ & s_i & \cdots & 0 \\ SYM. & & \ddots & \vdots \\ & & & s_i \end{bmatrix} \quad (4.9)$$

and

$$\{ F \} = \begin{Bmatrix} \{ F_1 \} \\ \{ F_2 \} \\ \vdots \\ \{ F_{q-1} \} \\ \{ F_q \} \end{Bmatrix} \quad (4.10)$$

where

$$\begin{aligned} \{ F_1 \} &= -[S_1] \begin{Bmatrix} g_1 \\ \vdots \\ g_1 \end{Bmatrix} \\ \{ F_2 \} &= [S_1] \begin{Bmatrix} g_1 \\ \vdots \\ g_1 \end{Bmatrix} - [S_2] \begin{Bmatrix} g_2 \\ \vdots \\ g_2 \end{Bmatrix} \\ \{ F_{q-1} \} &= [S_{q-2}] \begin{Bmatrix} g_{q-2} \\ \vdots \\ g_{q-2} \end{Bmatrix} - [S_{q-1}] \begin{Bmatrix} g_{q-1} \\ \vdots \\ g_{q-1} \end{Bmatrix} \\ \{ F_q \} &= [S_{q-1}] \begin{Bmatrix} g_{q-1} \\ \vdots \\ g_{q-1} \end{Bmatrix} \end{aligned} \quad (4.11)$$

Each structure is described by stiffness matrix $[K_n]$, damping matrix $[C_n]$, and mass

matrix $[M_n]$, where $n = 1, \dots, q$. They are the same as those defined in chapter 2. The matrix $[D]$ in equation 4.6 is of the same form as matrix $[S]$, except that s_i in equation 4.8 are replaced by d_i to obtain $[D]$. It is noted that matrix $[S]$ is of order q and submatrices $[S_i]$ are of order p .

The system of equations 4.4 is solved by the Newmark- β approach to obtain numerical results for the parametric study.

4.3 Numerical Results

Numerical results have been obtained for three pounding shear beam structures in a row. Each structure has ten stories. The “observed” structure or “examined” structure for which the response values are presented in the following pages could be an interior or an exterior structure. The structural parameters for the examined structure are: the floor mass $= 6.02E + 5 \text{ Kg}$, story stiffness $= 1.81E + 9 \text{ N/m}$ and the fundamental frequency $= 1.304 \text{ cps}$. All the results discussed in the following and presented in Figures 4.4 through 4.7 are for this structure with these mass and stiffness properties. When this structure is placed at the corner, it is referred to as the exterior structure and when it is in the middle of the row, it is called the interior structure. The stiffness of the impact spring is chosen as $8.76E + 9 \text{ N/m}$ and a dashpot with coefficient $d_i = 2.04E + 7 \text{ Kg/sec}$ has been added at each pounding interface to include some loss of energy due to pounding in the analysis. The damping ratio of 0.05 has been assumed in each mode.

Based on the study in the previous chapter, the effect of varying the important parameters of fundamental frequency, floor mass, gap size and impact element stiffness on the pounding response is examined in this chapter.

The seismic base motion used to obtain the numerical results is the 1941 N-S El Centro component with maximum ground acceleration level of $0.2 G$.

Effect of Adjacent Building Frequency

In Figure 4.4 we show the pounding to no-pounding displacement, story shear, floor

acceleration and overturning moment responses of the exterior and interior structures for different frequency ratios (β_1). Here, the floor masses of all three buildings in the row are equal to $6.02E + 5 \text{ Kg}$. The parameter β_1 denotes the ratio of the fundamental frequency of the examined structure (for which the results are shown in the figure) to that of the neighboring structure. When the parameter $\beta_1 = 0.5$, the fundamental frequency of the neighboring structure is 2.608 cps . To obtain this value of the frequency, the stiffness parameter for the neighboring structure must be $7.24E + 9 \text{ N/m}$. For $\beta_1 = 1.5$, which corresponds to a softer neighboring structure, the stiffness and frequency of the neighboring structure are equal to $8.04E + 8 \text{ N/m}$ and 0.869 cps , respectively. From Figure 4.4 it is observed that:

1. A softer (than its neighbor) exterior building will experience a higher response than a softer interior building. That is, one-sided pounding will aggravate the situation more than two-sided pounding for a softer building.
2. If the observed building is stiffer than its neighbor, then the story shear is slightly higher when it is placed on the exterior (except at top). The acceleration and overturning moment responses, on the other hand, are increased for a stiffer building placed in the interior.
3. For an interior structure, the displacement and story shear responses are greatly affected by changes in the stiffness of the adjacent structures. On the other hand, the acceleration and overturning moment responses are not very sensitive to the changes in the stiffness of adjacent structure.
4. For an exterior structure, the opposites of the statements made in paragraph (3) above are true. That is, displacement and story shear responses are less sensitive to the stiffness changes in the adjacent structure than the acceleration and overturning moment responses.
5. A softer exterior structure will feel a large increase in acceleration and overturning

moment responses due to pounding.

Effect of Adjacent Building Mass

In Figure 4.5 we examine the effect of changing the mass of pounding structures. The mass of the observed structure is kept the same as in the previous figure, and the masses of the adjacent structures are varied. The spring constant of the adjacent structures is also varied to keep the frequency of these structures at 0.95 *cps*. Here, the ratio of the mass of the examined structure to that of the neighboring structure is denoted by β_2 . For $\beta_2 = 0.5$, which corresponds to a heavier neighboring structure, the mass, stiffness and fundamental frequency of the neighboring structure are $1.204E + 6$ *Kg*, $1.92E + 9$ *N/m* and 0.95 *cps*, respectively. For $\beta_2 = 2.0$, which corresponds to a lighter neighboring structure, these parameters are equal to $3.01E + 5$ *Kg*, $4.80E + 8$ *N/m* and 0.95 *cps*, respectively. The following observations can be made from Figure 4.5:

1. The displacement of a building on the exterior is amplified by pounding, whereas for an interior building it may be reduced.
2. The story shear for an exterior building, whether heavier or lighter than its neighbor, is amplified by pounding. For an interior building, the shear is in general reduced by pounding, except for a building whose neighboring buildings are heavier. The shear at the top may be increased by pounding.
3. Pounding increases the acceleration of all buildings. However, for an exterior heavier building this increase is not as large as for other three cases.
4. The overturning moment is also increased due to pounding, except that for a heavy exterior building the increase is not as significant as it is for the other three cases.

Effect of Gap Size

In Figure 4.6 we examine the effect of increasing the gap size on the pounding response of the interior and exterior structure. The structural parameters for the neighbouring structure are: the floor mass $=6.02E + 5 \text{ Kg}$, story stiffness $=9.60E + 8 \text{ N/m}$ and the fundamental frequency $=0.95 \text{ cps}$. It is observed that:

1. For smaller gap size, the displacement and story shear ratios of the exterior building are larger than those of the interior structure. The acceleration ratio of the exterior building is somewhat smaller than that of the interior structure. The overturning moment ratios of the exterior and interior structures are almost the same.
2. For larger gap size, the response ratios of the exterior and interior structures are almost the same, except the overturning moment ratios, which are larger for the interior structure.
3. The increase in the gap size does not seem to reduce the effect of pounding as far as acceleration response is concerned. However for the overturning moment response, a larger gap size does mean a smaller overturning moment, especially for lower stories, both for interior and exterior structures.

Effect of Impact Element Stiffness

In Figure 4.7 the effect of impact element stiffness on the response of the exterior and interior buildings is examined. The structural parameters for the neighboring structure are: the floor mass $=6.02E + 5 \text{ Kg}$, story stiffness $=9.60E + 8 \text{ N/m}$ and the fundamental frequency $=0.95 \text{ cps}$. The following observations can be made from this figure:

1. For both impact element stiffnesses examined, the displacement and story shear ratios (except at the top floor) of the exterior structure are larger than those of the interior structure, whereas the acceleration and overturning moment ratios of the interior structure are larger than those of the exterior structure.

2. Increasing the impact element stiffness by four times does not affect the displacement and story shear very much, but there is a relatively large increase in the acceleration and overturning moment responses of both interior and exterior structures.

4.4 Summary

In this chapter the effects of different parameters on the pounding responses of the exterior and interior structure of the same height in a row were investigated. The results show that the pounding responses of the exterior structure (subjected to one-sided impact) are very different from those of the interior structure (subjected to two-sided impact). Due to pounding, the exterior structure is usually penalized more than the interior structure when it is adjacent to either a stiffer or a heavier structure. If the neighboring structure is either softer or lighter, then the floor acceleration and overturning moment responses of the interior structure are larger than those of the exterior structure. The parametric study showed that, although the displacement and story shear responses are not very sensitive to the impact element stiffness, the floor acceleration and overturning moment responses are very sensitive to this parameter.

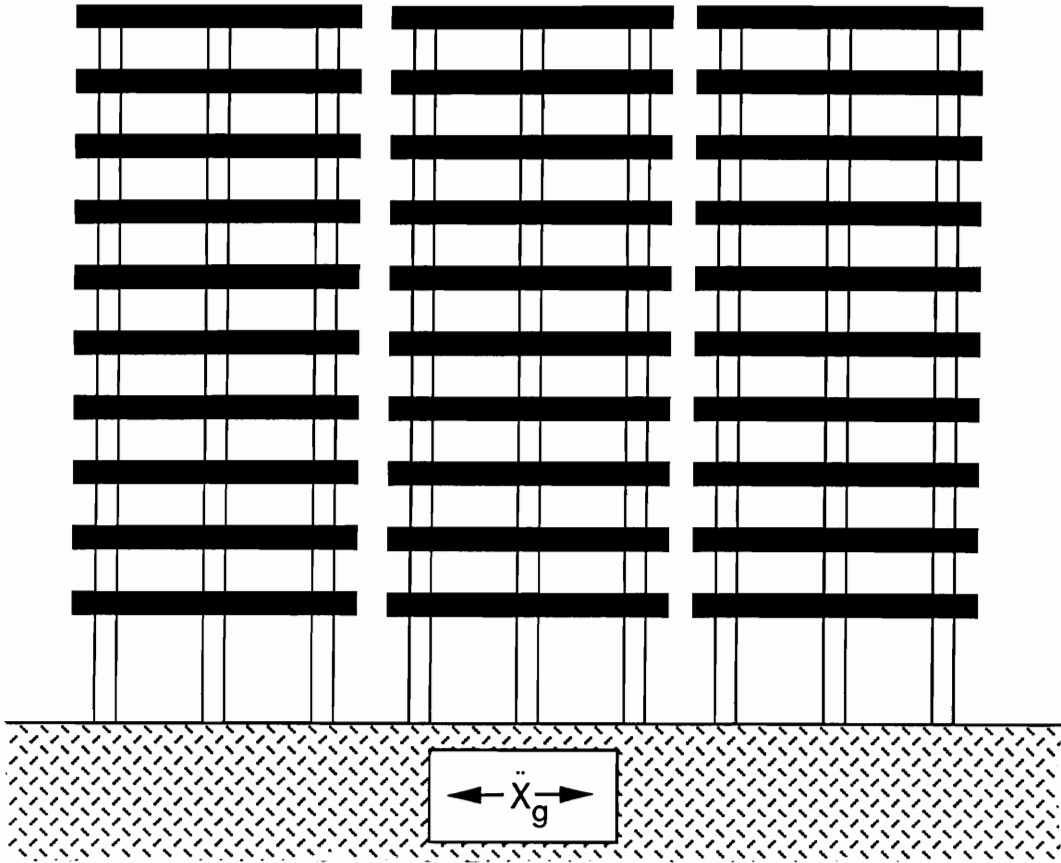


Figure 4.1: Schematic of adjacent structures in series undergoing the pounding

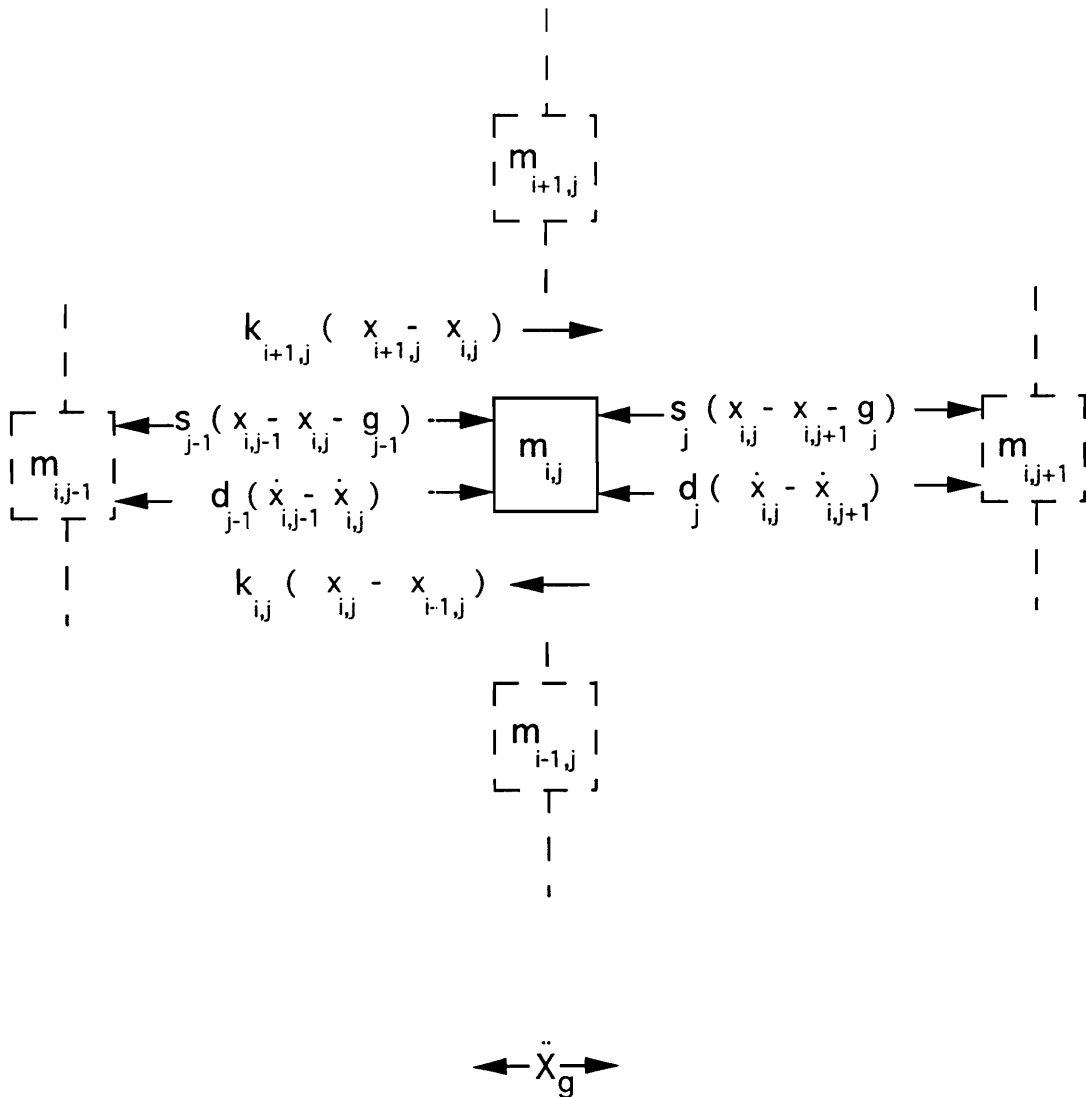


Figure 4.2: Free body diagram of a typical floor mass of the interior structure undergoing the two-sided pounding

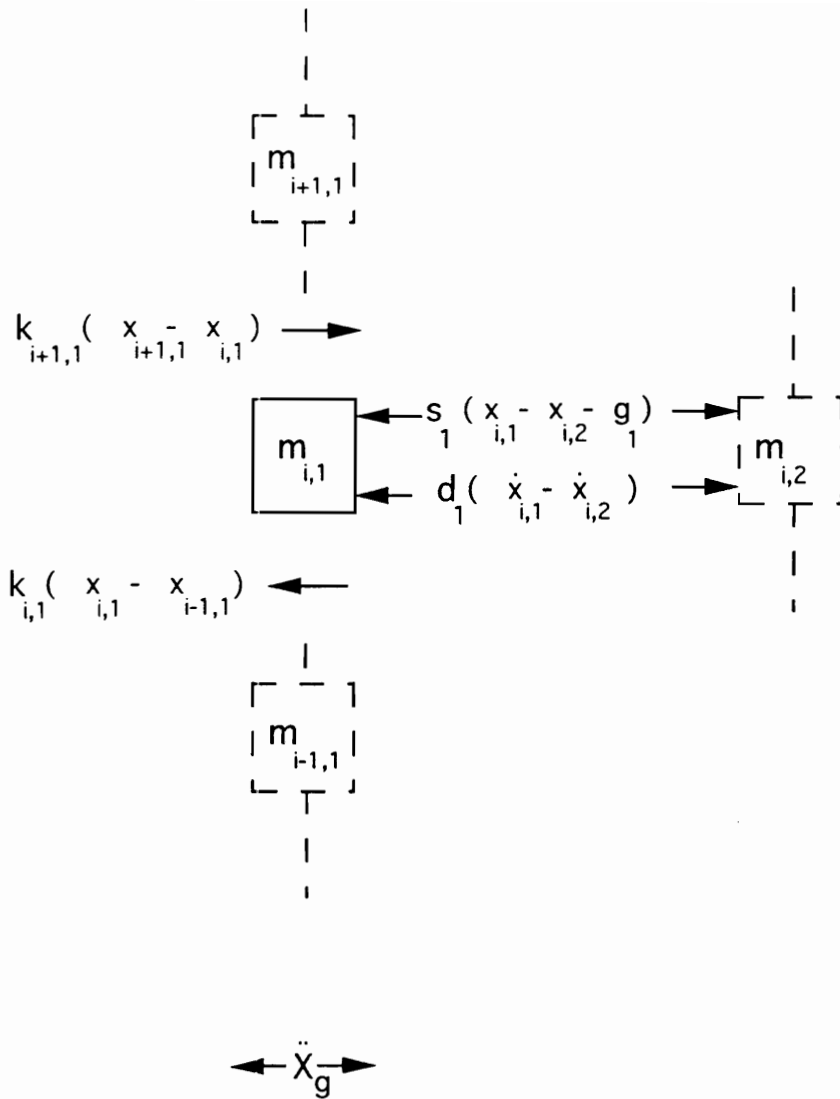


Figure 4.3: Free body diagram of a typical floor mass of the exterior structure undergoing the one-sided pounding

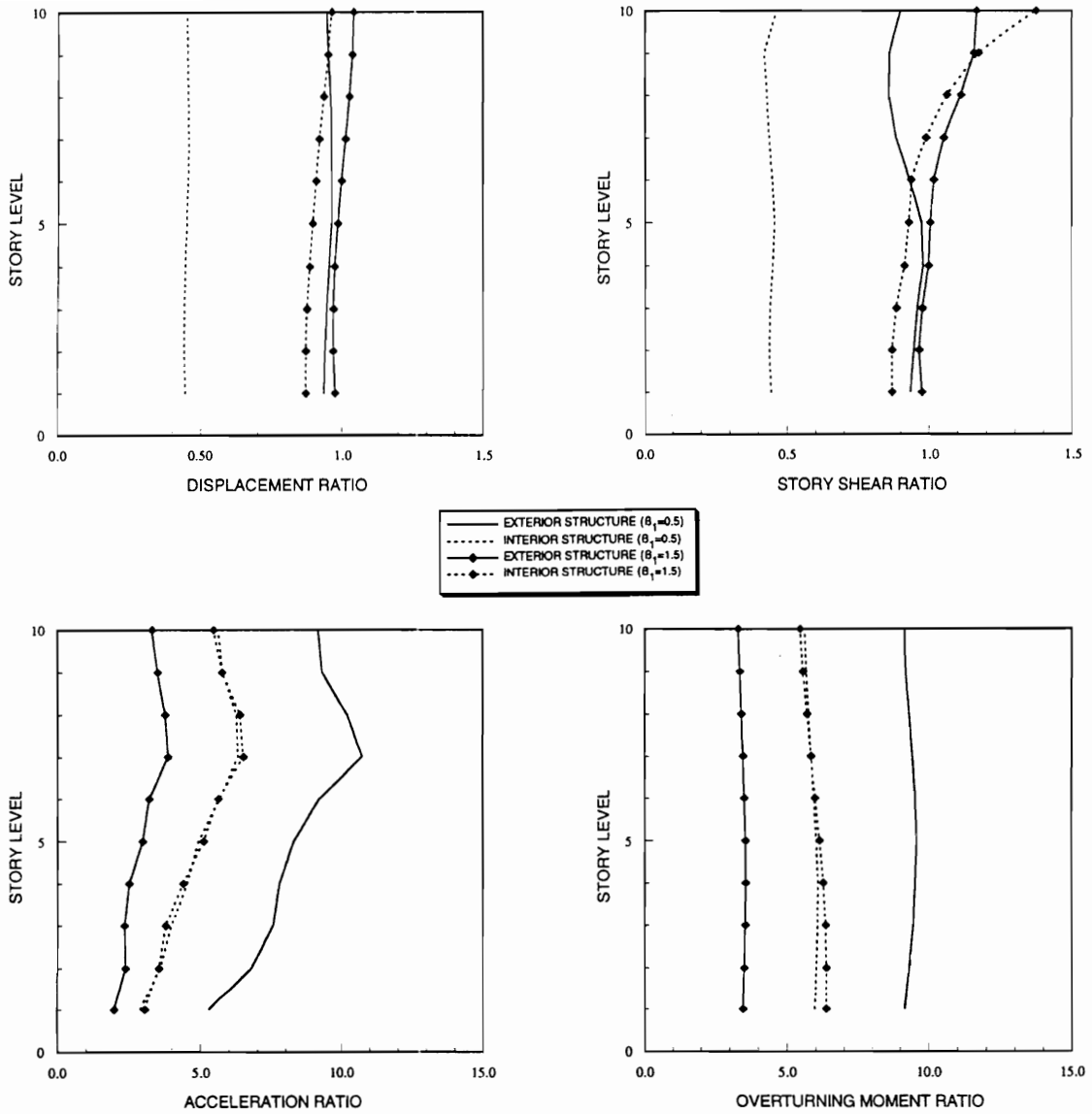


Figure 4.4: Pounding to no-pounding response ratios of the observed structure (exterior or interior) for different fundamental frequencies of its neighboring building

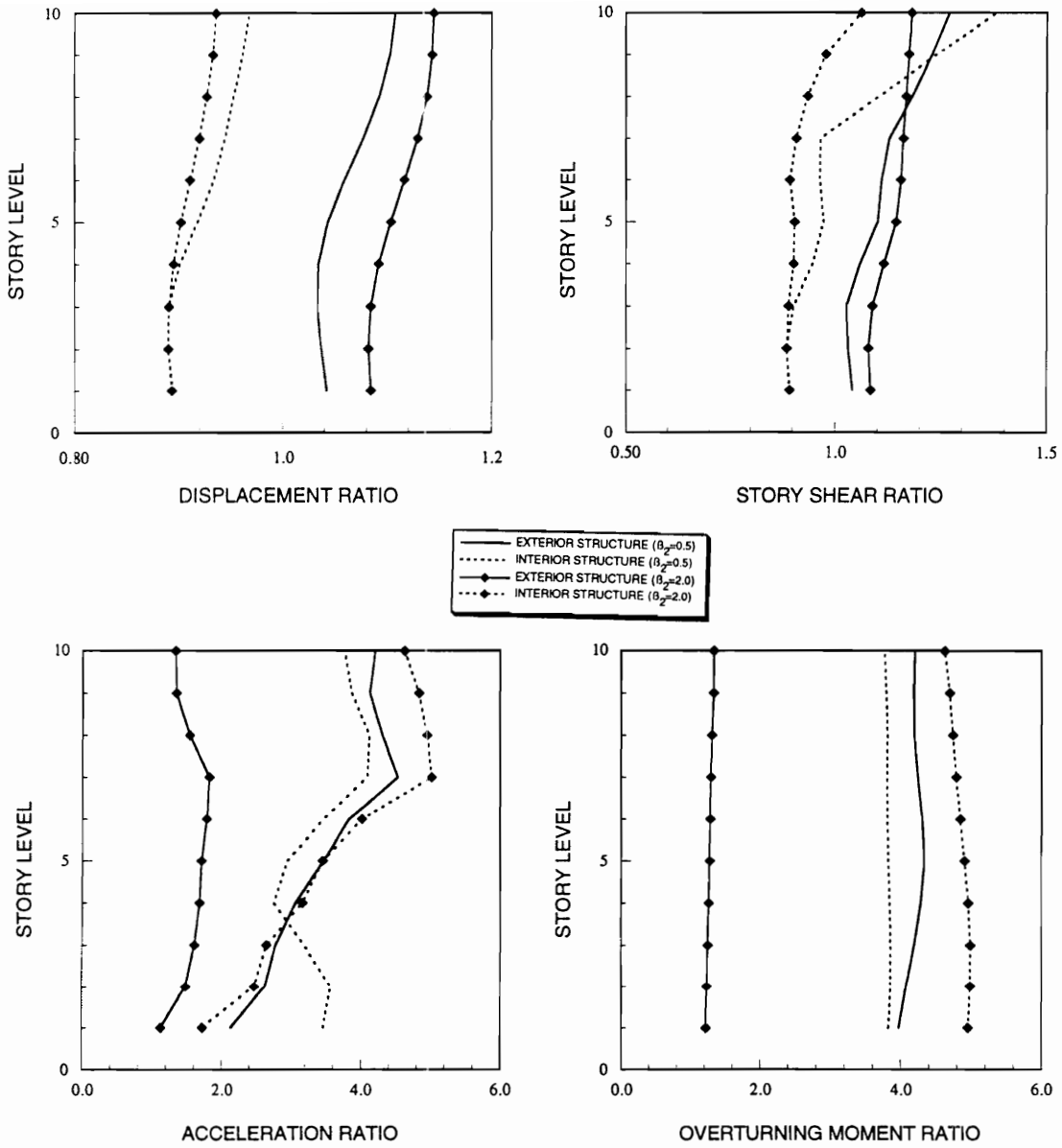


Figure 4.5: Pounding to no-pounding response ratios of the observed structure (exterior or interior) for different floor masses of its neighboring building

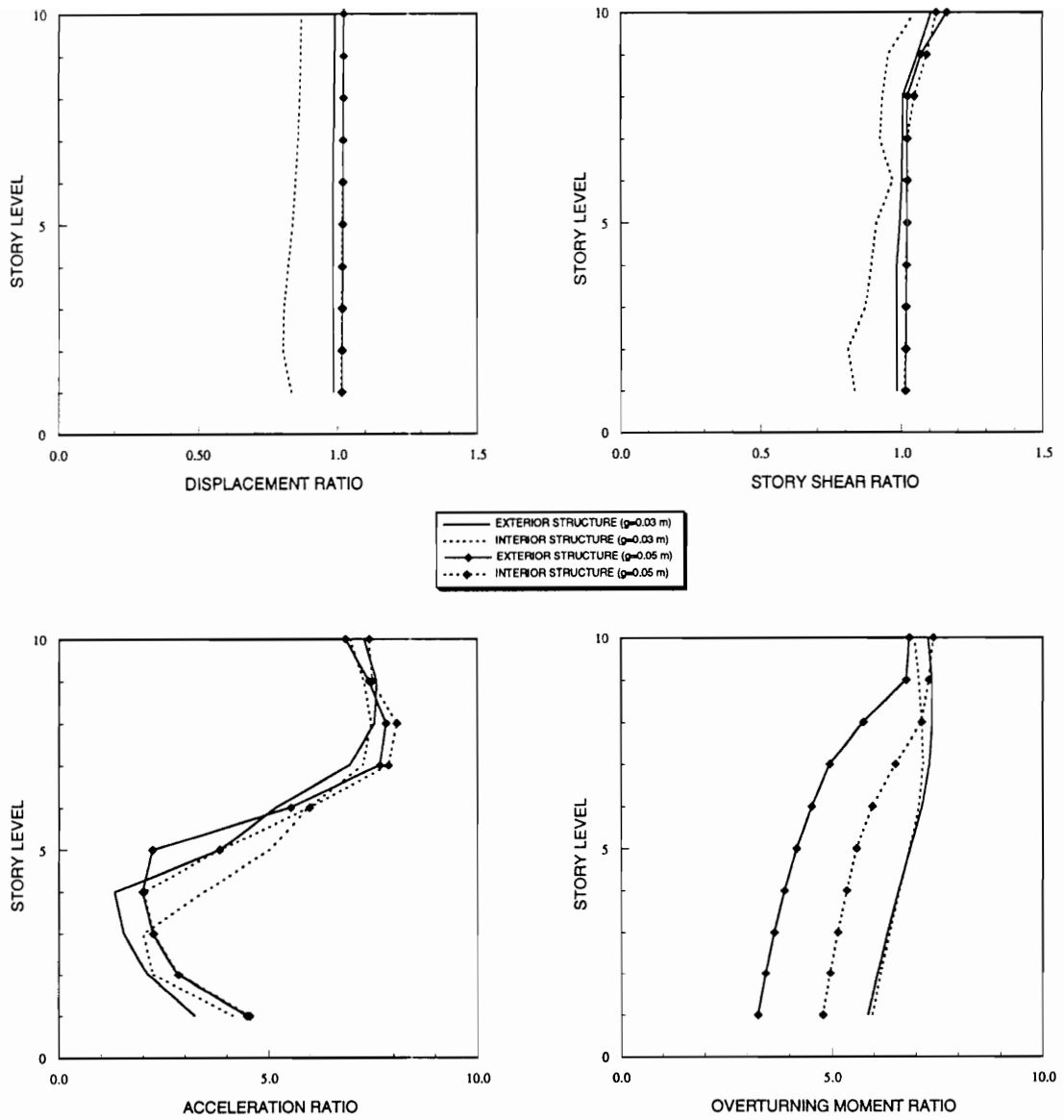


Figure 4.6: Pounding to no-pounding response ratios of the observed structure (exterior or interior) for different gap sizes

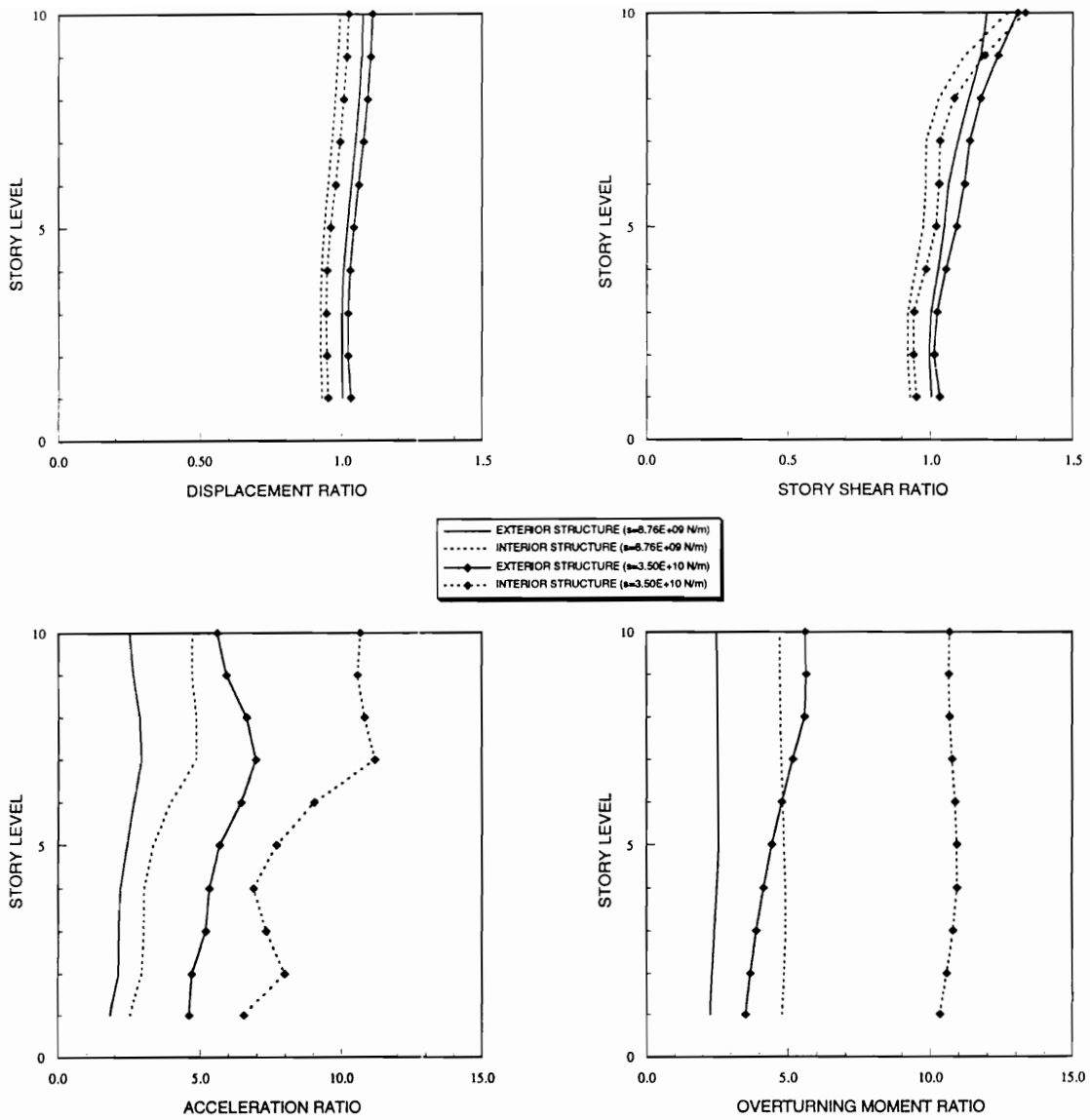


Figure 4.7: Pounding to no-pounding response ratios of the observed structure (exterior or interior) for different impact element stiffnesses

Chapter 5

EFFECT OF SOIL-STRUCTURE INTERACTION ON THE STRUCTURAL POUNDING

5.1 Introduction

In the previous chapters, it was assumed that the two pounding structures were supported on a rigid base. In this chapter, we will consider structures supported on a flexible soil foundation to examine the effect of soil-structure interaction on the pounding response. Inclusion of a flexible foundation will also permit us to evaluate the effect of pounding on the foundation forces. In the later chapters, we will be considering various pounding mitigation strategies. The consideration of foundation flexibility will also permit us to evaluate the effect of various pounding mitigation strategies on the forces transmitted to the foundation.

5.2 Model for Foundation Flexibility

The topic of soil-structure interaction has been the subject of extensive studies in the 1970's in connection with the design of nuclear power plants for seismic loads. Various analytical methods were considered then to incorporate the effect of soil foundation on the response of superstructures and supported subsystems. One of the popular and simpler approaches has been to use soil springs to represent the foundation flexibility. To include the dissipation of vibration energy due to internal friction and radiation damping in the foundation, viscous dampers have been utilized. In this study, the spring and dashpot coefficients proposed by Parmelee et al. [32] have been adopted. Although these coefficients are frequency-dependent, Parmelee et al. have shown that for most practical considerations

they can be assumed to be frequency-independent. The frequency-independent spring and damping coefficients corresponding to the translation and rocking degrees of freedom are defined by Parmelee et al. [32] as follows:

$$k_x = 4.4V_s^2\rho r \quad (5.1)$$

$$c_x = 2.7V_s\rho r^2 \quad (5.2)$$

$$k_\theta = 2.3V_s^2\rho r^3 \quad (5.3)$$

$$c_\theta = 0.31V_s\rho r^4 \quad (5.4)$$

where k_x and k_θ are the spring coefficients for the translation and rotation springs, respectively, and c_x and c_θ are the corresponding damping coefficients for the two degrees of freedom. V_s = the shear wave velocity of the foundation medium, ρ = the mass density of the foundation soil and r = the radius of the base mat of the structure. For the numerical values of these parameters, r has been assumed to be one-half of the base dimensions of the structures. The numerical values used in this study for ρ and r are shown in Table 5.1.

The shear wave velocity V_s is an important parameter representing the foundation stiffness. A higher shear wave velocity means a stiffer soil. Here in the parametric study several values of the shear wave velocities between the range of 77 *m/sec* to 600 *m/sec* have been considered to calculate the numerical results.

5.3 Equations of Motion

Two multi-story flexible shear buildings, identified as p and q-structures, are considered. It is assumed that the number of floors in the p- and q-structures are, respectively, p and

q. As before, the properties associated with these structures will be identified by subscripts p and q, respectively.

As in chapters 2 and 3, it is again assumed that the floor heights of both structures are the same, and therefore the pounding will occur only at their floor levels. A schematic of the two structures is shown in Figure 5.1. The impact is again modeled by a linear spring and dashpot element introduced between the colliding floor masses of the two structures.

Considering the translation and rocking motions of the base, the equations of motion for the i th colliding masses of the two structures can be written as:

$$\begin{aligned}
 m_{i_p} [\ddot{x}_{i_p}(t) + \ddot{u}_p(t) + h_i \ddot{\theta}_p(t)] + \sum_{j=1}^p c_{ij_p} \dot{x}_{j_p}(t) + d_i \{ [\dot{x}_{i_p}(t) + \dot{u}_p(t) + \\
 h_i \dot{\theta}_p(t)] - [\dot{x}_{i_q}(t) + \dot{u}_q(t) + h_i \dot{\theta}_q(t)] \} + (k_{i_p} + k_{(i+1)_p}) x_{i_p}(t) - \\
 k_{i_p} x_{(i-1)_p}(t) - k_{(i+1)_p} x_{(i+1)_p}(t) + s_i \{ [x_{i_p}(t) + u_p(t) + h_i \theta_p(t)] - \\
 [x_{i_q}(t) + u_q(t) + h_i \theta_q(t) + g_i] \} = -m_{i_p} \ddot{x}_g(t)
 \end{aligned} \tag{5.5}$$

$$\begin{aligned}
 m_{i_q} [\ddot{x}_{i_q}(t) + \ddot{u}_q(t) + h_i \ddot{\theta}_q(t)] + \sum_{j=1}^q c_{ij_q} \dot{x}_{j_q}(t) + d_i \{ [\dot{x}_{i_q}(t) + \dot{u}_q(t) + \\
 h_i \dot{\theta}_q(t)] - [\dot{x}_{i_p}(t) + \dot{u}_p(t) + h_i \dot{\theta}_p(t)] \} + (k_{i_q} + k_{(i+1)_q}) x_{i_q}(t) - \\
 k_{i_q} x_{(i-1)_q}(t) - k_{(i+1)_q} x_{(i+1)_q}(t) + s_i \{ [x_{i_q}(t) + u_q(t) + h_i \theta_q(t)] - \\
 [x_{i_p}(t) + u_p(t) + h_i \theta_p(t) - g_i] \} = -m_{i_q} \ddot{x}_g(t)
 \end{aligned} \tag{5.6}$$

where x_{i_p} is the relative displacement with respect to the base of the i th mass m_{i_p} of the p-structure; k_{i_p} and c_{ij_p} , respectively, are the stiffness and damping coefficients for the i th story of p-structure; u_p = relative displacement with respect to the ground and θ_p = rotation, both of the foundation mat; h_i = the height of the i th story; and s_i and d_i , respectively, are the stiffness and damping coefficients of the impact elements at the i th level. Similar quantities appearing in equation 5.6 with subscript q pertain to the q-structure. The at-rest gap between the two colliding masses is denoted by g_i and $\ddot{x}_g(t)$ is the ground acceleration.

Two additional equations of motion associated with the translational and rotational DOF of the foundation are derived by summing the external forces and moments of the entire structure about the base. These equations for the p-structure can be written as:

$$\begin{aligned}
& \sum_{i=1}^p m_{i_p} \ddot{x}_{i_p}(t) + \left(\sum_{i=1}^p m_{i_p} + m_p \right) \ddot{u}_p(t) + \left(\sum_{i=1}^p m_{i_p} h_i \right) \ddot{\theta}_p(t) + \sum_{i=1}^q d_i \{ [\dot{x}_{i_p}(t) + \\
& \dot{u}_p(t) + h_i \dot{\theta}_p(t)] - [\dot{x}_{i_q}(t) + \dot{u}_q(t) + h_i \dot{\theta}_q(t)] \} + \sum_{i=1}^q s_i \{ [x_{i_p}(t) + \\
& u_p(t) + h_i \theta_p(t)] - [x_{i_q}(t) + u_q(t) + h_i \theta_q(t) + g_i] \} + k_x u_p(t) + \\
& c_x \dot{u}_p(t) = - \left(\sum_{i=1}^p m_{i_p} + m_p \right) \ddot{x}_g(t)
\end{aligned} \tag{5.7}$$

$$\begin{aligned}
& \sum_{i=1}^p m_{i_p} h_i [\ddot{x}_{i_p}(t) + \ddot{u}_p(t) + h_i \ddot{\theta}_p(t)] + \left(\sum_{i=1}^p I_i + I_p \right) \ddot{\theta}_p(t) + \sum_{i=1}^q d_i h_i \{ [\dot{x}_{i_p}(t) + \\
& \dot{u}_p(t) + h_i \dot{\theta}_p(t)] - [\dot{x}_{i_q}(t) + \dot{u}_q(t) + h_i \dot{\theta}_q(t)] \} + \sum_{i=1}^q s_i h_i \{ [x_{i_p}(t) + \\
& u_p(t) + h_i \theta_p(t)] - [x_{i_q}(t) + u_q(t) + h_i \theta_q(t) + g_i] \} + k_\theta \theta_p(t) + \\
& c_\theta \dot{\theta}_p(t) = - \left(\sum_{i=1}^p m_{i_p} h_i \right) \ddot{x}_g(t)
\end{aligned} \tag{5.8}$$

Equations similar to equations 5.7 and 5.8 can be written for the q-structure by merely changing the subscript p to q.

It is noted that when $\delta_i = x_{i_p} - x_{i_q} - g_i < 0$, there will be no pounding. In that case the terms containing s_i and d_i in equations 5.5, 5.6, 5.7 and 5.8 are set equal to zero.

Collecting equation 5.5 for each mass of the p-structure and q-structure along with equations 5.7 and 5.8 and similar equations for the q-structure, the coupled system of equations of motion of the two pounding structures can be written as:

$$[M]\{\ddot{X}\} + [C]\{\dot{X}\} + [K]\{X\} = -([M]\{r\} + \{m_b\})\ddot{x}_g(t) - \{F\} \tag{5.9}$$

where $[M]$ = system mass matrix; $[C]$ = system damping matrix and $[K]$ = system stiffness matrix are defined as:

$$[M] = \begin{bmatrix} [M_p] & 0 \\ 0 & [M_q] \end{bmatrix} \quad (5.10)$$

$$[C] = \begin{bmatrix} [C_p] & 0 \\ 0 & [C_q] \end{bmatrix} + [D] \quad (5.11)$$

$$[K] = \begin{bmatrix} [K_p] & 0 \\ 0 & [K_q] \end{bmatrix} + [S] \quad (5.12)$$

The unknown displacement vector $\{X\}$, the influence coefficient vectors $\{r\}$, the base mass vector $\{m_b\}$ and the supplemental force vector $\{F\}$ are defined as:

$$\{X\}^T = [x_{1p}, \dots, x_{pp}, u_p, \theta_p, x_{1q}, \dots, x_{qq}, u_q, \theta_q] \quad (5.13)$$

$$\{r\}^T = [\overbrace{1, \dots, 1}^p, \overbrace{0, 0}^2, \overbrace{1, \dots, 1}^q, \overbrace{0, 0}^2] \quad (5.14)$$

$$\{m_b\}^T = [\overbrace{0, \dots, 0}^p, \overbrace{m_p, 0}^2, \overbrace{0, \dots, 0}^q, \overbrace{m_q, 0}^2] \quad (5.15)$$

$$\{F\} = -[S]\{g\} \quad (5.16)$$

where

$$\{g\}^T = [\overbrace{g_1, g_2, \dots, g_q}^q, \overbrace{0, \dots, 0}^{p+4}] \quad (5.17)$$

In equations 5.10, 5.11 and 5.12, $[M_p]$, $[C_p]$ and $[K_p]$ are, respectively, the mass, damping and stiffness matrices of the p-structure. The matrices associated with subscript q belong to the q-structure. The matrices $[M_p]$, $[K_p]$ and $[C_p]$ are defined as:

$$[M_p] = \begin{bmatrix} m_1 & 0 & \dots & 0 & m_1 & m_1 h_1 \\ & m_2 & \dots & 0 & m_2 & m_2 h_2 \\ & & \ddots & \vdots & \vdots & \vdots \\ & & & m_p & m_p & m_p h_p \\ SYM. & & & & \alpha_1 & \alpha_2 \\ & & & & & \alpha_3 \end{bmatrix} \quad (5.18)$$

$$[K_p] = \begin{bmatrix} k_1 + k_2 & -k_2 & 0 & \dots & 0 & 0 & 0 & 0 \\ & k_2 + k_3 & -k_3 & \dots & 0 & 0 & 0 & 0 \\ & & k_3 + k_4 & \dots & 0 & 0 & 0 & 0 \\ & & & \ddots & \vdots & \vdots & \vdots & \vdots \\ & & & & k_{p-1} + k_p & -k_p & 0 & 0 \\ SYM. & & & & & k_p & 0 & 0 \\ & & & & & & k_x & 0 \\ & & & & & & & k_\theta \end{bmatrix} \quad (5.19)$$

$$[C_p] = \begin{bmatrix} [C'_p] \\ & c_x \\ & & c_\theta \end{bmatrix} \quad (5.20)$$

These matrices are of dimension $(p + 2) \times (p + 2)$. The structural damping matrix $[C'_p]$ is added to include the energy dissipation effects. This matrix is defined in terms of the modal damping ratio and eigenproperties of the structure using standard procedures [6].

The matrix $[S]$ in equation 5.12 is the supplemental stiffness matrix provided by the contact spring whenever pounding occurs. This matrix is defined as:

$$[S] = \begin{bmatrix}
 \overbrace{s_1 \ \dots \ 0}^q & \overbrace{0 \ \dots \ 0}^{p-q} & \overbrace{s_1 \ s_1 h_1}^2 & \overbrace{-s_1 \ \dots \ 0}^q & \overbrace{-s_1 \ -s_1 h_1}^2 \\
 \vdots & \vdots & \vdots & \vdots & \vdots \\
 & s_q \ 0 \ \dots \ 0 & s_q \ s_q h_q & 0 \ \dots \ -s_q & -s_q \ -s_q h_q \\
 & 0 \ \dots \ 0 & 0 \ 0 & 0 \ \dots \ 0 & 0 \ 0 \\
 & & \vdots & \vdots & \vdots \\
 & & 0 \ 0 \ 0 & 0 \ \dots \ 0 & 0 \ 0 \\
 & & \alpha_4 \ \alpha_5 & -s_1 \ \dots \ -s_q & -\alpha_4 \ -\alpha_5 \\
 & & \alpha_6 & -s_1 h_1 \ \dots \ -s_q h_q & -\alpha_5 \ -\alpha_6 \\
 & & & s_1 \ \dots \ 0 & s_1 \ s_1 h_1 \\
 & & & \vdots & \vdots \\
 & & & & s_q \ s_q \ s_q h_q \\
 & & & & \alpha_4 \ \alpha_5 \\
 & & & & \alpha_6
 \end{bmatrix}$$

SYM.

(5.21)

The combined structural damping matrix in equation 5.11 is supplemented by the damping matrix $[D]$ coming from the dashpots provided at the pounding surfaces. These dashpots are provided to include the loss of energy which occurs during any pounding. The matrix $[D]$ is of the same form as matrix $[S]$, except that s_i in equation 5.21 are replaced by d_i to obtain $[D]$. The s_i and d_i in these matrices are zero for the floors which do not pound. The supplemental matrices $[S]$ and $[D]$ are of size $(p + q + 4) \times (p + q + 4)$.

The coefficients $\alpha_1, \dots, \alpha_6$ in equations 5.18 and 5.21 are defined as:

$$\alpha_1 = \sum_{i=1}^p m_i + m_p \quad , \quad \alpha_2 = \sum_{i=1}^p m_i h_i$$

$$\alpha_3 = \sum_{i=1}^p (m_i h_i^2 + I_i) + I_p \quad , \quad \alpha_4 = \sum_{i=1}^q s_i$$

$$\alpha_5 = \sum_{i=1}^q s_i h_i \quad , \quad \alpha_6 = \sum_{i=1}^q s_i h_i^2 \quad (5.22)$$

The equations of motion 5.9, with and without pounding, are both linear. However, since $[D]$ and $[S]$ matrices constantly change because of the pounding and no-pounding situations, the problem is essentially nonlinear. It was, therefore, found to be best to solve it by a step-by-step integration approach. Here the Newmark- β [6] approach has been used. The time steps of the integration were kept very small to capture the everchanging “pounding” and “no-pounding” states as the motion proceeded.

5.4 Numerical Results

5.4.1 Force and acceleration responses

Numerical results have been obtained for several configurations of two pounding structures. The assumed basic configuration is a ten-story shear building pounding against a five-story shear building. Table 5.1 shows the assumed building parameters for the numerical analysis. This table summarizes the floor masses, m_i , column stiffness, k_i , modal damping as a percentage of critical, ξ , centroidal mass moment of inertia, I_i , and the story heights, h_i .

Table 5.1 also shows the impact element stiffness and damping coefficients. These coefficients were estimated based on practical considerations [1, 24, 41, 46]. A parametric study [35] indicated that the system pounding responses are not sensitive to the stiffness and damping values of the impact element for the numerical values of these parameters considered. The at-rest gaps between the floors of the two structures, g_i , are assumed to be zero.

To avoid the effect of individual variation in the ground motion, here an ensemble of 50 accelerograms with similar frequency characteristics are used. These accelerograms were generated for a broad-band spectral density function. The average ground spectra for these accelerograms are shown in Figure 5.2.

The numerical results presented in the following pages represent the average of the maximum response values obtained for the 50 accelerograms.

In Figures 5.3 and 5.4, we demonstrate the effect of foundation stiffness on the displacement, story shear, overturning moment and absolute acceleration response of the two structures when they pound. The results are presented for 6 shear wave velocity values of 77 *m/sec*, 100 *m/sec*, 200 *m/sec*, 300 *m/sec*, 600 *m/sec* and ∞ , representing six different foundation media of increasing stiffness. The lowest value of 77 *m/sec* is taken from reference [43]. This represents a rather flexible foundation with a unit weight of 100 *lbs/cft* and a shear modulus of 2×10^5 *lbs/ft²* which gives a shear wave velocity of 250 *ft/sec* (or 77 *m/sec*). The value $V_s = \infty$ *m/sec* corresponds to a fixed base case.

From the response results shown in Figure 5.3 for the ten-story structure, we observe that:

1. The pounding displacement at all floors decreases with increasing flexibility of the base.
2. The story shears in general increase with the increasing foundation stiffness, except in the top and bottom stories where there is some crossover in the story shear values for different shear wave velocities. We also notice that, for a more flexible foundation there is a more dramatic increase in the shear force in the stories above the top pounding level. That is, the increase in the shear force from pounding to no-pounding stories is more pronounced for softer foundations.
3. The overturning moments at the lower levels are higher for more flexible foundation.
4. The absolute accelerations of the pounding floors are also increased by the flexibility of the foundation.

Similar observations can also be made from the response values shown in Figure 5.4 for the five-story structure.

In general, therefore, we observe that a more flexible foundation may give somewhat smaller story shear forces, but will tend to attract higher overturning moments and higher floor accelerations. Later the significance of these higher floor accelerations on the response of secondary systems will be examined further when the floor response spectra results will be presented.

In the previous two figures we examined the effect of changing the shear wave velocity on various response quantities. In the following figures we now compare the pounding and no pounding responses for structures with flexible foundation. To avoid crowding of the figures, we will consider only two cases of flexible foundations, with shear wave velocities of 77 m/sec and 300 m/sec . As mentioned before, the first case represents a rather flexible foundation on a soil medium of organic clay silt. The second case is for a medium stiff soil which is between the case of a very rigid and very flexible base. For these two cases the numerical results obtained with and without pounding are compared with each other and also with the results for the case of a rigid base.

The results in Figure 5.5 are for the ten-story structure, whereas those in Figure 5.6 are for the five-story structure. From the results of the ten-story structure one observes that:

1. For the softer foundation medium, the pounding causes a higher displacement response. This is, however, not the case for stiffer media, where one observes that the pounding reduces the displacement response.
2. For the softer foundation medium, the pounding causes an increase in the shear force in all the stories which is especially large for all stories above the top pounding story. However, as the foundation medium becomes stiffer, the shear force in the pounding stories is in fact decreased by pounding. The stories above the top pounding story, on the other hand, always experience a significant increase in the shear force due to pounding. This increase is, however, more dramatic for the softer foundation medium.

3. The pounding causes a significant increase in the overturning moment especially for lower stories, for all cases of foundation flexibility. This increase is larger for softer foundations.
4. The floor acceleration response is also significantly increased by pounding for all cases of foundation flexibility. This increase for the cases examined here is larger for softer foundations.

The results for the five-story structure, shown in Figure 5.6, also follow a similar trend, except in the case of shear force of the top pounding story where we observe a clear increase in the shear force due to this pounding for all foundation medium stiffnesses.

5.4.2 Forces in foundation media

It is also of interest to examine the effect of pounding on the foundation media. This effect is shown in terms of the force in the translational spring and moment in the rotational spring for the ten-story and five-story structures in the next two figures (Figures 5.7 and 5.8). From the figures for the ten-story structure we note that flexible foundations will experience a significant increase in the shear force. The stiffer foundations, on the other hand, show a decrease in the shear. The overturning moment is reduced for all foundation stiffnesses. For the five-story structure, both shear and moment are reduced by pounding. This is clearly shown in Figure 5.9 where we plot the ratio of pounding to no-pounding values. The ratios greater than unity mean an increase in the value due to pounding. Only the shear force values in the ten-story structure for flexible foundations are increased by pounding.

5.4.3 Floor spectral response

In the results presented in section 5.4.1 we examined the effect of foundation flexibility and pounding on the displacement, story shear, overturning moment and floor acceleration responses. In particular, it was observed that the flexibility of the foundation caused an increased acceleration response of pounding floors in most cases. In this section, we explore

this effect further by examining the effect of flexibility and pounding on the frequency content of floor acceleration, expressed in terms of floor response spectra.

In Figures 5.10 and 5.11 we show the floor response spectra for floors 1 to 10 of the ten-story structure obtained for various values of shear wave velocities. Here no particular trend dependent upon the shear wave velocity is apparent in these figures. However, for the pounding floors, all floor spectra have their peaks in the frequency range of 30 to 50 cps. The peaks of the floor spectra for the higher floors are, however, shifted to lower values. Floors 6, 7 and 9 have a predominant peak at a frequency of about 12.5 cps. In these cases it appears that pounding seems to excite one of the higher modes of the system significantly. The peaks for the 8th and 10th floors occur at lower frequencies than the peaks of 6th, 7th and 9th floors. Again no predictions about these peaks can be made in advance of an analysis. To get a better resolution between various curves, the floor spectra for floors 1, 5 and 10 are plotted in enlarged form in Figures 5.12, 5.13 and 5.14.

The floor spectra for the pounding floors of the five-story structure are similar to the floor spectra of pounding floors of the ten-story structure. Again, no particular trend dependent upon the flexibility of foundation media is detected from these figures. Here again we plot the spectra for floors 1 and 5 in enlarged form in Figures 5.16 and 5.17.

In Figures 5.18, 5.19 and 5.20 we compare the floor spectra with and without pounding for the softest foundation ($V_s = 77 \text{ m/sec}$) for the ten-story and five-story structures. The effect of pounding on the spectra in the higher-frequency range is quite clearly seen. Of course, the pounding floors see a large increase in the spectral values in the high-frequency range due to pounding. But we also note a significant increase in the spectra of higher floors which do not pound.

5.5 Summary

In this chapter we have investigated the effect of foundation flexibility on the pounding response. The results clearly show that the flexibility of the foundation is an important char-

acteristic to be considered in pounding response evaluations. The flexibility may increase or decrease the displacement and shear responses in pounding situations. The overturning moment response was seen to increase with flexibility. Also the floor acceleration response was seen to increase in most cases by the flexibility of the foundation. The effect of flexibility on the floor spectra of various pounding and no-pounding floors was also observed to be significant. The foundation itself may experience an increase or decrease in forces due to pounding. This depends upon the stiffness of the foundation.

In general it is observed that to properly evaluate the effect of pounding on a structural response, a proper consideration of its foundation flexibility must be included in the analysis; the assumption of a fixed base structure, when in fact it is not, can produce erroneous results and conclusions about the effect of pounding.

Table 5.1: Properties of the ten and five-story pounding structures including the impact element and the foundation medium properties.

m_i (Kg)	3.76E + 04
k_i (N/m)	7.78E + 07
ξ	0.05
I_i (Kg - m ²)	2.88E + 04
h_i (m)	4.00
s_i (N/m)	8.76E + 09
d_i (Kg/sec)	2.46E + 06
V_s (m/sec)	77.00
ρ (Kg/m ³)	1.60E + 03
r (m)	1.75

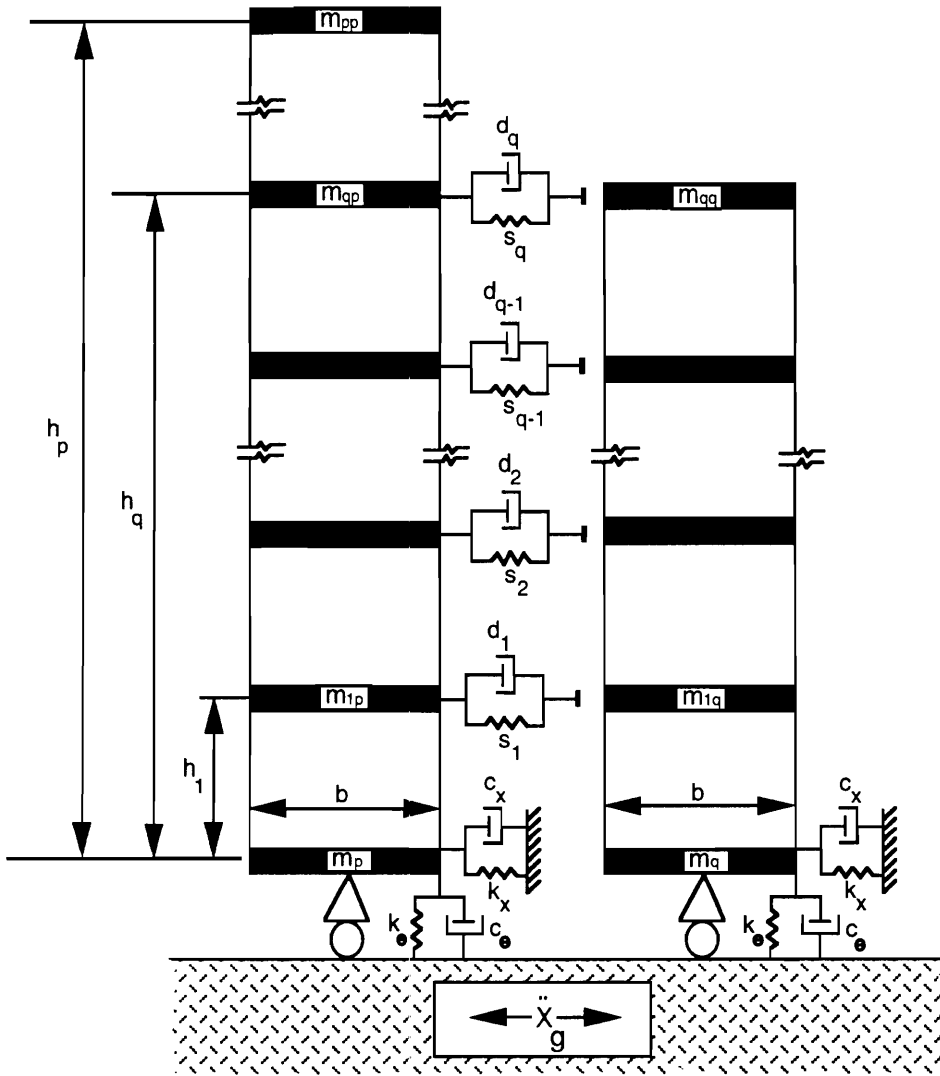


Figure 5.1: Schematic of pounding structures supported on the flexible foundation

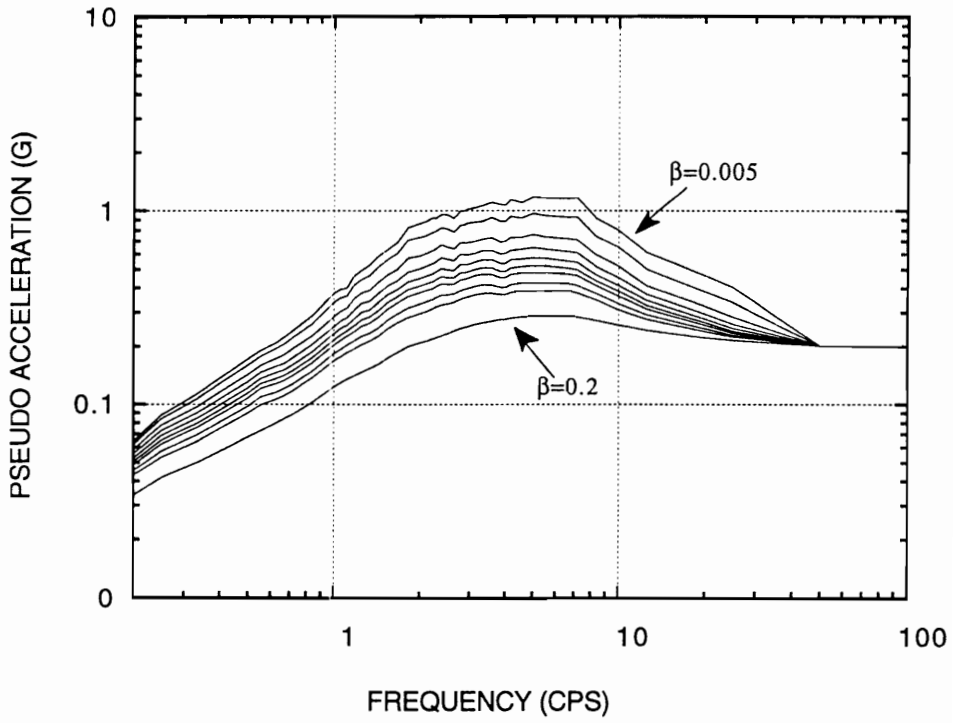


Figure 5.2: The average input ground acceleration spectra

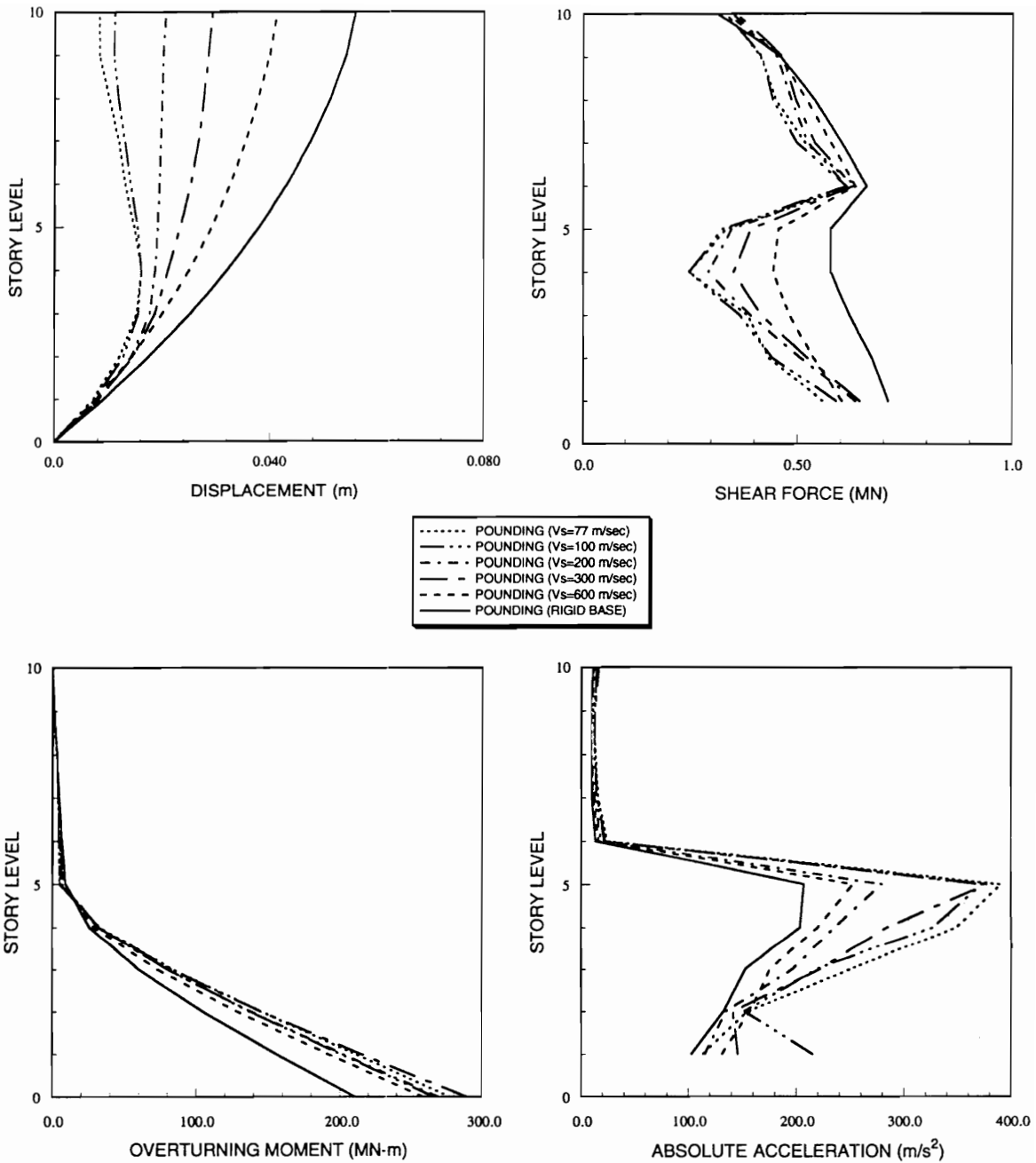


Figure 5.3: The effect of foundation stiffness on the pounding responses of the 10-story structure

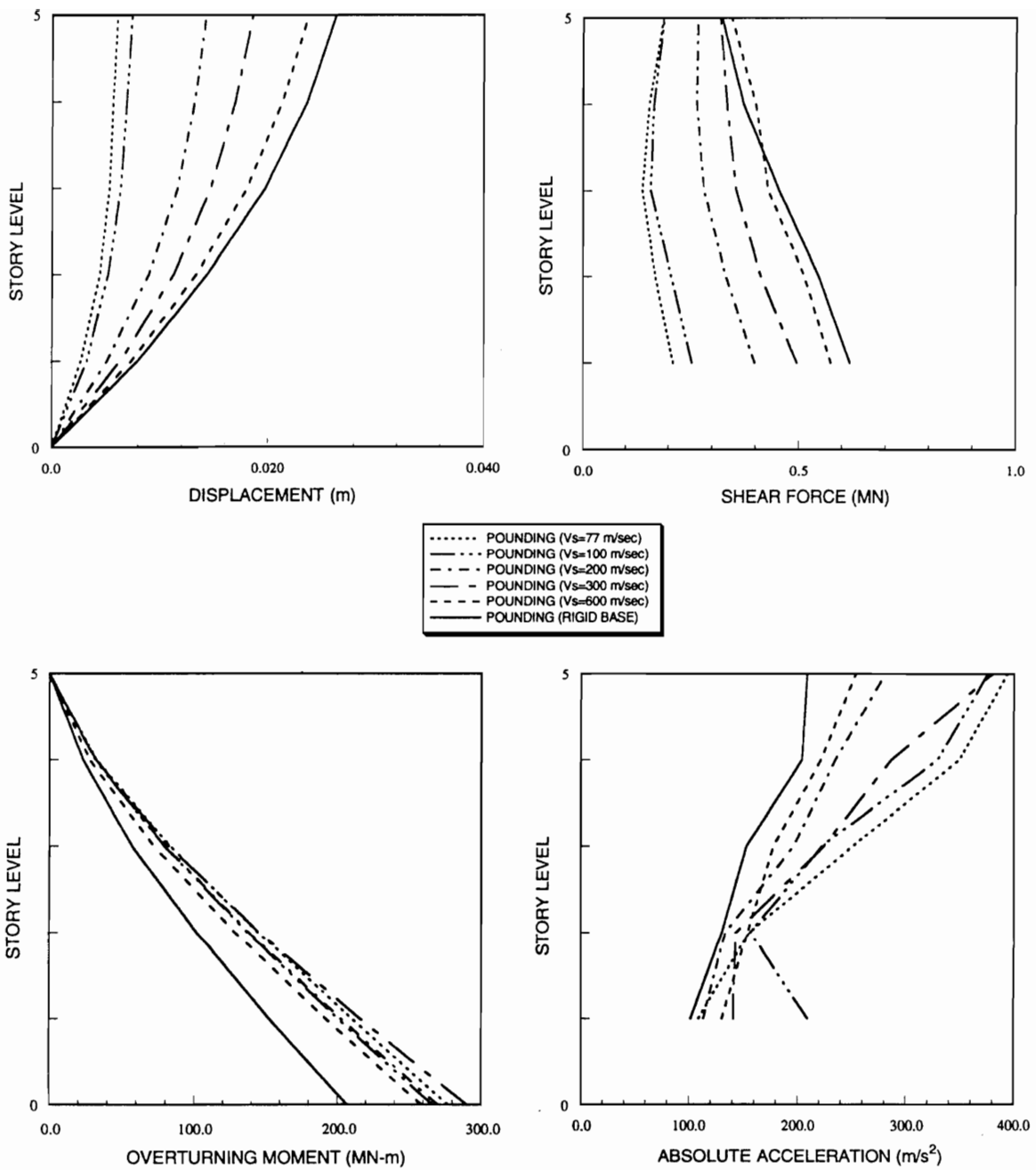


Figure 5.4: The effect of foundation stiffness on the pounding responses of the 5-story structure

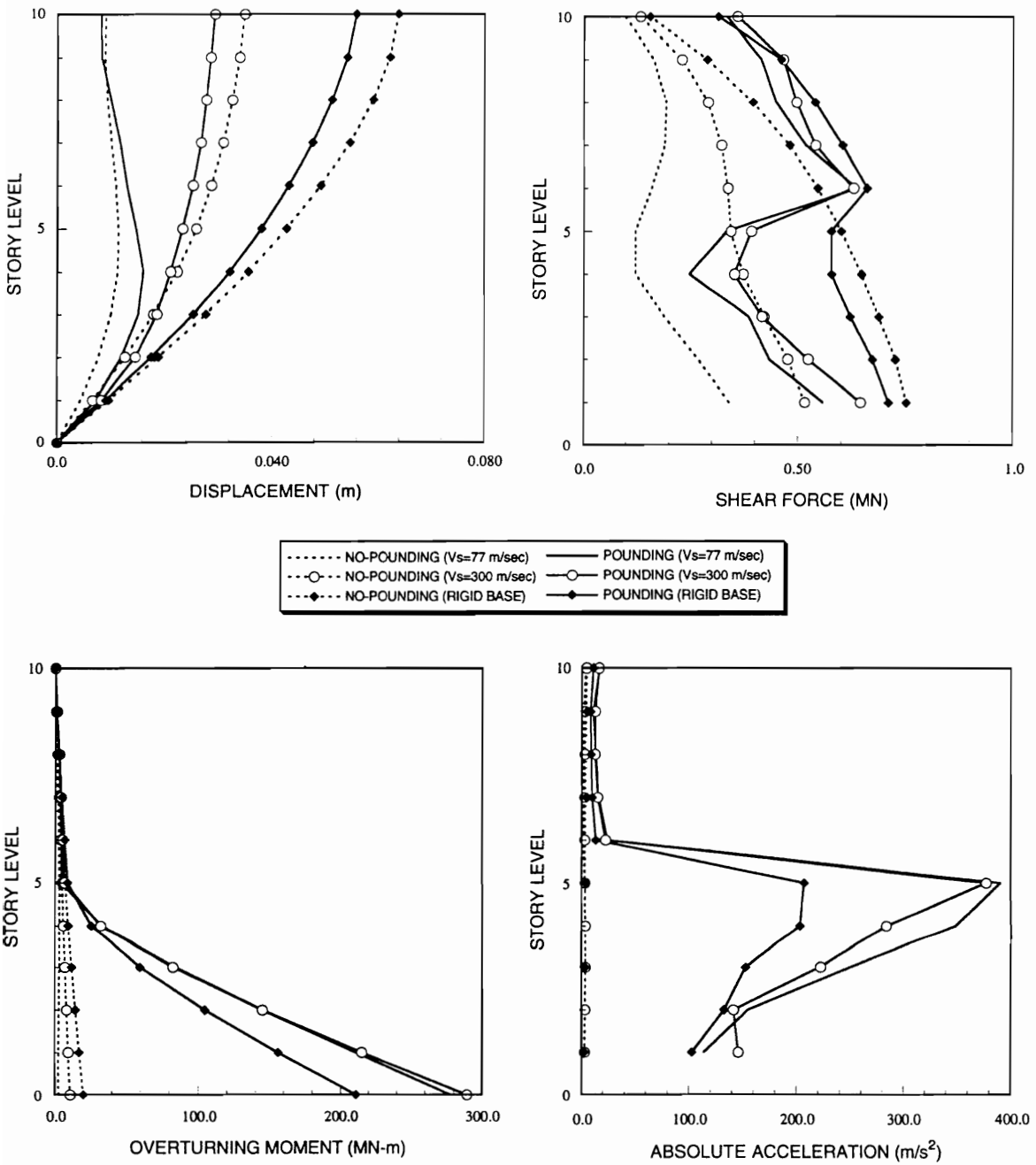


Figure 5.5: Comparison of the pounding and no-pounding responses of the 10-story structure obtained for different flexible foundations with the corresponding responses obtained for the rigid foundation model

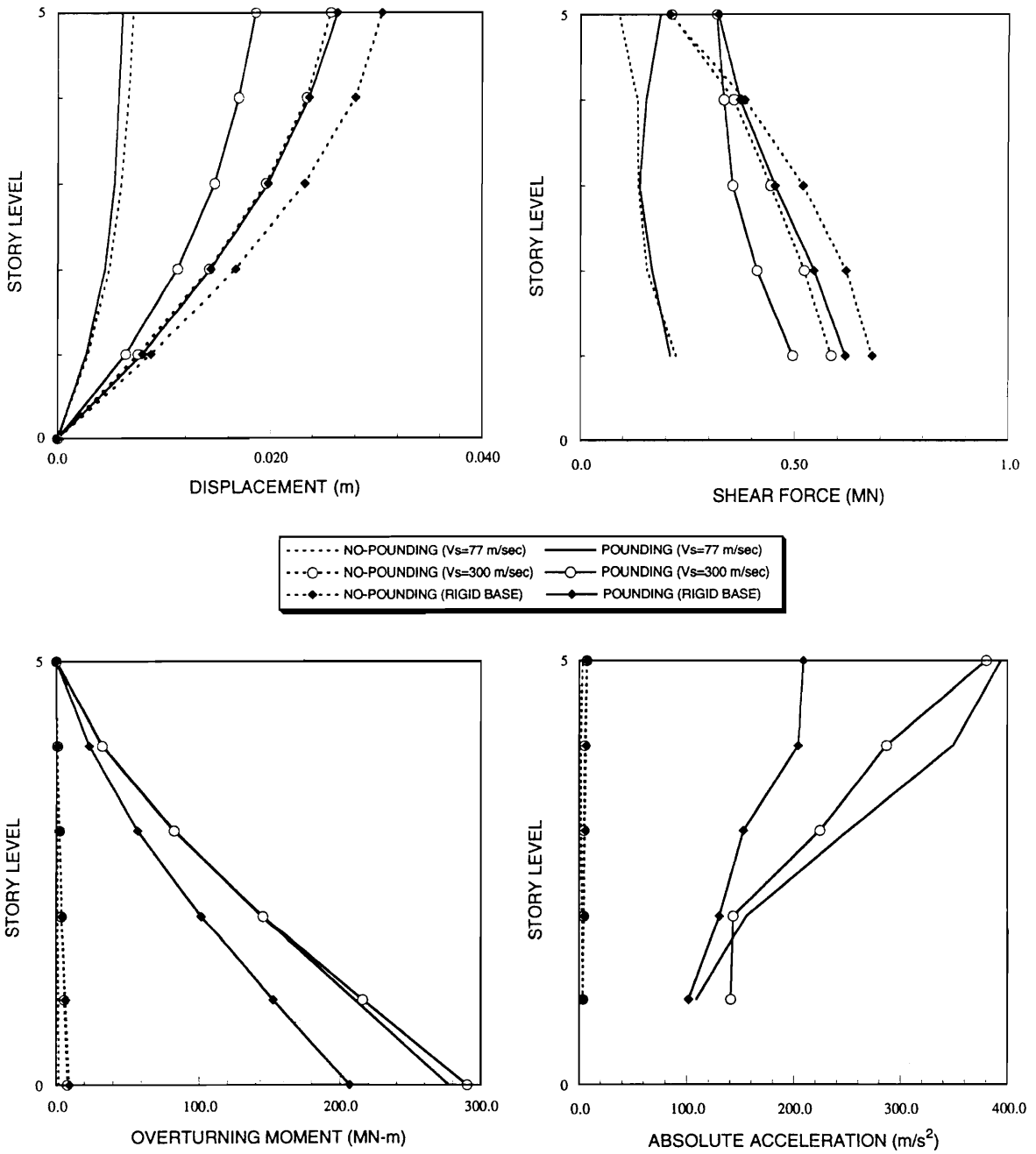


Figure 5.6: Comparison of the pounding and no-pounding responses of the 5-story structure obtained for different flexible foundations with the corresponding responses obtained for the rigid foundation model

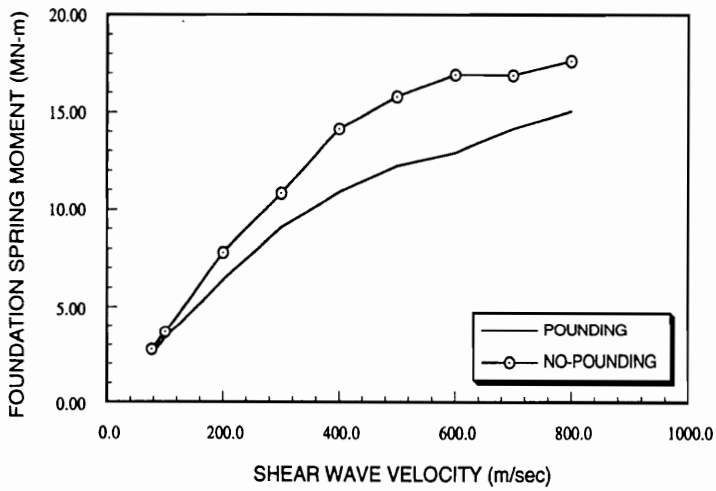
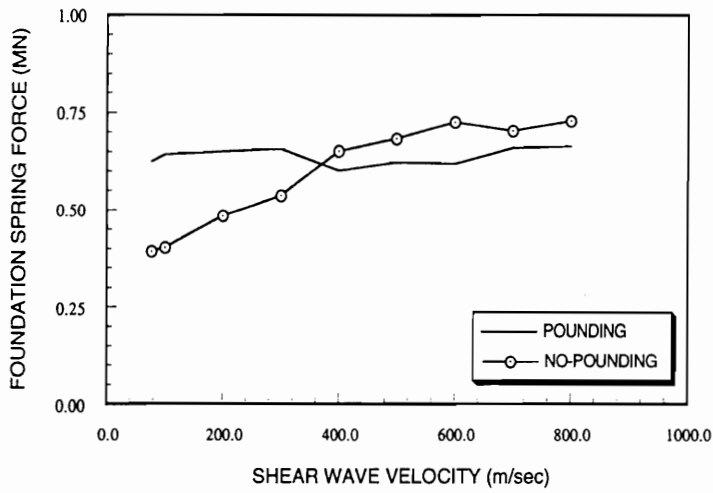


Figure 5.7: The effect of pounding on the force and moment responses of the translational and rotational foundation springs for the 10-story structure

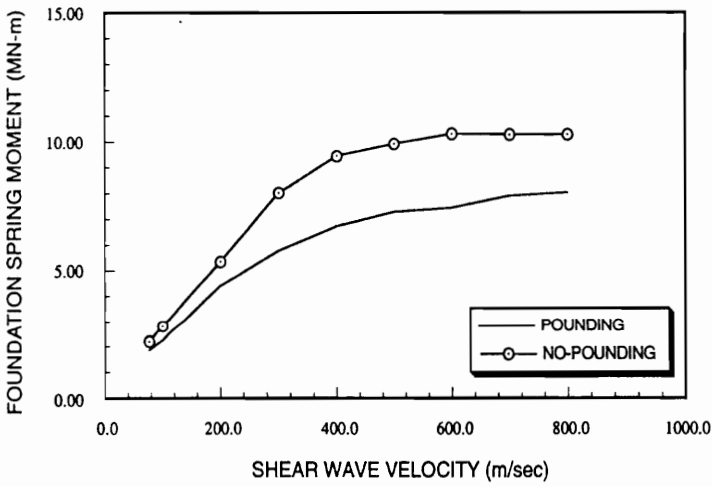
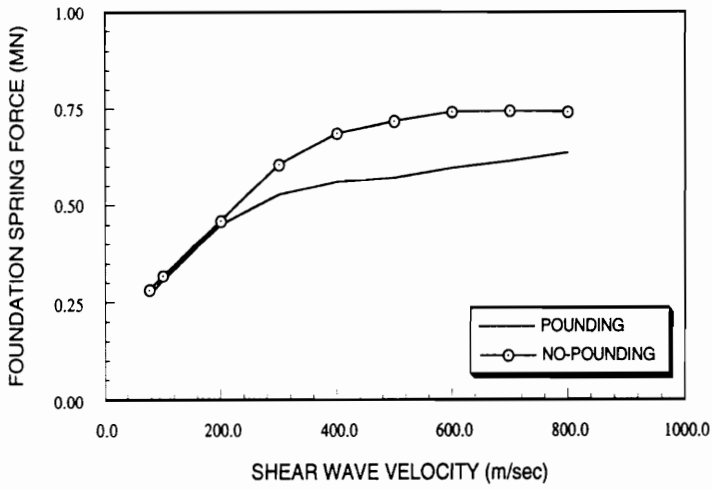


Figure 5.8: The effect of pounding on the force and moment responses of the translational and rotational foundation springs for the 5-story structure

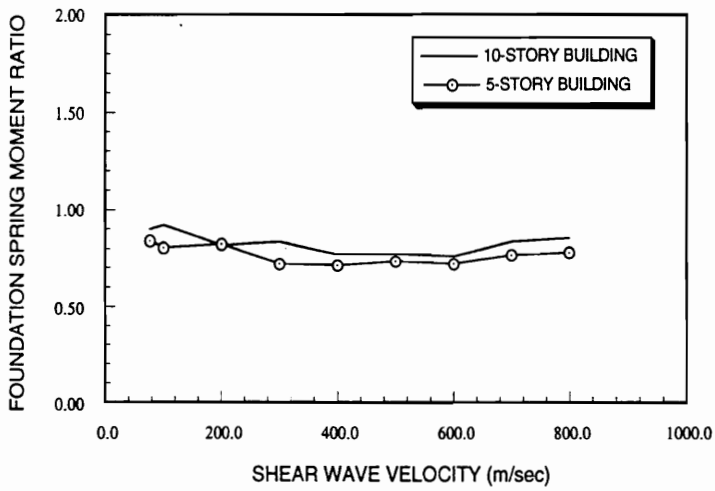
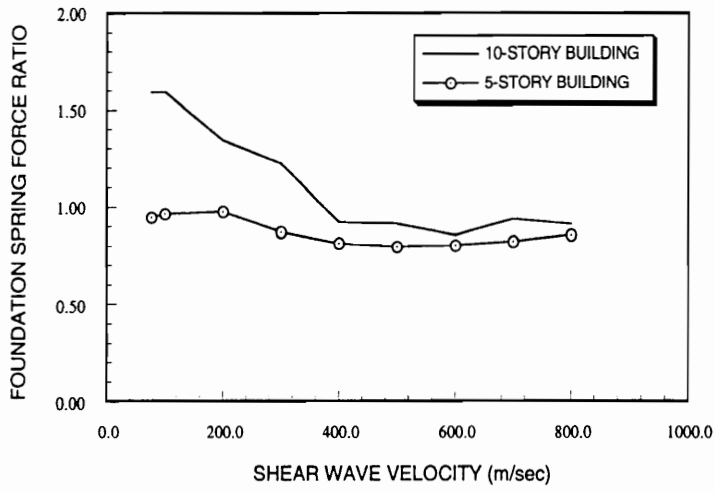


Figure 5.9: Pounding to no-pounding foundation springs force and moment ratios for the 5- and 10-story structures

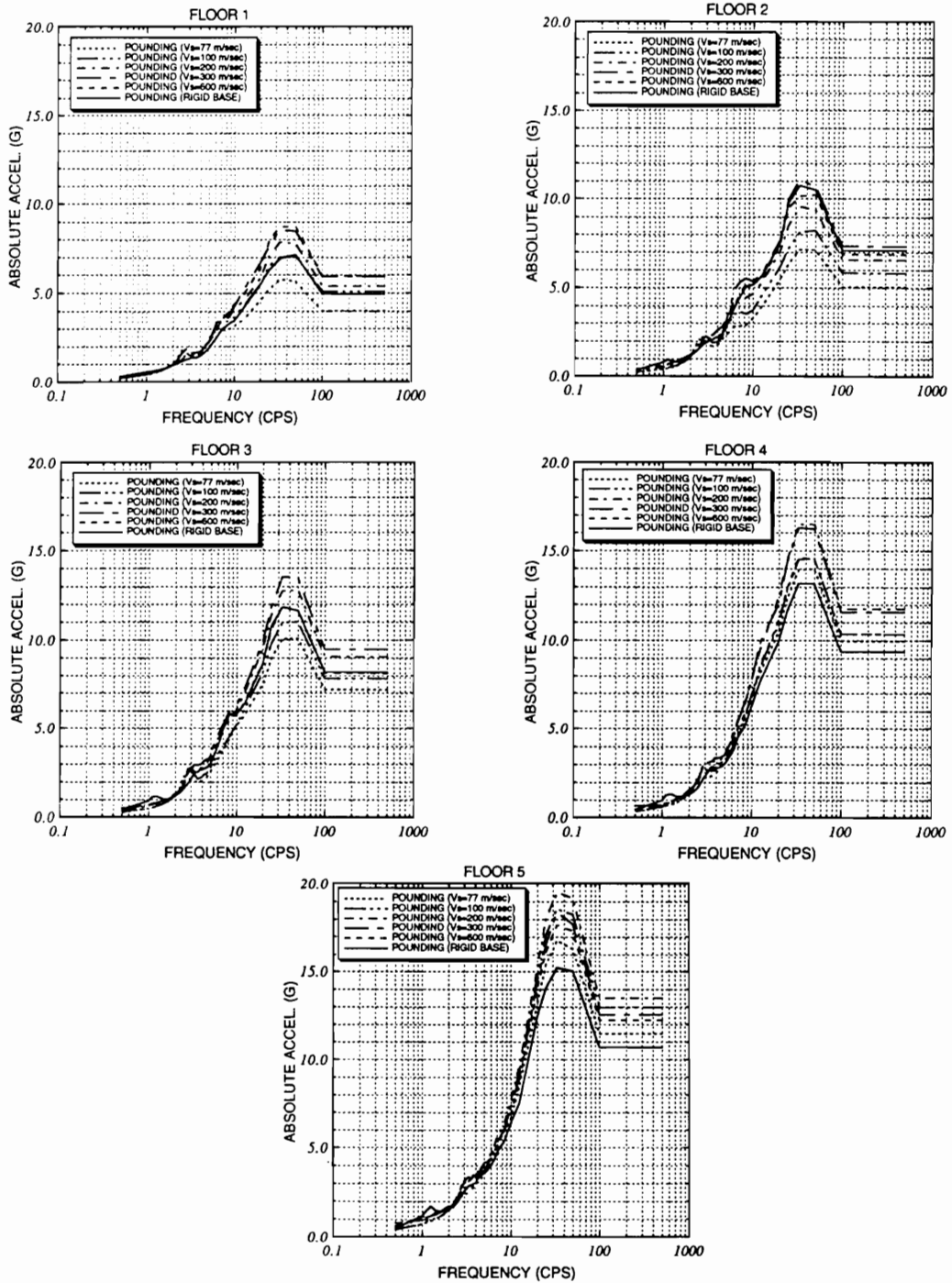


Figure 5.10: The effect of foundation shear wave velocity on the floor acceleration response spectra of various floors of the 10-story structure – floors 1 through 5

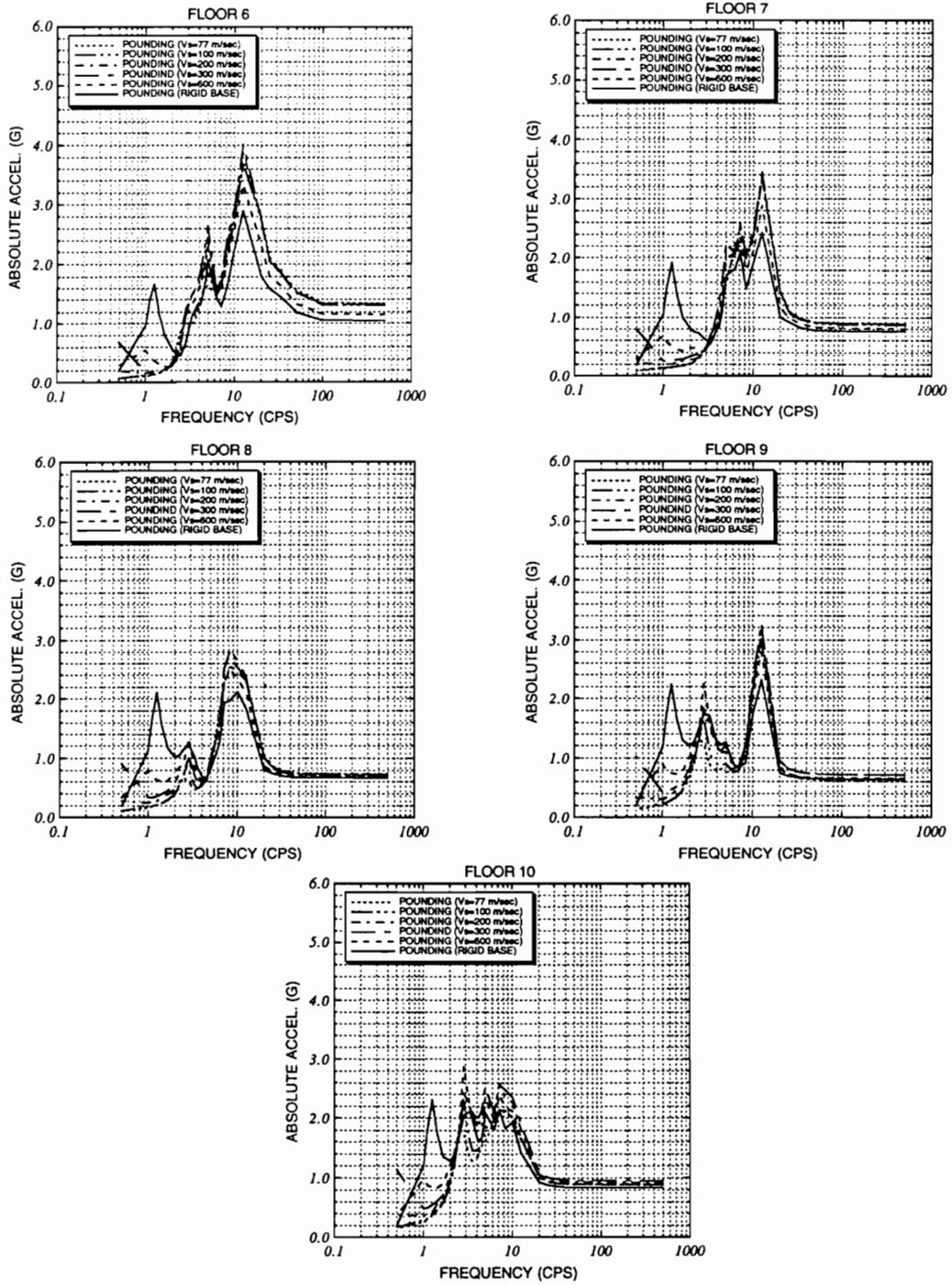


Figure 5.11: The effect of foundation shear wave velocity on the floor acceleration response spectra of various floors of the 10-story structure – floors 6 through 10

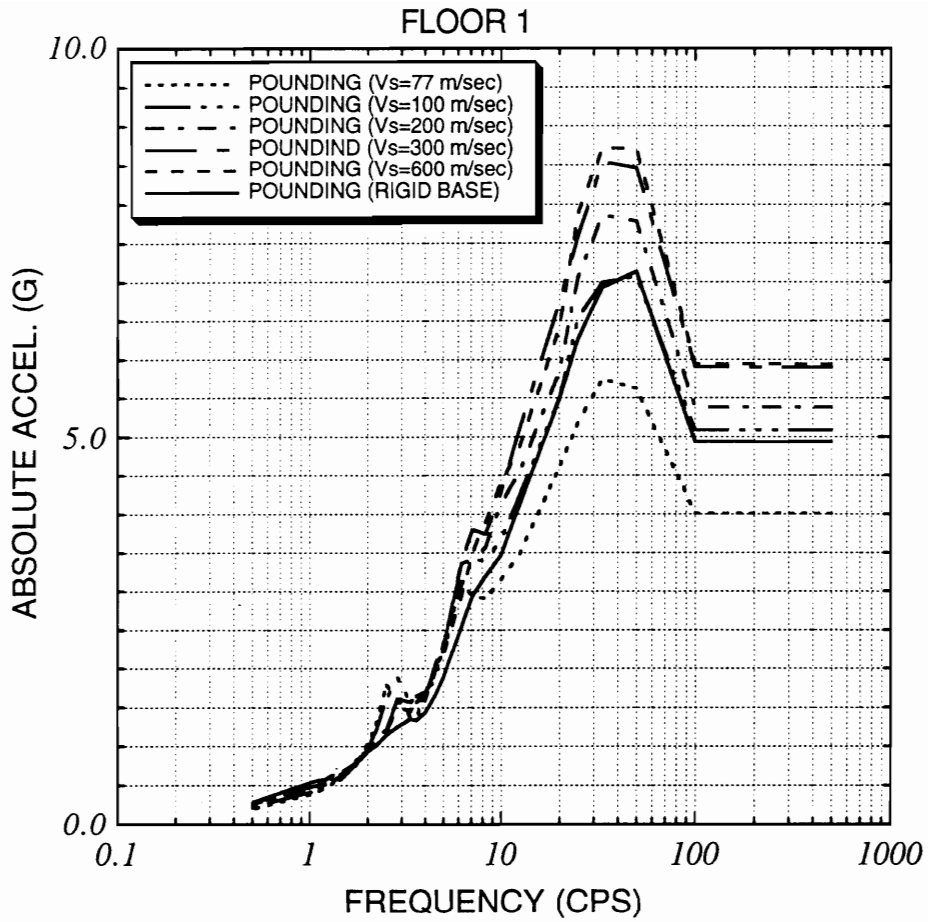


Figure 5.12: The effect of foundation shear wave velocity on the floor acceleration response spectra of floor 1 of the 10-story structure in enlarged form

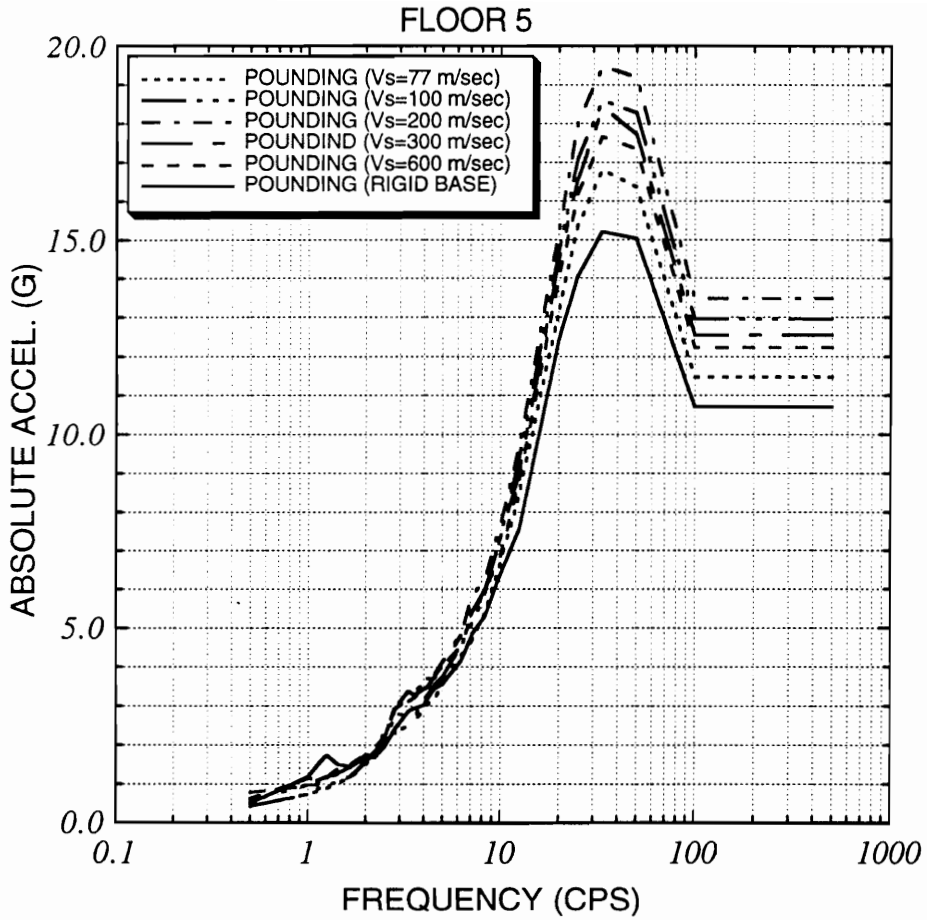


Figure 5.13: The effect of foundation shear wave velocity on the floor acceleration response spectra of floor 5 of the 10-story structure in enlarged form

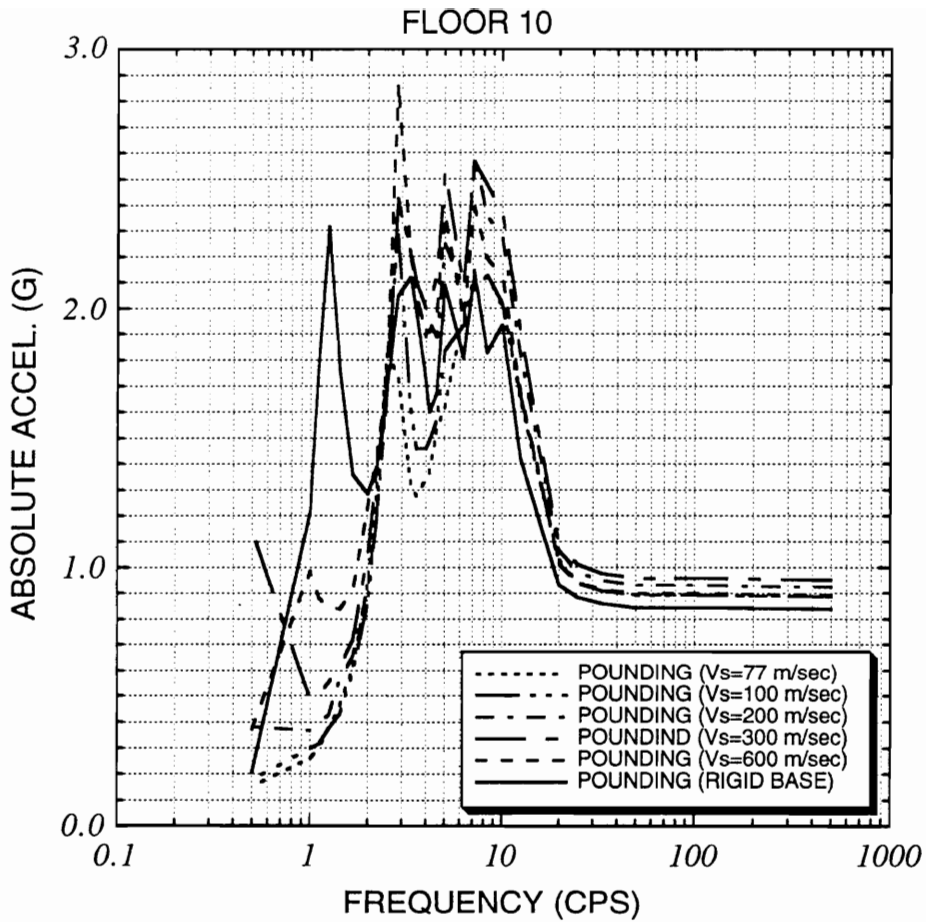


Figure 5.14: The effect of foundation shear wave velocity on the floor acceleration response spectra of floor 10 of the 10-story structure in enlarged form

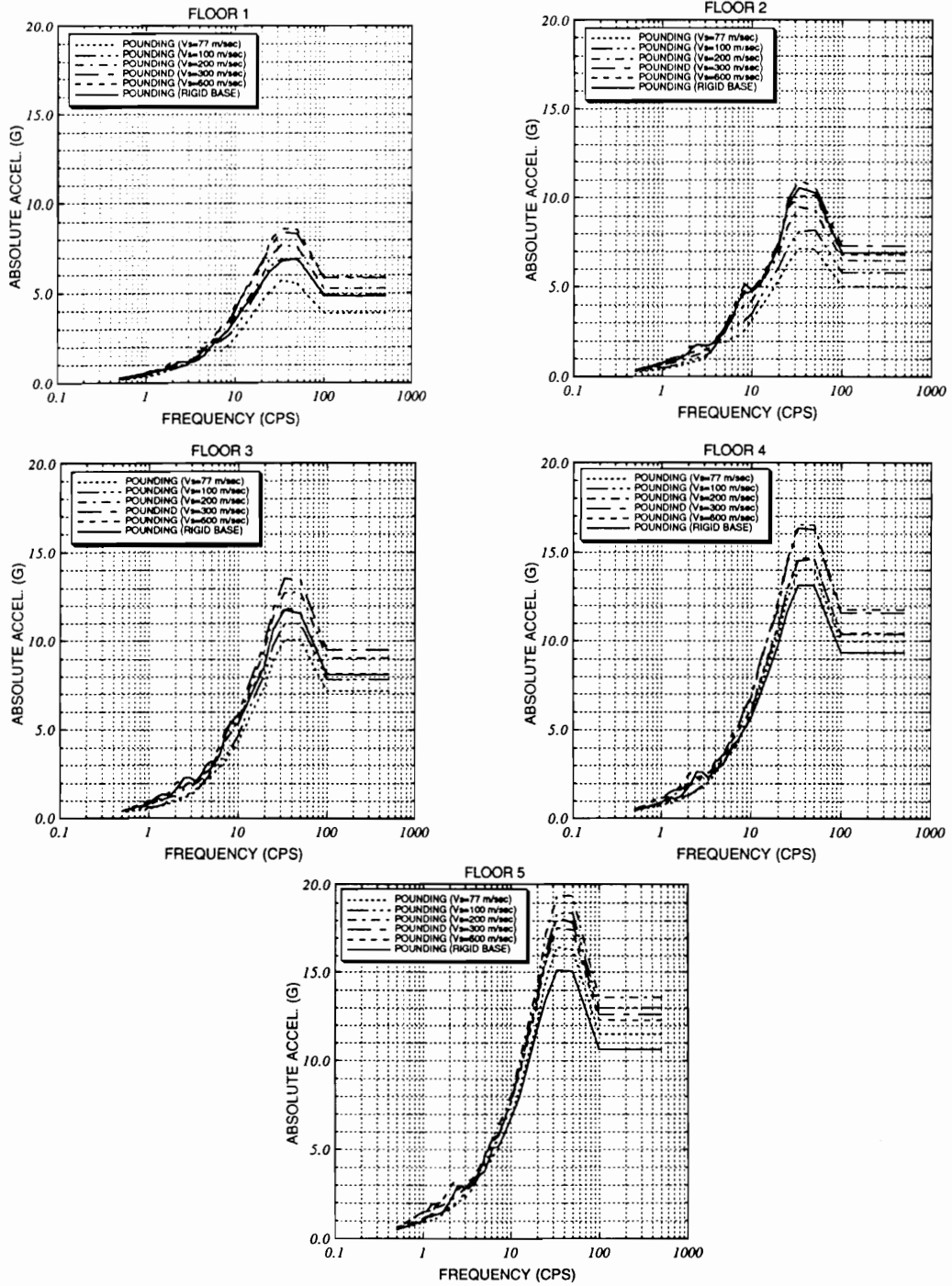


Figure 5.15: The effect of the foundation shear wave velocity on the floor acceleration response spectra of various floors of the 5-story structure

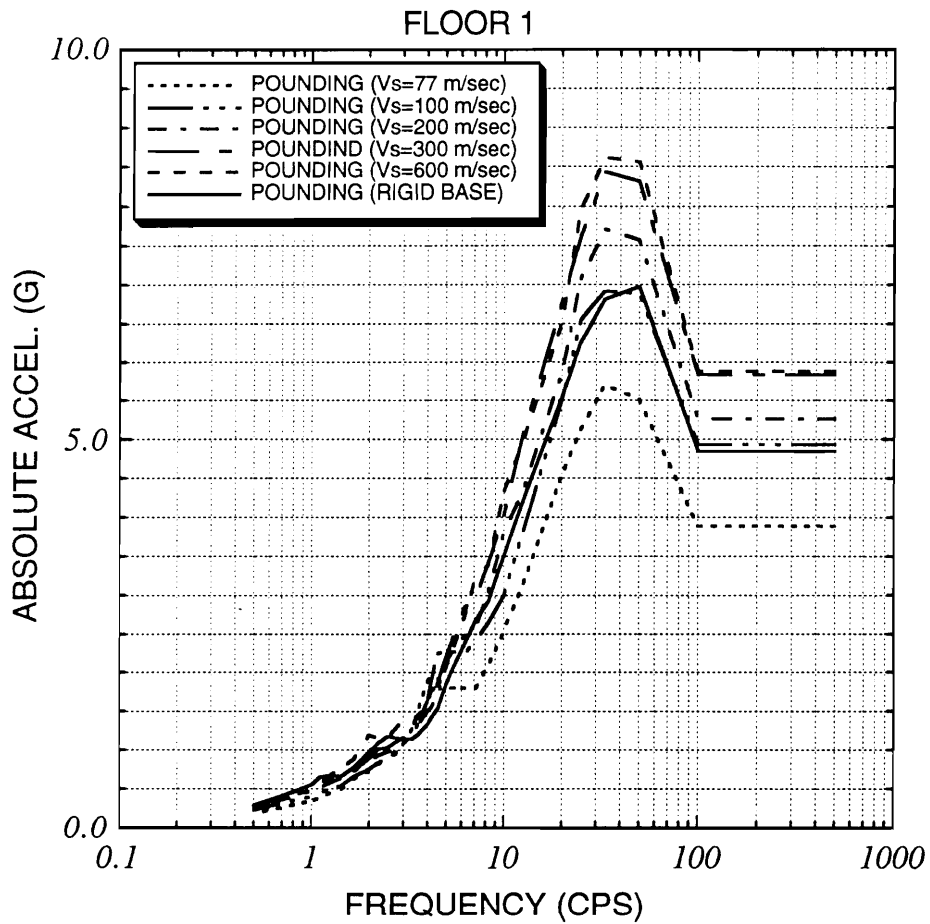


Figure 5.16: The effect of foundation shear wave velocity on the floor acceleration response spectra of floor 1 of the 5-story structure in enlarged form

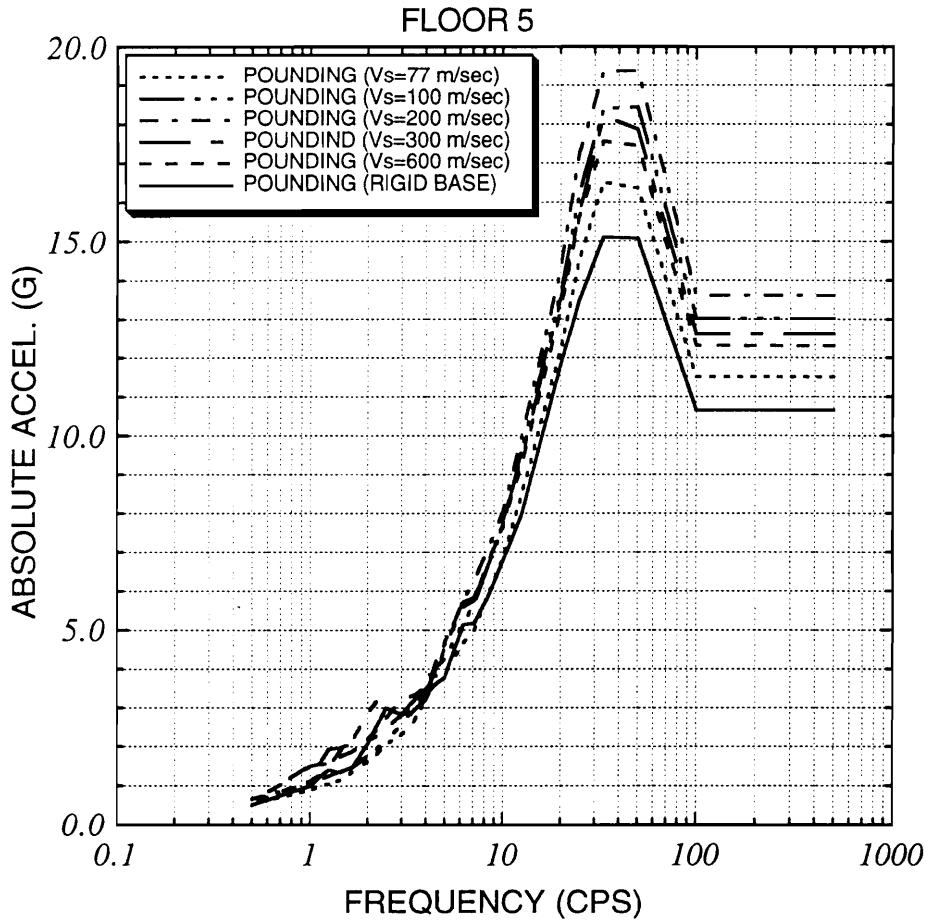


Figure 5.17: The effect of foundation shear wave velocity on the floor acceleration response spectra of floor 5 of the 5-story structure in enlarged form

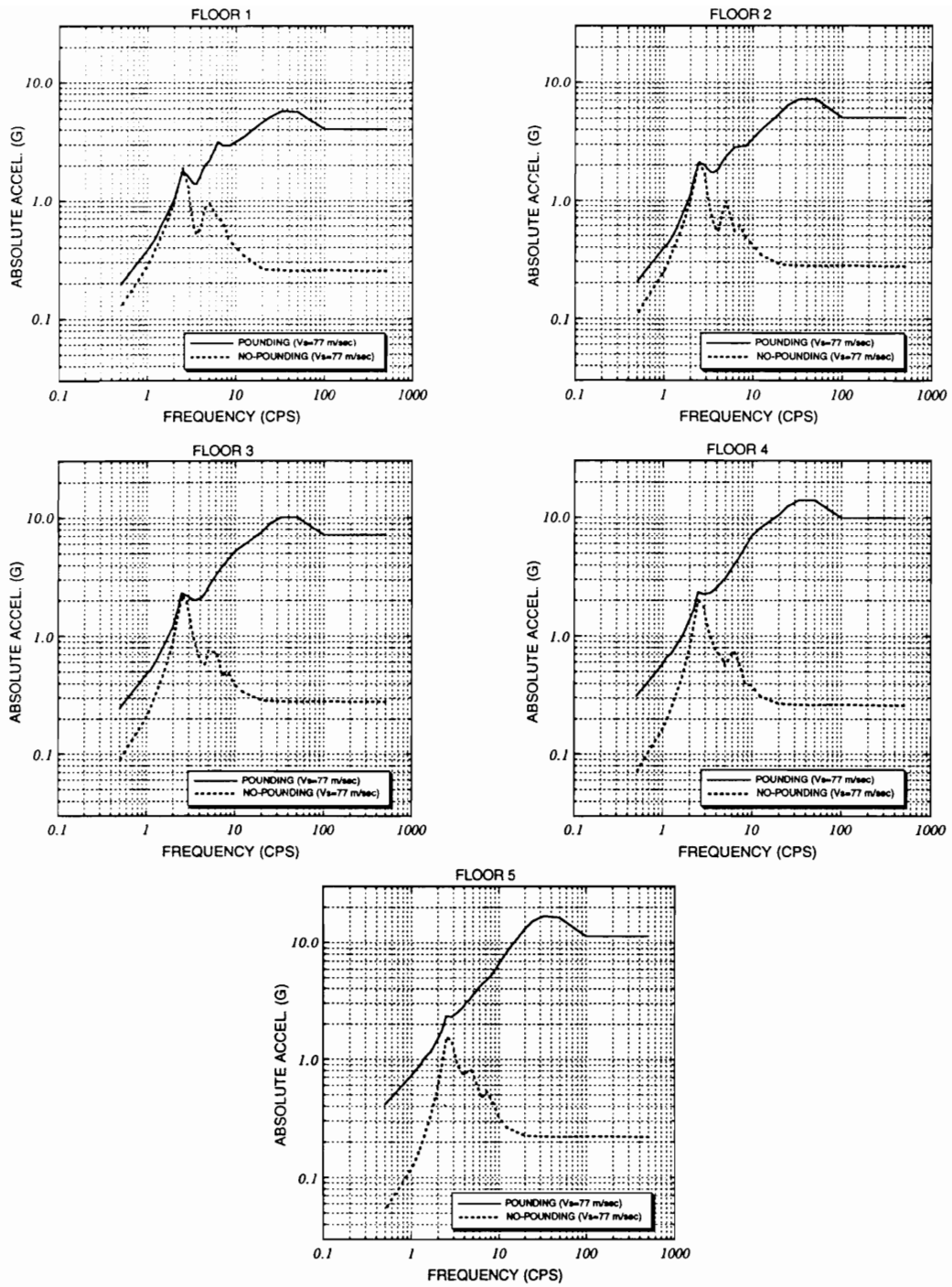


Figure 5.18: Floor acceleration response spectra of various floors in pounding and no-pounding cases for 10-story structure supported on the flexible foundation – floors 1 through 5

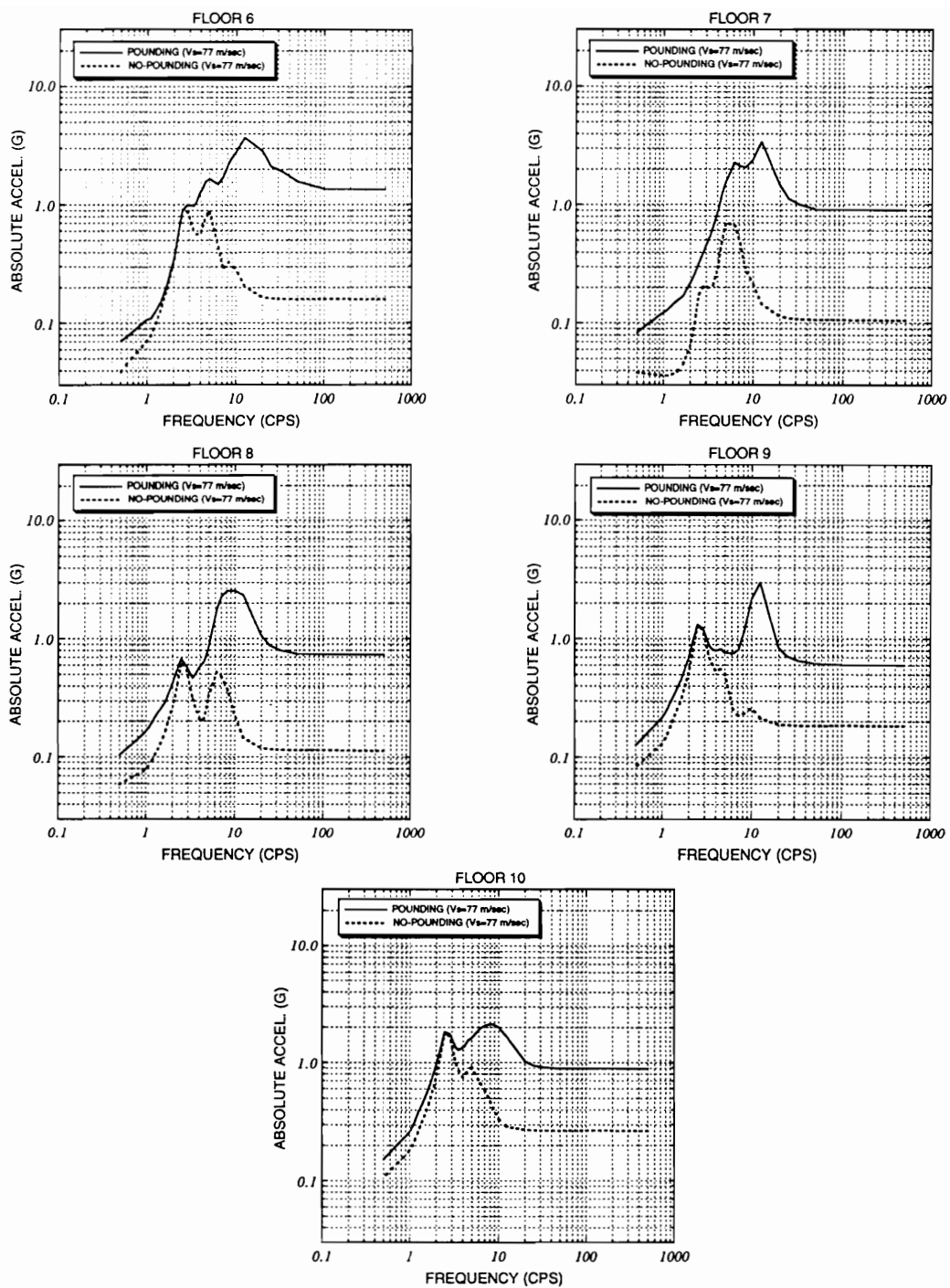


Figure 5.19: Floor acceleration response spectra of various floors in pounding and no-pounding cases for 10-story structure supported on the flexible foundation – floors 6 through 10

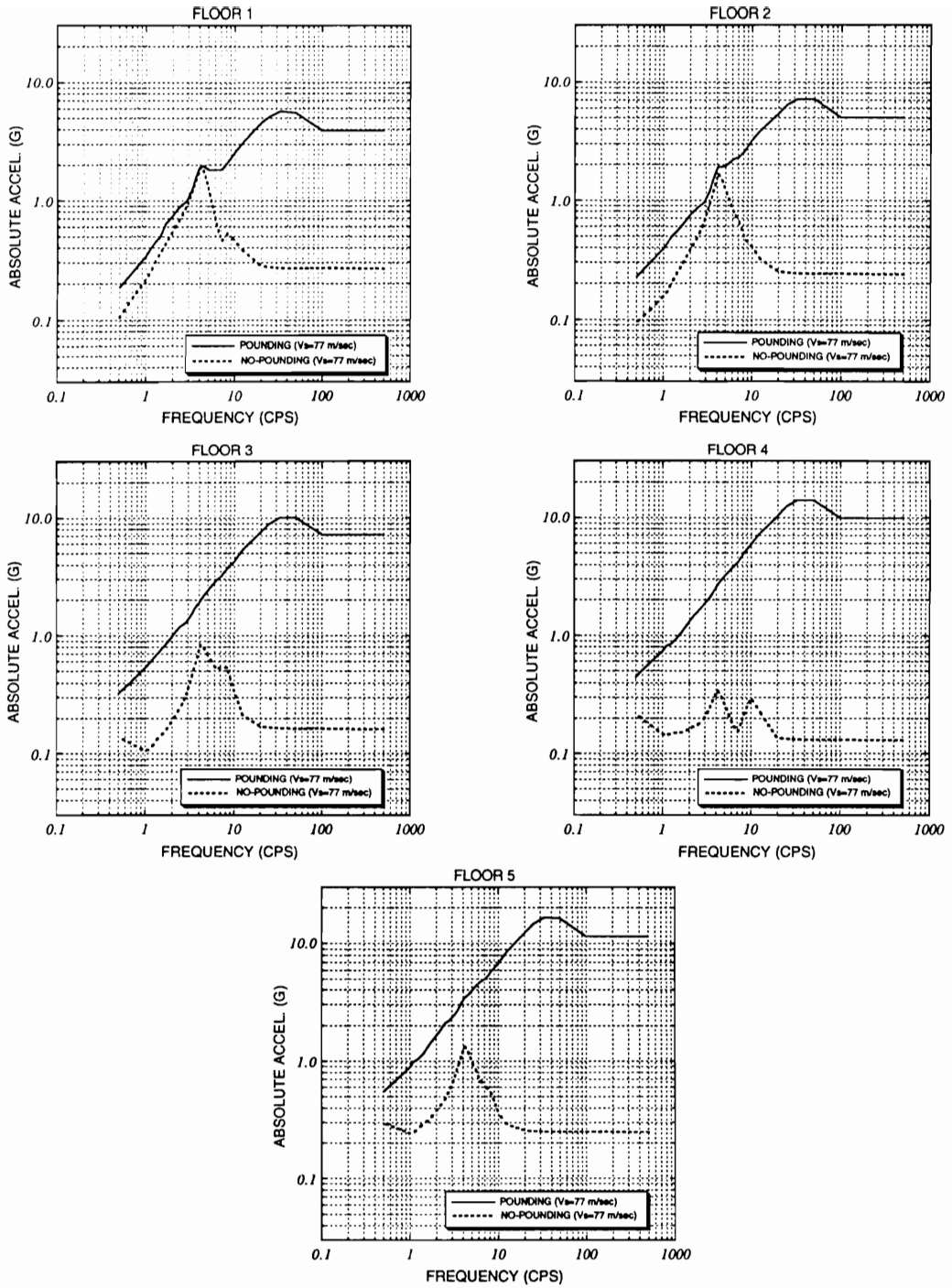


Figure 5.20: Floor acceleration response spectra of various floors in pounding and no-pounding cases for 5-story structure supported on the flexible foundation

Chapter 6

MITIGATION OF POUNDING PROBLEM

6.1 Introduction

In chapters 2 and 3, we studied the pounding response of two deformable structures during earthquakes. The parametric studies showed that the pounding, in general, increased the response of structures. In particular the two most significant effects of pounding were observed to be:

1. A large increase in the story shear response of the structures, especially in the stories above the top pounding floor of the taller structure. Increased story shear means that the story columns will experience larger bending moment response.
2. A dramatic increase in the absolute acceleration, especially of the pounding floors of both structures. This increase in floor accelerations can be detrimental to the supported secondary systems. The overturning moments at the lower levels were also increased.

These response increases require that the design of pounding structures be modified to either alleviate the pounding effects or increase the strength of the structural members to prevent their damage. In this chapter, therefore, we examine different methods for reducing or eliminating the effect of pounding on the response of structures.

The best alternative to a structural pounding problem is not to have pounding at all. This can be achieved by separating the buildings with a clearance larger than their maximum unobstructed displacement response. This may, however, be only possible for new construction. For existing buildings constructed next to each other with no or small spacing

between them, this option of increasing the clearance is not available. For these structures, other options of alleviating pounding effects must be sought.

The options considered are:

1. Installation of soft springs or precompressed springs at the pounding interface.
2. Installation of diagonal bracings to withstand large impact forces with and without joining the two structures.

In the following sections, these alternative options are examined with numerical examples.

6.2 Pounding on Soft Springs

In Chapters 2 and 3, we conducted a parametric study where the stiffness coefficient of the impact spring was changed. It was noticed that as the impact spring became softer the response of the structures decreased to their no-pounding cases. In this chapter, therefore, we examine the effect on response of using very soft springs.

Numerical results have been obtained for the basic configuration of the two systems discussed in chapter 3. At the pounding interface, springs with stiffness coefficients several orders of magnitude smaller than the story column stiffnesses have been used. The ratios of multiple pounding to no-pounding responses for different impact spring stiffnesses are shown in Figures 6.1 and 6.2. For the softer springs, we observe that the ratio of the pounding to no-pounding response is nearly equal to or less than 1.0. However, as the impact spring stiffness is increased, the story shear ratio for higher stories becomes greater than 1.0 indicating that pounding response is higher than the no-pounding response. Similar observations are applicable to overturning moment response, which also increases due to pounding as the impact spring stiffness is increased.

From Figure 6.3, where we have plotted story shears versus pounding stiffness coefficient, we again note that for lower values of the coefficients, the story shears are nearly constant

at about the no-pounding shear values. However, the shear values start to increase when the pounding stiffness becomes greater than $\frac{1}{100}$ th of the story stiffness. After a stiffness coefficient of about $2.0E + 9 \text{ N/m}$ the story shears approach a constant level; for higher values of pounding stiffness coefficients, similar observations were made in Chapter 3 where the parametric variation study on the pounding stiffness was performed.

In Figure 6.4 we show the acceleration variations of the pounding floors of the ten-story structure with the stiffness coefficient of the impact springs. As observed earlier for the story shears, softer springs cause lower floor accelerations. The acceleration response is also seen to be insensitive to small values of the stiffness coefficient, but for stiffness coefficients higher than $1.0E + 8 \text{ N/m}$ the accelerations increase monotonically with the coefficient.

The above observations indicate that allowing the floors to pound on soft springs instead of pounding on the floor slabs will reduce the structural response significantly, even sometimes to less than the no-pounding response value. The use of a soft spring to reduce the response is, however, only possible if it can be physically inserted between the pounding floors. For a zero-gap case this will require cutting of the pounding floor slabs. The amount of cutting will depend upon how much the spring will deform and its physical size. A softer spring will, of course, also require a larger clearance to avoid impacting. Figure 6.5 shows the maximum deformations of various springs during vibration. It is seen that the impacting springs of stiffness coefficient $1.81E + 7 \text{ N/m}$ (which is $\frac{1}{100}$ of the story stiffness), should be allowed to deform by about 4.5 cm, 3.8 cm, 2.9 cm, 2 cm and 1.1 cm at floors 5, 4, 3, 2 and 1 respectively. The largest spring deformation of 4.5 cm is nearly equal to the maximum gap required for no-pounding of the structures. Thus provision of the softer springs at the pounding interfaces to insure a soft impact is not a feasible alternative.

The insertion of precompressed springs between the pounding surfaces was also considered, but it became immediately apparent that this would not reduce the response. The precompressed springs would apply an equal and opposite force to both structures. These forces will always be there and are in addition to the forces the two structures will experience when vibrating with the connecting springs. As the structural response with

connecting springs is more than the no-pounding response, unless the springs are very soft, no advantage is gained by providing precompressed springs at the pounding interfaces.

To examine what effect an energy dissipation device (viscous damper) introduced between the pounding floors will have on the response, here the story shear and floor acceleration responses obtained for increasing values of the damping coefficients are plotted in Figures 6.6 and 6.7. It is noted that the shears in the higher stories do decrease if dampers with very high coefficients are provided, although the story shear in the 6th story which is just above the highest pounding floor seems to be rather insensitive to changes in the damping coefficient. Also, for the chosen example problem, the floor acceleration response seems to be specially sensitive with respect to the damping coefficient values shown in the middle range of Figure 6.7. Thus the effectiveness of providing energy dissipation devices to alleviate the pounding effect, especially for reducing the story shear, is also questionable.

6.3 Response of Rigidly Joined Structures

One approach to avoid pounding is to join the pounding structures rigidly. To examine what effect this rigid joining will have on the response of the two structures, compared to the response when they are allowed to pound freely, the following set of numerical results is presented. The first five floors of the two structures are assumed to be connected by rigid links. A schematic of the joined structures is shown in Figure 6.8.

Figures 6.9 and 6.10, respectively, show the column bending moments and floor accelerations for the two structures for the El-Centro accelerogram and a synthetically generated accelerogram. To include the effect of variations in the base motion input, we also present similar results, but the average of the maximum values, obtained for an ensemble of fifty time histories which have similar frequency content as the accelerogram used in Figure 5.2. For comparison, the responses obtained for the no-pounding and free pounding cases are also shown.

It is clearly seen that by joining the two structures, the maximum floor acceleration

values are drastically reduced. The effect of joining the two structures on the column bending moment is, however, not entirely beneficial. In Figure 6.9, which is for the El-Centro accelerogram, we note that in the ten-story structure the column bending moments in the first few stories and also in the story immediately above the top pounding story are increased and those in the other stories are somewhat reduced. The bending moments in the five-story structure are increased by joining. A similar observation can be made from the results presented in Figure 6.10, which are for a synthetically generated time history. However, when we consider the average results for an ensemble of time histories, as shown in Figure 6.11, there are some differences. For example, the bending moments in all pounding stories are now decreased; they are even smaller than those for the no-pounding case. The bending moments in some stories above the top pounding story are increased. Also increased are the bending moments in the five-story structure.

Thus, joining the two structures is definitely advantageous in reducing the high floor acceleration caused by pounding. It will be helpful in protecting the supported secondary systems. But joining cannot reduce the increased story shears or bending moments in columns caused by pounding; in fact, it can even be detrimental as it could lead to higher bending moments in some stories. The situation of the smaller structure is definitely worsened by joining of the two structures because it introduces higher bending moments in the story columns.

6.4 Pounding of Braced Structures - Analytical Formulation

As observed in previous chapters, another detrimental effect of pounding was to increase shear in stories above the pounding stories, which results in higher bending moments in the columns. As seen in the previous section, these higher bending moments could not be reduced by joining of the two structures. To reduce this bending moment, we will examine the use of diagonal bracings. Several different configurations of the bracings will be considered. To strengthen the pounding structures of unequal story heights, the use of

bracings has been suggested by Rosenblueth and Esteva [36] and Newmark and Rosenblueth [29], and strengthening by links and beams has been suggested by Westermo [42].

In the previous section, we considered the pounding structures as shear beam structures. Now since diagonal bracings will be introduced in various stories, we will model the pounding structures as frame structures. The columns, beams and braces of the frames are modeled as beam finite elements. Each node will now have three degrees of freedom. In the following we will develop the equations of motion of two pounding structures for the general case of a flexible foundation. The results for a rigid foundation can be simply obtained by choosing a high value for the foundation springs.

The two pounding structures are identified as p- and q-structures. The properties associated with these structures will be identified by subscripts p and q, respectively.

Let the p-structure be modeled as a p-story structure with n nodes and $3n$ degrees of freedom [DOF]. This system is characterized by stiffness matrix \mathbf{K}_p , damping matrix \mathbf{C}_p and mass matrix \mathbf{M}_p . Similarly the q-structure is modeled as a q-story structure with m nodes and $3m$ DOF. This system is characterized by stiffness matrix \mathbf{K}_q , damping matrix \mathbf{C}_q and mass matrix \mathbf{M}_q . It is assumed that $n \geq m$.

It is assumed that the floor heights of both structures are the same and therefore the pounding will occur only at their floor levels. A schematic of the two structures is shown in Figure 6.12. As assumed before, the impact is modeled by a linear spring and dashpot element introduced between the colliding floor masses of the two structures.

The Lagrangian formulation is utilized to develop the equations of motion of the pounding structures. For the two pounding structures, the elastic potential energy of the structural components, the translational and rocking springs at the base, and the floor pounding springs can be written as:

$$\begin{aligned}
 V = & \frac{1}{2} \left[\mathbf{u}_p^T \mathbf{K}_p \mathbf{u}_p + \mathbf{u}_q^T \mathbf{K}_q \mathbf{u}_q + k_x (x_{bp}^2 + x_{bq}^2) + k_\theta (\theta_{bp}^2 + \theta_{bq}^2) \right] + \\
 & \frac{1}{2} \sum_{i=1}^q s_i [(x_{ip} + x_{bp} + h_i \theta_{bp}) - (x_{iq} + x_{bq} + h_i \theta_{bq}) - g_i]^2 \quad (6.1)
 \end{aligned}$$

where k_x and k_θ are the stiffness coefficients of the translational and rotational soil springs at the base; x_{bp} and θ_{bp} are the relative translation and rotation displacements of the base of the p-structure; x_{bq} and θ_{bq} similarly are the degrees of freedom of the base of the q-structure; h_i is the height of the i th floor measured from the base; g_i is the at-rest gap at the i th floor levels of the pounding structures; s_i is the stiffness coefficient of the impact element; and x_{ip} and x_{iq} are the displacements of the i th floor in the p- and q-structure. Here it is assumed that the soil springs at the base of the two structures are the same, although there will not be any difficulty in the formulation to have different springs. The vectors \mathbf{u}_p and \mathbf{u}_q are the nodal displacements vectors for the p- and q-structure, respectively, defined as:

$$\mathbf{u}_p^T = [\overbrace{x_{1p}, y_{1p}, \theta_{1p}, x_{2p}, y_{2p}, \theta_{2p}, \dots, x_{np}, y_{np}, \theta_{np}}^{3n}] \quad (6.2)$$

$$\mathbf{u}_q^T = [\overbrace{x_{1q}, y_{1q}, \theta_{1q}, x_{2q}, y_{2q}, \theta_{2q}, \dots, x_{mq}, y_{mq}, \theta_{mq}}^{3m}] \quad (6.3)$$

They define the nodal displacements measured with respect to the bases of the two structures.

The kinetic energy of the combined system of structures can be written as:

$$T = \frac{1}{2} \left[\dot{\mathbf{v}}_p^T \mathbf{M}_p \dot{\mathbf{v}}_p + \dot{\mathbf{v}}_q^T \mathbf{M}_q \dot{\mathbf{v}}_q + m_{bp}(\dot{x}_{bp} + \dot{x}_g)^2 + m_{bq}(\dot{x}_{bq} + \dot{x}_g)^2 + I_{bp} \dot{\theta}_{bp}^2 + I_{bq} \dot{\theta}_{bq}^2 \right] \quad (6.4)$$

where I_{bp} and I_{bq} represent the moments of inertia of the base mats of the p- and q-structure, respectively; m_{bp} and m_{bq} are the masses of the base mats of the p- and q-structure, respectively; x_g is the ground displacement and the dot indicates the time derivative with respect to time. The vectors \mathbf{v}_p and \mathbf{v}_q relate the nodal displacements \mathbf{u}_p and \mathbf{u}_q to the base displacements through the following equations:

$$\mathbf{v}_p = \mathbf{u}_p + \mathbf{r}_{gp}(x_g + x_{bp}) + \mathbf{r}_{\theta p} \theta_{bp} \quad (6.5)$$

$$\mathbf{v}_q = \mathbf{u}_q + \mathbf{r}_{gq}(x_g + x_{bq}) + \mathbf{r}_{\theta q}\theta_{bq} \quad (6.6)$$

The mass matrices \mathbf{M}_p and \mathbf{M}_q and the stiffness matrices \mathbf{K}_p and \mathbf{K}_q are derived by assembling the finite element mass and stiffness matrices using the standard finite element procedures [33]. The influence vectors for the ground displacement are defined as:

$$\mathbf{r}_{gp}^T = [\overbrace{1, 0, 0, 1, 0, 0, \dots, 1, 0, 0}^{3n}] \quad (6.7)$$

$$\mathbf{r}_{gq}^T = [\overbrace{1, 0, 0, 1, 0, 0, \dots, 1, 0, 0}^{3m}] \quad (6.8)$$

and the influence vectors for the base rotation are defined as:

$$\mathbf{r}_{\theta p}^T = [\overbrace{h_1, -b/2, -1, \dots, h_p, -b/2, -1, h_1, b/2, -1, \dots, h_p, b/2, -1}^{3n}] \quad (6.9)$$

$$\mathbf{r}_{\theta q}^T = [\overbrace{h_1, b/2, -1, \dots, h_q, b/2, -1, h_1, -b/2, -1, \dots, h_q, -b/2, -1}^{3m}] \quad (6.10)$$

where h_p and h_q are the heights of the top floors of the p- and q-structure, respectively and b is the bay span of the two structures, assumed to be the same. Substituting for \mathbf{v}_p and \mathbf{v}_q in T , we can write the Lagrangian as:

$$\begin{aligned} \mathbf{L} &= T - V \\ &= \frac{1}{2} \left[\dot{\mathbf{u}}_p^T + \mathbf{r}_{gp}^T(\dot{x}_{bp} + \dot{x}_g) + \mathbf{r}_{\theta p}^T\dot{\theta}_{bp} \right] \mathbf{M}_p \left[\dot{\mathbf{u}}_p + \mathbf{r}_{gp}(\dot{x}_{bp} + \dot{x}_g) + \mathbf{r}_{\theta p}\dot{\theta}_{bp} \right] + \\ &\quad \frac{1}{2} \left[\dot{\mathbf{u}}_q^T + \mathbf{r}_{gq}^T(\dot{x}_{bq} + \dot{x}_g) + \mathbf{r}_{\theta q}^T\dot{\theta}_{bq} \right] \mathbf{M}_q \left[\dot{\mathbf{u}}_q + \mathbf{r}_{gq}(\dot{x}_{bq} + \dot{x}_g) + \mathbf{r}_{\theta q}\dot{\theta}_{bq} \right] + \\ &\quad \frac{1}{2} \left[m_{bp}(\dot{x}_{bp} + \dot{x}_g)^2 + I_{bp}\dot{\theta}_{bp}^2 - \mathbf{u}_p^T \mathbf{K}_p \mathbf{u}_p - k_x x_{bp}^2 - k_\theta \theta_{bp}^2 \right] + \end{aligned}$$

$$\begin{aligned} & \frac{1}{2} \left[m_{bq}(\dot{x}_{bq} + \dot{x}_g)^2 + I_{bq}\dot{\theta}_{bq}^2 - \mathbf{u}_q^T \mathbf{K}_q \mathbf{u}_q - k_x x_{bq}^2 - k_\theta \theta_{bq}^2 \right] - \\ & \frac{1}{2} \sum_{i=1}^q s_i [(x_{ip} + x_{bp} + h_i \theta_{bp}) - (x_{iq} + x_{bq} + h_i \theta_{bq}) - g_i]^2 \end{aligned} \quad (6.11)$$

The Rayleigh dissipation function for the energy dissipated through viscous damping in the structures, radiation damping in the soil medium and in the impact damping elements can be written as:

$$\begin{aligned} D = & \frac{1}{2} \left[\dot{\mathbf{u}}_p^T \mathbf{C}_p \dot{\mathbf{u}}_p + c_x \dot{x}_{bp}^2 + c_\theta \dot{\theta}_{bp}^2 \right] + \frac{1}{2} \left[\dot{\mathbf{u}}_q^T \mathbf{C}_q \dot{\mathbf{u}}_q + c_x \dot{x}_{bq}^2 + c_\theta \dot{\theta}_{bq}^2 \right] + \\ & \frac{1}{2} \sum_{i=1}^q d_i \left[(\dot{x}_{ip} + \dot{x}_{bp} + h_i \dot{\theta}_{bp}) - (\dot{x}_{iq} + \dot{x}_{bq} + h_i \dot{\theta}_{bq}) \right]^2 \end{aligned} \quad (6.12)$$

where \mathbf{C}_p and \mathbf{C}_q are the damping matrices for the p- and q-structures. As in the previous chapters, these matrices have been defined in terms of the modal damping ratio and eigen-properties of the structure using standard procedures. The damping coefficient of the impact element is indicated by d_i and the translational and rocking radiation damping coefficients are denoted by c_x and c_θ , respectively. Using the Lagrangian of equation 6.11 along with equation 6.12, we can develop the equations of motion in the generalized coordinates \mathbf{q} as follows:

$$\frac{d}{dt} \left[\frac{\partial \mathbf{L}}{\partial \dot{\mathbf{q}}} \right] - \frac{\partial \mathbf{L}}{\partial \mathbf{q}} + \frac{\partial D}{\partial \dot{\mathbf{q}}} = 0 \quad (6.13)$$

where \mathbf{q} is defined as:

$$\mathbf{q}^T = \left[\overbrace{\mathbf{u}_p, x_{bp}, \theta_{bp}, \mathbf{u}_q, x_{bq}, \theta_{bq}}^{3(n+m)+4} \right] \quad (6.14)$$

Utilizing equations 6.11 and 6.12 in equation 6.13, after some simplifications the equations of motion for the p-structure can be written in the following form:

$$\mathbf{M}_p \ddot{\mathbf{u}}_p + \mathbf{M}_p \mathbf{r}_{gp} \ddot{x}_{bp} + \mathbf{M}_p \mathbf{r}_{\theta p} \ddot{\theta}_{bp} + \mathbf{C}_p \dot{\mathbf{u}}_p + \mathbf{f}_d + \mathbf{K}_p \mathbf{u}_p + \mathbf{f}_s = -\mathbf{M}_p \mathbf{r}_{gp} \ddot{x}_g \quad (6.15)$$

$$\begin{aligned} & \mathbf{r}_{gp}^T \mathbf{M}_p \ddot{\mathbf{u}}_p + (\mathbf{r}_{gp}^T \mathbf{M}_p \mathbf{r}_{gp} + m_{bp}) \ddot{x}_{bp} + \mathbf{r}_{gp}^T \mathbf{M}_p \mathbf{r}_{\theta p} \ddot{\theta}_{bp} + \sum_{i=1}^q d_i [(\dot{x}_{ip} + \dot{x}_{bp} + h_i \dot{\theta}_{bp}) - \\ & (\dot{x}_{iq} + \dot{x}_{bq} + h_i \dot{\theta}_{bq})] + c_x \dot{x}_{bp} + k_x x_{bp} + \sum_{i=1}^q s_i [(x_{ip} + x_{bp} + h_i \theta_{bp}) - \\ & (x_{iq} + x_{bq} + h_i \theta_{bq}) - g_i] = -(\mathbf{r}_{gp}^T \mathbf{M}_p \mathbf{r}_{gp} + m_{bp}) \ddot{x}_g \end{aligned} \quad (6.16)$$

$$\begin{aligned} & \mathbf{r}_{\theta p}^T \mathbf{M}_p \ddot{\mathbf{u}}_p + \mathbf{r}_{\theta p}^T \mathbf{M}_p \mathbf{r}_{gp} \ddot{x}_{bp} + (\mathbf{r}_{\theta p}^T \mathbf{M}_p \mathbf{r}_{\theta p} + I_{bp}) \ddot{\theta}_{bp} + \sum_{i=1}^q d_i h_i [(\dot{x}_{ip} + \dot{x}_{bp} + \\ & h_i \dot{\theta}_{bp}) - (\dot{x}_{iq} + \dot{x}_{bq} + h_i \dot{\theta}_{bq})] + c_\theta \dot{\theta}_{bp} + k_\theta \theta_{bp} + \sum_{i=1}^q s_i h_i [(x_{ip} + x_{bp} + h_i \theta_{bp}) - \\ & (x_{iq} + x_{bq} + h_i \theta_{bq}) - g_i] = -\mathbf{r}_{\theta p}^T \mathbf{M}_p \mathbf{r}_{gp} \ddot{x}_g \end{aligned} \quad (6.17)$$

where \mathbf{f}_s is a $3n \times 1$ vector containing the coupling terms between the two pounding structures due to impact force. It is noted that when $\delta_i = (x_{ip} + x_{bp} + h_i \theta_{bp}) - (x_{iq} + x_{bq} + h_i \theta_{bq}) - g_i < 0$, there will be no pounding. In that case the terms containing s_i and d_i in equations 6.15, 6.16 and 6.17 are set equal to zero. The vector \mathbf{f}_s is defined as:

$$\mathbf{f}_s = \left\{ \begin{array}{c} s_1 [(x_{1p} + x_{bp} + h_1 \theta_{bp}) - (x_{1q} + x_{bq} + h_1 \theta_{bq}) - g_1] \\ 0 \\ 0 \\ s_2 [(x_{2p} + x_{bp} + h_2 \theta_{bp}) - (x_{2q} + x_{bq} + h_2 \theta_{bq}) - g_2] \\ 0 \\ 0 \\ \vdots \\ s_q [(x_{qp} + x_{bp} + h_q \theta_{bp}) - (x_{qq} + x_{bq} + h_q \theta_{bq}) - g_q] \\ 0 \\ 0 \\ \vdots \\ 0 \end{array} \right\} \quad (6.18)$$

Similarly \mathbf{f}_d is a $3n \times 1$ vector containing the coupling terms between the two pounding structures due to impact damping. This vector is defined as:

$$\mathbf{f}_d = \left\{ \begin{array}{c} d_1 [(\dot{x}_{1p} + \dot{x}_{bp} + h_1 \dot{\theta}_{bp}) - (\dot{x}_{1q} + \dot{x}_{bq} + h_1 \dot{\theta}_{bq})] \\ 0 \\ 0 \\ d_2 [(\dot{x}_{2p} + \dot{x}_{bp} + h_2 \dot{\theta}_{bp}) - (\dot{x}_{2q} + \dot{x}_{bq} + h_2 \dot{\theta}_{bq})] \\ 0 \\ 0 \\ \vdots \\ d_q [(\dot{x}_{qp} + \dot{x}_{bp} + h_q \dot{\theta}_{bp}) - (\dot{x}_{qq} + \dot{x}_{bq} + h_q \dot{\theta}_{bq})] \\ 0 \\ 0 \\ \vdots \\ 0 \end{array} \right\} \quad (6.19)$$

Using a similar procedure, the equations of motion for the q-structure can be derived. In this case there are $3m + 2$ equations of motion where q of them are coupled with the p-system of equations. By combining the coupled equations of motion of the two pounding structures, we can write the system equations of motion as:

$$\mathbf{M} \ddot{\mathbf{u}} + (\mathbf{C} + \mathbf{D}) \dot{\mathbf{u}} + (\mathbf{K} + \mathbf{S}) \mathbf{u} = \mathbf{f} \quad (6.20)$$

where the system mass matrix is defined as:

$$\mathbf{M} = \begin{bmatrix} \mathbf{M}_1 & \\ & \mathbf{M}_2 \end{bmatrix} \quad (6.21)$$

The sub-matrix \mathbf{M}_1 corresponding to the p-structure is defined as:

$$\mathbf{M}_1 = \begin{bmatrix} \mathbf{M}_p & \mathbf{M}_p \mathbf{r}_{gp} & \mathbf{M}_p \mathbf{r}_{\theta p} \\ \mathbf{r}_{gp}^T \mathbf{M}_p & \mathbf{r}_{gp}^T \mathbf{M}_p \mathbf{r}_{gp} + m_{bp} & \mathbf{r}_{gp}^T \mathbf{M}_p \mathbf{r}_{\theta p} \\ \mathbf{r}_{\theta p}^T \mathbf{M}_p & \mathbf{r}_{\theta p}^T \mathbf{M}_p \mathbf{r}_{gp} & \mathbf{r}_{\theta p}^T \mathbf{M}_p \mathbf{r}_{\theta p} + I_{bp} \end{bmatrix} \quad (6.22)$$

and the sub-matrix \mathbf{M}_2 corresponding to the q-structure is defined as:

$$\mathbf{M}_2 = \begin{bmatrix} \mathbf{M}_q & \mathbf{M}_q \mathbf{r}_{gq} & \mathbf{M}_q \mathbf{r}_{\theta q} \\ \mathbf{r}_{gq}^T \mathbf{M}_q & \mathbf{r}_{gq}^T \mathbf{M}_q \mathbf{r}_{gq} + m_{bq} & \mathbf{r}_{gq}^T \mathbf{M}_q \mathbf{r}_{\theta q} \\ \mathbf{r}_{\theta q}^T \mathbf{M}_q & \mathbf{r}_{\theta q}^T \mathbf{M}_q \mathbf{r}_{gq} & \mathbf{r}_{\theta q}^T \mathbf{M}_q \mathbf{r}_{\theta q} + I_{bq} \end{bmatrix} \quad (6.23)$$

The vector of the unknown displacements, \mathbf{u} is given as in equation 6.14 and the damping matrix \mathbf{C} and the stiffness matrix \mathbf{K} are given as:

$$\mathbf{S}_2^T = \begin{bmatrix} s_1 & 0 & 0 & s_2 & 0 & 0 & \dots & s_q & 0 & 0 \\ s_1 h_1 & 0 & 0 & s_2 h_2 & 0 & 0 & \dots & s_q h_q & 0 & 0 \end{bmatrix} \quad (6.27)$$

$$\mathbf{S}_3 = \begin{bmatrix} \sum_{i=1}^q s_i & \sum_{i=1}^q s_i h_i \\ \sum_{i=1}^q s_i h_i & \sum_{i=1}^q s_i h_i^2 \end{bmatrix} \quad (6.28)$$

The $\mathbf{0}_1$, $\mathbf{0}_2$, $\mathbf{0}_3$, $\mathbf{0}_4$ and $\mathbf{0}_5$ are null matrices with the dimensions of $3q \times (3n - 3q)$, $3q \times 3q$, $(3n - 3q) \times (3n - 3q)$, $2 \times (3n - 3q)$ and $2 \times 3q$, respectively.

The supplemental damping matrix \mathbf{D} in equation 6.20 is of the same form as matrix \mathbf{S} , except that the s_i are replaced by d_i in equations 6.25, 6.26 and 6.27 to obtain \mathbf{D} .

The system force vector \mathbf{f} in equation 6.20 consists of the forces due to ground excitation as well as the forces due to the structural pounding. This vector is defined as:

$$\mathbf{f} = - \left\{ \begin{array}{c} \mathbf{M}_p \mathbf{r}_{gp} \\ \mathbf{r}_{gp}^T \mathbf{M}_p \mathbf{r}_{gp} + m_{bp} \\ \mathbf{r}_{\theta p}^T \mathbf{M}_p \mathbf{r}_{gp} \\ \mathbf{M}_q \mathbf{r}_{gq} \\ \mathbf{r}_{gq}^T \mathbf{M}_q \mathbf{r}_{gq} + m_{bq} \\ \mathbf{r}_{\theta q}^T \mathbf{M}_q \mathbf{r}_{gq} \end{array} \right\} \ddot{x}_g + \mathbf{S} \mathbf{g} \quad (6.29)$$

where \mathbf{g} is defined as:

$$\mathbf{g}^T = [\overbrace{g_1, 0, 0, g_2, 0, 0, \dots, g_q, 0, 0}^{3q}, \overbrace{0, 0, \dots, 0}^{3n-3q}] \quad (6.30)$$

The system of equations 6.20 is solved by the Newmark- β approach to obtain numerical results, which are presented in the following section.

6.5 Structures on Rigid Foundation

Equations derived in the previous section are used to obtain the numerical results for various bracing configurations.

Since the story above the top pounding story had the highest increase in its shear force, the strengthening of this story by a diagonal bracing has been examined first. These results are presented in Figures 6.13, 6.14 and 6.15, again for El-Centro, one synthetic time history and fifty synthetic time histories. Comparing the response of the braced and unbraced ten-story structure, it is seen that the column bending moment in the braced story is drastically reduced, but at the same time there is an increase in the moments of the other stories, especially the pounding stories, for the results presented for one accelerogram in Figures 6.13 and 6.14. This increase in the bending moment is, however, not seen when the average of several ground motions is considered, as is seen from Figure 6.15. The bending moment in the top stories is still higher than the bending moment for the no-pounding case. From the bottom set of the sketches in Figures 6.13, 6.14 and 6.15, we note that bracing of a story does not reduce the floor acceleration significantly.

Next we show the results, again for El-Centro, for one synthetic time history and the ensemble of fifty time histories in Figures 6.16, 6.17 and 6.18 for different bracing arrangements. From the results in Figure 6.17 for one time history input, we note that if we brace all non-pounding stories to reduce the bending moment in them, we end up getting higher bending moments in all the pounding stories. (This increase in the moment in the pounding stories is not very significant, however, when we consider the averaging effect of fifty time histories, Figure 6.18). Thus, in general, this arrangement only transfers the problem from

the top stories to the bottom stories. It also worsens the acceleration response situation.

The effect of only bracing the pounding stories is also not beneficial, as it causes even higher bending moment response in the non-pounding stories. However, because this arrangement makes the structure more stiff, it reduces the relative displacement between the pounding stories and thus the accelerations of the pounding floors compared to the accelerations we obtain for the case of free pounding.

From these results, we observe that, in general, bracing one or more stories only has a local effect. In most cases, it only transfers the problem from the braced stories to the remaining unbraced stories. It may, therefore, be necessary to brace all stories. With this motivation, we have also examined the case of bracing all ten stories of the structure, and corresponding results are presented and compared with other bracing arrangements in Figures 6.16, 6.17 and 6.18.

We observe that bracing all stories of the taller structure does reduce the bending moment response in all stories; the response becomes even smaller than the no-pounding response, except in the smaller structure in which its top story experiences somewhat higher bending moment. However, we also note that although the floor accelerations have been reduced, they are still much higher than the accelerations of the no-pounding case.

It is, therefore, now apparent that one must brace all the stories of at least the taller structure to reduce the bending moment response. At the same time, to reduce high acceleration caused by pounding, one must also join the two structures by rigid links. In the next set of three figures (Figures 6.19, 6.20 and 6.21), we therefore show the combined effect of joining the two structures and bracing the taller structure. From these results, we note that, even for the joined case, a partial bracing of the structure does not solve the problem completely; it only transfers the effect to the remaining part which is not braced. However, joining and complete bracing of the taller structure provides the best solution. It reduces the bending moments in all the stories of the taller structure. The higher pounding stories of the shorter structure experience moments higher than the no-pounding case and may, therefore, require bracing as well.

In the next set of three figures (Figures 6.22, 6.23 and 6.24) we examine the acceleration response, again for three different inputs. As we noted earlier, joining reduces the pounding accelerations of floors drastically. In the lower portions of the Figures 6.22, 6.23 and 6.24, we compare the acceleration response for different arrangements of bracing of the joined structures. We note that bracing all floors causes higher acceleration compared to other bracing arrangements, simply because the taller structure now becomes more rigid. Nevertheless this acceleration is much smaller than the acceleration for the case of freely pounding structures.

The next set of figures (Figures 6.25, 6.26 and 6.27) shows the response of the joined and separate, but completely braced, ten-story structures. We observe that joining does not change story bending moments. It mainly reduces the floor accelerations.

In the next set of figures, we examine the sensitivity of various response quantities with respect to the bracing size used. The case with all stories of the taller structure braced is considered. Also the results are only for the average of fifty time histories. In Figure 6.28 we plot the story column bending moment and acceleration responses obtained for various bracing sizes. As expected, we note that column bending moments are reduced by a larger bracing. However, the reduction is not very sensitive to size as all moment curves are not much separated. The acceleration values are seen to be more sensitive to bracing size. But even a large bracing does not reduce them to the no-pounding level.

In the next figure (Figure 6.29) we compare the axial force in the bracing in the upper part of the figure and combined axial plus bending stress in the bracing in the lower part of the figure. We observe that a larger bracing attracts a larger force, whereas the stresses in the bracing do not change much with the sizes. This is more clearly shown in the lower part of Figure 6.30, where we notice that stresses in the bracings in different stories do not change drastically as their sizes are changed. This suggests that a smaller size bracing may be as effective as a larger bracing, as far as the stresses in bracing themselves are concerned. Thus for design purposes, we can start with a smallest size bracing which can reduce the column bending moment to its no-pounding level. Similar observations can also be made

from the results presented in the next two figures (Figures 6.31 and 6.32) which pertain to the case of joined structures.

6.6 Structures on Flexible Foundations

In the preceding section, we considered various options to reduce the detrimental effects of pounding of two structures with a rigid foundation. In this section, we present parallel results for the structures on flexible foundations. The flexibility of the foundation is introduced through a set of two soil springs (translational and rotational) provided under each structure. The soil spring constants corresponding to a shear wave velocity of 77 *m/sec* are used.

Again we will consider the effect of joining the structures, providing bracing only and joining and bracing of the two structures. For calculating the response of pounding structures on a flexible foundation, the formulation of section 6.4 is used. For joined, braced or unbraced, structures on a flexible foundation, the formulation is developed in the following section.

6.6.1 Rigidly joined structures - equations of motion

In this section we develop the equations of motion of two structures rigidly joined at their floor levels. However, their foundation mats and soil springs are separate. The schematic of this system is shown in Figure 6.33.

Again the Lagrangian formulation is used. The kinetic energy of the combined system can be written as:

$$T = \frac{1}{2} \left[\dot{\mathbf{v}}_p^T \mathbf{M}_p \dot{\mathbf{v}}_p + \dot{\mathbf{v}}_q^T \mathbf{M}_q \dot{\mathbf{v}}_q + m_{bp} (\dot{x}_{bp} + \dot{x}_g)^2 + m_{bq} (\dot{x}_{bq} + \dot{x}_g)^2 + I_{bp} \dot{\theta}_{bp}^2 + I_{bq} \dot{\theta}_{bq}^2 \right] \quad (6.31)$$

where \mathbf{M}_p and \mathbf{M}_q are the mass matrices of the p- and q-structures considered separately; m_{bp} and m_{bq} are the masses of the bases of the two structures; I_{bp} and I_{bq} are the mass

moments of inertia of the two bases; \mathbf{v}_p and \mathbf{v}_q are the absolute displacement vectors of the two structures; x_{bp} and x_{bq} are the translations, relative to ground, of the bases of the two structures; θ_{bp} and θ_{bq} are the rotations of two structures and x_g is the ground displacement. The dot over a quantity represents its time derivative.

The potential energy of the system is written in terms of the relative displacement vector as:

$$V = \frac{1}{2} \left[\mathbf{u}_p^T \mathbf{K}_p \mathbf{u}_p + \mathbf{u}_q^T \mathbf{K}_q \mathbf{u}_q + k_x(x_{bp}^2 + x_{bq}^2) + k_\theta(\theta_{bp}^2 + \theta_{bq}^2) \right] \quad (6.32)$$

where \mathbf{K}_p and \mathbf{K}_q are the stiffness matrices of the p- and q-structures; \mathbf{u}_p and \mathbf{u}_q are the displacement vectors of the p- and q- structures relative to their respective bases and k_x and k_θ are the stiffness coefficients of the translational and rotational soil springs at the bases of two structures.

The Rayleigh dissipation function for the energy dissipated through viscous damping in the structural damping and radiation damping in the soil medium can be written as:

$$D = \frac{1}{2} \left[\dot{\mathbf{u}}_p^T \mathbf{C}_p \dot{\mathbf{u}}_p + \dot{\mathbf{u}}_q^T \mathbf{C}_q \dot{\mathbf{u}}_q + c_x(\dot{x}_{bp}^2 + \dot{x}_{bq}^2) + c_\theta(\dot{\theta}_{bp}^2 + \dot{\theta}_{bq}^2) \right] \quad (6.33)$$

where \mathbf{C}_p and \mathbf{C}_q are the p- and q-structure damping matrices. As in the previous chapters, these matrices have been defined in terms of the modal damping ratios and eigenproperties of the structure using standard procedures. The translational and rocking radiation damping coefficients at the bases of two structures are denoted c_x and c_θ , respectively.

The absolute and relative displacement vectors are related as follows:

$$\mathbf{v}_p = \mathbf{u}_p + \mathbf{r}_{gp}(x_g + x_{bp}) + \mathbf{r}_{\theta p}\theta_{bp} \quad (6.34)$$

$$\mathbf{v}_q = \mathbf{u}_q + \mathbf{r}_{gq}(x_g + x_{bq}) + \mathbf{r}_{\theta q}\theta_{bq} \quad (6.35)$$

Since the two structures are joined, the absolute displacement values at the common points on the two structures are the same. Let the absolute displacement vector of these common nodes be denoted \mathbf{v}_c . In terms of this common vector, the absolute displacement vectors are written as follows:

$$\mathbf{v}_p = \begin{Bmatrix} \mathbf{v}_{fp} \\ \mathbf{v}_c \end{Bmatrix} \quad (6.36)$$

$$\mathbf{v}_q = \begin{Bmatrix} \mathbf{v}_{fq} \\ \mathbf{v}_c \end{Bmatrix} \quad (6.37)$$

where \mathbf{v}_{fp} and \mathbf{v}_{fq} are the absolute displacement vectors of the unconnected nodes of the p- and q-structure, respectively.

Similarly, the influence vectors \mathbf{r}_{gp} , $\mathbf{r}_{\theta p}$, \mathbf{r}_{gq} and $\mathbf{r}_{\theta q}$ can be subdivided as:

$$\mathbf{r}_{gp} = \begin{Bmatrix} \mathbf{r}_{gfp} \\ \mathbf{r}_{gcp} \end{Bmatrix} \quad (6.38)$$

$$\mathbf{r}_{\theta p} = \begin{Bmatrix} \mathbf{r}_{\theta fp} \\ \mathbf{r}_{\theta cp} \end{Bmatrix} \quad (6.39)$$

$$\mathbf{r}_{gq} = \begin{Bmatrix} \mathbf{r}_{gfq} \\ \mathbf{r}_{gcq} \end{Bmatrix} \quad (6.40)$$

$$\mathbf{r}_{\theta q} = \begin{Bmatrix} \mathbf{r}_{\theta fq} \\ \mathbf{r}_{\theta cq} \end{Bmatrix} \quad (6.41)$$

where \mathbf{r}_{gfp} and \mathbf{r}_{gfq} are the influence vectors due to the ground motion of the unconnected nodes of the p- and q-structure; \mathbf{r}_{gcp} and \mathbf{r}_{gcq} are the influence vectors due to the ground

motion of the common nodes of the p- and q-structure; $\mathbf{r}_{\theta fp}$ and $\mathbf{r}_{\theta fq}$ are the influence vectors due to the base rotation of the unconnected nodes of the p- and q-structure and $\mathbf{r}_{\theta cp}$ and $\mathbf{r}_{\theta cq}$ are the influence vectors due to the base rotation of the common nodes of the p- and q-structure. These influence vectors are defined in Appendix A.

Substituting equations 6.36, 6.38 and 6.39 in equation 6.34, one obtains:

$$\mathbf{u}_p = \begin{Bmatrix} \mathbf{v}_{fp} \\ \mathbf{v}_c \end{Bmatrix} - \begin{Bmatrix} \mathbf{r}_{gfp} \\ \mathbf{r}_{gcp} \end{Bmatrix} (\mathbf{x}_g + \mathbf{x}_{bp}) - \begin{Bmatrix} \mathbf{r}_{\theta fp} \\ \mathbf{r}_{\theta cp} \end{Bmatrix} \theta_{bp} \quad (6.42)$$

Similarly by substituting equations 6.37, 6.40 and 6.41 in equation 6.35, we can write:

$$\mathbf{u}_q = \begin{Bmatrix} \mathbf{v}_{fq} \\ \mathbf{v}_c \end{Bmatrix} - \begin{Bmatrix} \mathbf{r}_{gfq} \\ \mathbf{r}_{gcq} \end{Bmatrix} (\mathbf{x}_g + \mathbf{x}_{bq}) - \begin{Bmatrix} \mathbf{r}_{\theta fq} \\ \mathbf{r}_{\theta cq} \end{Bmatrix} \theta_{bq} \quad (6.43)$$

Substituting equations 6.42 and 6.43 in equations 6.32 and 6.33 and by partitioning the mass, damping and stiffness matrices of the two structures in terms of their unconnected and common nodes, the kinetic energy T, potential energy V and dissipation function D can be written, respectively, as:

$$T = \frac{1}{2} \begin{Bmatrix} \dot{\mathbf{v}}_{fp}^T \\ \dot{\mathbf{v}}_c^T \end{Bmatrix} \begin{bmatrix} \mathbf{M}_{11p} & \mathbf{M}_{12p} \\ \mathbf{M}_{21p} & \mathbf{M}_{22p} \end{bmatrix} \begin{Bmatrix} \dot{\mathbf{v}}_{fp} \\ \dot{\mathbf{v}}_c \end{Bmatrix} + \frac{1}{2} \begin{Bmatrix} \dot{\mathbf{v}}_{fq}^T \\ \dot{\mathbf{v}}_c^T \end{Bmatrix} \begin{bmatrix} \mathbf{M}_{11q} & \mathbf{M}_{12q} \\ \mathbf{M}_{21q} & \mathbf{M}_{22q} \end{bmatrix} \begin{Bmatrix} \dot{\mathbf{v}}_{fq} \\ \dot{\mathbf{v}}_c \end{Bmatrix} + \frac{1}{2} [m_{bp}(\dot{\mathbf{x}}_{bp} + \dot{\mathbf{x}}_g)^2 + m_{bq}(\dot{\mathbf{x}}_{bq} + \dot{\mathbf{x}}_g)^2 + I_{bp}\dot{\theta}_{bp}^2 + I_{bq}\dot{\theta}_{bq}^2] \quad (6.44)$$

$$V = \frac{1}{2} \left[\begin{Bmatrix} \mathbf{v}_{fp}^T \\ \mathbf{v}_c^T \end{Bmatrix} - \begin{Bmatrix} \mathbf{r}_{gfp}^T \\ \mathbf{r}_{gcp}^T \end{Bmatrix} (\mathbf{x}_g + \mathbf{x}_{bp}) - \begin{Bmatrix} \mathbf{r}_{\theta fp}^T \\ \mathbf{r}_{\theta cp}^T \end{Bmatrix} \theta_{bp} \right] \begin{bmatrix} \mathbf{K}_{11p} & \mathbf{K}_{12p} \\ \mathbf{K}_{21p} & \mathbf{K}_{22p} \end{bmatrix} \left[\begin{Bmatrix} \mathbf{v}_{fp} \\ \mathbf{v}_c \end{Bmatrix} - \begin{Bmatrix} \mathbf{r}_{gfp} \\ \mathbf{r}_{gcp} \end{Bmatrix} (\mathbf{x}_g + \mathbf{x}_{bp}) - \begin{Bmatrix} \mathbf{r}_{\theta fp} \\ \mathbf{r}_{\theta cp} \end{Bmatrix} \theta_{bp} \right] +$$

$$\begin{aligned}
& \frac{1}{2} \left[\begin{array}{c} \left\{ \begin{array}{c} \mathbf{v}_{fq}^T \\ \mathbf{v}_c^T \end{array} \right\} - \left\{ \begin{array}{c} \mathbf{r}_{gfq}^T \\ \mathbf{r}_{gcq}^T \end{array} \right\} (x_g + x_{bq}) - \left\{ \begin{array}{c} \mathbf{r}_{\theta fq}^T \\ \mathbf{r}_{\theta cq}^T \end{array} \right\} \theta_{bq} \end{array} \right] \begin{bmatrix} \mathbf{K}_{11q} & \mathbf{K}_{12q} \\ \mathbf{K}_{21q} & \mathbf{K}_{22q} \end{bmatrix} \\
& \left[\begin{array}{c} \left\{ \begin{array}{c} \mathbf{v}_{fq} \\ \mathbf{v}_c \end{array} \right\} - \left\{ \begin{array}{c} \mathbf{r}_{gfq} \\ \mathbf{r}_{gcq} \end{array} \right\} (x_g + x_{bq}) - \left\{ \begin{array}{c} \mathbf{r}_{\theta fq} \\ \mathbf{r}_{\theta cq} \end{array} \right\} \theta_{bq} \end{array} \right] + \\
& \frac{1}{2} [k_x(x_{bp}^2 + x_{bq}^2) + k_\theta(\theta_{bp}^2 + \theta_{bq}^2)] \tag{6.45}
\end{aligned}$$

$$\begin{aligned}
D = & \frac{1}{2} \left[\begin{array}{c} \left\{ \begin{array}{c} \dot{\mathbf{v}}_{fp}^T \\ \dot{\mathbf{v}}_c^T \end{array} \right\} - \left\{ \begin{array}{c} \mathbf{r}_{gfp}^T \\ \mathbf{r}_{gcp}^T \end{array} \right\} (\dot{x}_g + \dot{x}_{bp}) - \left\{ \begin{array}{c} \mathbf{r}_{\theta fp}^T \\ \mathbf{r}_{\theta cp}^T \end{array} \right\} \dot{\theta}_{bp} \end{array} \right] \begin{bmatrix} \mathbf{C}_{11p} & \mathbf{C}_{12p} \\ \mathbf{C}_{21p} & \mathbf{C}_{22p} \end{bmatrix} \\
& \left[\begin{array}{c} \left\{ \begin{array}{c} \dot{\mathbf{v}}_{fp} \\ \dot{\mathbf{v}}_c \end{array} \right\} - \left\{ \begin{array}{c} \mathbf{r}_{gfp} \\ \mathbf{r}_{gcp} \end{array} \right\} (\dot{x}_g + \dot{x}_{bp}) - \left\{ \begin{array}{c} \mathbf{r}_{\theta fp} \\ \mathbf{r}_{\theta cp} \end{array} \right\} \dot{\theta}_{bp} \end{array} \right] + \\
& \frac{1}{2} \left[\begin{array}{c} \left\{ \begin{array}{c} \dot{\mathbf{v}}_{fq}^T \\ \dot{\mathbf{v}}_c^T \end{array} \right\} - \left\{ \begin{array}{c} \mathbf{r}_{gfq}^T \\ \mathbf{r}_{gcq}^T \end{array} \right\} (\dot{x}_g + \dot{x}_{bq}) - \left\{ \begin{array}{c} \mathbf{r}_{\theta fq}^T \\ \mathbf{r}_{\theta cq}^T \end{array} \right\} \dot{\theta}_{bq} \end{array} \right] \begin{bmatrix} \mathbf{C}_{11q} & \mathbf{C}_{12q} \\ \mathbf{C}_{21q} & \mathbf{C}_{22q} \end{bmatrix} \\
& \left[\begin{array}{c} \left\{ \begin{array}{c} \dot{\mathbf{v}}_{fq} \\ \dot{\mathbf{v}}_c \end{array} \right\} - \left\{ \begin{array}{c} \mathbf{r}_{gfq} \\ \mathbf{r}_{gcq} \end{array} \right\} (\dot{x}_g + \dot{x}_{bq}) - \left\{ \begin{array}{c} \mathbf{r}_{\theta fq} \\ \mathbf{r}_{\theta cq} \end{array} \right\} \dot{\theta}_{bq} \end{array} \right] + \\
& \frac{1}{2} [c_x(\dot{x}_{bp}^2 + \dot{x}_{bq}^2) + c_\theta(\dot{\theta}_{bp}^2 + \dot{\theta}_{bq}^2)] \tag{6.46}
\end{aligned}$$

Using the Lagrangian of equations 6.44 and 6.45 along with equation 6.46, we can develop the equations of motion in the generalized coordinates \mathbf{q} as follows:

$$\frac{d}{dt} \left[\frac{\partial \mathbf{L}}{\partial \dot{\mathbf{q}}} \right] - \frac{\partial \mathbf{L}}{\partial \mathbf{q}} + \frac{\partial D}{\partial \dot{\mathbf{q}}} = 0 \tag{6.47}$$

where \mathbf{q} is defined as

$$\mathbf{q}^T = \left[\overbrace{\mathbf{v}_{fp}, \mathbf{v}_c, \mathbf{v}_{fq}, x_{bp}, \theta_{bp}, x_{bq}, \theta_{bq}}^{3(n+\frac{m}{2})+4} \right] \tag{6.48}$$

and

$$L = T - V \quad (6.49)$$

Utilizing equations 6.49 and 6.46 in equation 6.47 and after some simplifications the equations of motion for the joined system in matrix form can be written as:

$$M\ddot{\mathbf{q}} + C\dot{\mathbf{q}} + K\mathbf{q} = \mathbf{f} \quad (6.50)$$

The matrices \mathbf{M} , \mathbf{C} , \mathbf{K} and the vector \mathbf{f} are defined in Appendix A.

6.6.2 Rigidly joined structures on flexible foundation - numerical results

In Figures 6.34, 6.35 and 6.36 we present the column bending moment and floor acceleration results for the two structures subjected to El-Centro (Figure 6.34), one synthetic time history (Figure 6.35) and fifty synthetic time histories (Figure 6.36). For fifty time histories the results are the average of the maximum values.

From the comparison of the results for joined and free pounding structures we notice that joining the two structures reduces the bending moments in the columns of the ten-story structure for all three inputs. It is pointed out here that this was not the case when we considered the structures on a rigid foundation (as shown in Figures 6.9, 6.10 and 6.11). So in this case, the pounding effects are reduced in the ten-story structure by joining the two structures, but the bending moments are still higher than those for the case of no-pounding. Also the smaller structure experiences larger bending moments than the moments for the free pounding or no-pounding cases. The main advantage of joining the two structures, however, lies in the fact that the pounding accelerations are now reduced drastically.

6.6.3 Braced structures on flexible foundation

In this section, we will present results for various configurations of bracings. When the structures, braced or unbraced, are freely pounding, the formulation presented in section 6.4

is used to obtain the numerical results. On the other hand, when the structures are rigidly joined, the formulation presented in section 6.6.1 is used.

First we consider bracing of the sixth story of the ten-story structure which experienced a large increase in the bending moment due to pounding. Again the results for three inputs are presented: (1) El-Centro in Figure 6.37, (2) one synthetic time history in Figure 6.38 and (3) fifty synthetic time histories in Figure 6.39. The most conspicuous effect of providing bracing in the sixth story is to reduce the bending moment in this particular story. The bending moments in other stories and pounding accelerations are not affected significantly. The top story of the five-story structure is seen to attract more bending moment in this case.

Thus the effect of providing bracing only in the sixth story did serve the purpose of reducing the bending moment in that story, but the benefits were localized.

In the next set of figures (Figures 6.40, 6.41 and 6.42) we compare the responses obtained for the three inputs for different configurations of the bracings used. The results are presented for: (1) no-pounding response, (2) free pounding without bracings, (3) pounding with first five stories braced, (4) pounding with top five stories braced and (5) pounding with all ten stories braced. In all three cases of inputs it is observed that:

1. Bracing of only the top five stories reduces the responses in the braced stories. The response in the unbraced lower stories may even be increased by this bracing arrangement (Figures 6.40, 6.41 and 6.42 for El-Centro and synthetic time history inputs).
2. Bracing of the lower five stories has a similar influence. That is, it does reduce the bending moment response in the lower five stories, but it may increase the response in the higher stories (Figure 6.40 for El-Centro input).
3. Bracing of all ten stories seems to be the best in reducing the bending moment due to pounding over the entire height. It is, however, noticed that this reduced response is still higher than the no-pounding response. Also, bracing all ten stories increases the bending moment in the top story of the five-story structure.

4. All these arrangements of bracing do not decrease the pounding acceleration responses.

In summary, we notice that bracing of all ten stories provides the best results, but at the same time it does not take care of all problems. That is, (1) it does not reduce the column moments adequately, (2) it does not decrease the pounding acceleration and (3) it increases the bending moment in the top story of the five-story structure. Therefore, next we want to examine if we can reduce these undesirable features by joining as well as bracing the two structures.

In the next three figures (Figures 6.43, 6.44 and 6.45) we compare the bending moment response for three different inputs for joined structures with different bracing configurations. We observe that bracing of either the top five or bottom five stories does not reduce the response in the remaining unbraced parts, whereas bracing of all ten stories reduces the bending moment response in all stories of ten- as well as five-story structures to a level less than the level of no-pounding response in almost all cases.

In the next three figures (Figures 6.46, 6.47 and 6.48) we compare the acceleration response for the three inputs for different bracing configurations of joined structures. Now since the pounding is avoided, the accelerations are drastically reduced as is seen from the top parts of Figures 6.46, 6.47 and 6.48. In the lower parts of these figures we only show the accelerations for the joined structures. We note that accelerations obtained for the braced cases are higher, especially in the top five stories, but they are still well below the accelerations we get when structures pound against each other.

6.6.4 Effect of bracing size

The previous set of results was obtained for bracing of size $W530 \times 66$. In the next few figures we examine the effect of reducing the bracing size on the pounding response as well as on the stresses in the brace itself.

Figure 6.49 shows the column bending moment in various stories and pounding acceleration for the ten-story structure braced with different size bracings. All ten stories are braced. It is noticed that a larger bracing reduces the bending moment more than a smaller

bracing. The bracing size, however, has no significant effect on the pounding acceleration response.

In Figure 6.50 we show the axial force and combined bending plus axial stress in different size bracings. From the top part of the figure we note that although larger braces attract larger forces, the combined stresses in different size bracings are not very different (lower part of the figure). This is more clearly shown in the next figure (Figure 6.51). The top part indicates the bracing forces plotted against the bracing size and the lower part shows the maximum stress in the brace. Since the curves in the lower part are nearly horizontal, they indicate that stress values are not sensitive to the size of the bracing used. This suggests that we could use the smallest possible bracing size which will produce a desired reduction in the bending moment of story columns.

In the next figure (Figure 6.52) we compare the responses obtained in the case of joined structures braced with smallest and largest size bracings in the group. It is seen that it is adequate to use the smaller bracing as it reduces the bending moment to the level of no-pounding. As seen from the stress in this bracing in Figure 6.53, it is well within the acceptable level for steel. Thus in pounding mitigation by bracing of stories, the stresses in the bracing will not be a critical factor. One can use the smallest bracing which will reduce the bending moment to a desirable level.

6.7 Foundation Shear

In this section we examine the effect of pounding mitigation schemes on the foundation forces. In Table 6.1 we show the force in the linear foundation spring for the five- and ten-story structures for (1) no-pounding, (2) pounding without bracing, (3) pounding with 1 through 5 stories braced, (4) pounding with 6 through 10 stories braced and (5) pounding with the most effective case of all stories braced. Also shown are the forces when the two structures are joined by rigid links. In the calculation of these forces it is assumed that the two base mats are also attached. The results in this table are for a soft soil (with shear

wave velocity of 77 m/sec). Also, the response for the braced case was obtained when the ten-story structure was braced with the largest size bracing in the group. It is noted that:

1. Pounding increases the shear force transmitted to the soil, by a factor of about 1.5 for this soft soil.
2. The shear transmitted to soil increases further if stories are braced. In the case when all ten stories are braced, there is a further increase in shear of about 25% due to pounding.
3. The situation is, however, improved dramatically when the two structures are joined. Joining, of course, changes the dynamic characteristics of the combined structures to bring about a change in the foundation forces. At the same time it reduces the pounding effect to reduce the foundation shear forces. As we will see later, this change is, of course, also affected by the stiffness of the foundation relative to the structural stiffness.
4. The shear force in the foundation of the five-story structure does not change much either due to pounding or bracing of the ten-story structure. When the two structures are joined, there is an increase in the foundation shear for the five-story structure as its foundation mat is assumed to move the same as the foundation mat for the ten-story structure.

In Table 6.2 we present the results for the ten-story structure braced by different size bracings. From these results we observe that the smaller the bracing, the lower the shear force due to pounding in the ten-story structure foundation. Again the force in the five-story structure is not affected much. Also the force for the joined case does not appear to be sensitive to the bracing size used.

In Table 6.3 we show the effect of shear wave velocity on foundation shear forces. We show the forces for the cases of (1) no-pounding of unbraced structures, (2) pounding of

ten-story structure braced with smallest size bracing in the group and (3) joined structures with ten-story structure braced.

For the ten-story structure we note that pounding with bracing seem to increase the shear forces for all foundation flexibilities, except that for the foundation with $V_s = 600 \text{ m/sec}$ no significant pounding effect is noticed. In the five-story structure the pounding is seen to reduce the foundation force for all cases of shear wave velocities. Joining of the two structures is seen to reduce the foundation force in soft soil only. For higher shear wave velocities, the joining also imposes a higher shear force on the foundation.

In summary, it is observed that except for the very soft soils, the mitigation scheme of joining the structures and bracing the ten-story structure will increase the shear force transmitted to the foundation, thus requiring a strengthening of the foundation. For the cases considered here, the foundation force may, however, be reduced in very flexible foundations. This effect, however, is significantly affected by the combined frequency characteristics of the structures and foundation soil.

6.8 Forces in the Rigid Links Joining the Structures

To get some idea what size rigid link we may need to connect the two structures, we have calculated the forces in the links provided at various levels.

Figure 6.54 shows the forces in the five links for various configuration of bracings. It is noticed that only the top link experiences a significant level of force. Also when braces are provided in all stories the force in the top link is also reduced, but then lower links experience some force.

In the next figure (Figure 6.55) we show the effect of different bracing sizes. We notice that bracing size does affect the forces in the links, but not very dramatically. In Figure 6.56 we show the effect of foundation flexibility on the link forces. We note that generally a rigid foundation will cause higher forces in the links. However, even the highest force is not very large. Assuming an allowable tensile stress of 150 MPa in steel, the maximum force of

0.32 MN can be easily carried by a 52 mm rod. Thus joining of the two structures does not pose any special problem and it can be easily accomplished by using large size steel rods or specially manufactured links.

6.9 Pounding of Structures at Unequal Levels - Column Pounding

Often structures in cities are not at the same level, or they may have unequal height stories. In such cases the floors of one structure will pound against the columns of the other structure, as shown in Figure 6.57. Here such pounding is referred to as column pounding. Such a pounding is most likely to cause collapse as most building columns are not designed for any impacting lateral load.

To alleviate the effect of such pounding, it is necessary that columns be K-braced, as suggested by Newmark and Rosenblueth [29]. The most critical case of column pounding will happen when the floor impacts in the middle of a column height. In the following, therefore, we have examined the responses for such a column pounding situation for various bracing configurations. The two pounding structures considered are three- and six-story structures.

The bracing configurations considered are:

1. Only bracing of pounded columns by K-braces, for both structures, Figure 6.58.
2. K-bracing of pounded columns with diagonal bracing of the higher stories of the six-story structure.

The column bending moment and floor acceleration responses for these two bracing arrangements are compared with the no-pounding response and response of joined and braced structures in Figures 6.59 and 6.60 for El-Centro ground motion and for an ensemble of fifty time histories.

From the results in these two figures we observe that K-bracing of the two structures is adequate to reduce the pounding effect on the column. However, bracing of the pounding

stories is seen to increase the column bending moment of the higher stories, especially for the fifty time history ensemble results, and also for the smaller size bracing results shown in Figures 6.61 and 6.62 for both the El-Centro and fifty time history results. If the higher stories are also braced, the bending moment response in all stories can be reduced significantly. But any of these bracing arrangements do not help much in reducing the pounding acceleration response. To reduce this, we must also join the two structures by rigid links. We observe that the bending moment response for the case of a joined and completely braced structure is significantly reduced. In fact, it is much smaller than the no-pounding response. The floor acceleration response in this case is now close to the response for the case of no-pounding.

Since the provision of the bracing reduces the bending moment response much more than what is necessary, it suggests that perhaps even a smaller size bracing may also be adequate. In the next two figures, therefore, the same results are presented for two smaller bracing sizes. The results in Figures 6.61 and 6.62 are for $W310 \times 23.8$ size bracing and those in Figure 6.63 and 6.64 are for even smaller size $W150 \times 13.5$ bracing. It is noted from these figures that if we only provide bracings in the pounding stories, then the higher stories attract responses higher than the no-pounding case. Thus we also need to provide bracing in those higher stories. Also providing bracing alone does not avoid high acceleration values due to impact; they can only be reduced by rigid joining of the two structures. We also note that by choosing the smallest possible size bracing it is possible to reduce the pounding effect to a desirable level.

6.10 Summary

In this chapter two proposals to alleviate pounding effects were examined. Providing a softer cushion, representing a softer spring was found impractical because of clearance requirements; the clearance requirement to permit the deformation of a soft spring is as much as the clearance required to avoid pounding. The introduction of energy dissipation

devices, even if possible to be installed, are not of much help in reducing the story shear, and in some cases may even be harmful as they may increase the floor acceleration response.

The best solution for alleviating pounding effects if it cannot be avoided by increasing the clearance is to rigidly connect the impacting floors and brace all the stories of at least the taller structure. Joining of the floors is required to reduce the excessive floor accelerations caused by impact, whereas the story bracings are required to reduce the excessive story shears or bending moments in the higher stories caused by pounding of the lower floors. Although the shears are increased only in the higher stories, it is necessary to brace all the stories of at least the taller structure. Also bracing of all the stories increases the floor acceleration response more than the no-pounding case because it makes the structure stiffer, but it is still necessary to protect the damage to the higher stories due to increased bending moment response.

The forces in the rigid links connecting the two structures were observed to be reasonable. Thus joining of the two structures does not seem to pose an insurmountable problem.

In the case of column pounding, the proposed mitigation strategy is to provide K-bracings on all pounding columns of the two structures and also to rigidly join them to avoid pounding acceleration.

The proposed pounding mitigation strategies were also examined for the structures supported on the flexible foundation media. It is observed that except for the very soft soils, the mitigation scheme of joining the structures and bracing the ten-story structure will increase the shear force transmitted to the foundation, thus requiring a strengthening of the foundation.

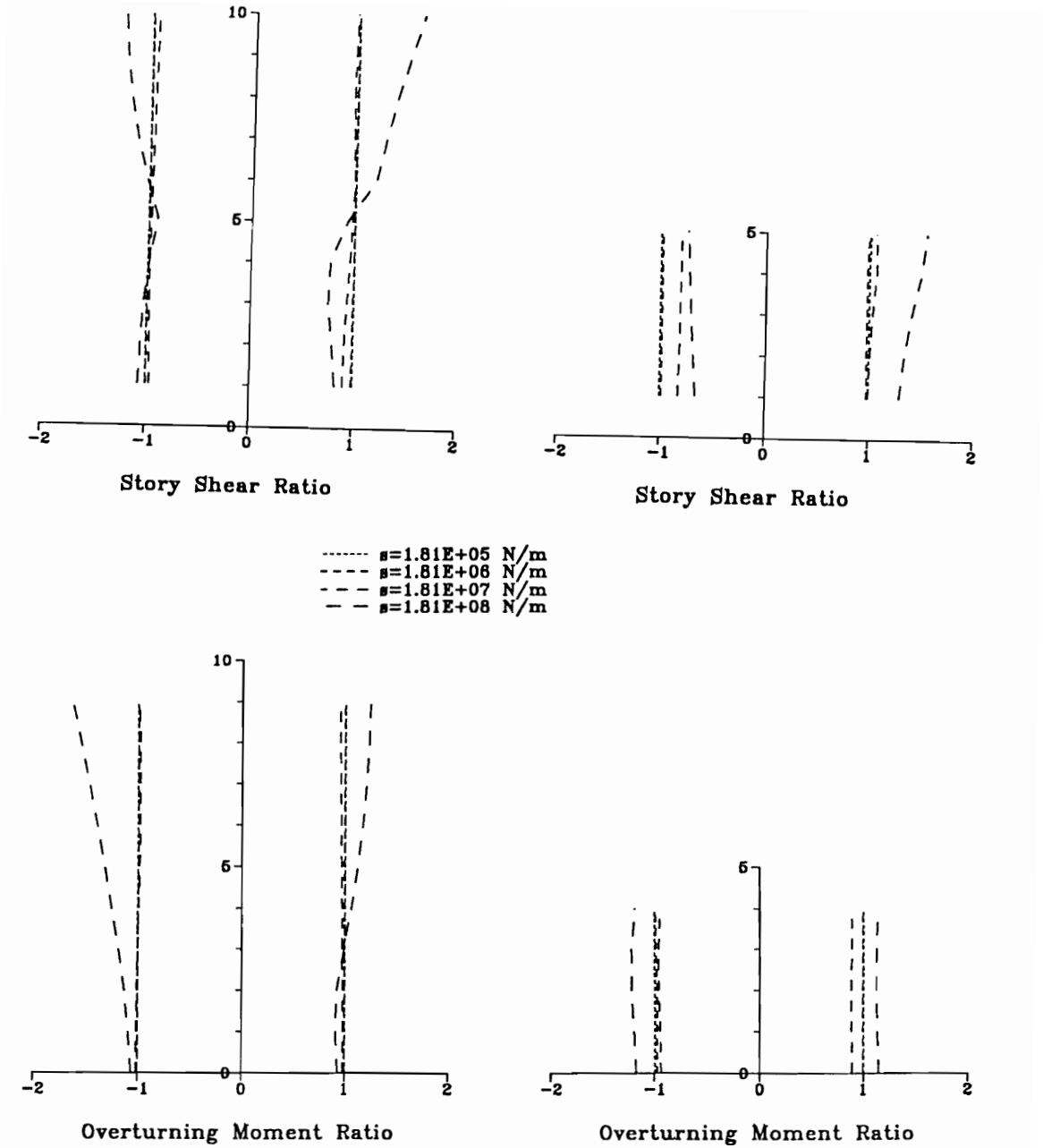


Figure 6.1: Response of structures with springs of varying stiffness coefficients provided at the pounding interfaces

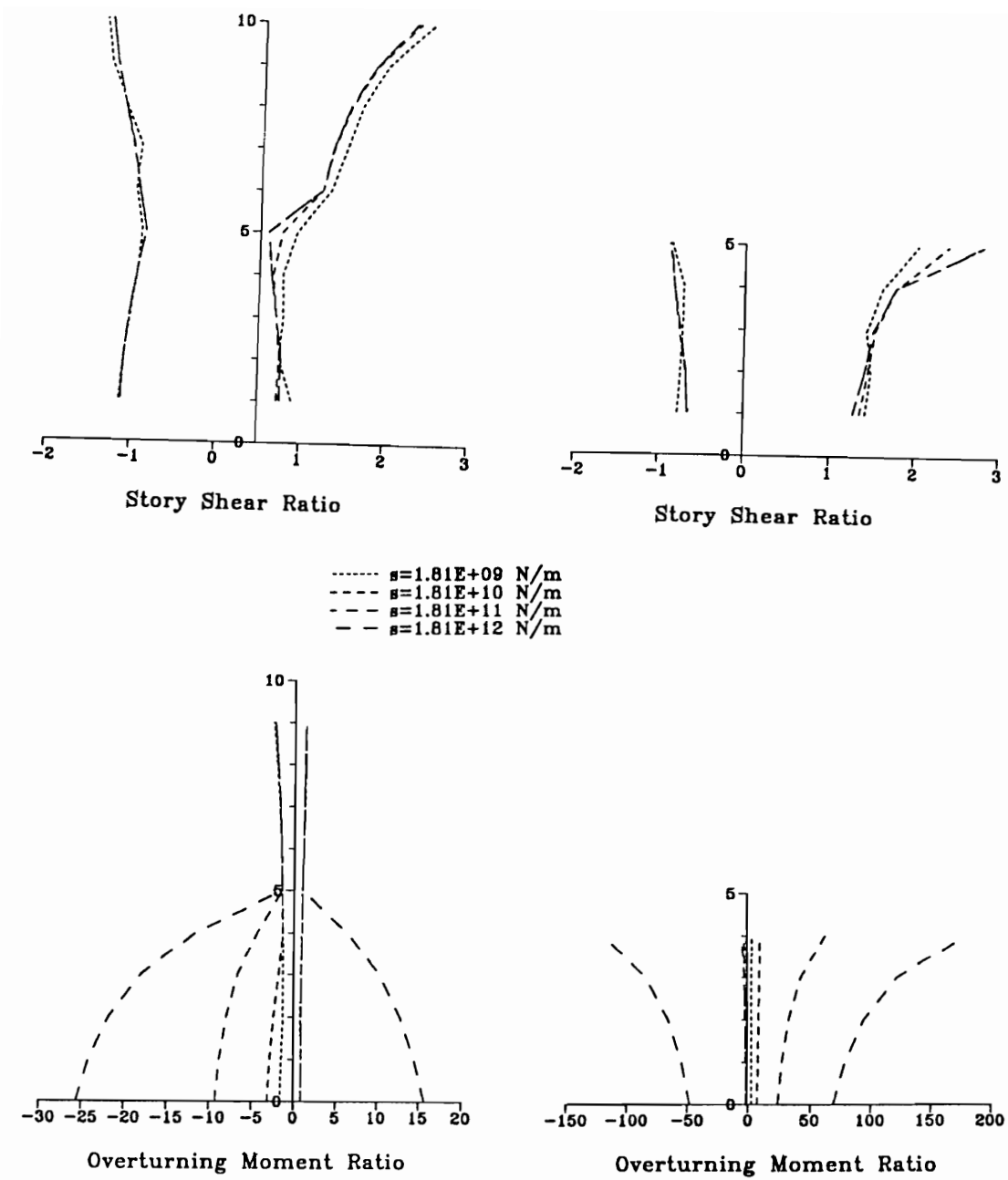


Figure 6.2: Response of structures with springs of varying stiffness coefficients provided at the pounding interfaces

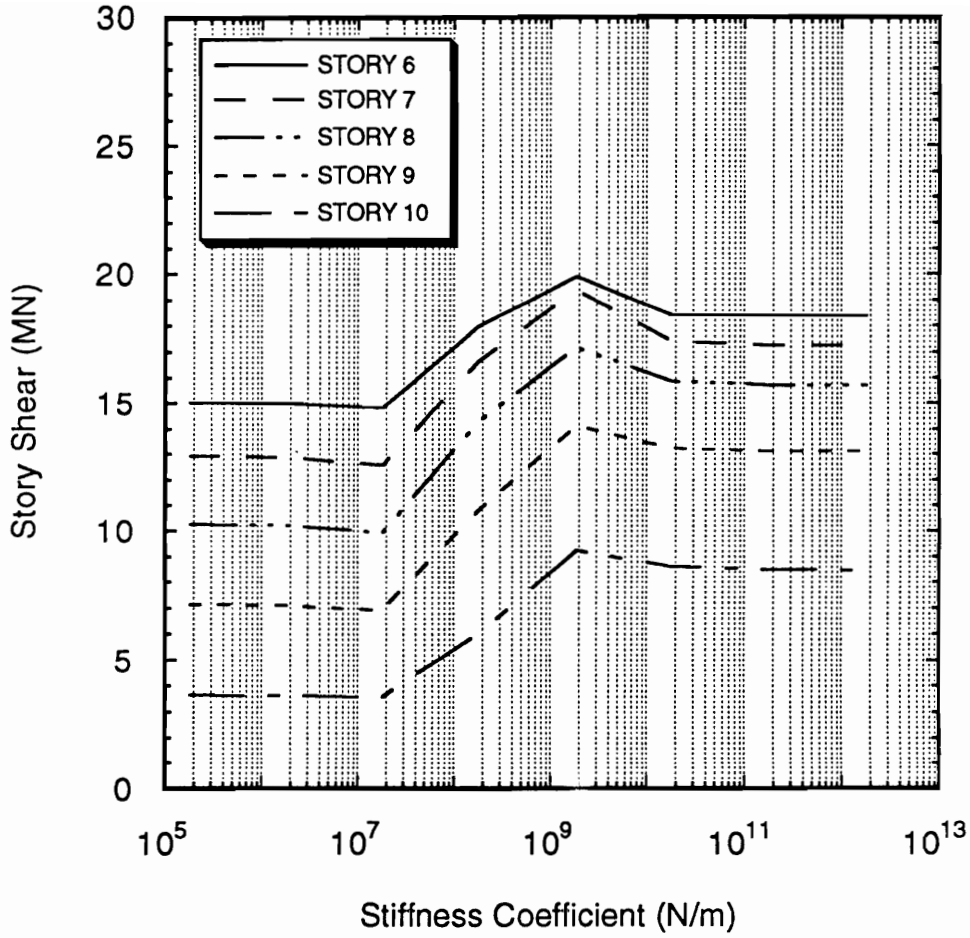


Figure 6.3: Variation of story shears of various stories versus impact spring stiffness coefficients

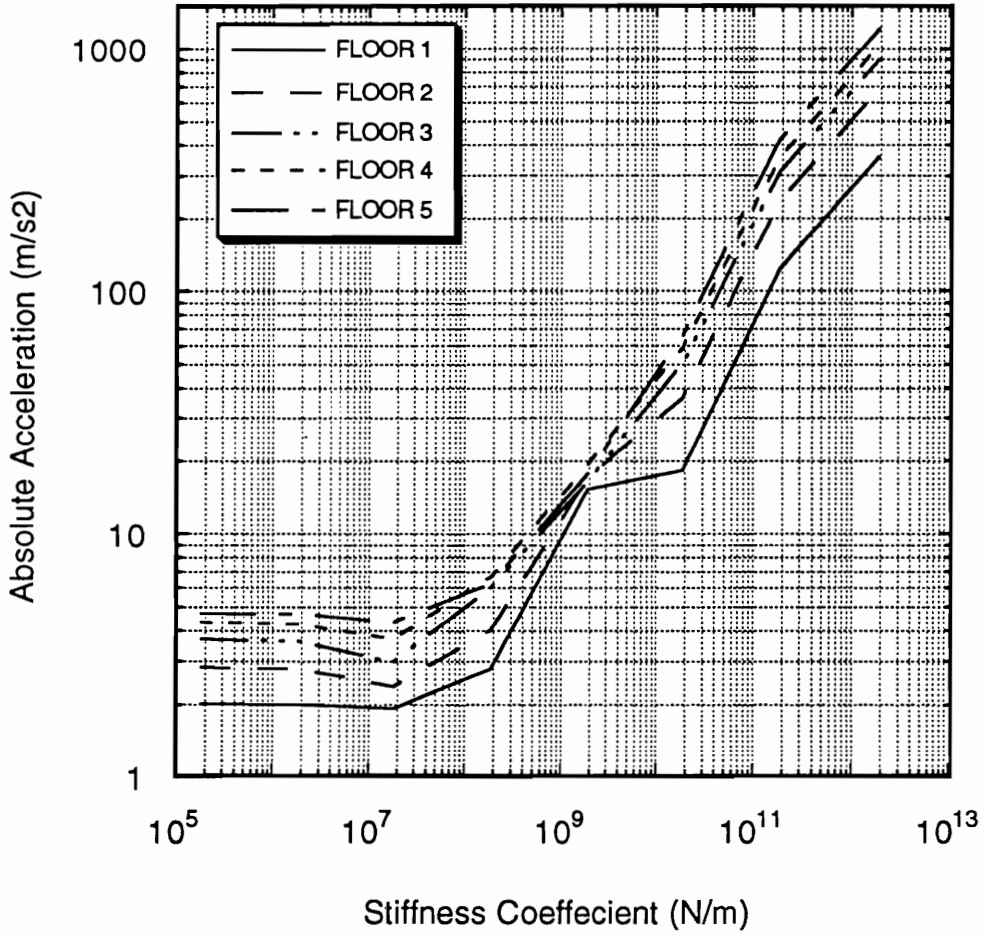


Figure 6.4: Variation of absolute accelerations of various impacting floors versus impact spring stiffness coefficients

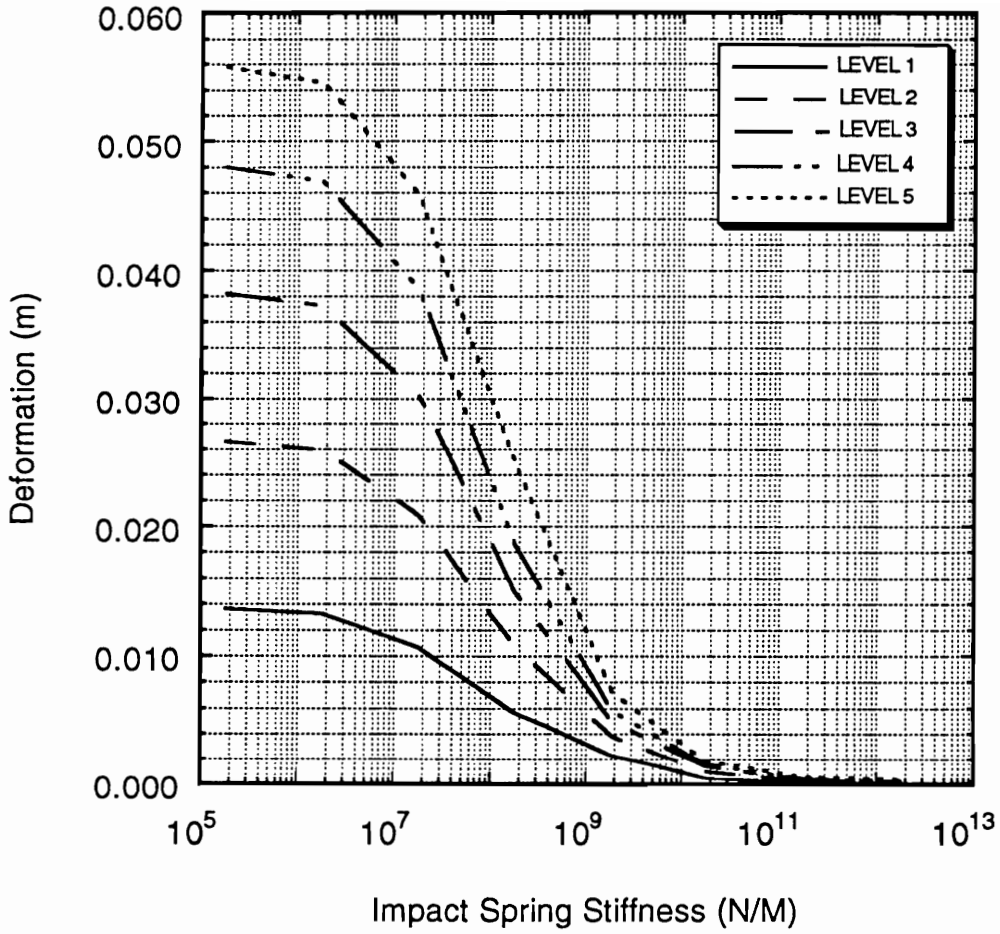


Figure 6.5: Maximum deformations versus stiffness coefficient of springs provided at different pounding interfaces

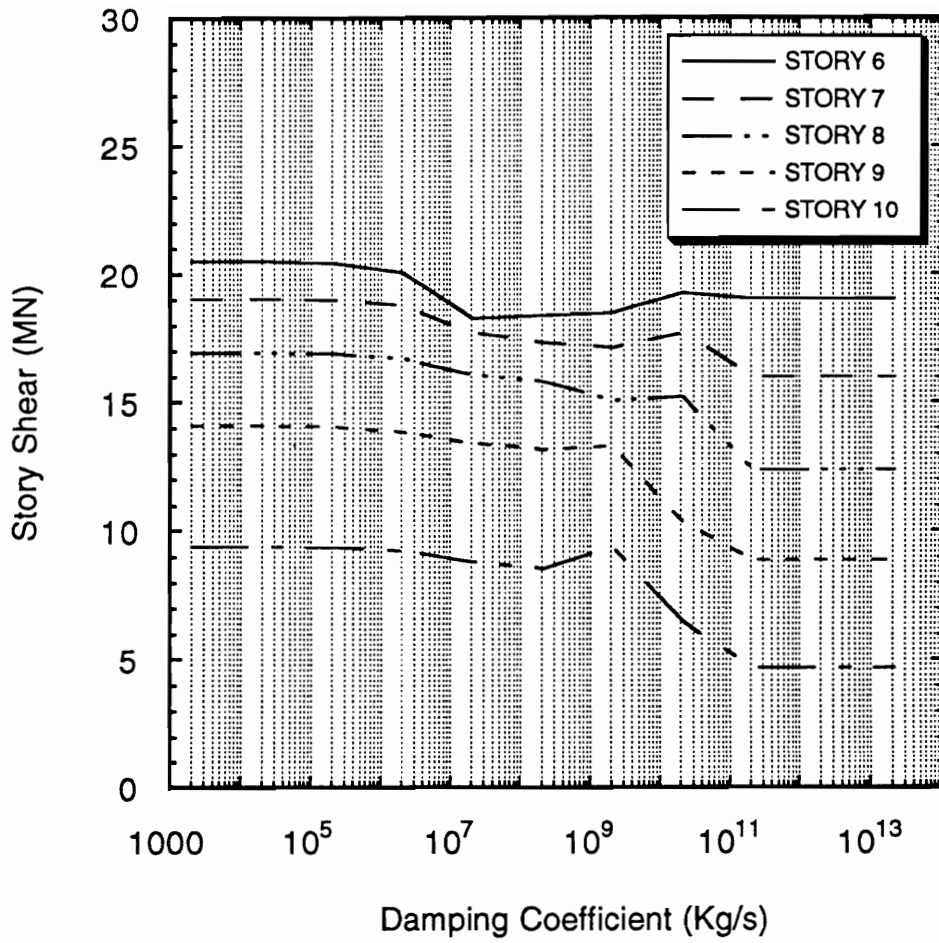


Figure 6.6: Effect of increasing the interface damping coefficient on the story shear response

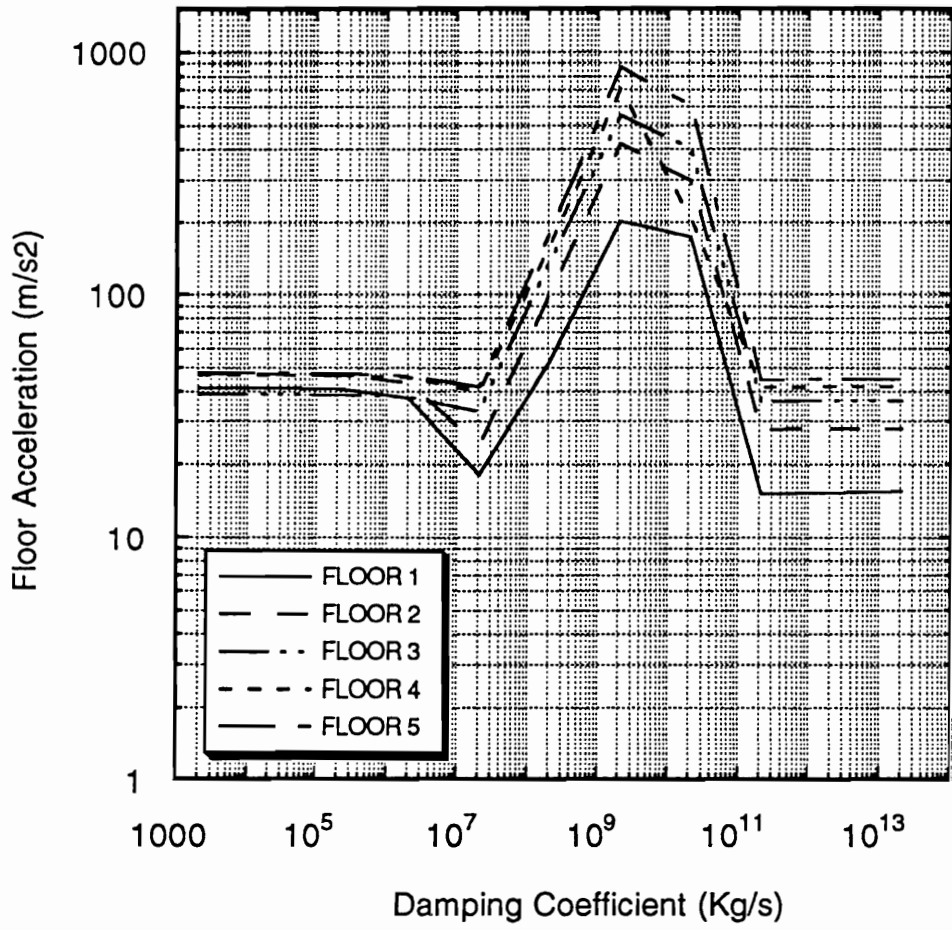


Figure 6.7: Effect of increasing the interface damping coefficient on the floor acceleration response

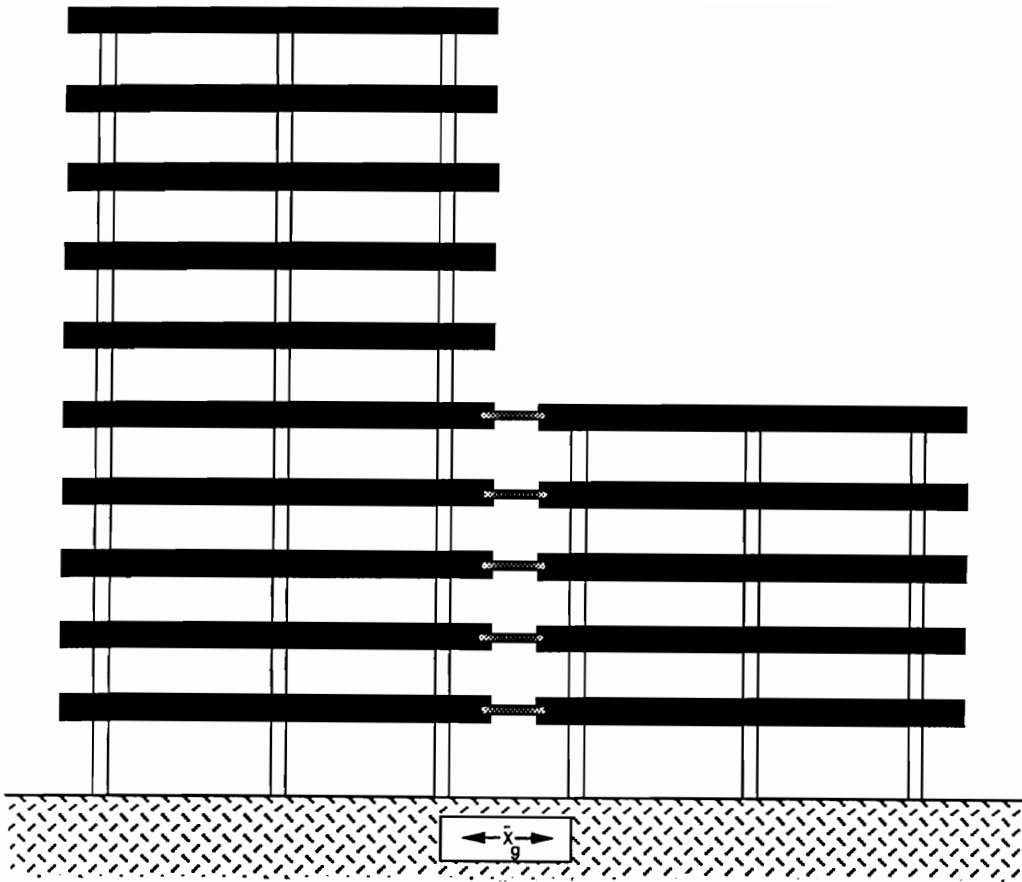


Figure 6.8: Schematic of rigidly joined structures supported on the rigid foundation

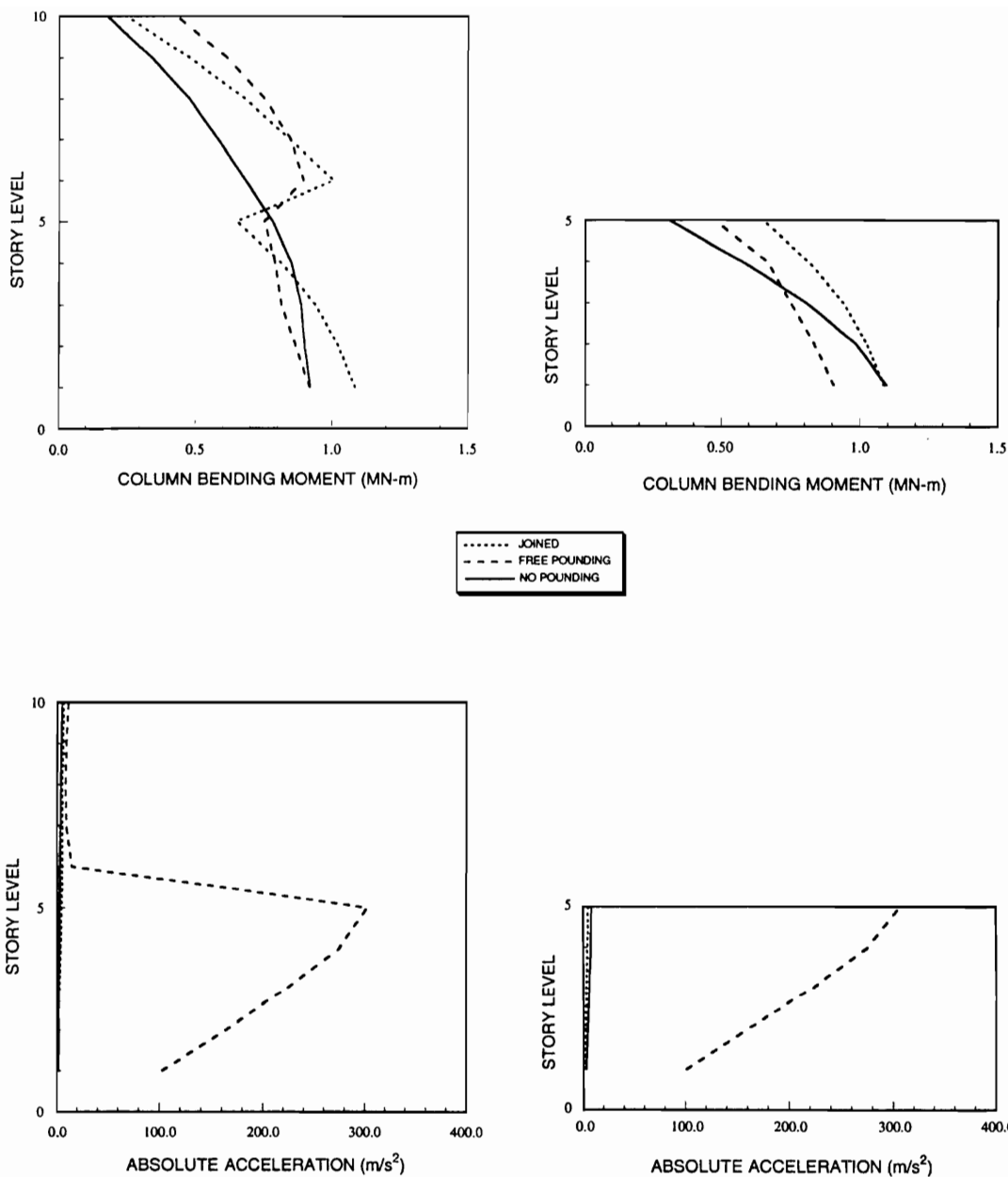


Figure 6.9: Comparison of the column bending moment and absolute floor acceleration responses of rigidly joined structures with the corresponding responses obtained for the no-pounding and free-pounding cases (rigid foundation model, El-Centro time history)

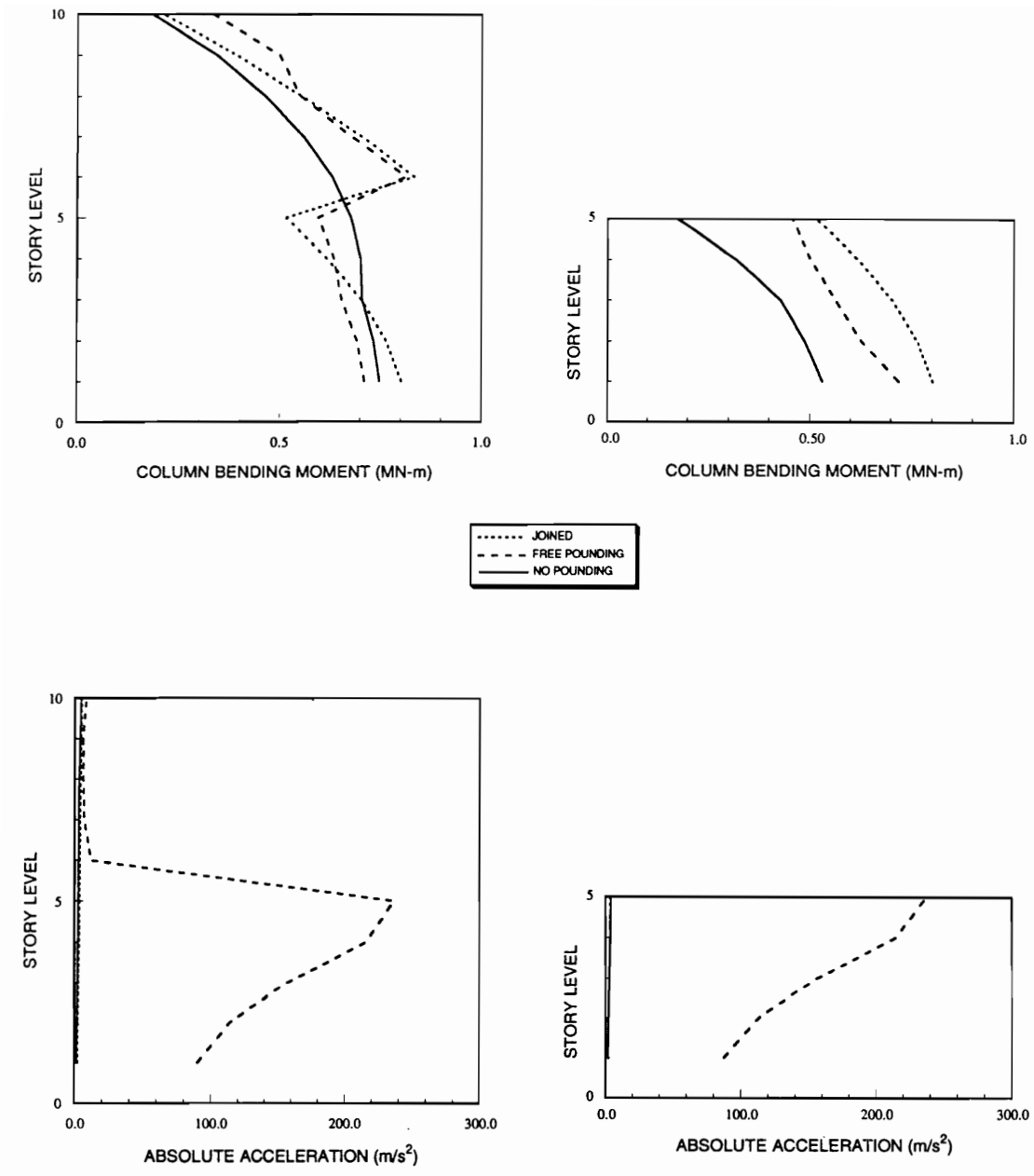


Figure 6.10: Comparison of the column bending moment and absolute floor acceleration responses of rigidly joined structures with the corresponding responses obtained for the no-pounding and free-pounding cases (rigid foundation model, 1 synthetic time history)

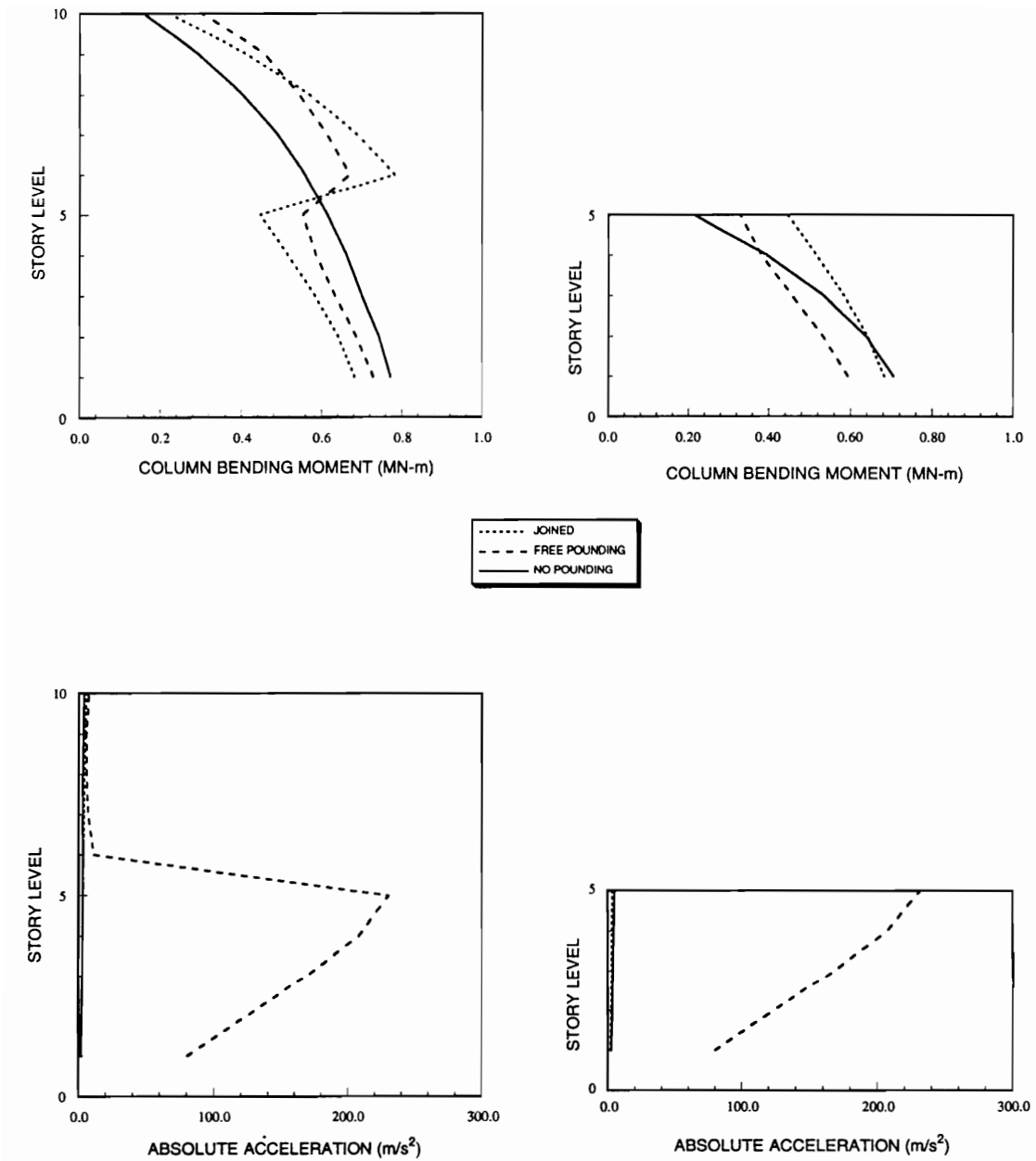


Figure 6.11: Comparison of the column bending moment and absolute floor acceleration responses of rigidly joined structures with the corresponding responses obtained for the no-pounding and free-pounding cases (rigid foundation model, 50 synthetic time histories)

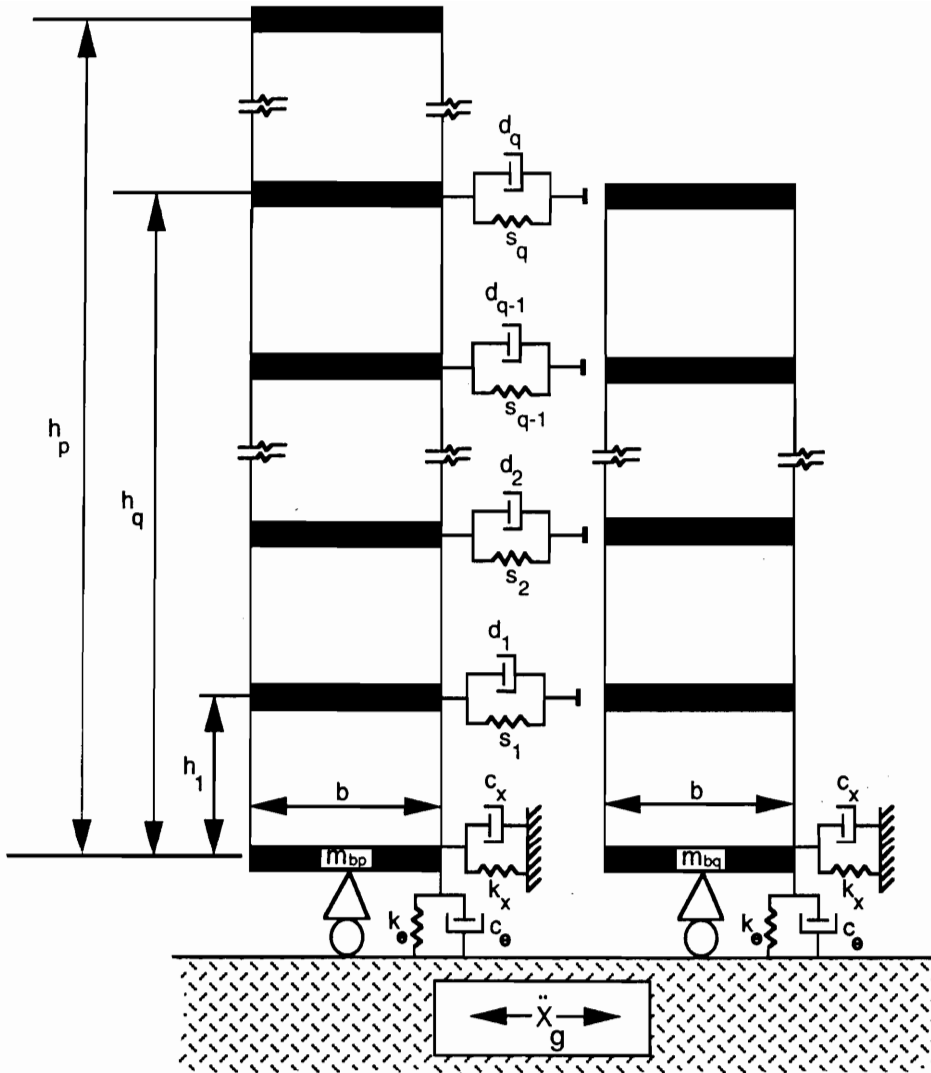


Figure 6.12: Schematic of pounding structures supported on the flexible foundation

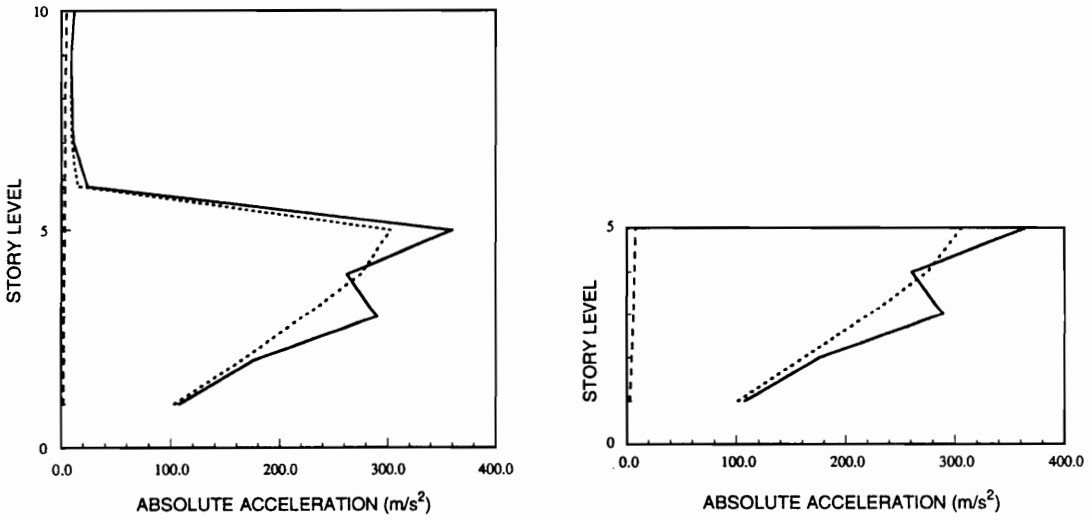
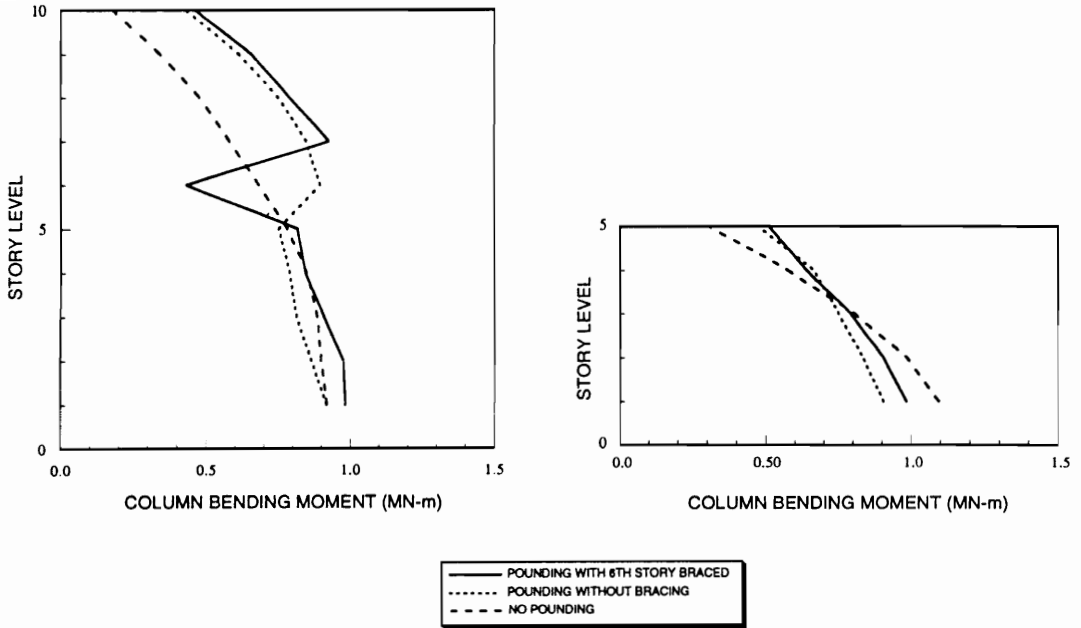


Figure 6.13: Comparison of responses obtained with bracing, without bracing and no-pounding cases (rigid foundation model, El-Centro time history)

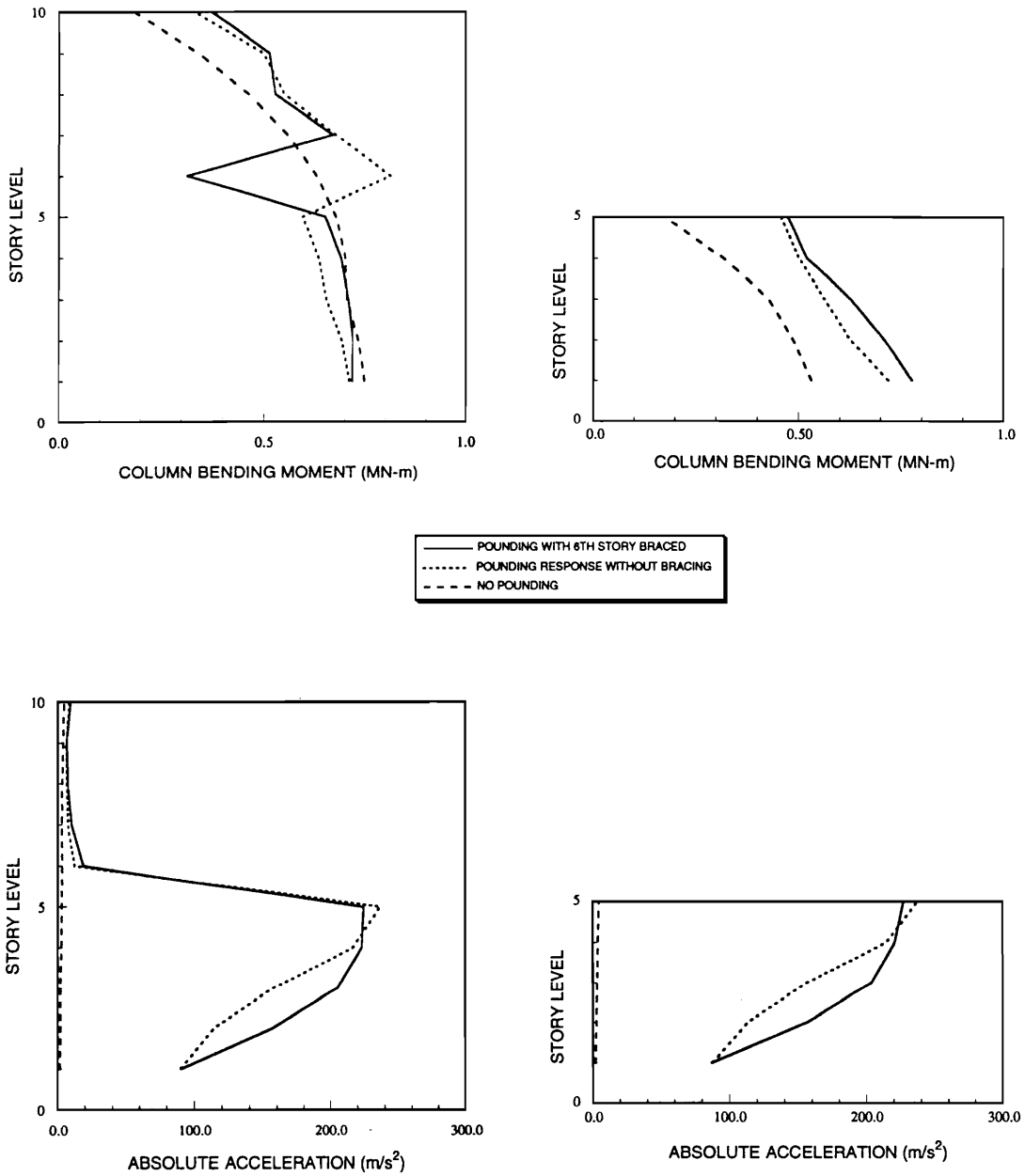


Figure 6.14: Comparison of responses obtained with bracing, without bracing and no-pounding cases (rigid foundation model, 1 synthetic time history)

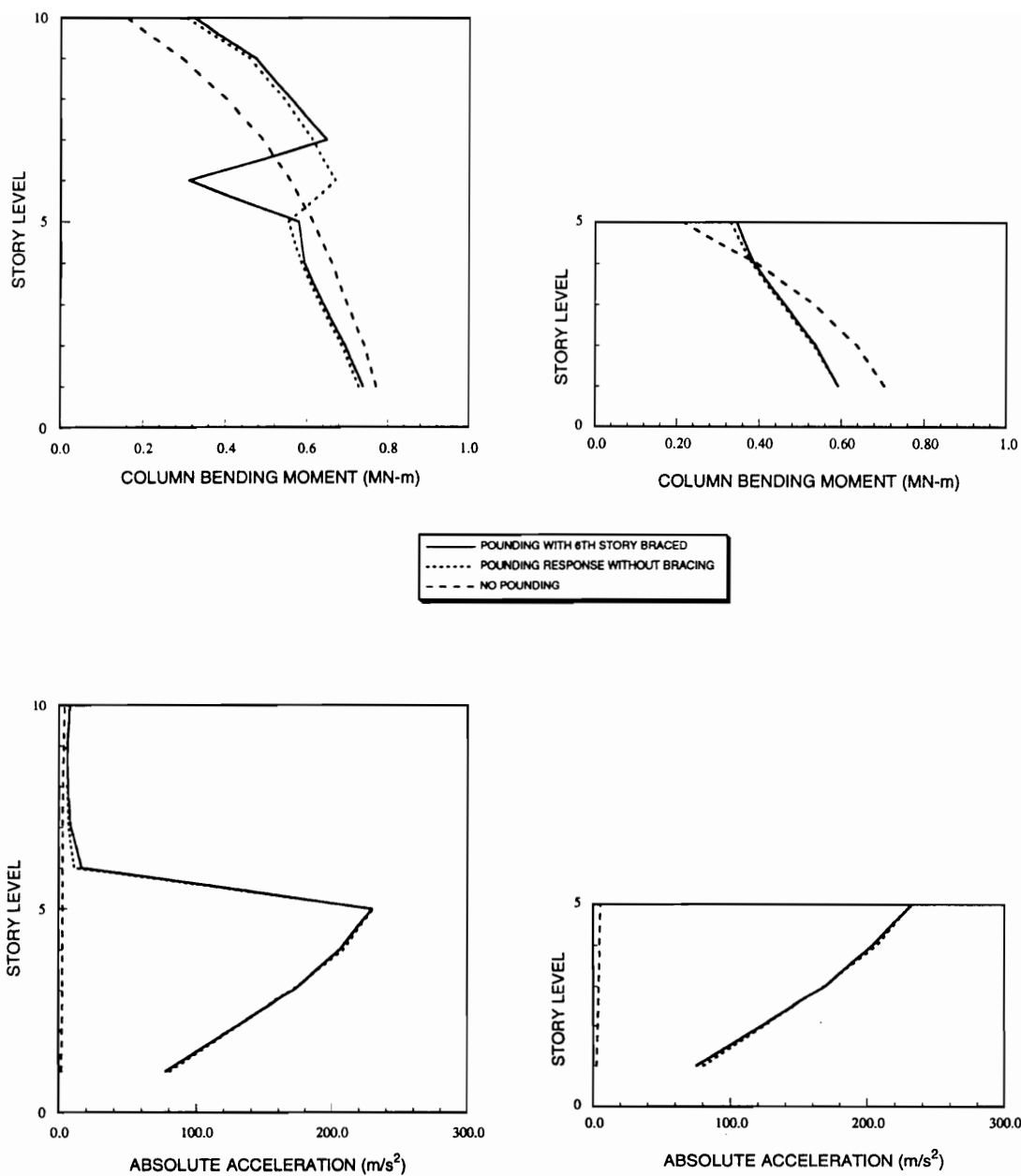


Figure 6.15: Comparison of responses obtained with bracing, without bracing and no-pounding cases (rigid foundation model, 50 synthetic time histories)

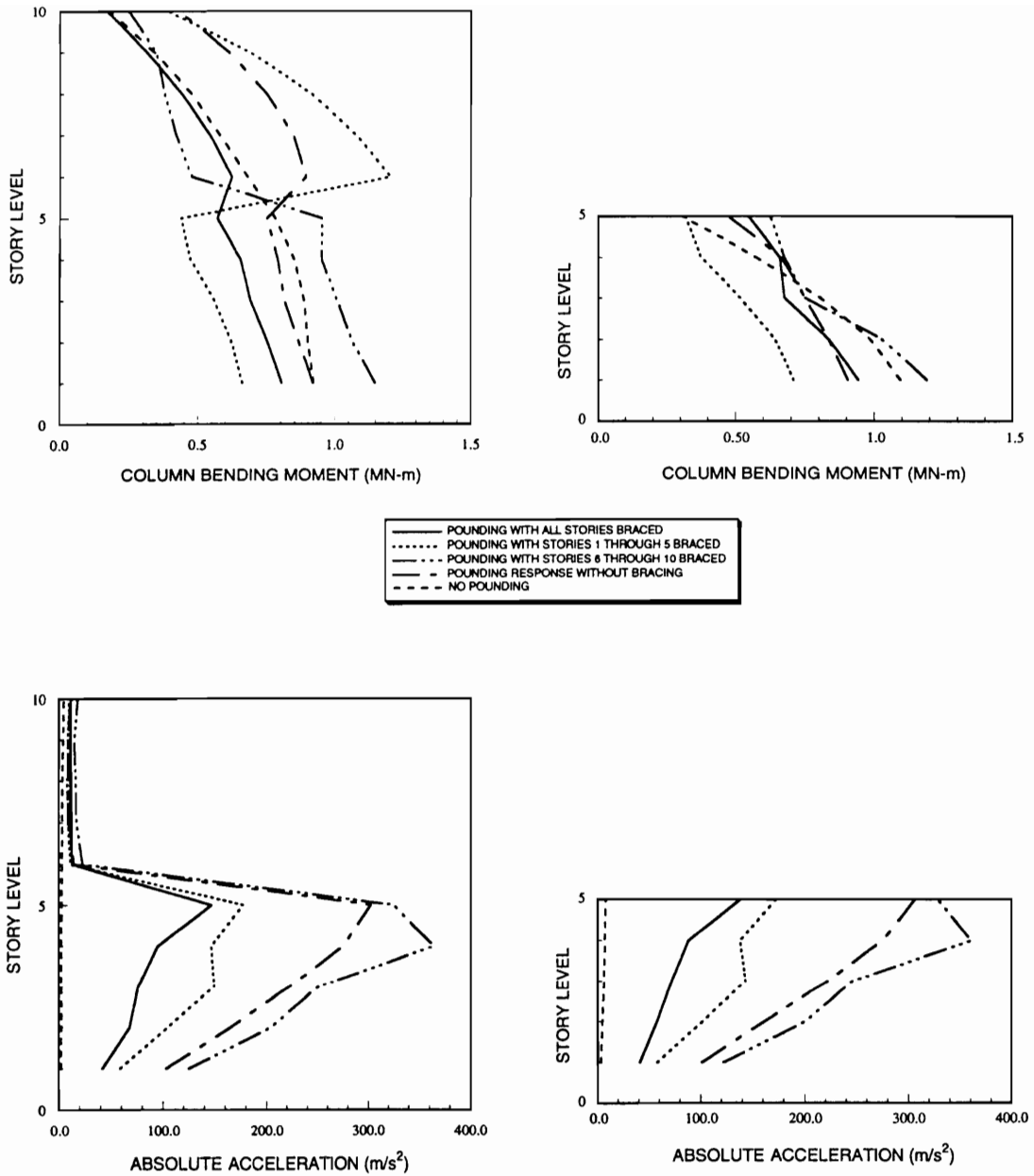


Figure 6.16: Comparison of responses obtained for different configurations of bracings with the responses obtained for unbraced and no-pounding cases (rigid foundation model, El-Centro time history)

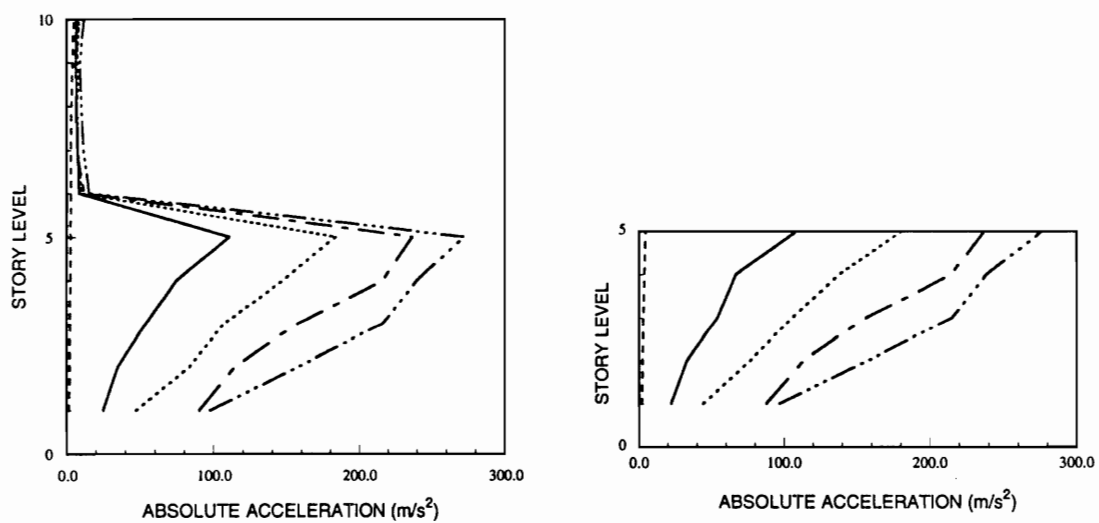
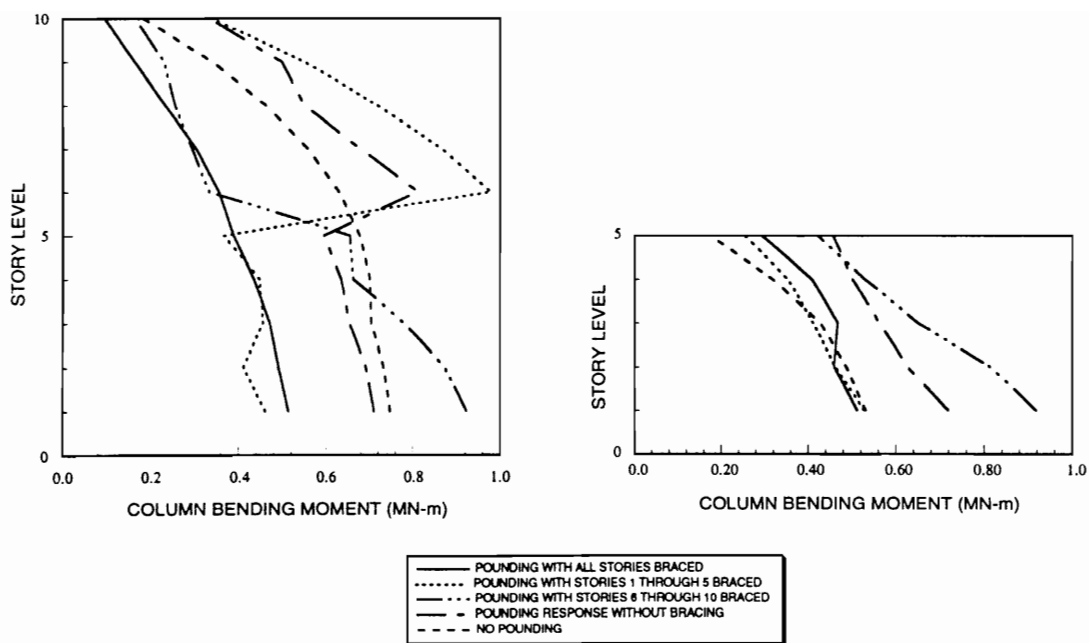


Figure 6.17: Comparison of responses obtained for different configurations of bracings with the responses obtained for unbraced and no-pounding cases (rigid foundation model, 1 synthetic time history)

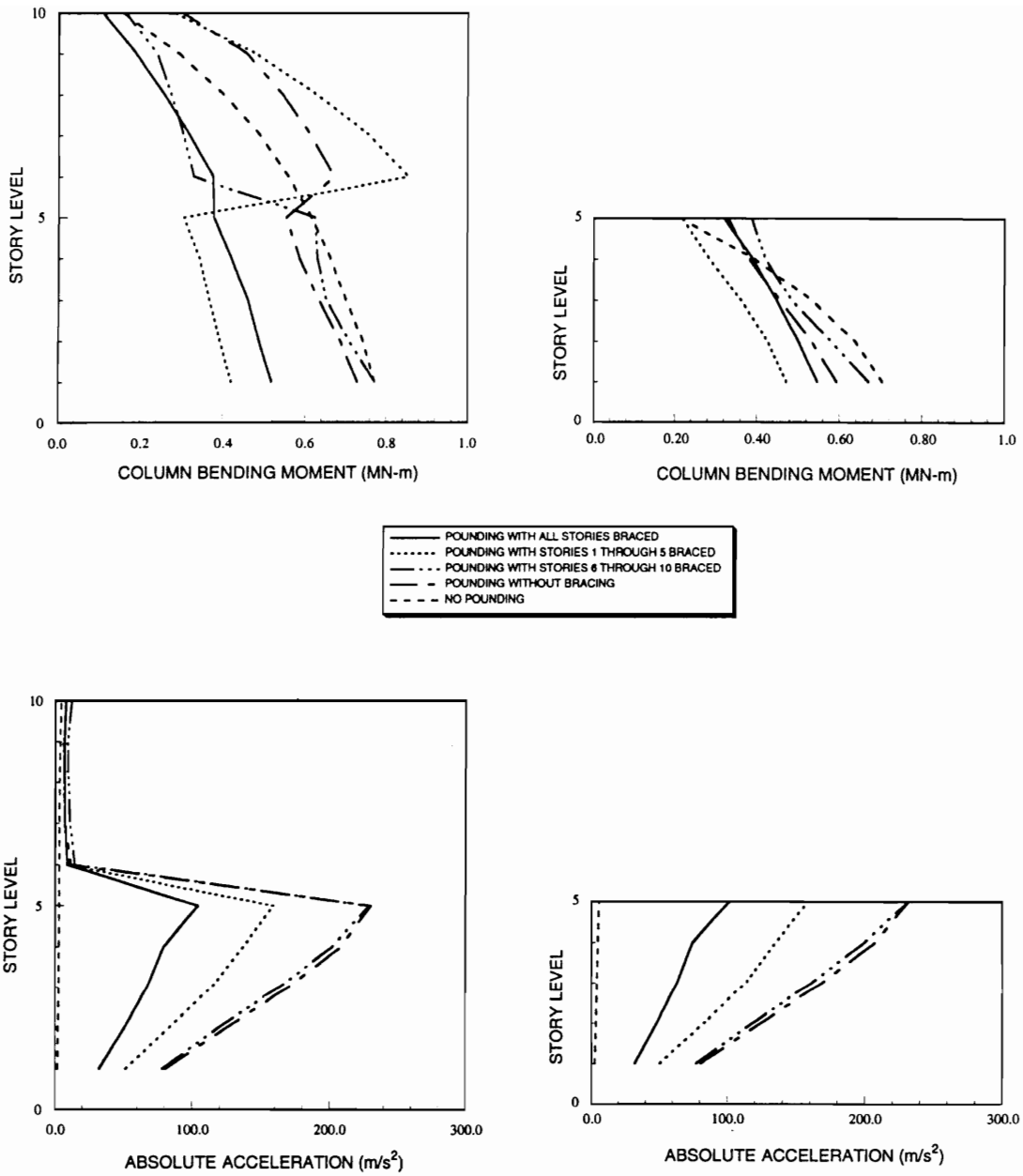


Figure 6.18: Comparison of responses obtained for different configurations of bracings with the responses obtained for unbraced and no-pounding cases (rigid foundation model, 50 synthetic time histories)

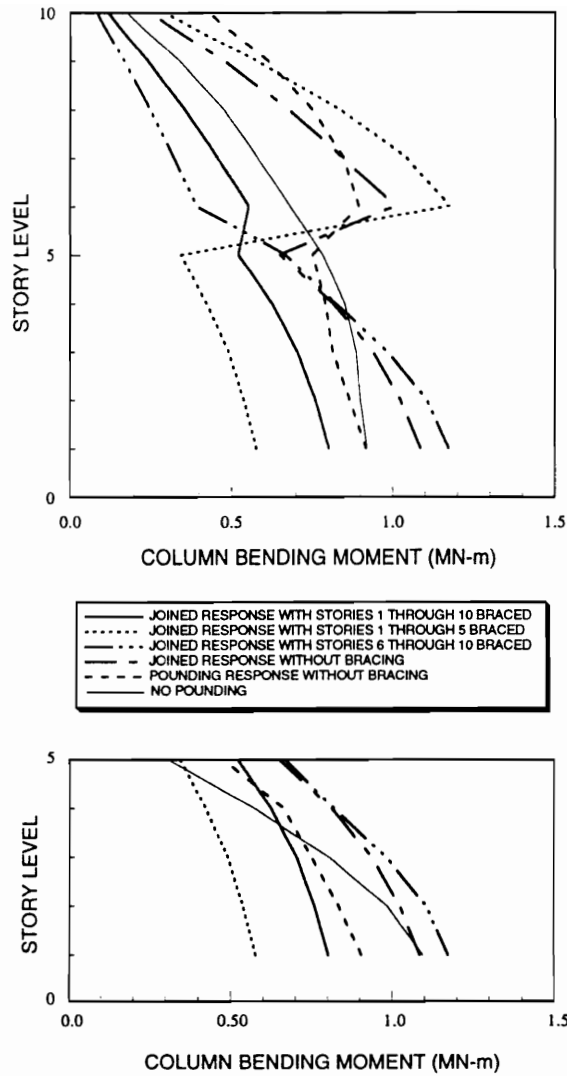


Figure 6.19: Comparison of the bending moment response obtained for joined structures with different bracing configurations with the response obtained for unbraced joined and unbraced disjoined freely pounding structures (rigid foundation model, El-Centro time history)

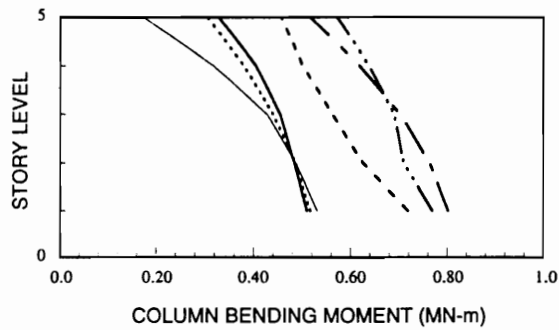
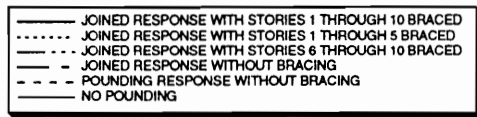
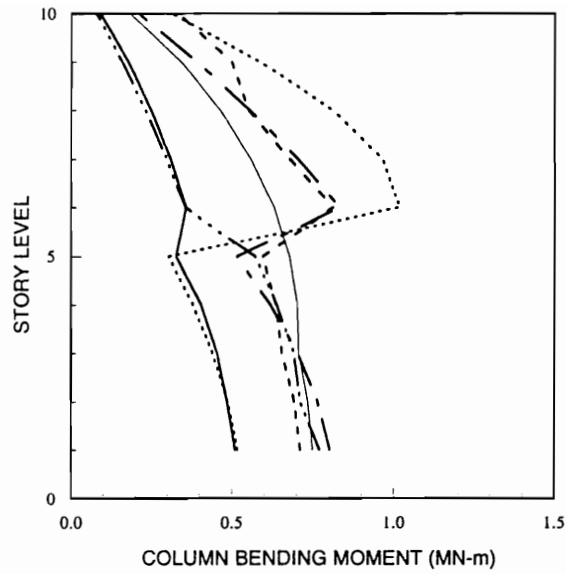


Figure 6.20: Comparison of the bending moment response obtained for joined structures with different bracing configurations with the response obtained for unbraced joined and unbraced disjoined freely pounding structures (rigid foundation model, 1 synthetic time history)

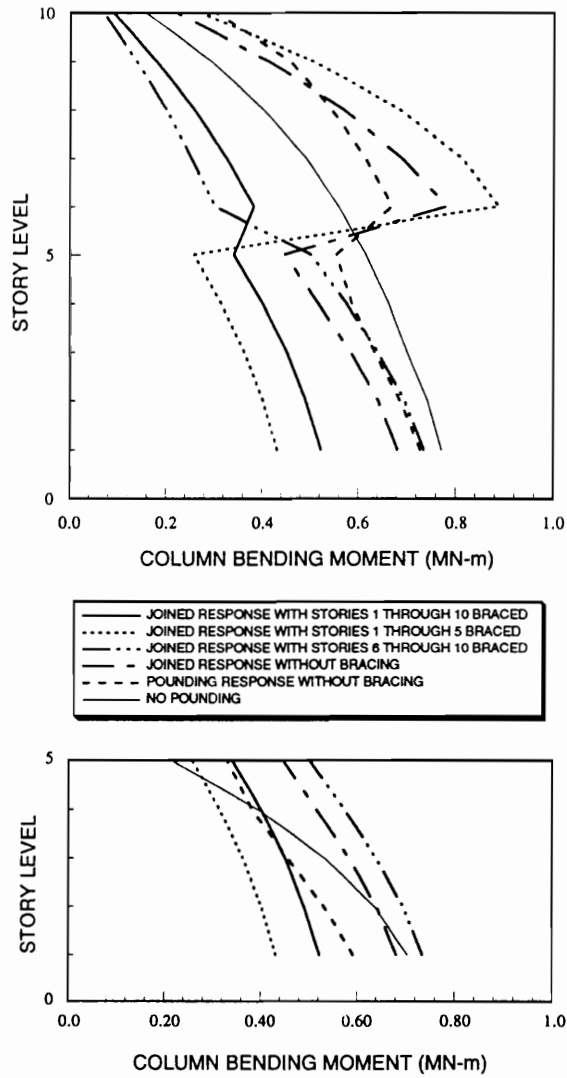


Figure 6.21: Comparison of the bending moment response obtained for joined structures with different bracing configurations with the response obtained for unbraced joined and unbraced disjoined freely pounding structures (rigid foundation model, 50 synthetic time histories)

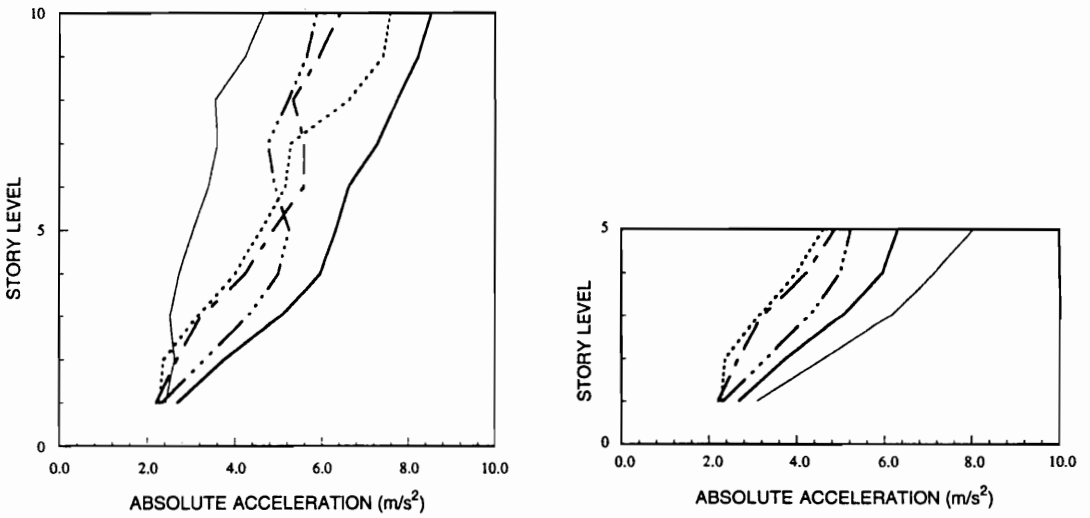
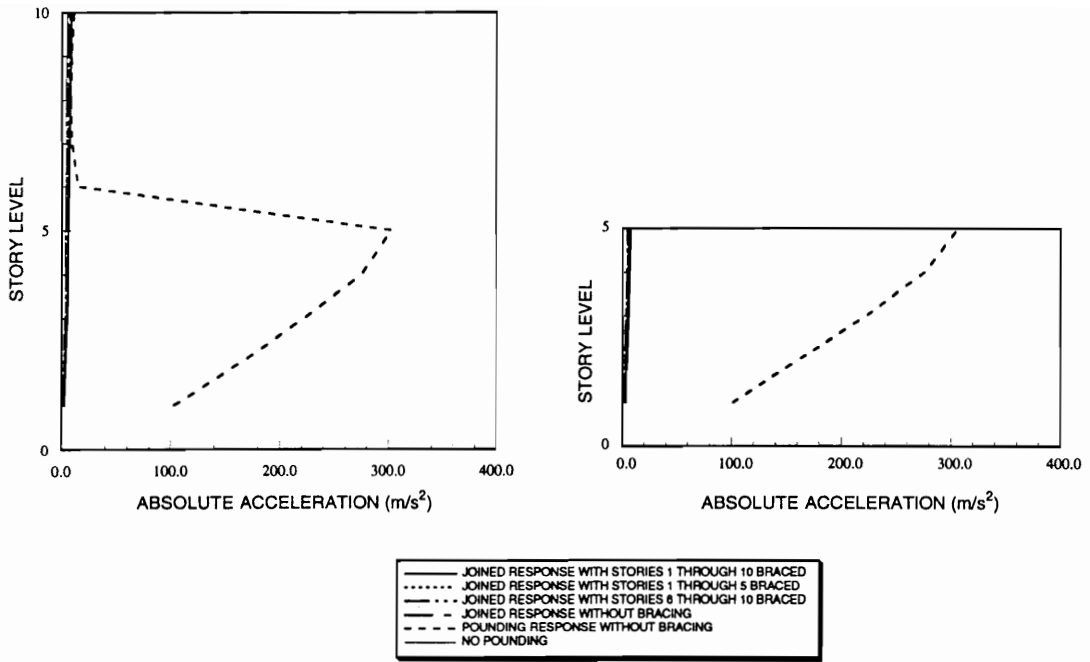


Figure 6.22: Comparison of the acceleration response obtained for joined structures with different bracing configurations with the response obtained for unbraced joined and unbraced disjointed freely pounding structures (rigid foundation model, El-Centro time history)

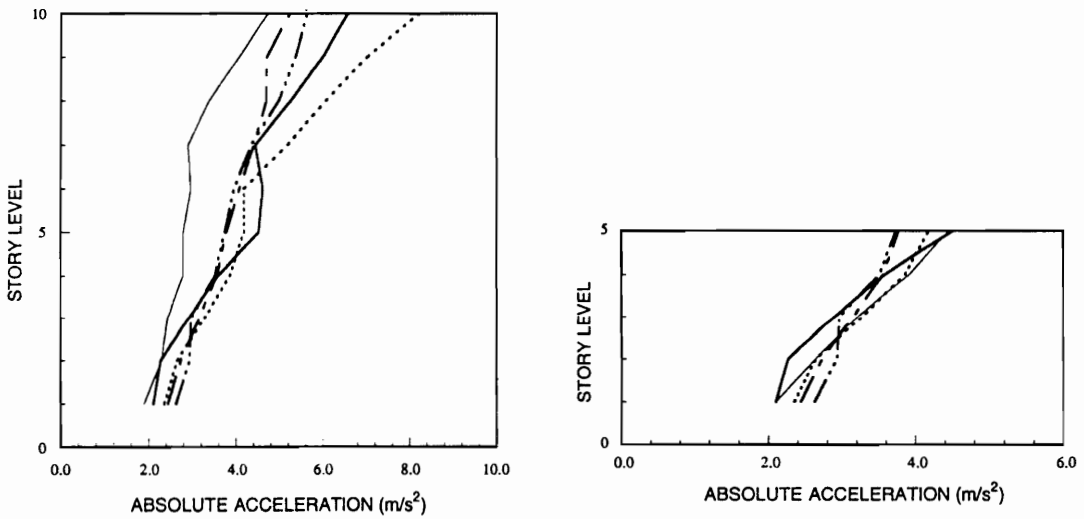
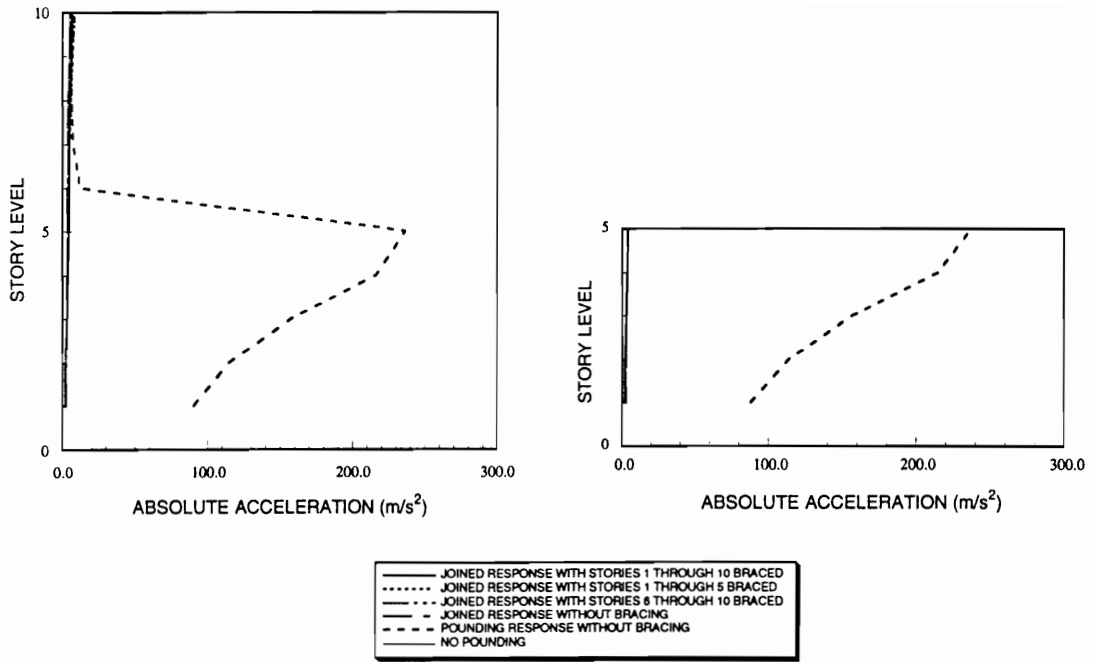


Figure 6.23: Comparison of the acceleration response obtained for joined structures with different bracing configurations with the response obtained for unbraced joined and unbraced disjointed freely pounding structures (rigid foundation model, 1 synthetic time history)

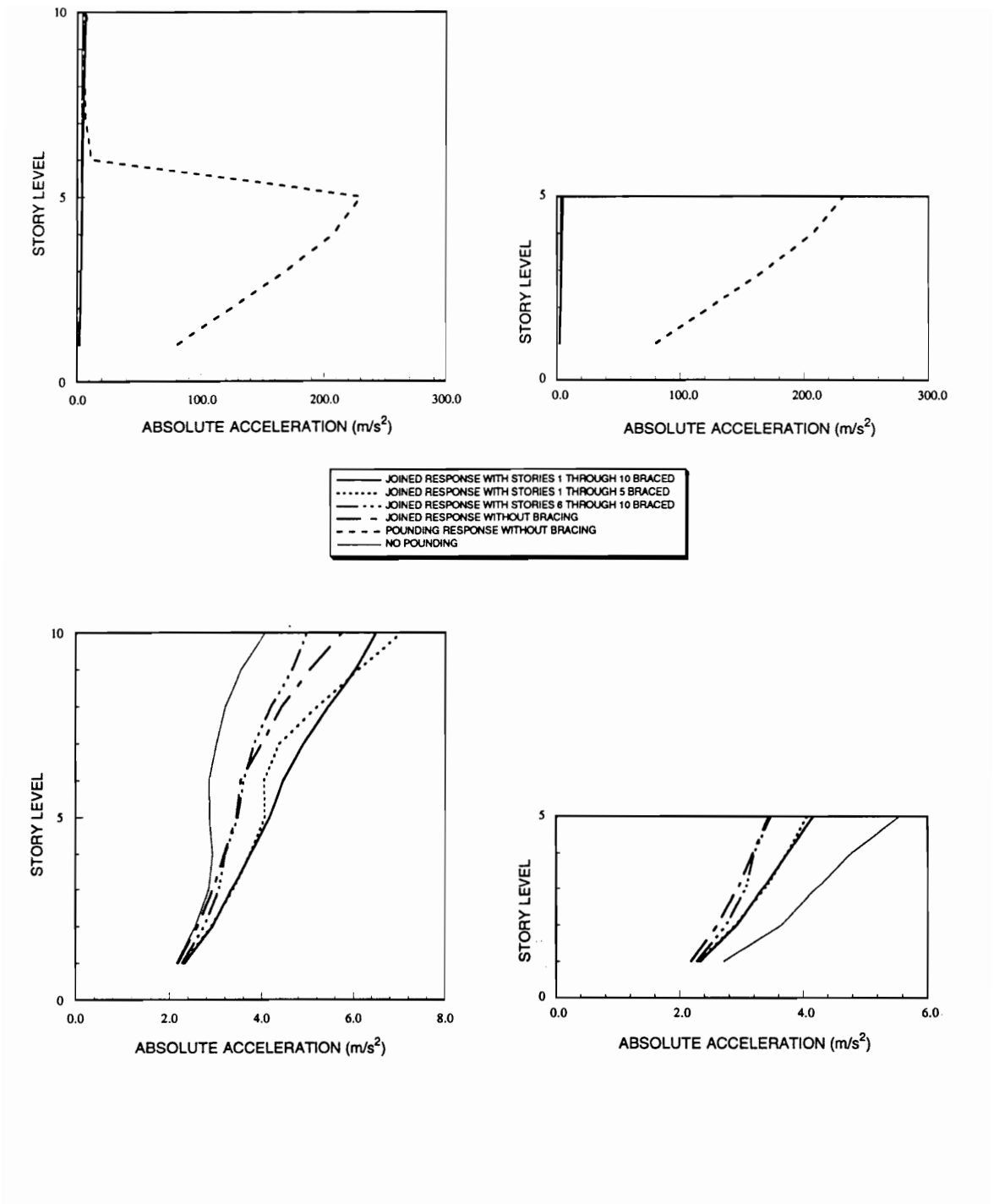


Figure 6.24: Comparison of the acceleration response obtained for joined structures with different bracing configurations with the response obtained for unbraced joined and unbraced disjoined freely pounding structures (rigid foundation model, 50 synthetic time histories)

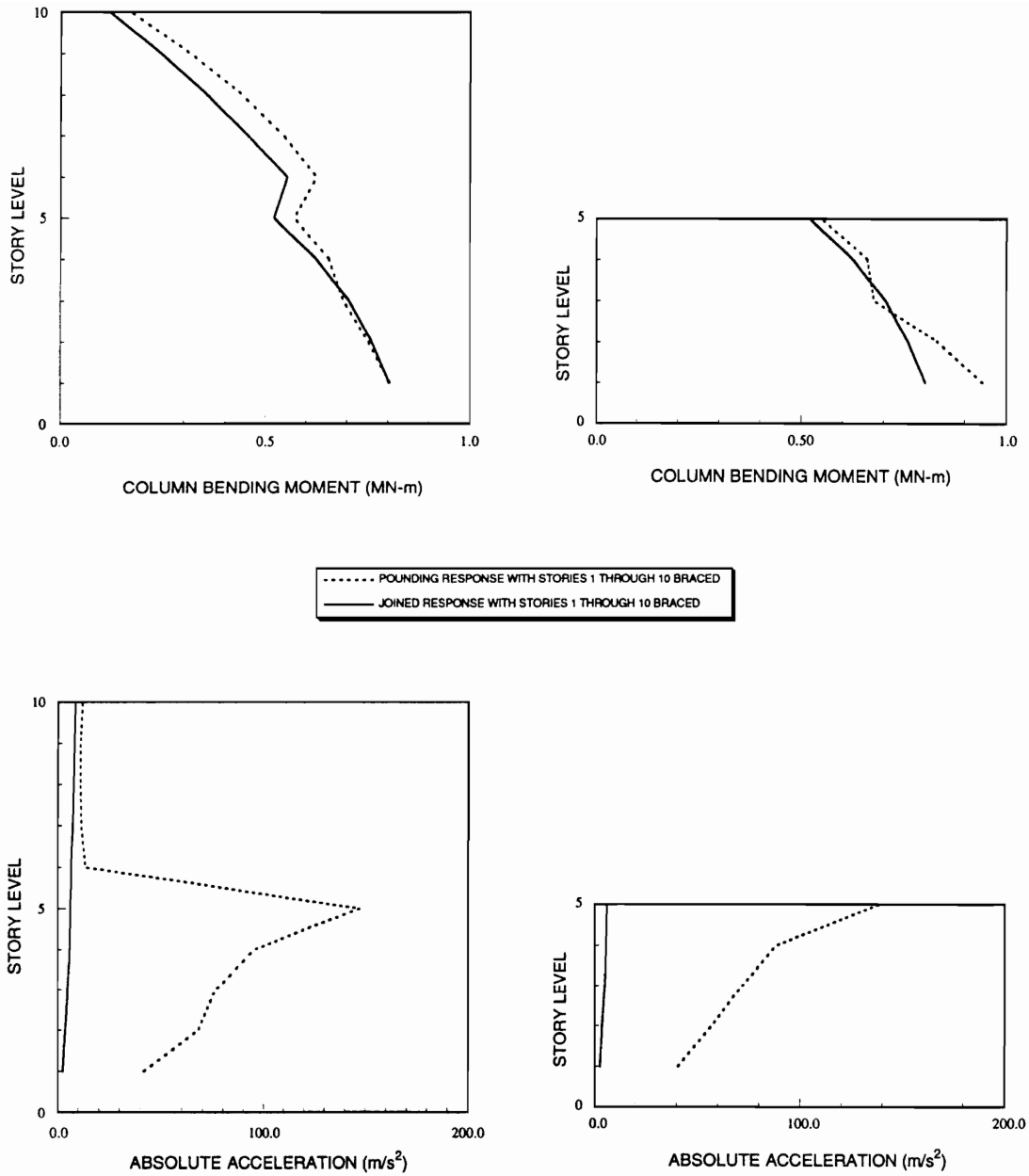


Figure 6.25: Comparison of responses obtained for joined and completely braced 10-story structure with the responses of the disjoined and completely braced 10-story structure (rigid foundation model, El-Centro time history)

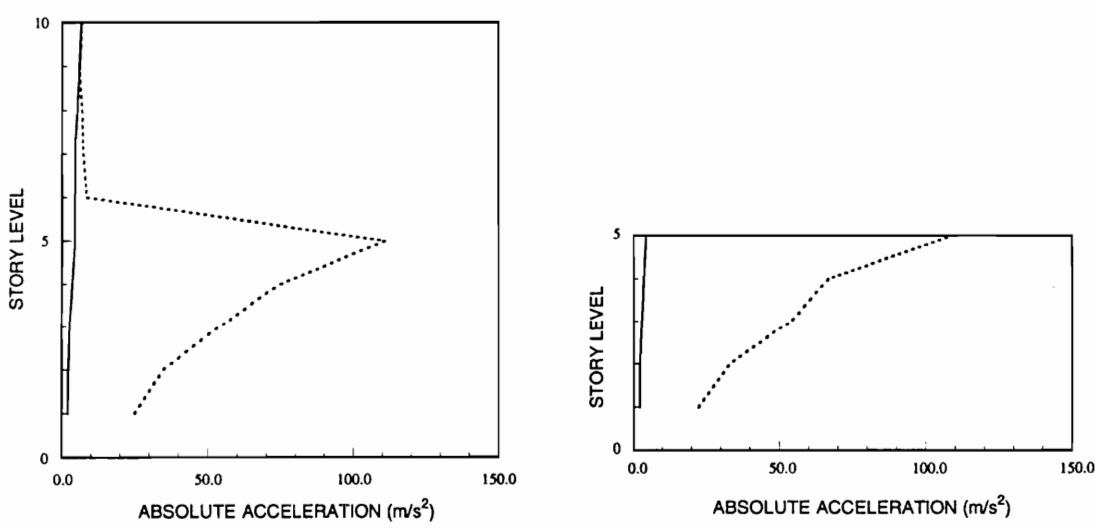
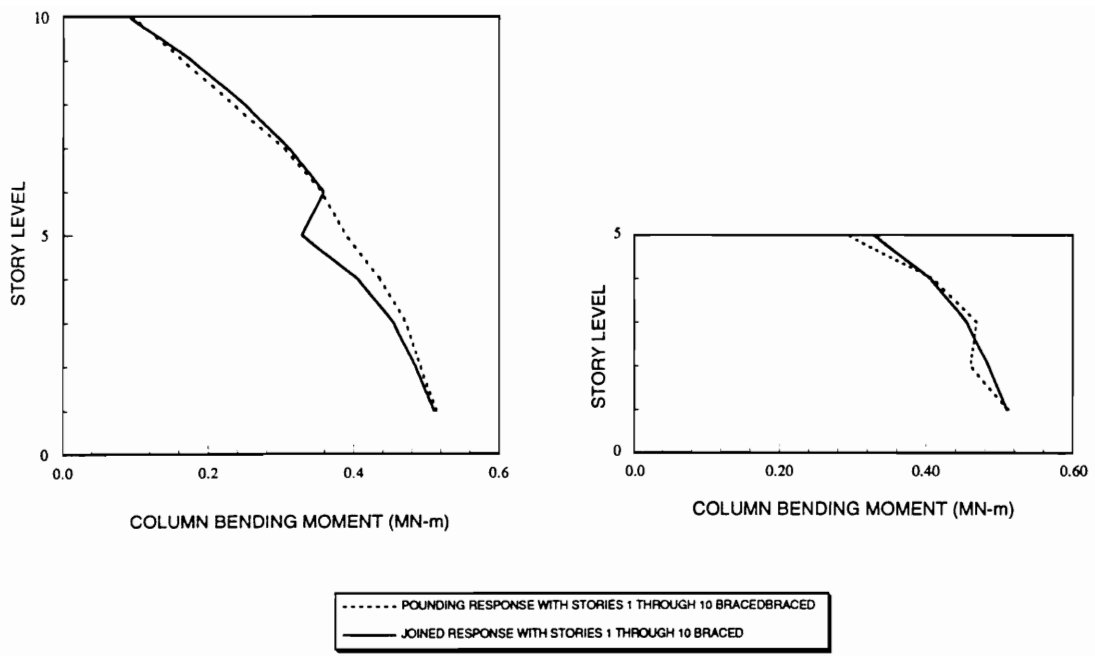


Figure 6.26: Comparison of responses obtained for joined and completely braced 10-story structure with the responses of the disjoined and completely braced 10-story structure (rigid foundation model, 1 synthetic time history)

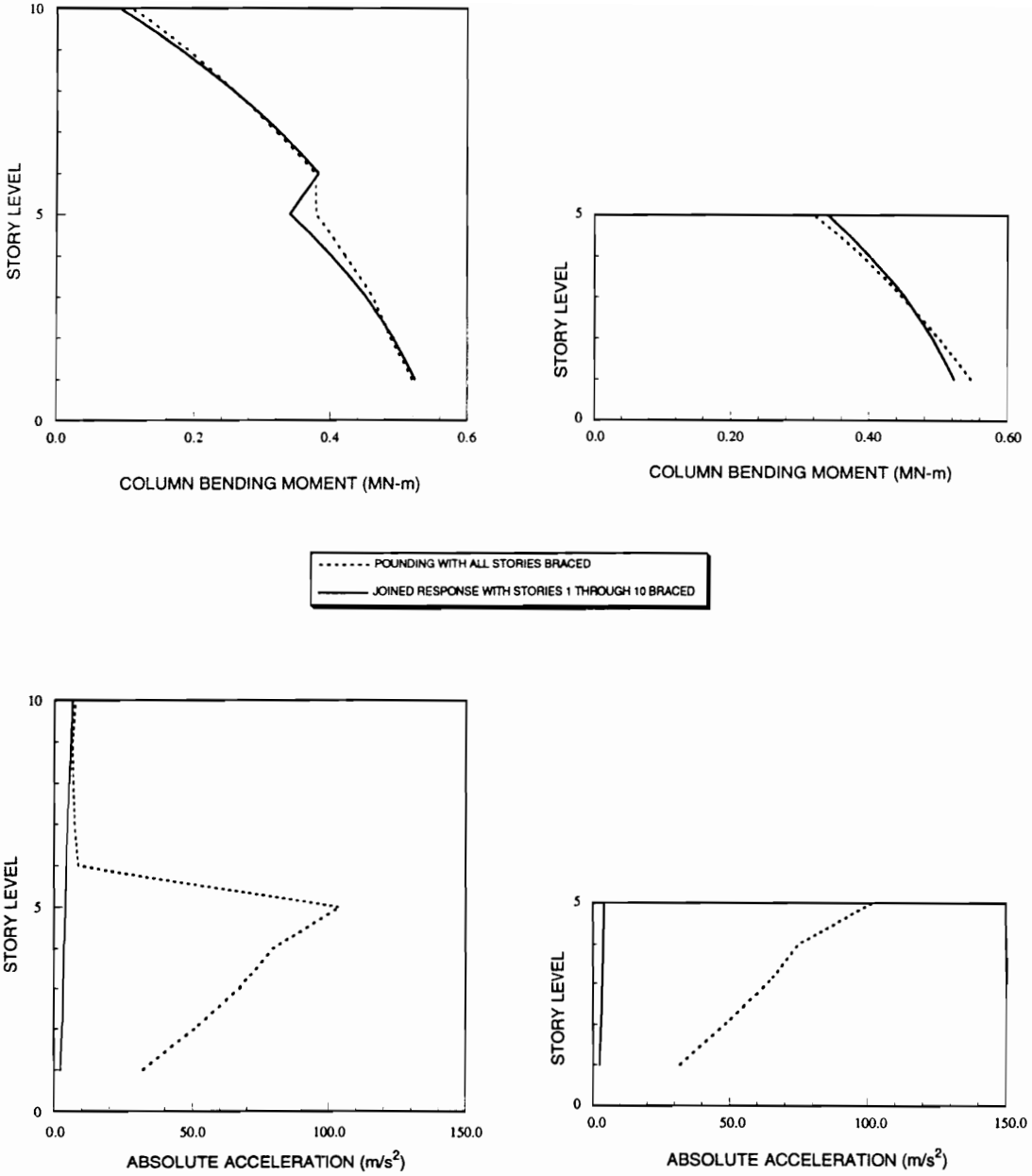


Figure 6.27: Comparison of responses obtained for joined and completely braced 10-story structure with the responses of the disjointed and completely braced 10-story structure (rigid foundation model, 50 synthetic time histories)

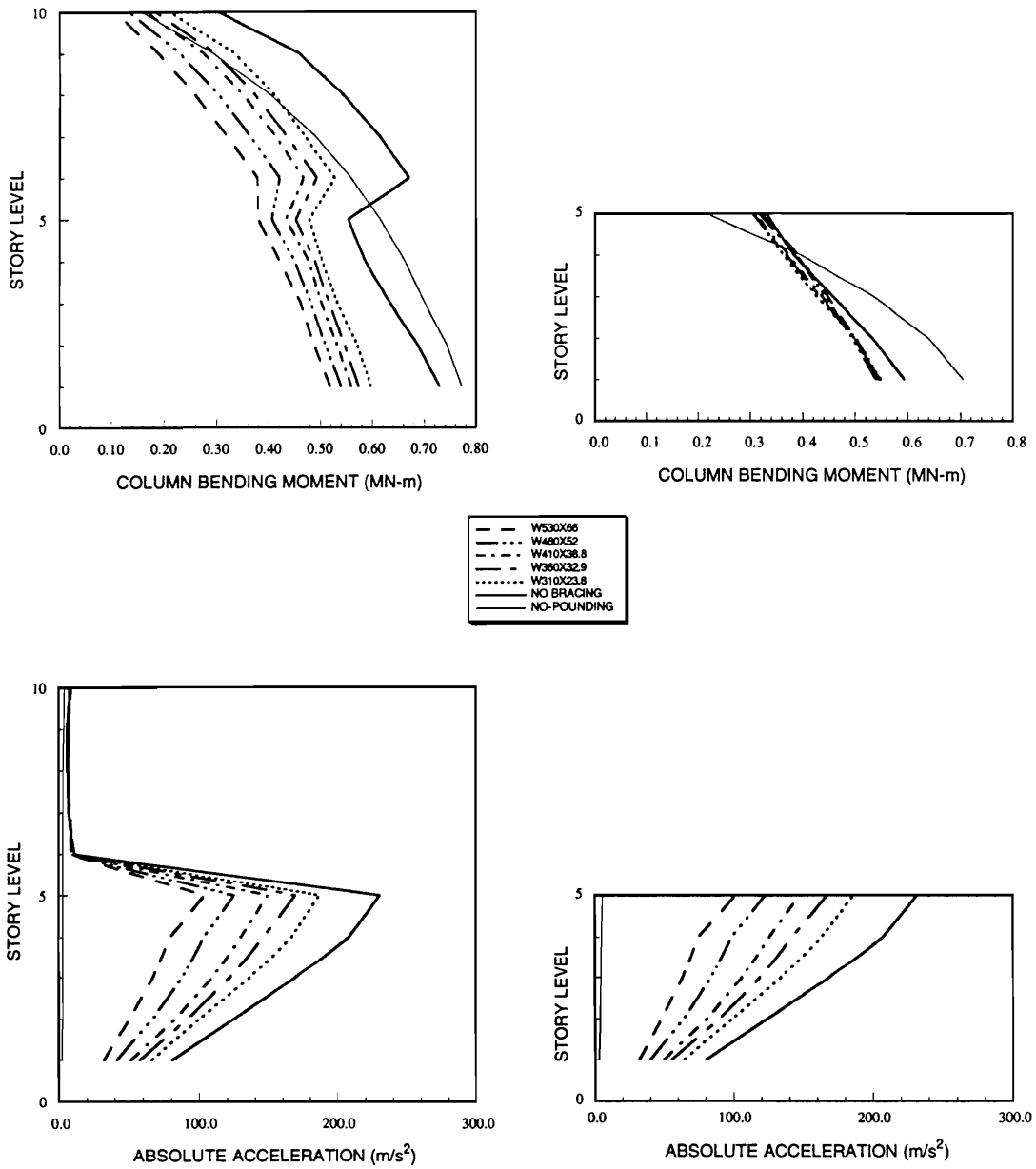


Figure 6.28: Comparison of responses obtained for different bracing sizes with the responses obtained for unbraced and no-pounding cases (rigid foundation model)

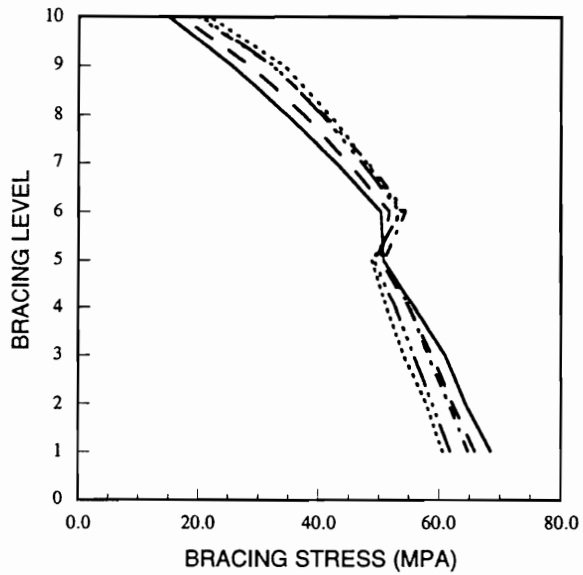
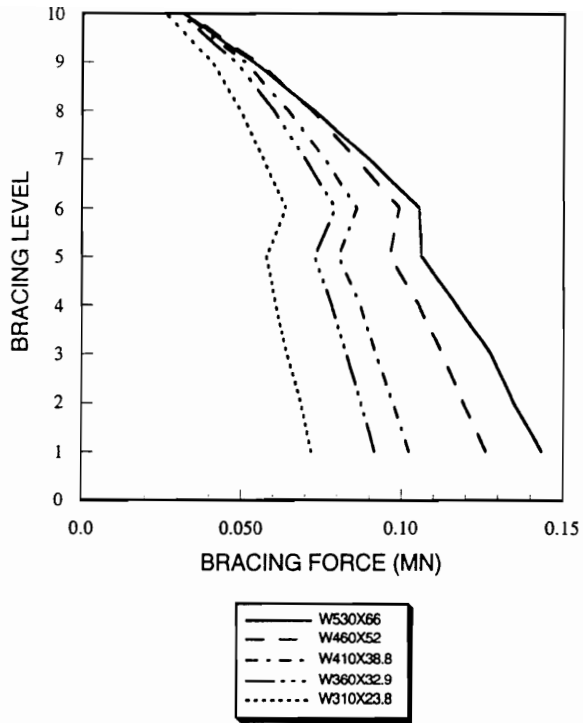


Figure 6.29: The effect of bracing sizes on the bracing force and stress responses in various bracings of the 10-story structure for pounding structures (rigid foundation model)

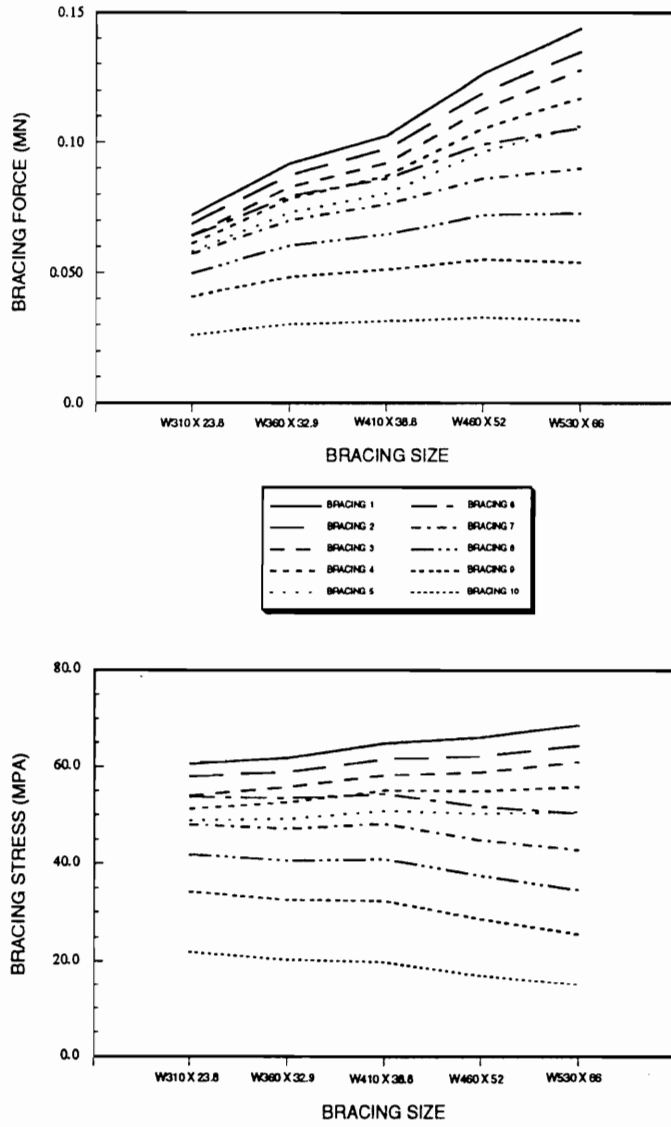


Figure 6.30: The effect of bracing sizes on the bracing force and stress pounding responses in various bracings of the 10-story structure (rigid foundation model)

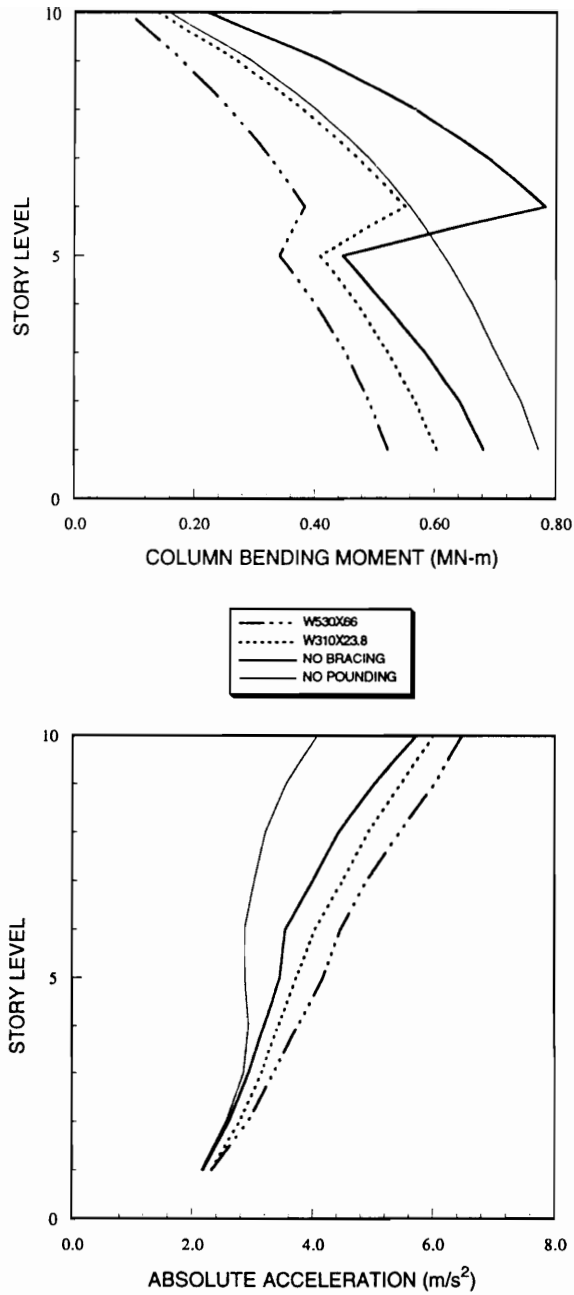


Figure 6.31: Comparison of responses obtained for joined and completely braced 10-story structure, with different bracing sizes, with the responses of unbraced joined and no-pounding cases (rigid foundation model)

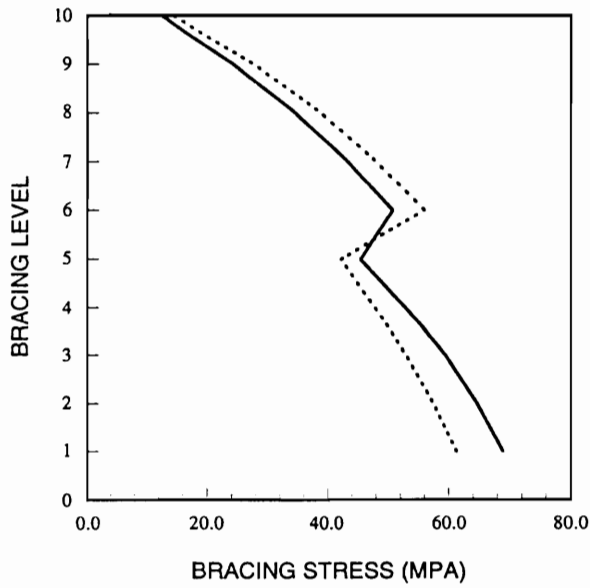
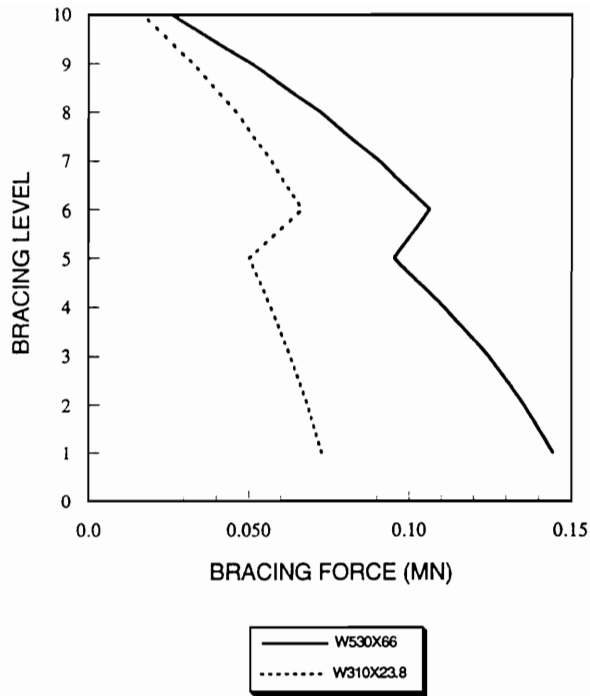


Figure 6.32: The effect of bracing sizes on the bracing force and stress responses in various bracings of the 10-story structure for joined structures (rigid foundation model)

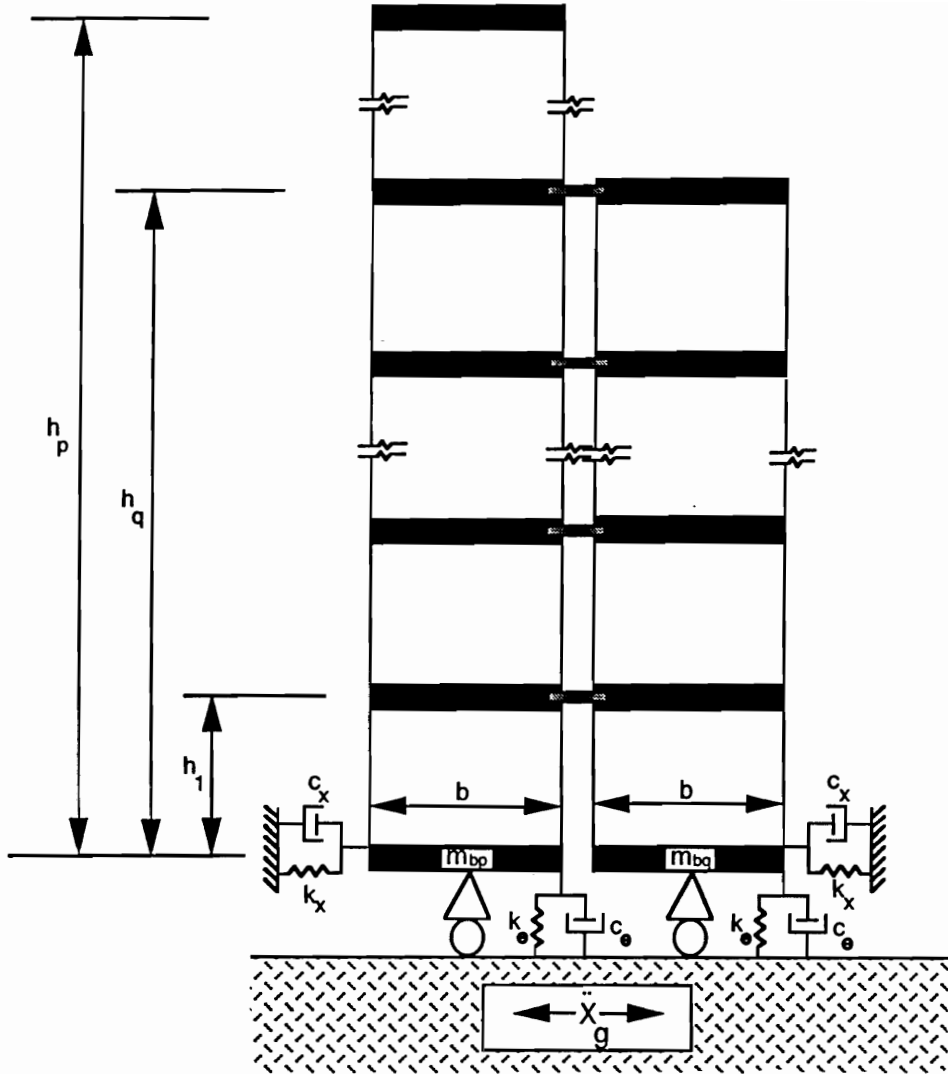


Figure 6.33: Schematic of rigidly joined structures supported on the flexible foundation

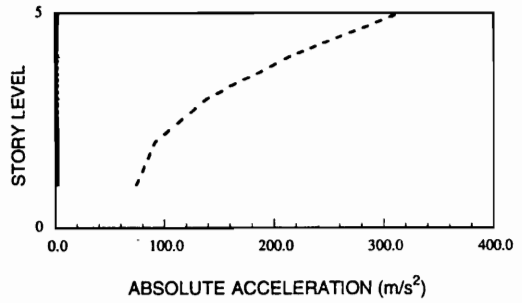
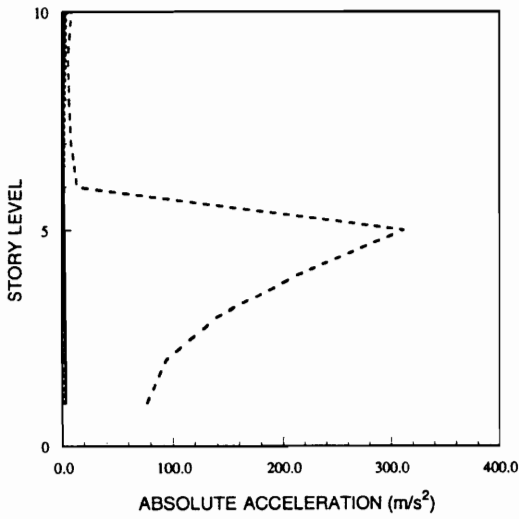
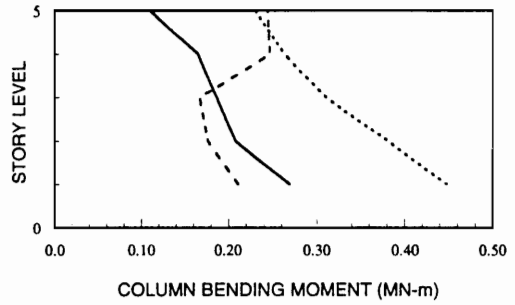
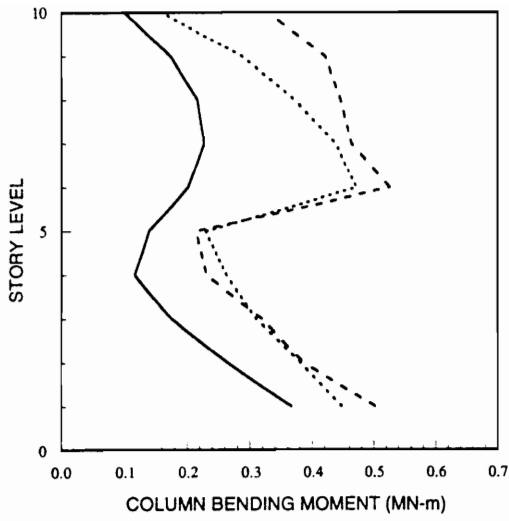


Figure 6.34: Comparison of the column bending moment and absolute floor acceleration responses of rigidly joined structures with the corresponding responses obtained for the no-pounding and free-pounding cases (flexible foundation model, El-Centro time history)

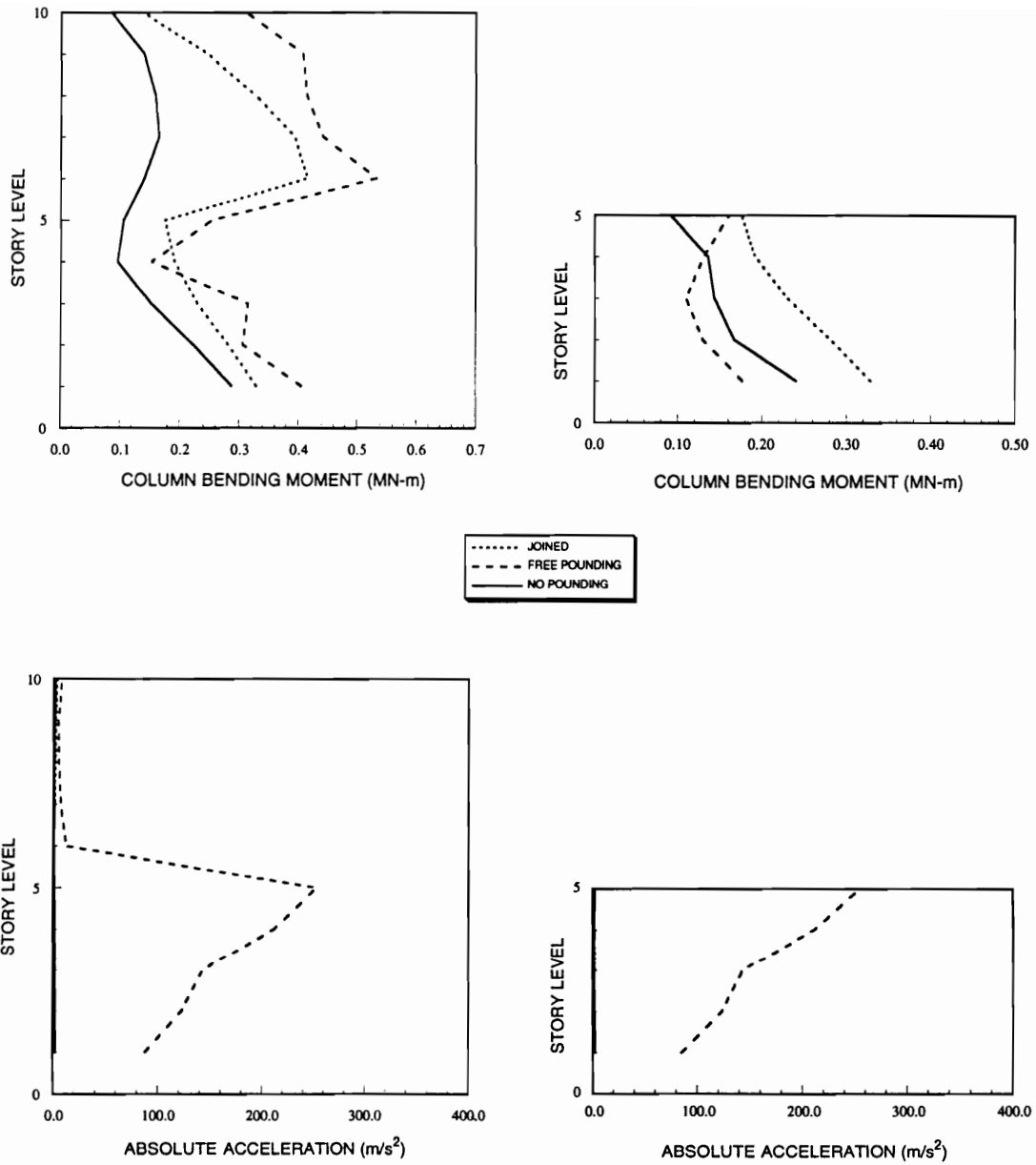


Figure 6.35: Comparison of the column bending moment and absolute floor acceleration responses of rigidly joined structures with the corresponding responses obtained for the no-pounding and free-pounding cases (flexible foundation model, 1 synthetic time history)

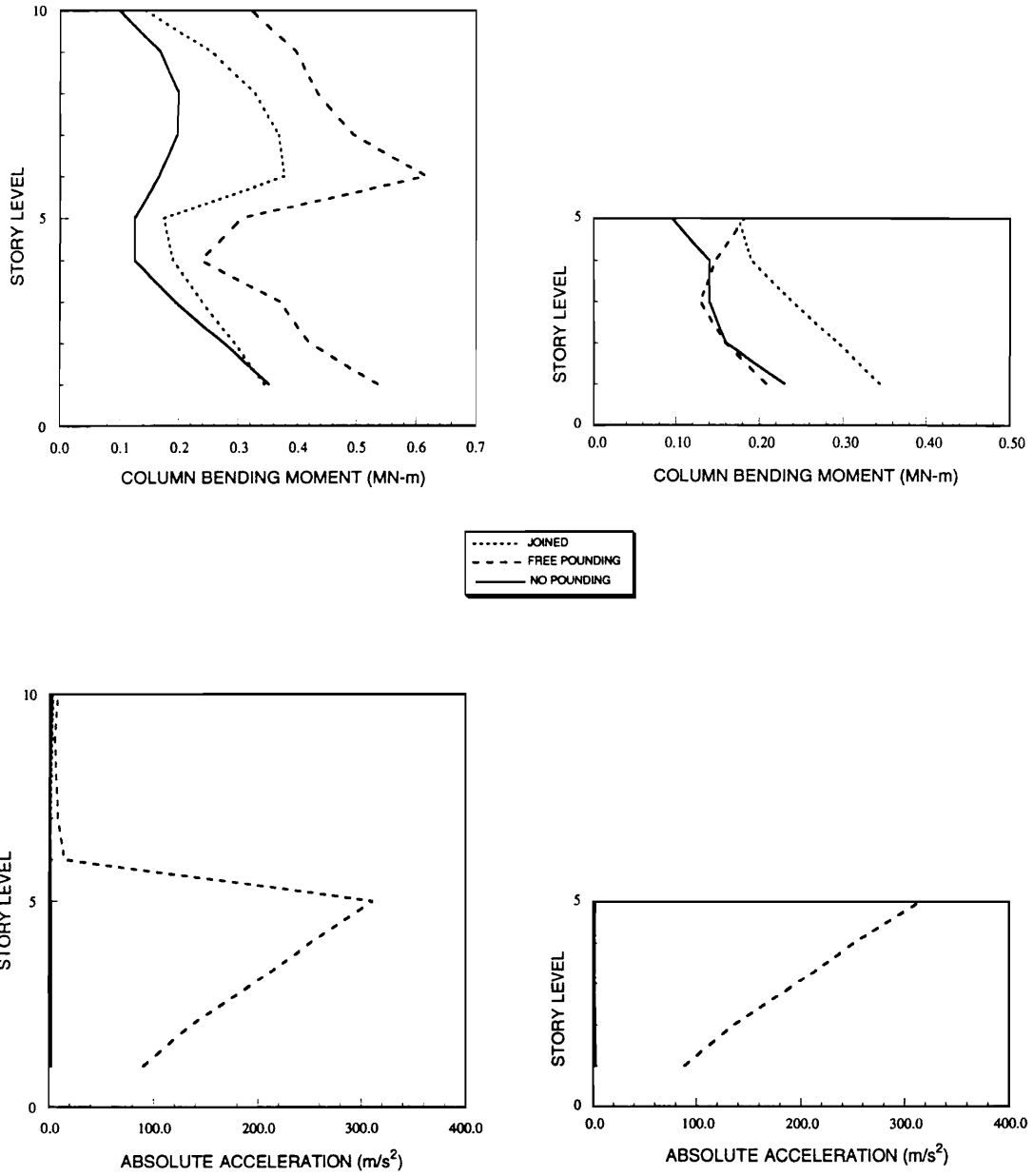


Figure 6.36: Comparison of the column bending moment and absolute floor acceleration responses of rigidly joined structures with the corresponding responses obtained for the no-pounding and free-pounding cases (flexible foundation model, 50 synthetic time histories)

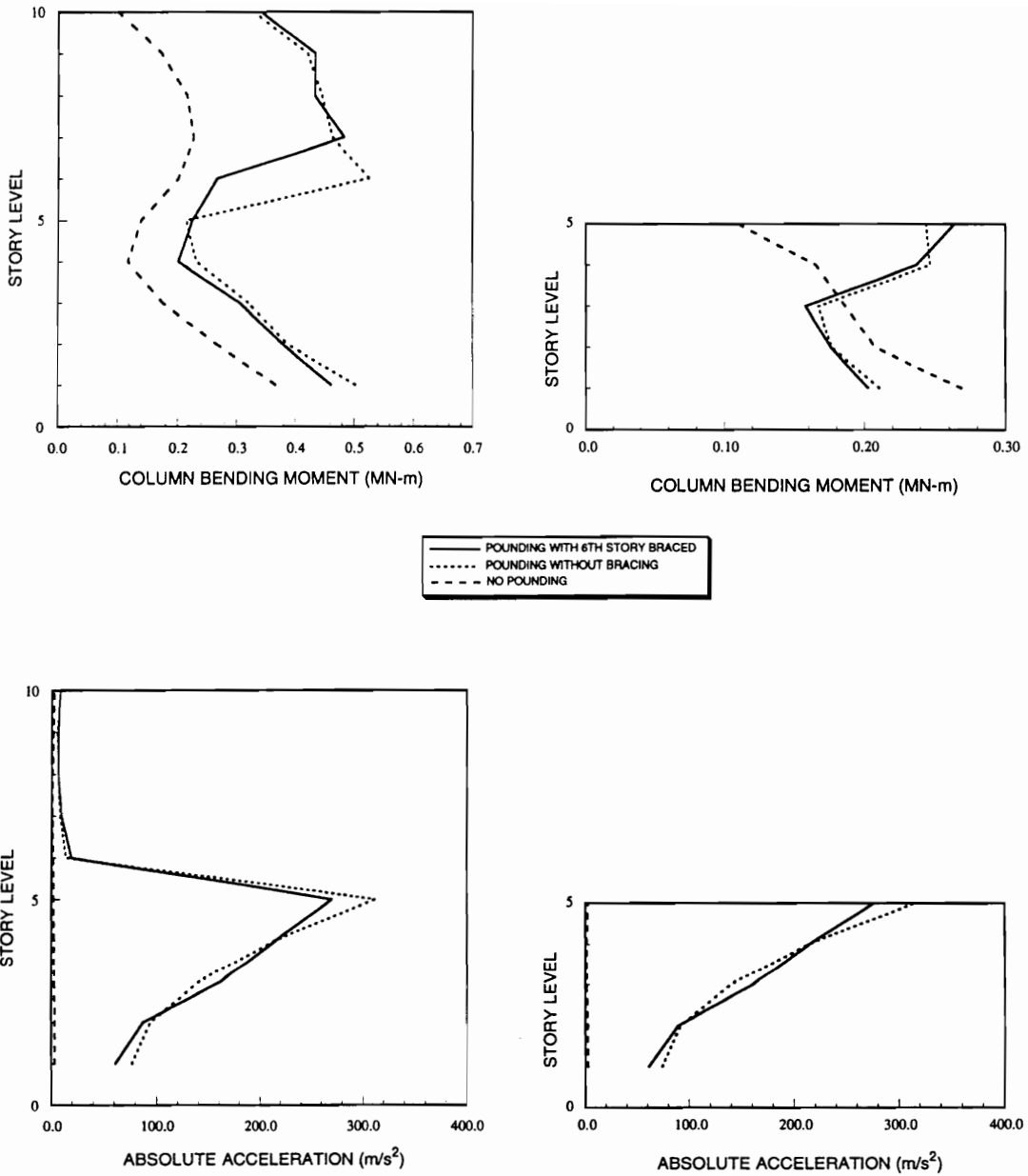
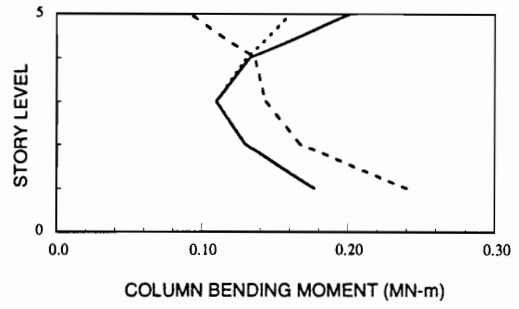
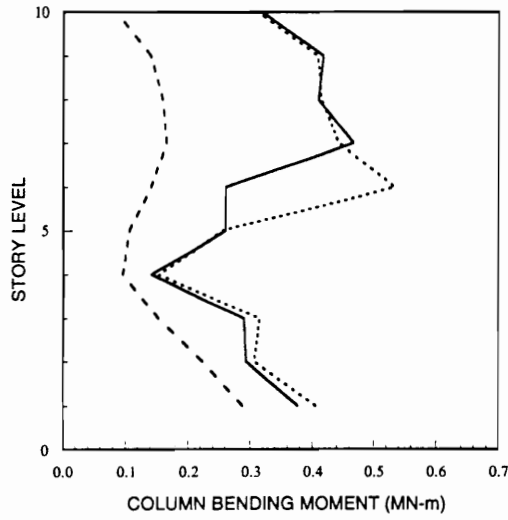


Figure 6.37: Comparison of responses obtained with bracing, without bracing and no-pounding cases (flexible foundation model, El-Centro time history)



— POUNDING WITH 8TH STORY BRACED
 - - - POUNDING RESPONSE WITHOUT BRACING
 - - - NO POUNDING

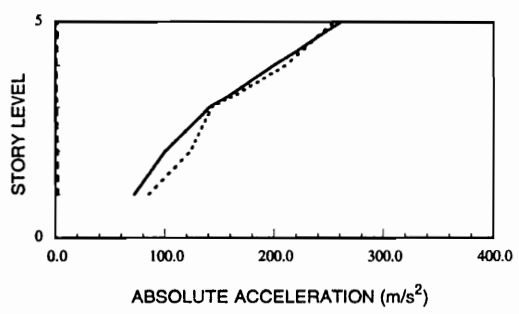
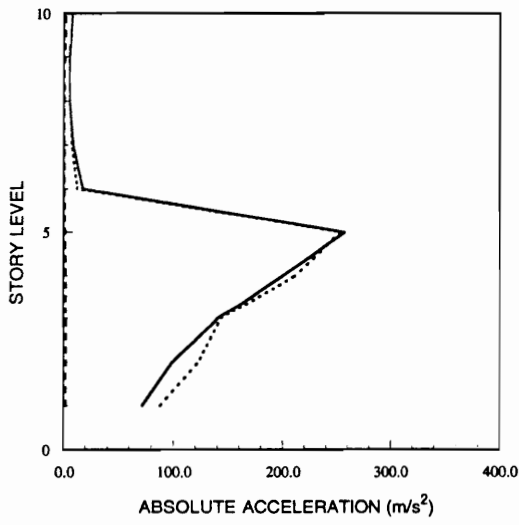


Figure 6.38: Comparison of responses obtained with bracing, without bracing and no-pounding cases (flexible foundation model, 1 synthetic time history)

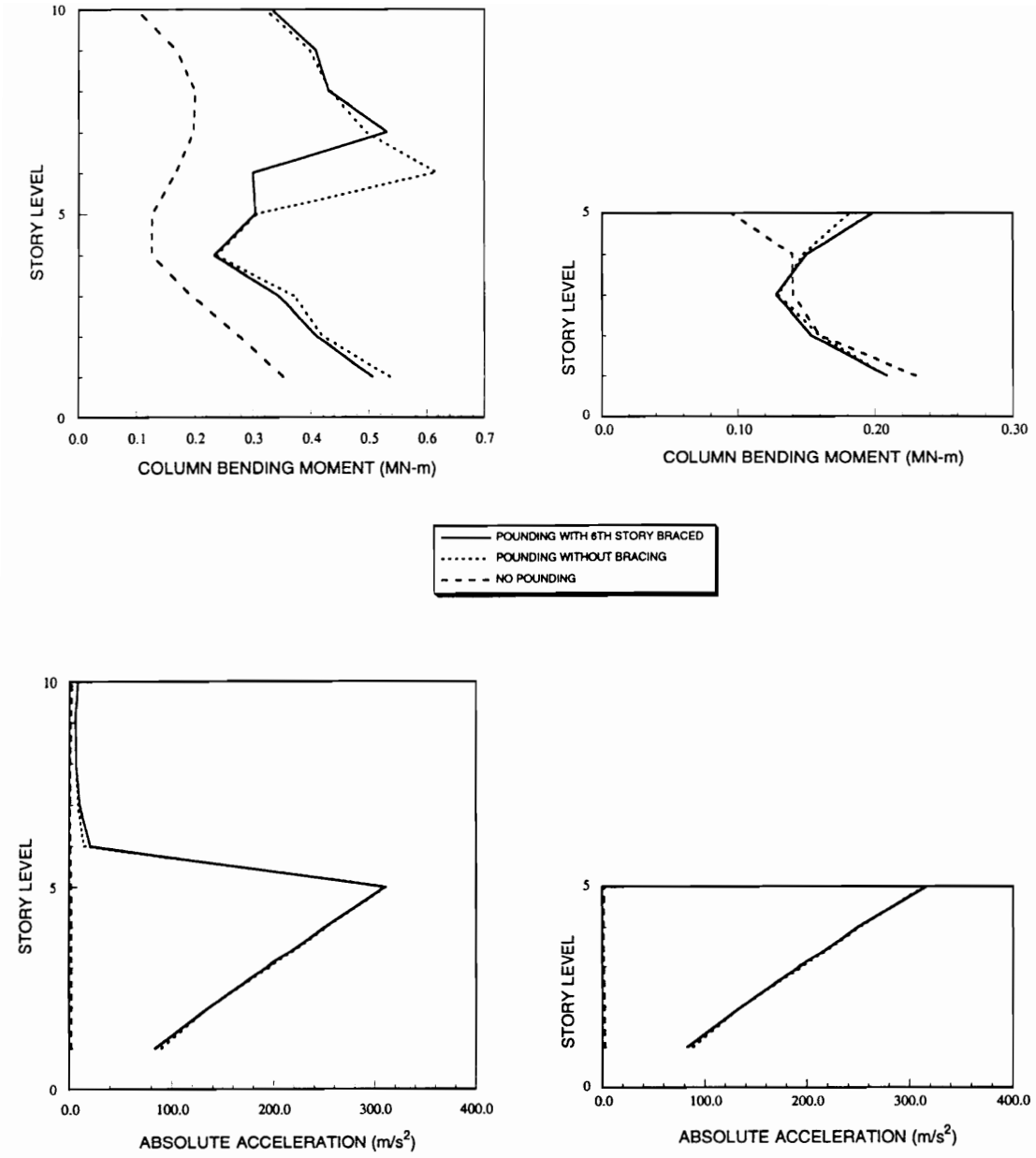


Figure 6.39: Comparison of responses obtained with bracing, without bracing and no-pounding cases (flexible foundation model, 50 synthetic time histories)

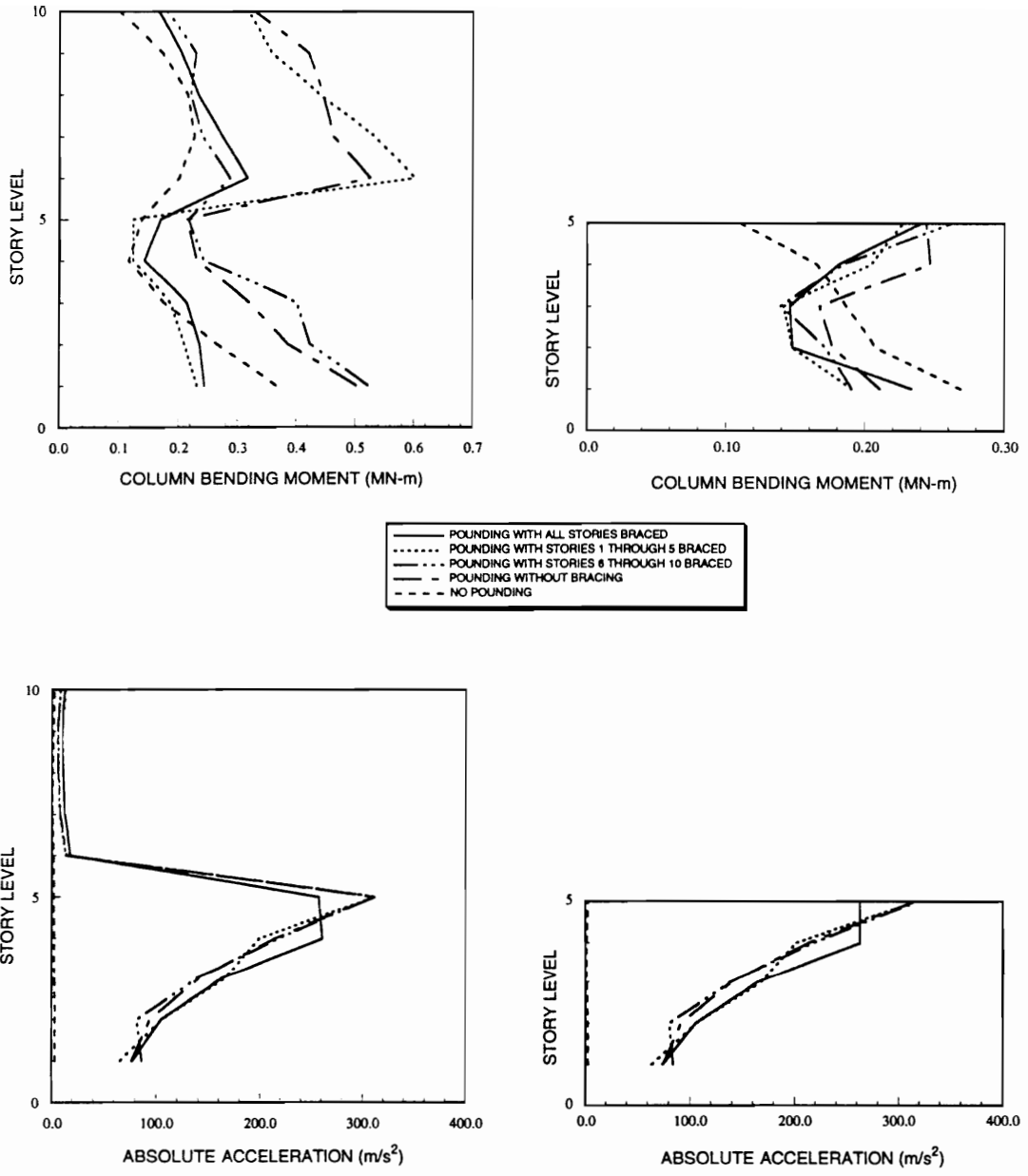


Figure 6.40: Comparison of responses obtained for different configurations of bracings with the responses obtained for unbraced and no-pounding cases (flexible foundation model, El-Centro time history)

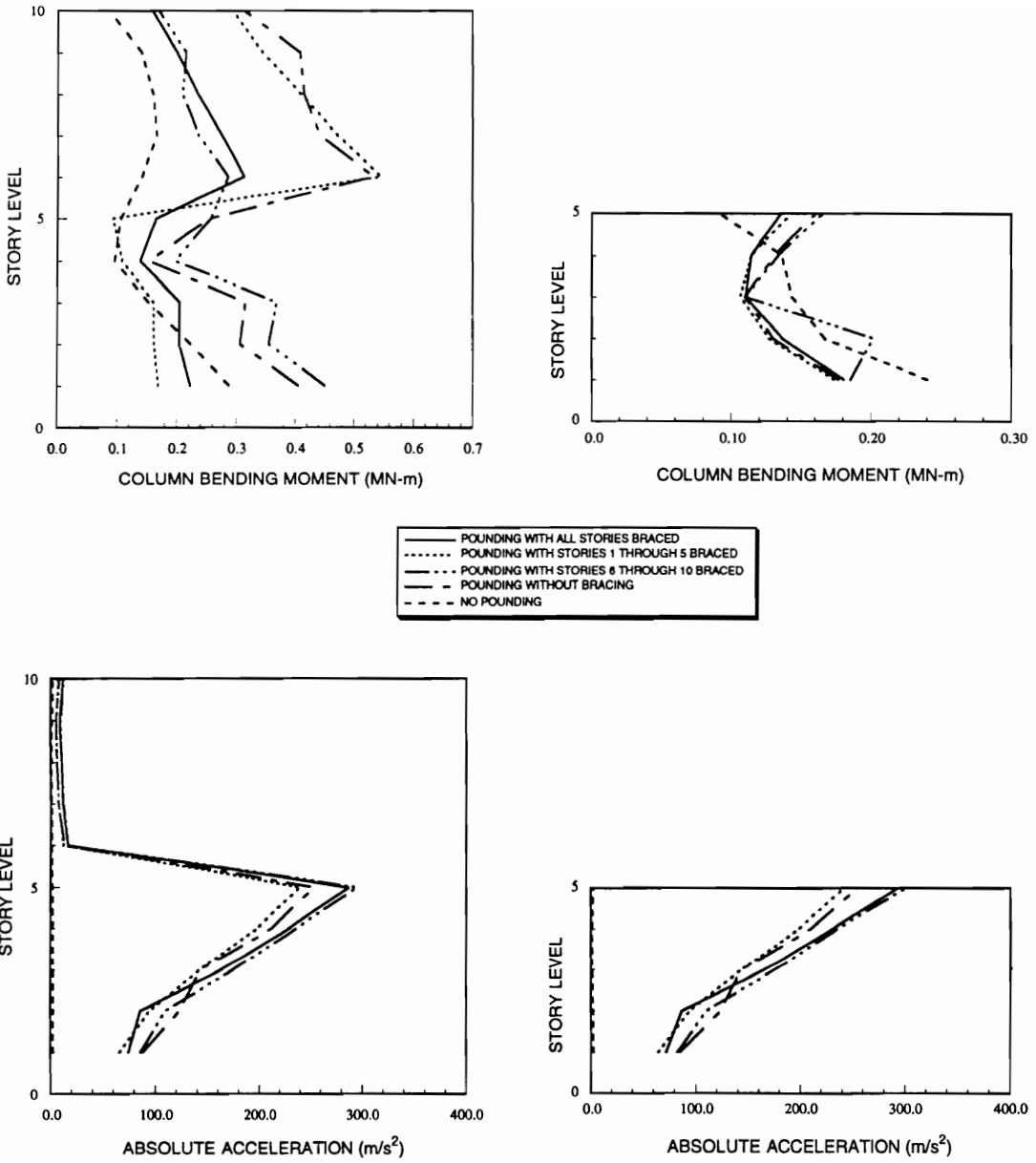


Figure 6.41: Comparison of responses obtained for different configurations of bracings with the responses obtained for unbraced and no-pounding cases (flexible foundation model, 1 synthetic time history)

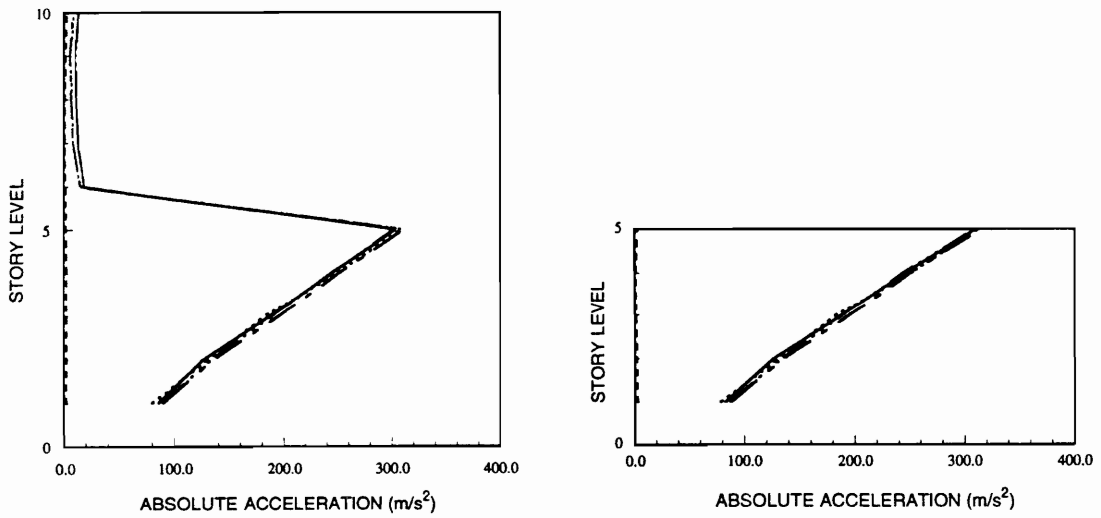
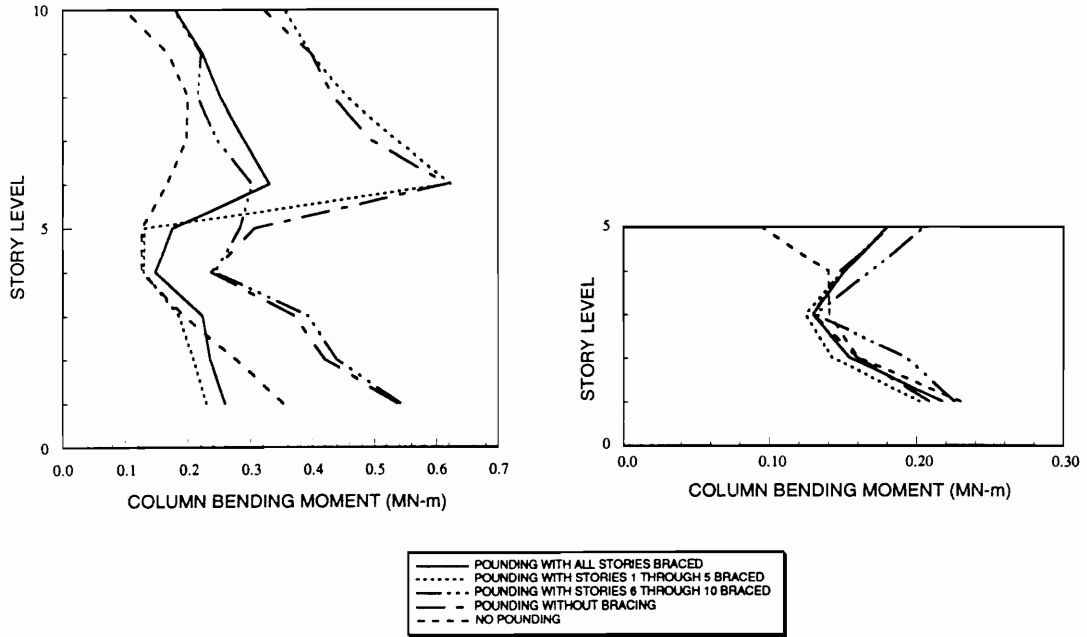


Figure 6.42: Comparison of responses obtained for different configurations of bracings with the responses obtained for unbraced and no-pounding cases (flexible foundation model, 50 synthetic time histories)

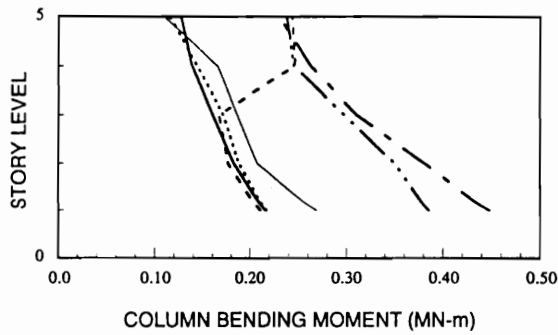
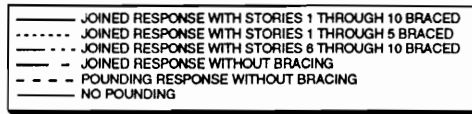
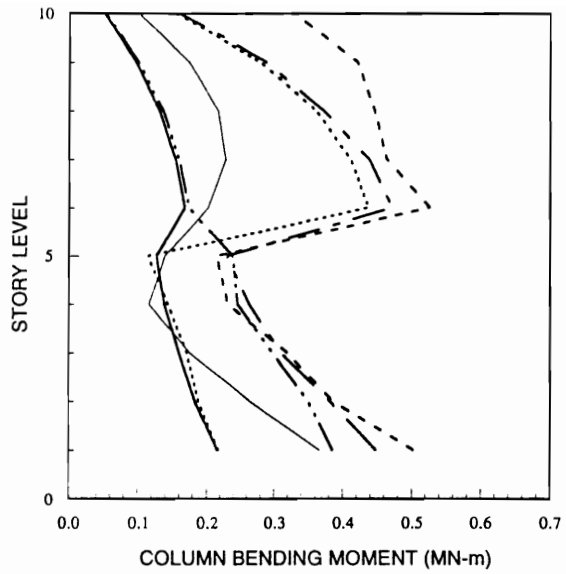


Figure 6.43: Comparison of the bending moment response obtained for joined structures with different bracing configurations with the response obtained for unbraced joined and unbraced disjoined freely pounding structures (flexible foundation model, El-Centro time history)

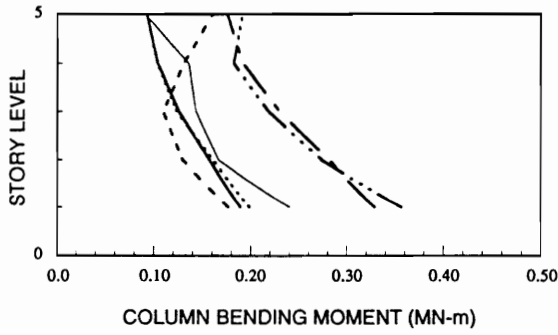
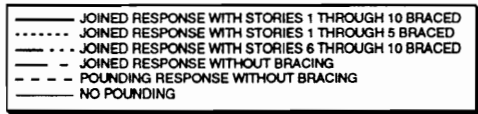
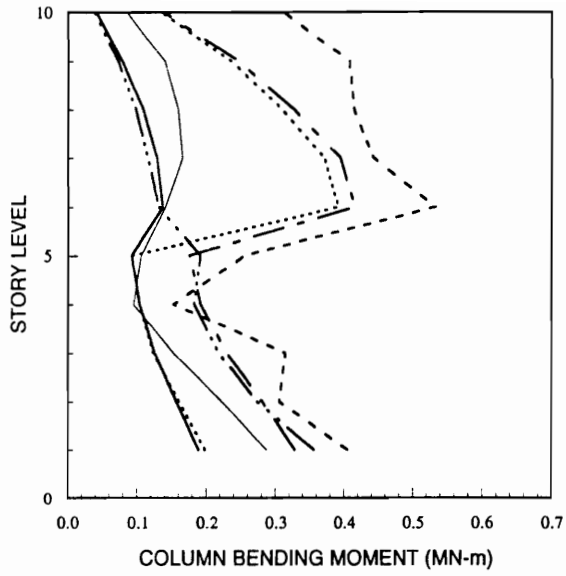


Figure 6.44: Comparison of the bending moment response obtained for joined structures with different bracing configurations with the response obtained for unbraced joined and unbraced disjointed freely pounding structures (flexible foundation model, 1 synthetic time history)

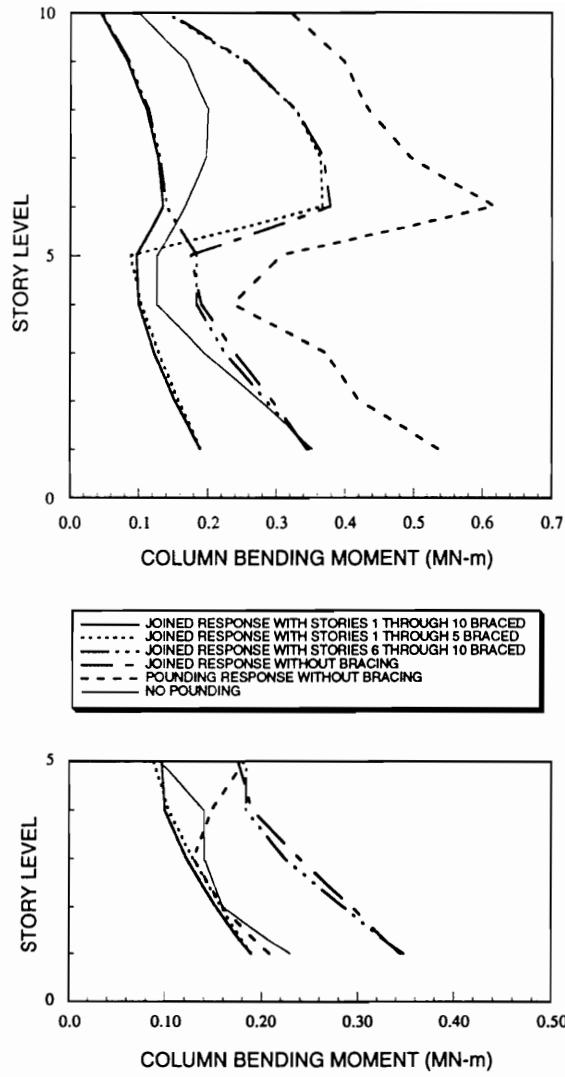


Figure 6.45: Comparison of the bending moment response obtained for joined structures with different bracing configurations with the response obtained for unbraced joined and unbraced disjoined freely pounding structures (flexible foundation model, 50 synthetic time histories)

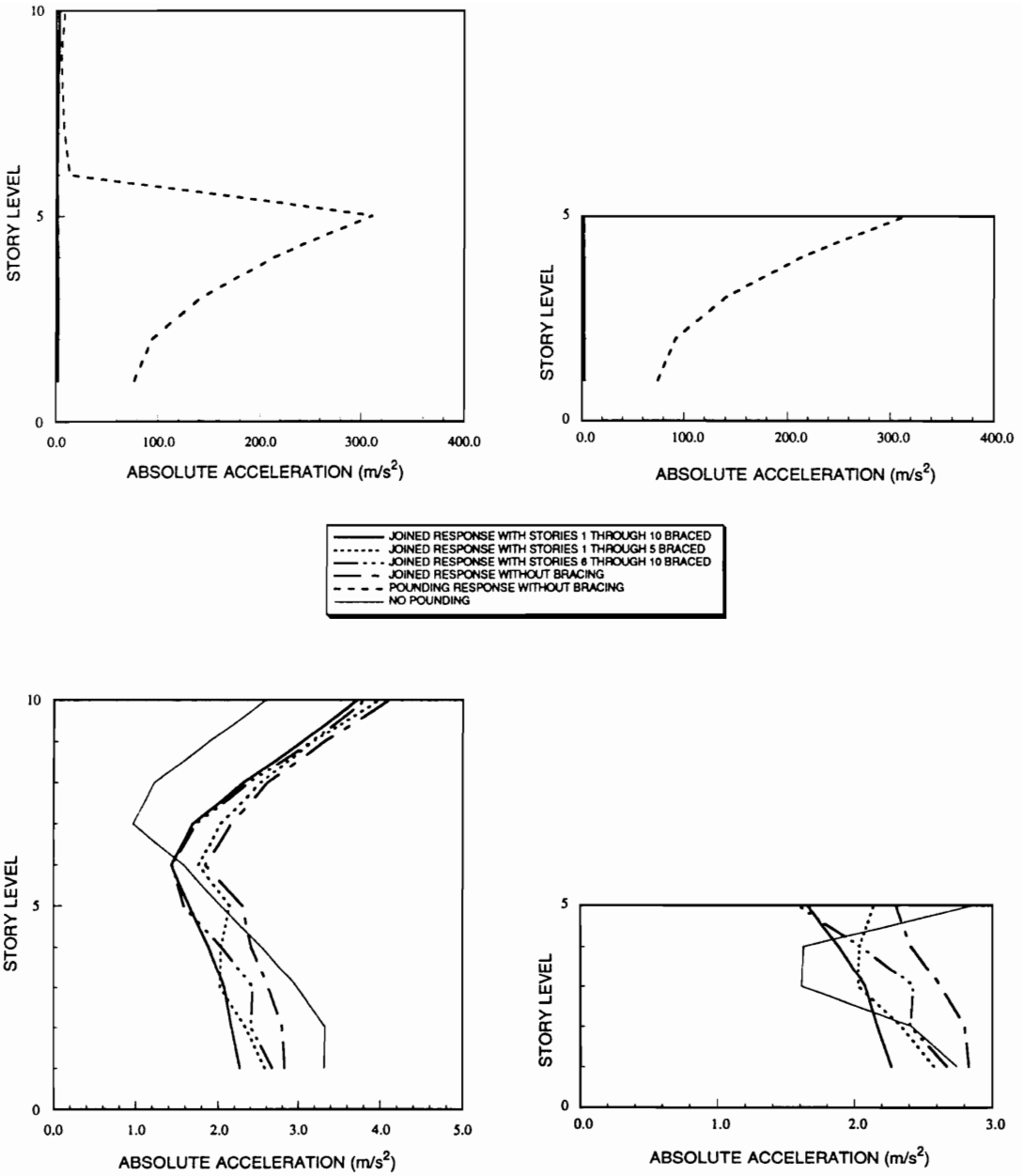


Figure 6.46: Comparison of the acceleration response obtained for joined structures with different bracing configurations with the response obtained for unbraced joined and unbraced disjoined freely pounding structures (flexible foundation model, El-Centro time history)

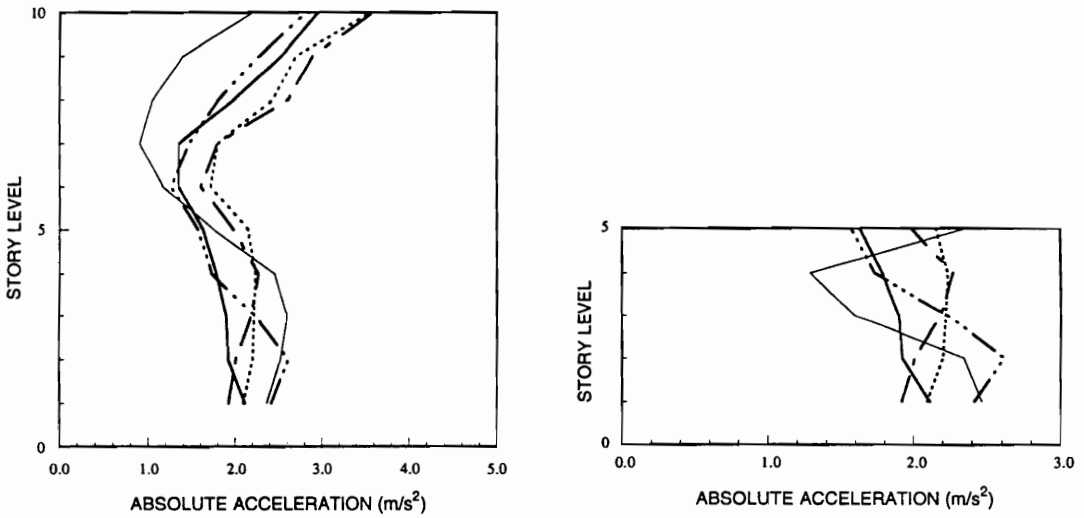
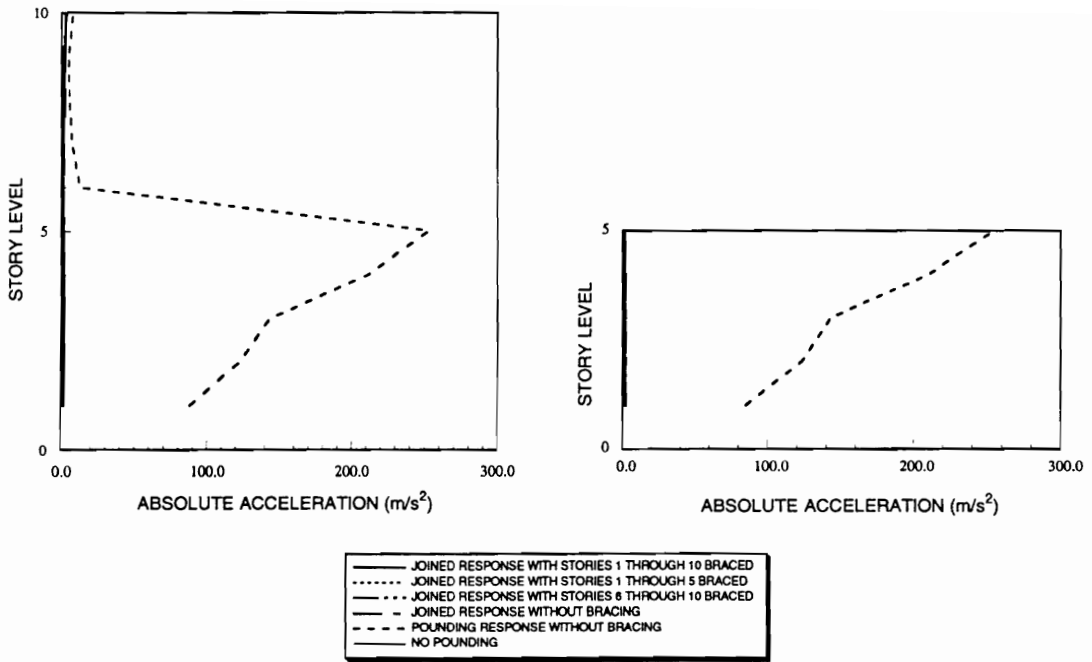


Figure 6.47: Comparison of the acceleration response obtained for joined structures with different bracing configurations with the response obtained for unbraced joined and unbraced disjointed freely pounding structures (flexible foundation model, 1 synthetic time history)

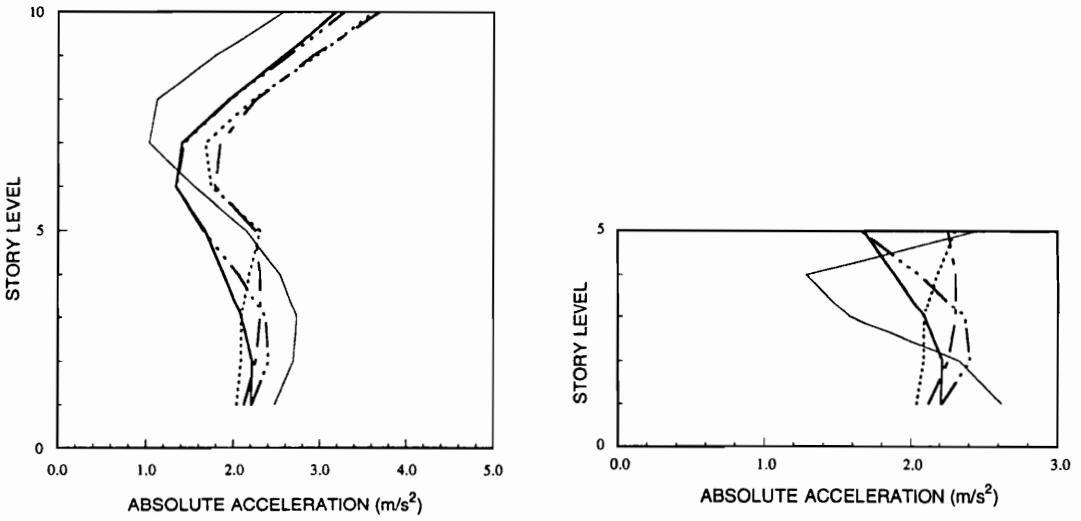
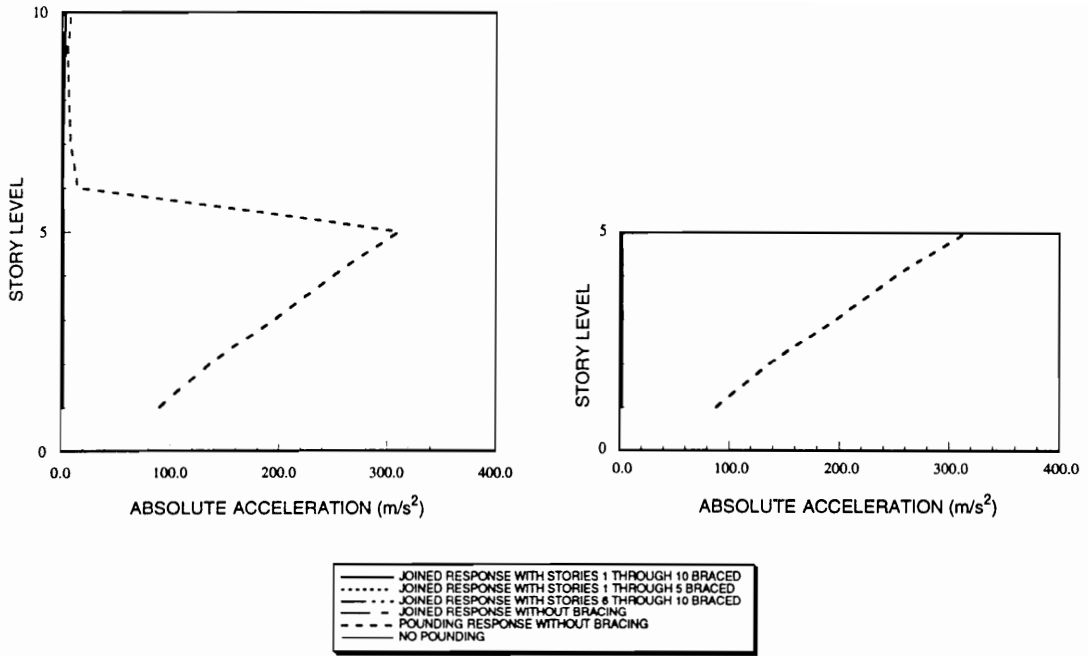


Figure 6.48: Comparison of the acceleration response obtained for joined structures with different bracing configurations with the response obtained for unbraced joined and unbraced disjoined freely pounding structures (flexible foundation model, 50 synthetic time histories)

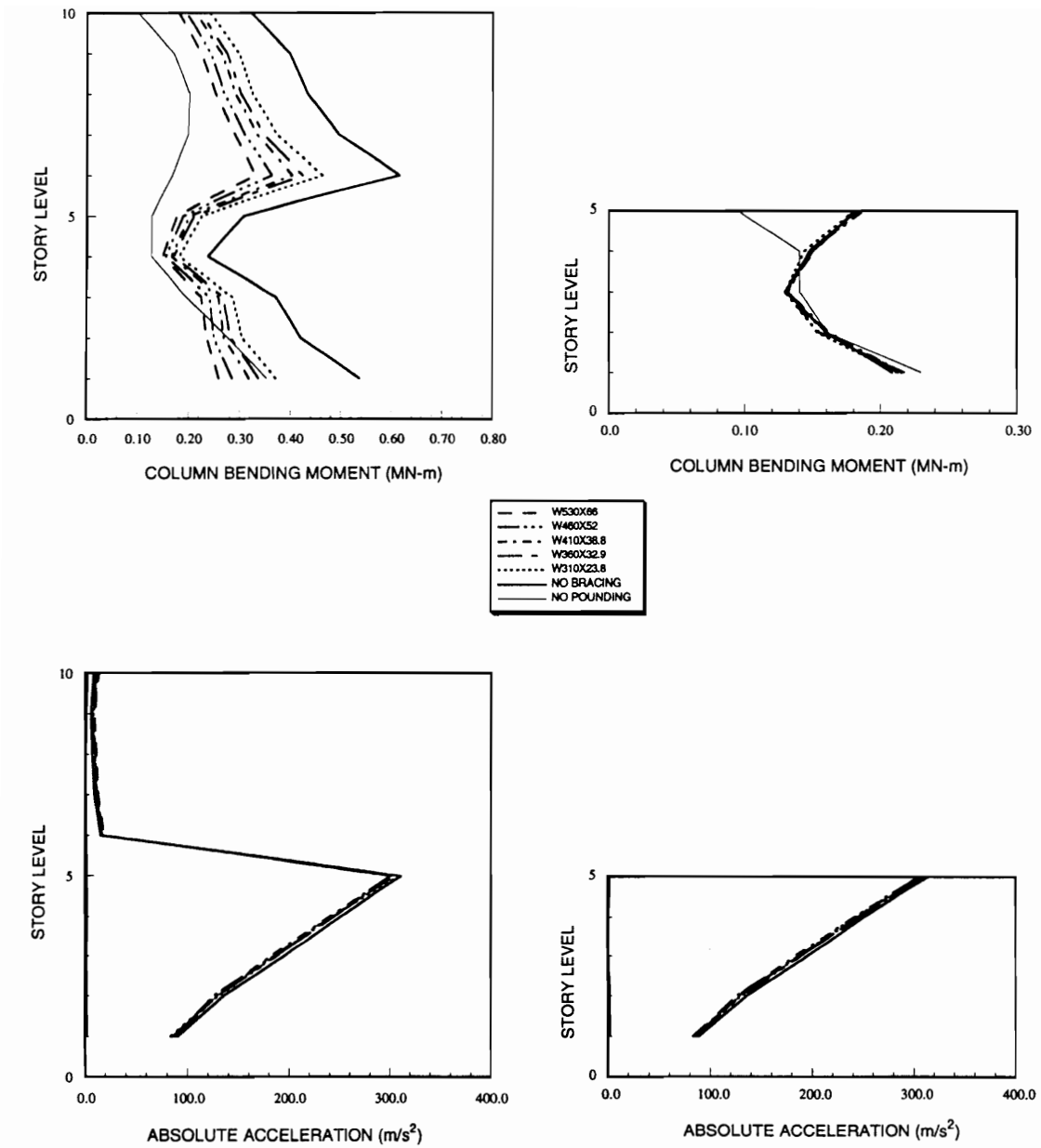


Figure 6.49: Comparison of responses obtained for different bracing sizes with the responses obtained for unbraced and no-pounding cases (flexible foundation model)

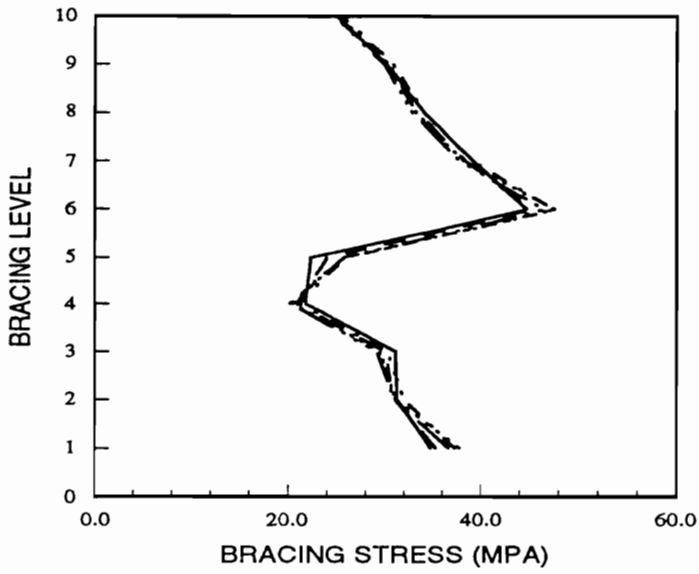
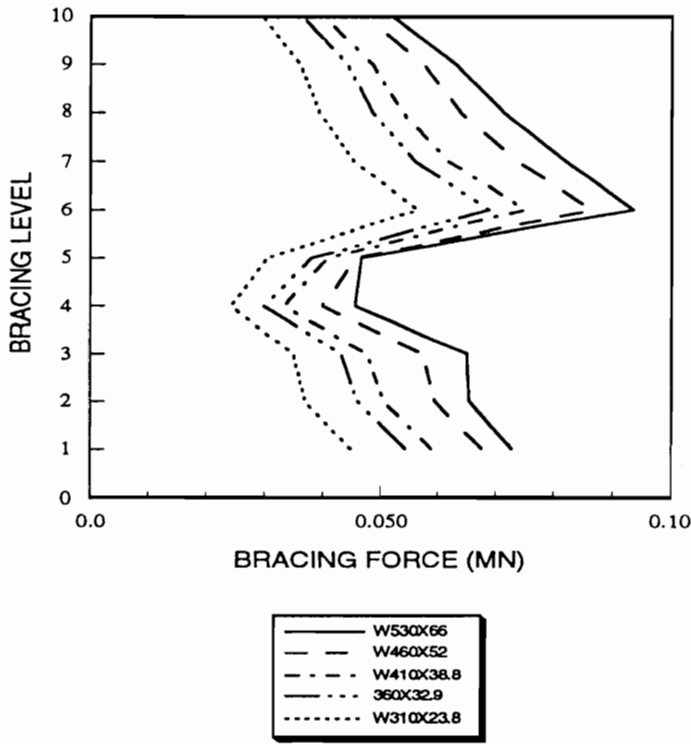


Figure 6.50: The effect of bracing sizes on the bracing force and stress responses in various bracings of the 10-story structure for pounding structures (flexible foundation model)

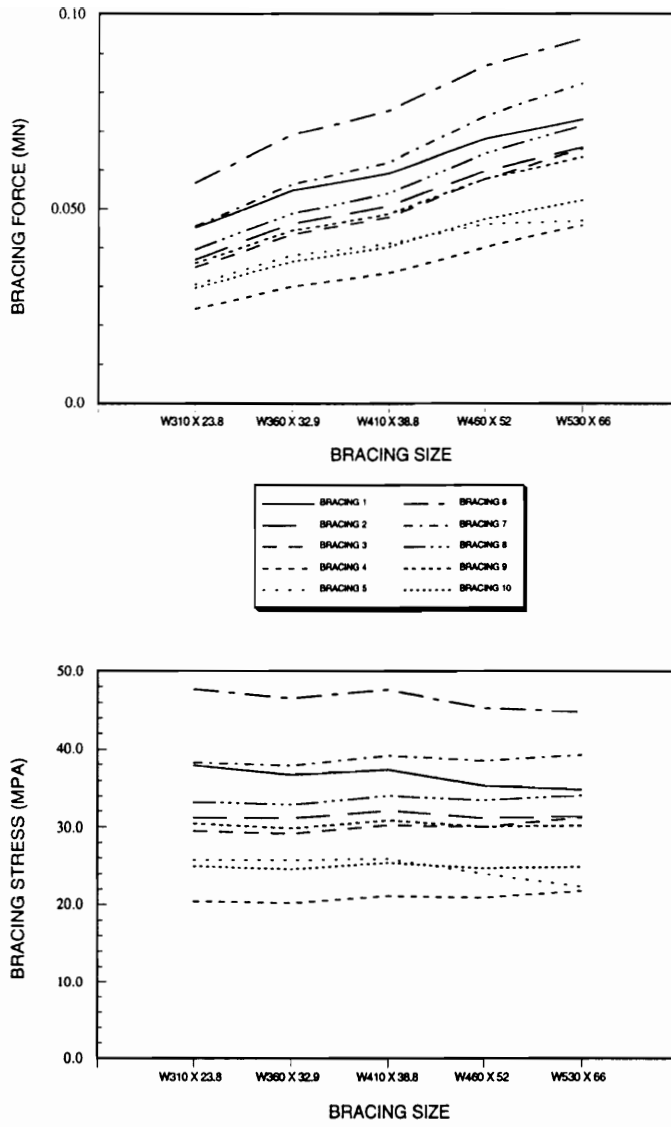


Figure 6.51: The effect of bracing sizes on the bracing force and stress pounding responses in various bracings of the 10-story structure (flexible foundation model)

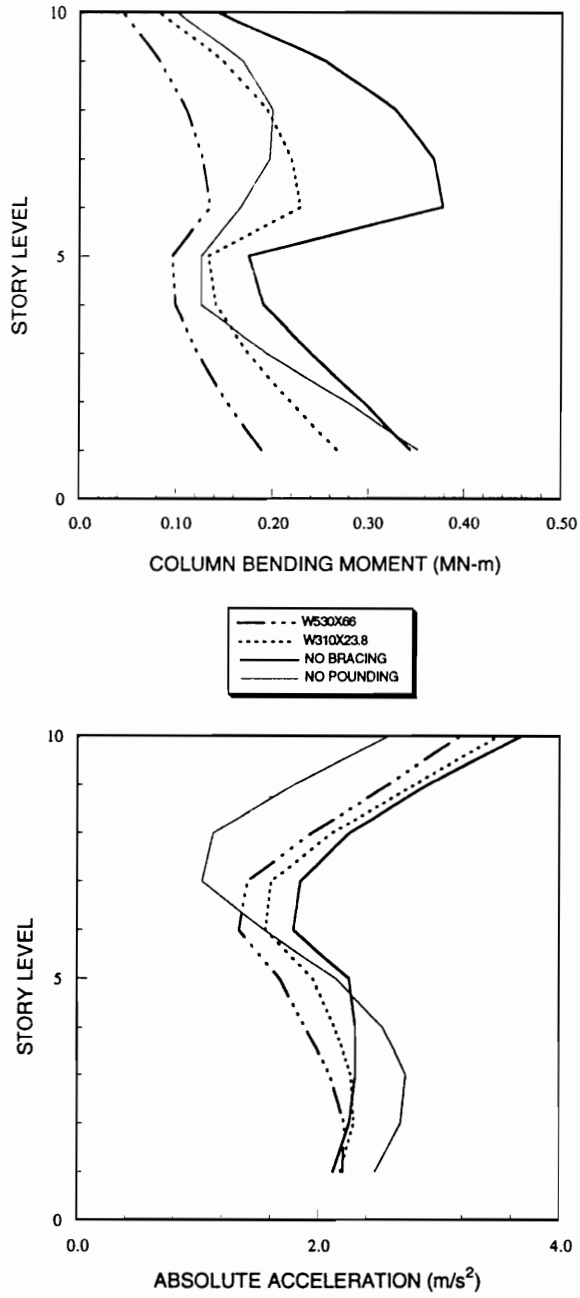


Figure 6.52: Comparison of responses obtained for joined and completely braced 10-story structure, with different bracing sizes, with the responses of unbraced joined and no-pounding cases (flexible foundation model)

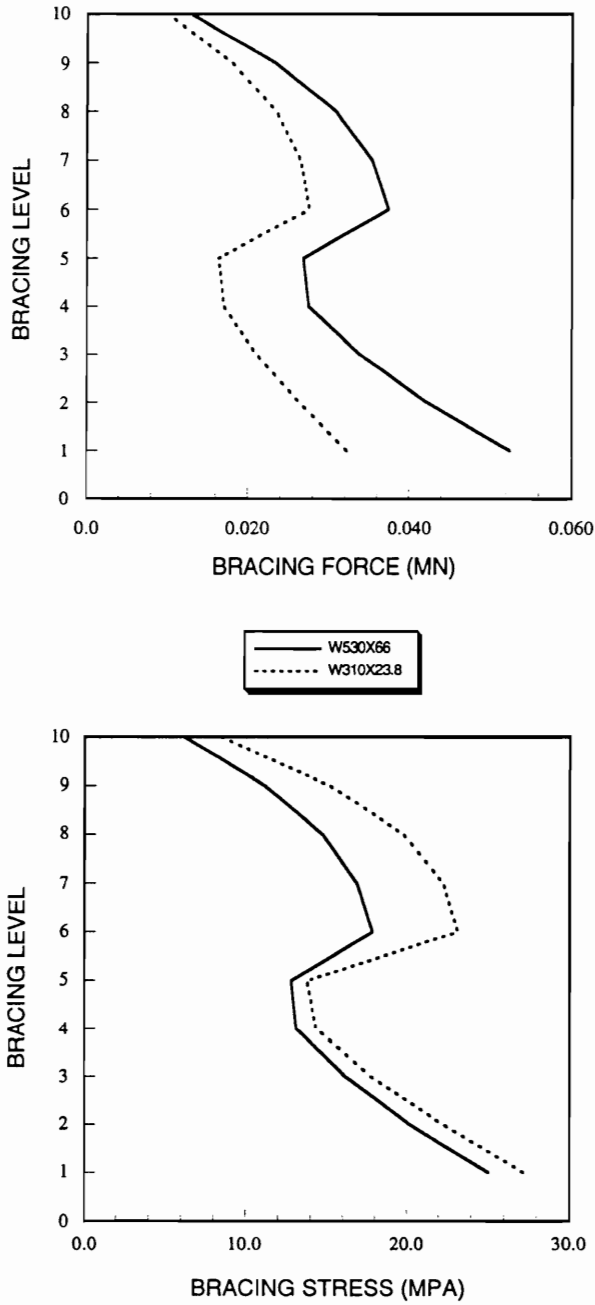


Figure 6.53: The effect of bracing sizes on the bracing force and stress responses in various bracings of the 10-story structure for joined structures (flexible foundation model)

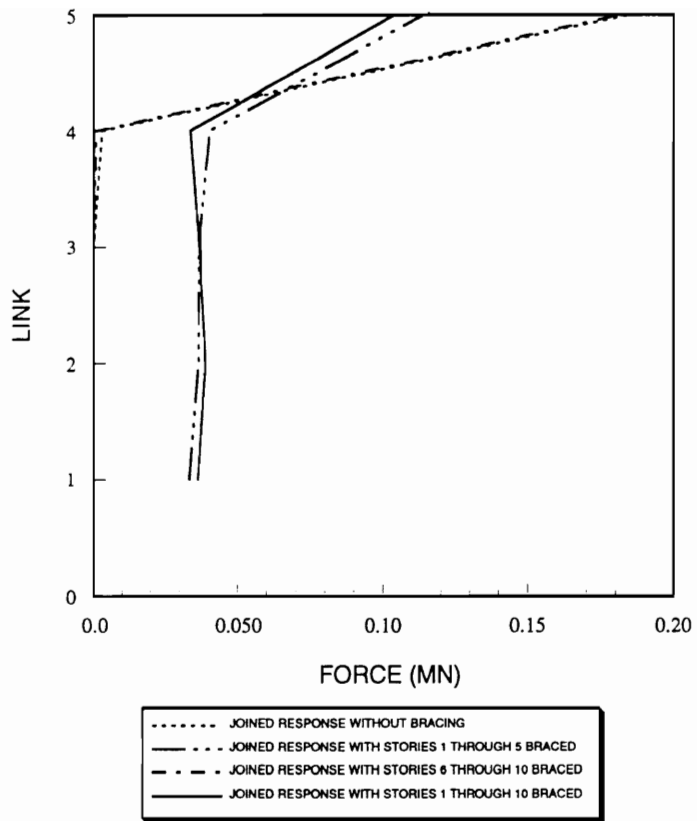


Figure 6.54: Forces in the rigid links for various configurations of bracings

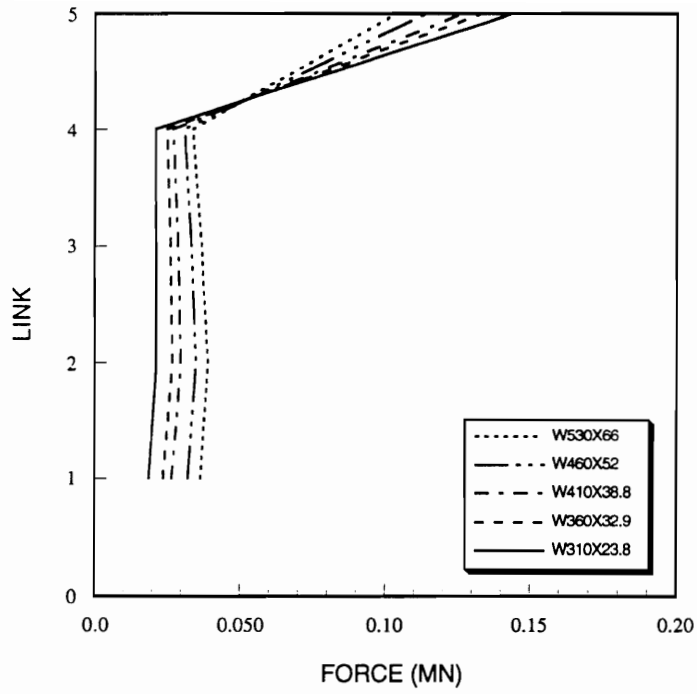


Figure 6.55: Forces in the rigid links for different bracing sizes of the 10-story structure

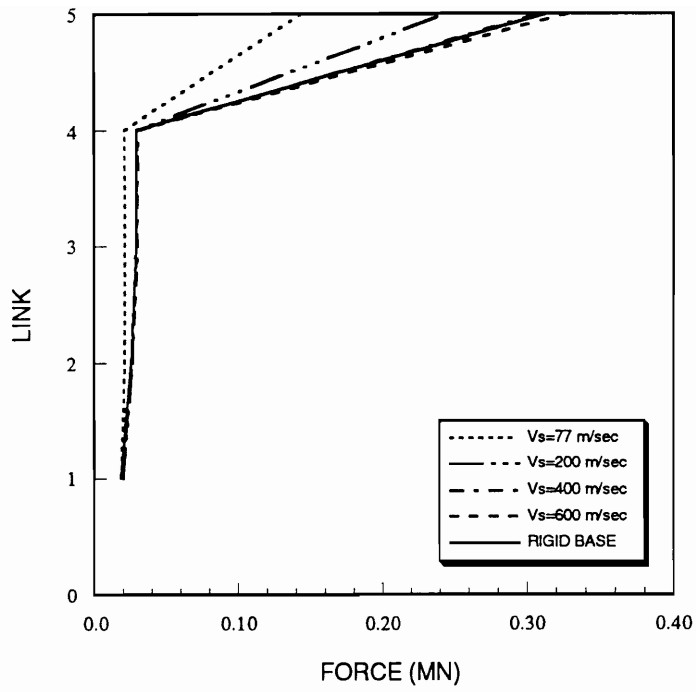


Figure 6.56: Forces in the rigid links for different shear wave velocities of the foundation media

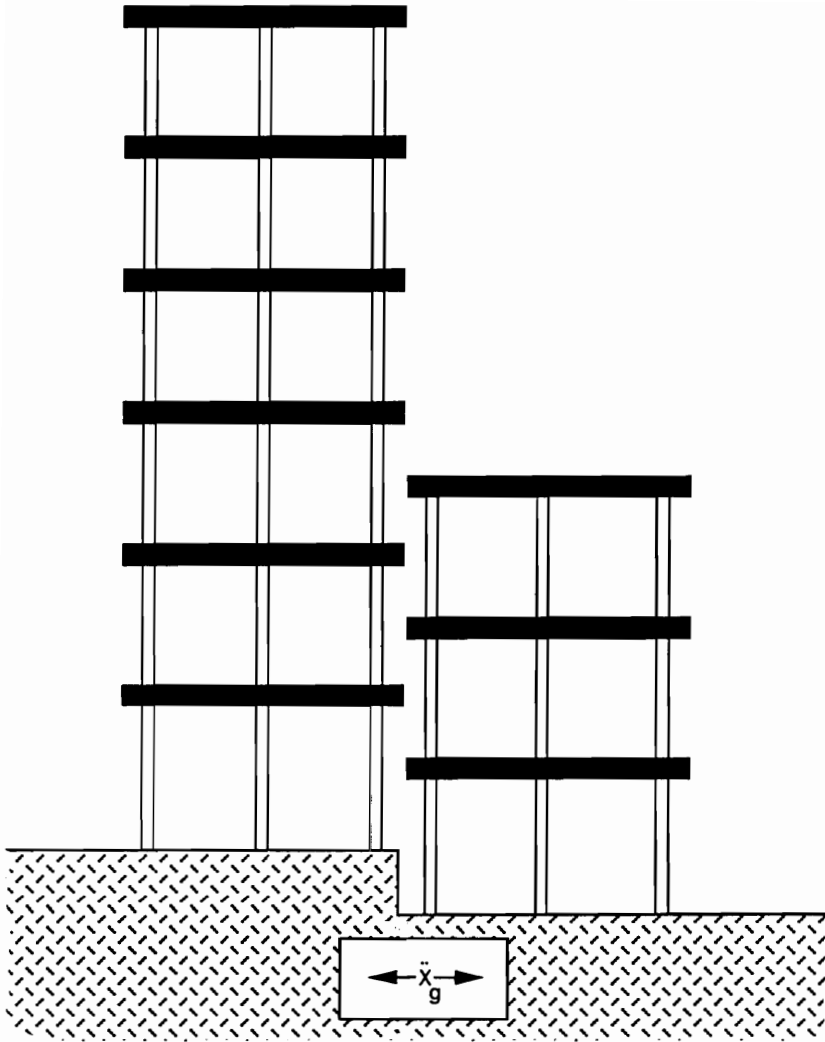


Figure 6.57: Schematic of column pounding structures

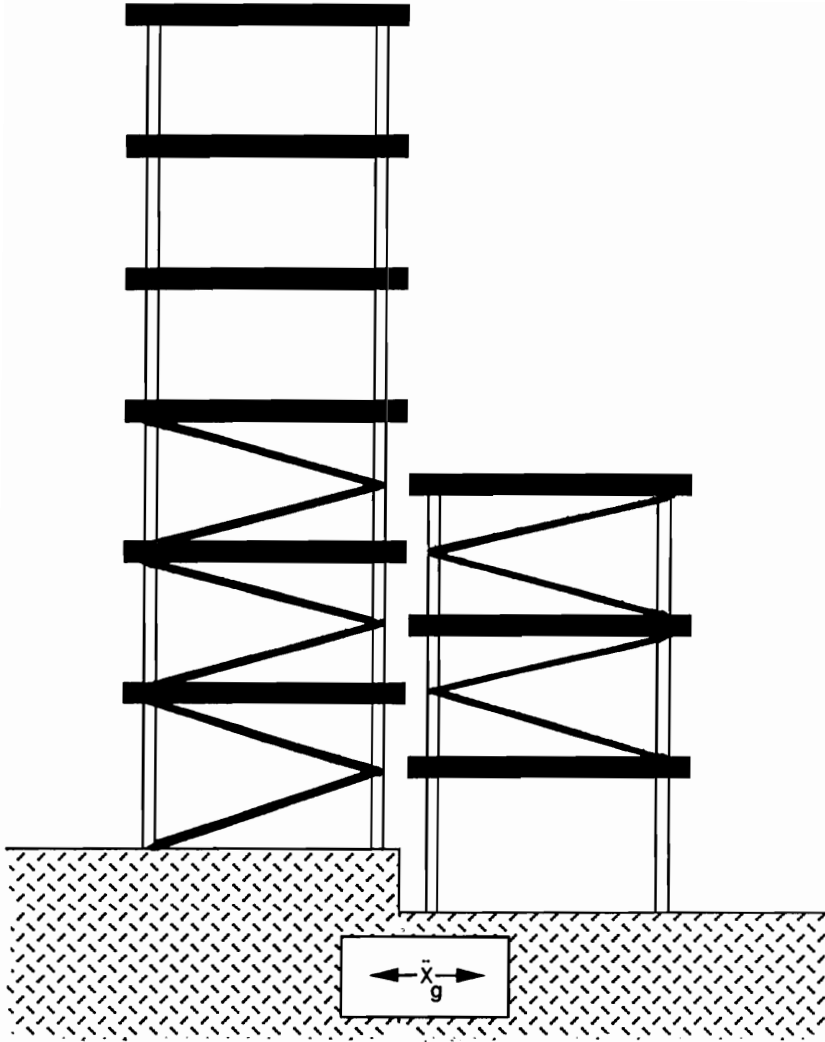


Figure 6.58: Schematic of K-braced column pounding structures

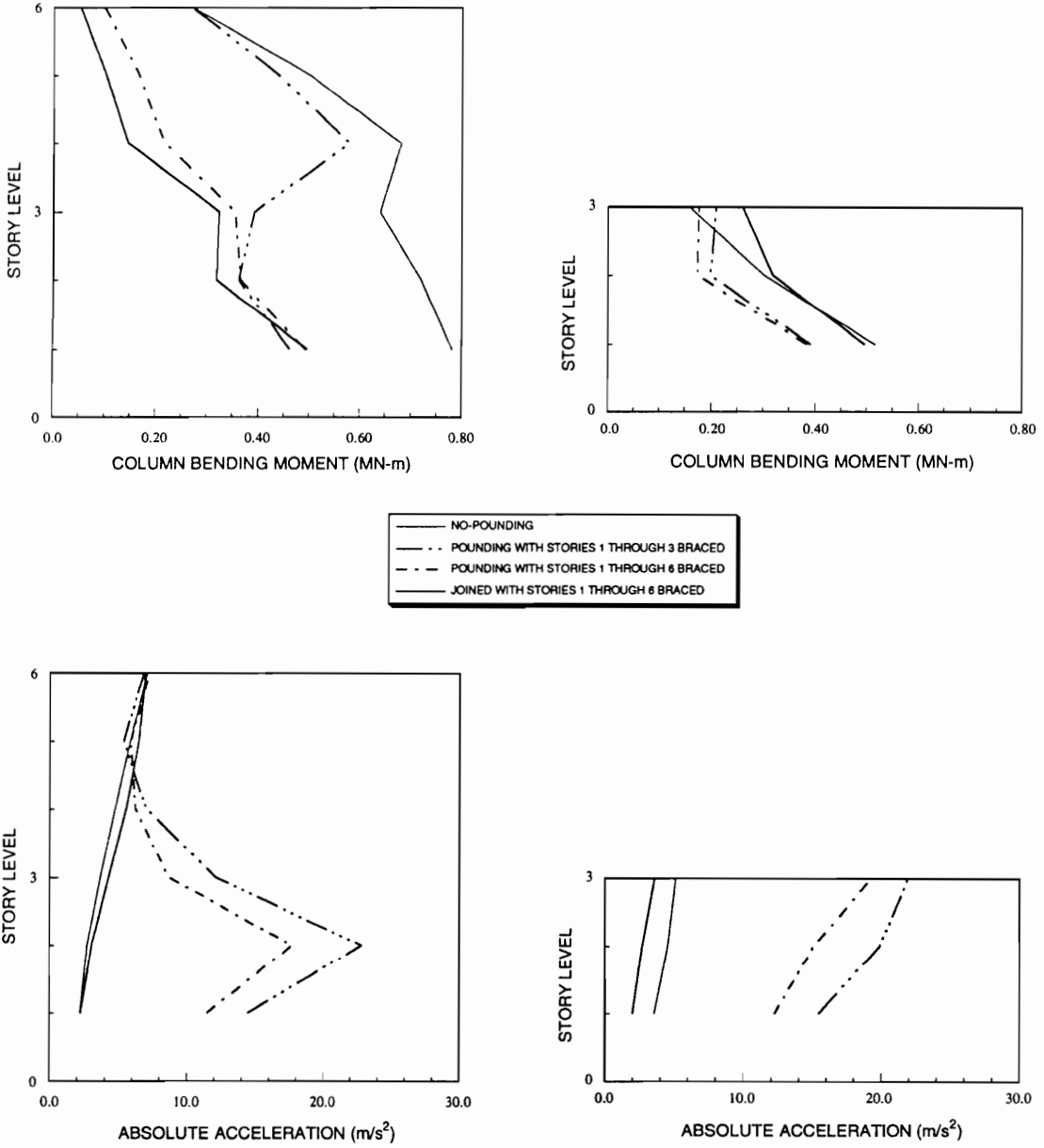


Figure 6.59: Comparison of the bending moment and acceleration responses obtained for braced pounding and unbraced no-pounding structures with different bracing configurations with the response obtained for braced joined structures (bracing size $W530 \times 66$, El-Centro time history)

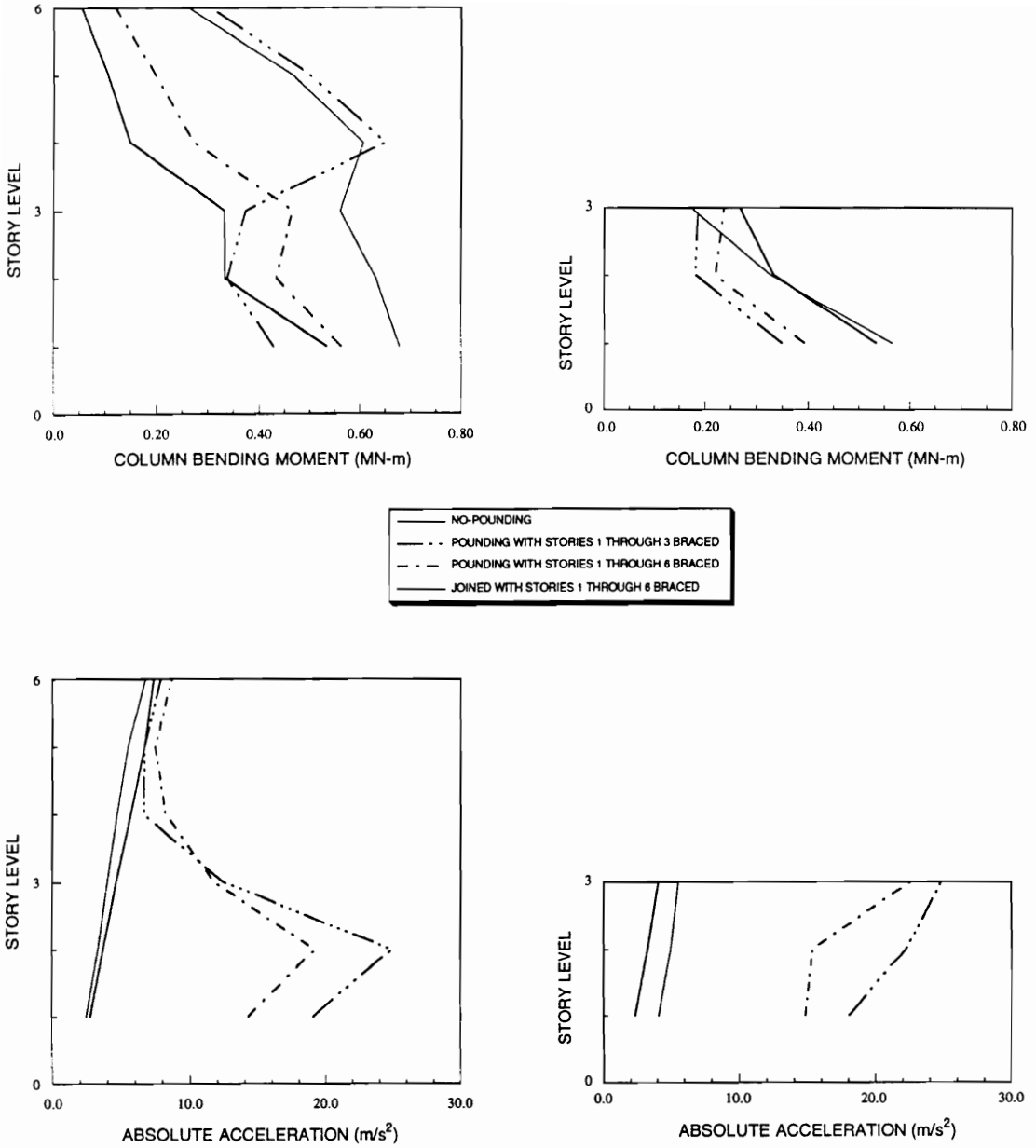


Figure 6.60: Comparison of the bending moment and acceleration responses obtained for braced pounding and unbraced no-pounding structures with different bracing configurations with the response obtained for braced joined structures (bracing size $W530 \times 66$, 50 synthetic time histories)

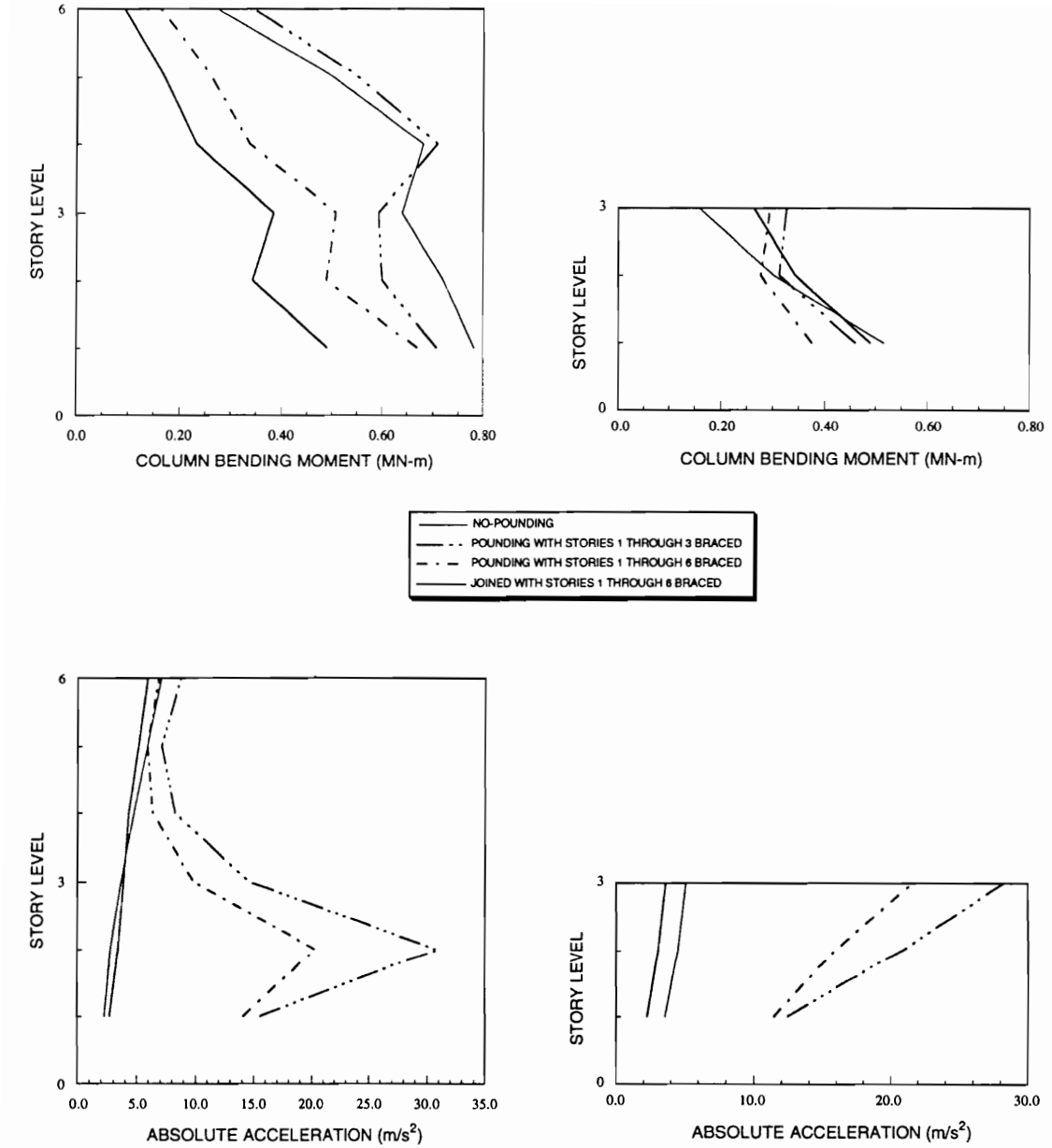


Figure 6.61: Comparison of the bending moment and acceleration responses obtained for braced pounding and unbraced no-pounding structures with different bracing configurations with the response obtained for braced joined structures (bracing size $W310 \times 23.8$, El-Centro time history)

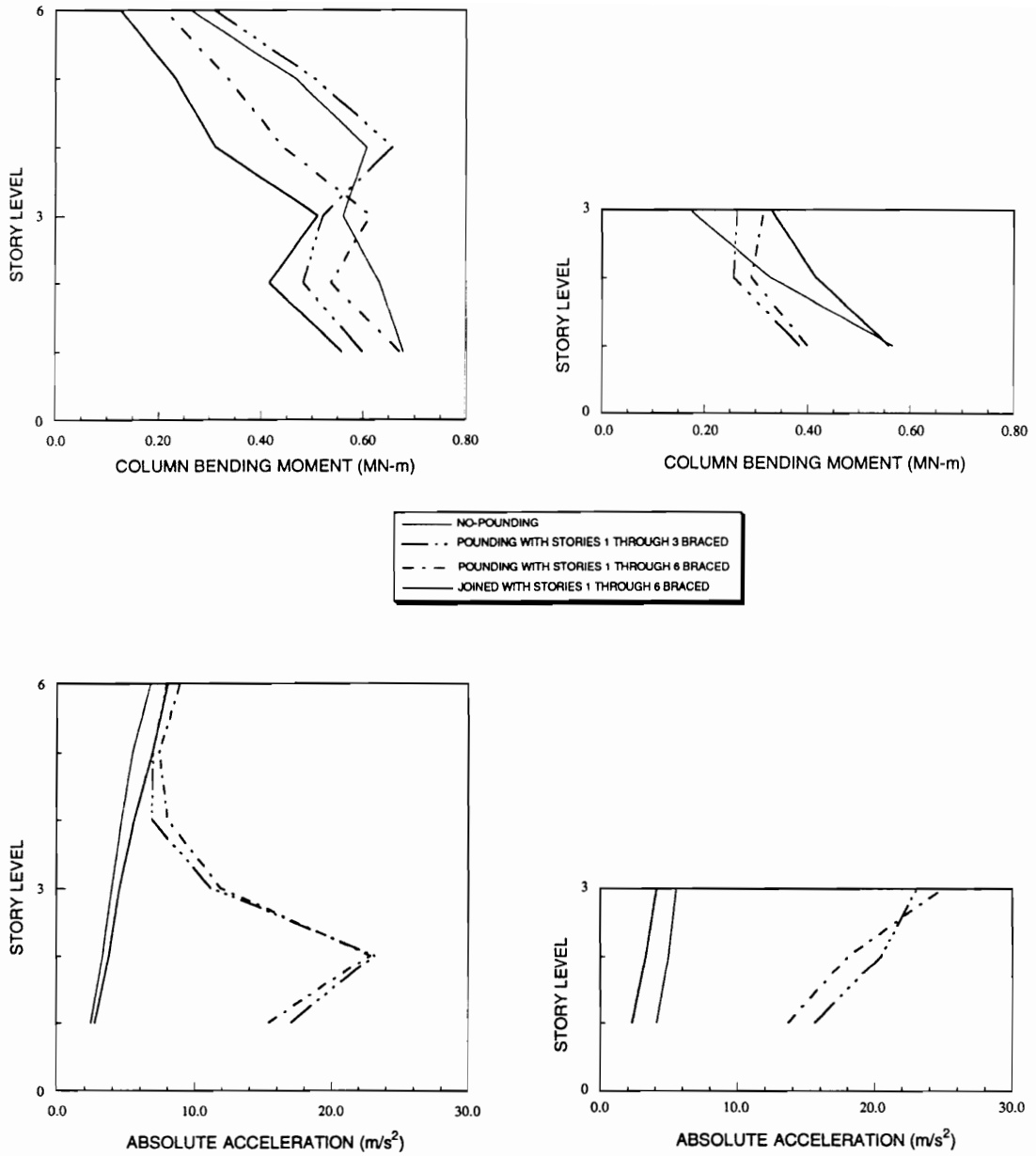


Figure 6.62: Comparison of the bending moment and acceleration responses obtained for braced pounding and unbraced no-pounding structures with different bracing configurations with the response obtained for braced joined structures (bracing size $W310 \times 23.8$, 50 synthetic time histories)

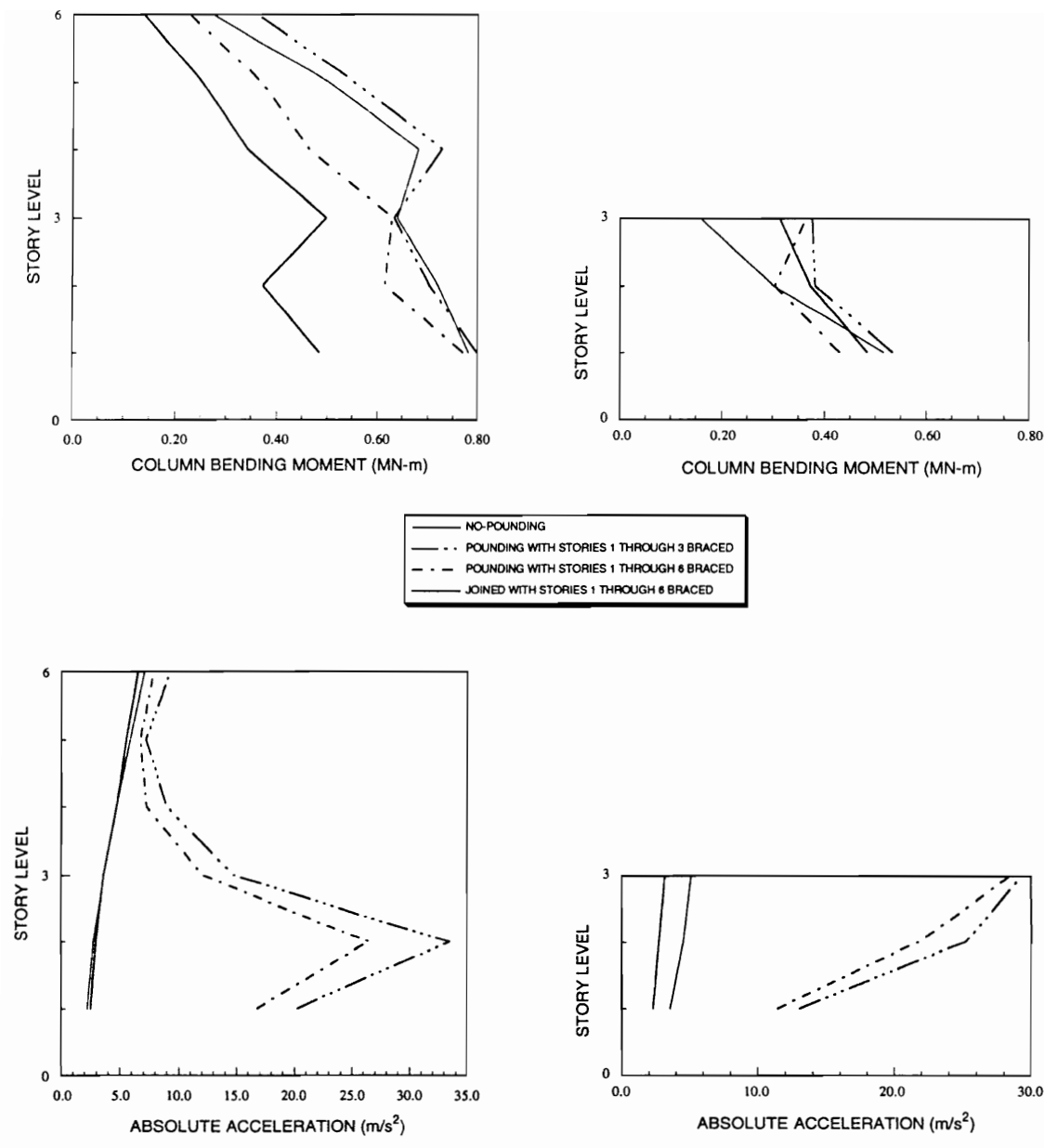


Figure 6.63: Comparison of the bending moment and acceleration responses obtained for braced pounding and unbraced no-pounding structures with different bracing configurations with the response obtained for braced joined structures (bracing size $W150 \times 13.5$, El-Centro time history)

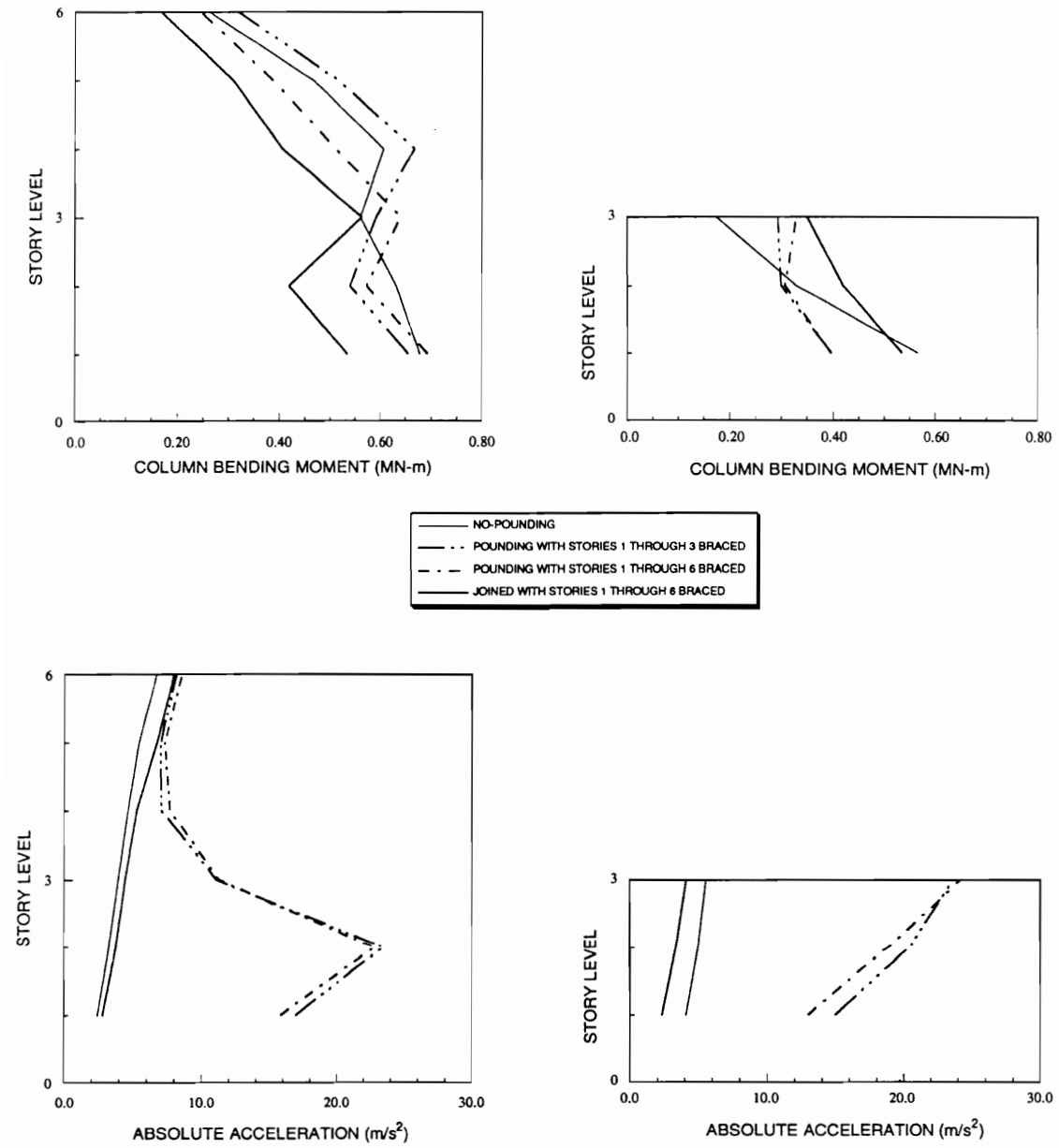


Figure 6.64: Comparison of the bending moment and acceleration responses obtained for braced pounding and unbraced no-pounding structures with different bracing configurations with the response obtained for braced joined structures (bracing size $W150 \times 13.5$, 50 synthetic time histories)

Table 6.1: The forces in the foundation springs of the 5- and 10-story structures for no-pounding, pounding and joined without bracing and with different bracing configurations

Braced stories of the 10-story structure	No-pounding		Pounding		Joined
	10-story structure	5-story structure	10-story structure	5-story structure	10- or 5-story structure
	Force (MN)	Force (MN)	Force (MN)	Force (MN)	Force (MN)
No-bracing	0.40450	0.28659	0.60232	0.26307	0.36543
1 through 5	-	-	0.68095	0.26033	0.36471
6 through 10	-	-	0.59583	0.28282	0.37188
1 through 10	-	-	0.74597	0.28362	0.36927

Table 6.2: The forces in the foundation springs of the 5- and 10-story structures for pounding and joined structures with different bracing sizes of the 10-story structure

Bracing size	pounding		Joined
	10-story structure Force (MN)	5-story structure Force (MN)	10- or 5-story structure Force (MN)
W530 × 66	0.74597	0.28362	0.36927
W460 × 52	0.73492	0.27996	0.37083
W410 × 38.8	0.71576	0.27299	0.37288
W360 × 32.9	0.70386	0.26971	0.37345
W310 × 23.8	0.68077	0.26682	0.37379

Table 6.3: The forces in the foundation springs of the 5- and 10-story structures for unbraced no-pounding, braced pounding and joined structures with different shear wave velocities of the foundation media

Shear wave velocity in the foundation media V_s (m/sec)	No-pounding without braces		Pounding with braces		Joined with braces
	10-story structure Force (MN)	5-story structure Force (MN)	10-story structure Force (MN)	5-story structure Force (MN)	10- or 5-story structure Force (MN)
77	0.40450	0.28659	0.68077	0.26682	0.37379
200	0.48485	0.45922	0.79315	0.39981	0.60740
400	0.65093	0.68661	0.73197	0.50940	0.77040
600	0.72542	0.73999	0.72835	0.55388	0.80870
∞	0.76954	0.70212	0.98415	0.57298	0.81210

Chapter 7

SUMMARY AND CONCLUDING REMARKS

In this study, the effect of pounding caused by earthquake induced vibrations of closely spaced structures was examined. Several structural systems with different floor mass, column stiffness, impact spring stiffness, and seismic joint gaps, subjected to several different input motions, were considered. To evaluate the effects of pounding, the numerical results with and without pounding were obtained. To study the characteristics of the response during pounding, the problem of a multi-degree-of-freedom shear structure pounding against a rigid structure was considered in Chapter 2 and pounding against a deformable structure was considered in Chapter 3. The structural responses obtained during rigid and flexible pounding were observed to be different numerically but similar qualitatively. A comprehensive parametric study was conducted to evaluate the importance of various problem parameters.

The most conspicuous effects of pounding were observed to be: (1) a large increase in the shear force in the stories higher than the top pounding story and (2) a large increase in the accelerations of the pounding floors. The pounding can also cause large overturning effects on both structures.

In chapter 4 the parametric study of the structural pounding was extended to the pounding of structures in series. The results showed that: (1) due to pounding, the exterior structure is usually penalized more than the interior structure when it is adjacent to either a stiffer or a heavier structure, (2) if the neighboring structure is either softer or lighter, then the floor acceleration and overturning moment responses of the interior structure are larger than those of the exterior structure, (3) the displacement and story shear responses are not very sensitive to the impact element stiffness, whereas the floor acceleration and

overturning moment responses are quite sensitive to this parameter.

In Chapter 5 the effect of foundation flexibility on the structural pounding response was investigated. The foundation flexibility may increase or decrease the displacement and shear responses in pounding situations. It will depend upon the relative stiffness of the foundation media with respect to the structure, as well as combined dynamic characteristics of the foundation and the structure. For the example problem considered in this study it was observed that for a stiffer foundation the transmitted force increased due to pounding. Such force increases may also necessitate foundation treatment to increase its load carrying capacity. The overturning moment and floor acceleration responses were seen to increase in most cases due to the flexibility of the foundation. In general it was observed that to correctly evaluate the effect of pounding on a structural response, a proper consideration of its foundation flexibility must be included in the analysis.

It is necessary to alleviate these pounding effects to avoid damage to the structural elements and supported secondary equipment. In Chapter 6, therefore, methods to reduce the pounding effects have been investigated. It was found necessary to join the structures by rigid links to avoid high accelerations caused by pounding. Joining of the structures, however, does not reduce the high shear force (or bending moment in the story columns) caused in the upper stories by pounding. To reduce the high bending moment, it is necessary to brace all the stories of the taller structure; a partial bracing of the structure transfers the force to the unbraced stories and thus does not solve the problem. The floor accelerations in the completely braced structures are, however, increased slightly when compared to the accelerations in the unbraced but joined structures.

The forces in the rigid links connecting the two structures were observed to be reasonable. Thus joining of the two structures does not seem to pose an insurmountable problem.

The proposed pounding mitigation strategies were also examined for the structures supported on the flexible foundation medium. It was observed that except for the very soft soils, the mitigation scheme of joining the structures and bracing the ten-story structure will increase the shear force transmitted to the foundation, thus requiring a strengthening

of the foundation.

This study was mostly limited to linearly behaving structures, although it is realized that nonlinear force deformation characteristics play an important role in the design of structures. The nonlinearity of the pounding problem arising from the fact that the state of contact between the two colliding structures keeps changing constantly as the structures vibrate was, however, considered in the analysis. Also, as a part of the parametric study, the nonlinear Hertz model for the contact stiffness at the pounding interface has been considered in the study. A natural extension of this work is to study the effect of pounding and its mitigation when the lateral load carrying members (columns) can yield or go in the inelastic range.

REFERENCES

- [1] Anagnostopoulos, S. A., "Pounding of Buildings in Series During Earthquakes," 8th European Conference on Earthquake Engineering, Lisbon, Portugal, September 1986.
- [2] Anagnostopoulos, S. A. and Spiliopoulos, K. V., "An Investigation of Earthquake Induced Pounding Between Adjacent Buildings," *Earthquake Engineering and Structural Dynamics*, Vol. 21, 289–302, 1992.
- [3] Benuska L., "Loma Prieta Earthquake Reconnaissance Report," *Earthquake Spectra*, EERI, Supplement to Vol. 6, May 1990.
- [4] Berg, G. V. and Degenkolb, H. J., "Engineering Lessons from the Managua Earthquake," American Iron and Steel Institute Report, 1973.
- [5] Bertero V., "Observations on Structural Pounding," Proc. International Conference: The Mexico Earthquake–1985, ASCE.
- [6] Clough, R. W. and Penzien, J., Dynamics of Structures, McGraw–Hill, Inc., New York, 1975.
- [7] Cranahan, B., Luther, H. A. and Wilkes, J. O., Applied Numerical Methods, John Wiley, Inc., New York, 1969.
- [8] Davis, R. O., "Pounding of Buildings Modelled by an Impact Oscillator," *Earthquake Engineering and Structural Dynamics*, Vol. 21, 253–274, 1992.
- [9] Dubowsky, S. and Freudenstein, F., "Dynamic Analysis of Mechanical Systems with Clearances, Part I: Formation of Dynamic Model; Part 2: Dynamic Response," *Journal of Engineering for Industry*, Vol. 93, 305–316, 1971.
- [10] Dubowsky, S., "On Predicting the Dynamic Effects of Clearance in One Dimensional Closed Loop Systems," *Journal of Engineering for Industry*, Vol. 93, 324–329, 1974.
- [11] Goldsmith, W., Impact – The Theory and Physical Behavior of Colliding Solids, Edward Arnold Ltd., London, 1960.
- [12] Huang, R. C., Haug, E. J. Jr. and Andrews, J. G., "Sensitivity Analysis and Optimal Design of a Mechanical System with Intermittent Motion," *Journal of Mechanical Design*, Vol. 100, 492–499, 1978.

- [13] Hunt, K. H. and Crossley, F. R. E., "Coefficient of Restitution Interpreted as Damping in Vibroimpact," *Journal of Applied Mechanics*, Vol. 42, 440–445, 1975.
- [14] "Impressions of the Guerrero-Michoacan, Mexico Earthquake of 19 September 1985," Preliminary Reconnaissance Report, Earthquake Engineering Research Institute, 1985.
- [15] Iwan, W. D., "Predicting the Earthquake Response of Resiliently Mounted Equipment with Motion Limiting Constraints," *Proceedings, 6th World Conference on Earthquake Engineering*, New Dehli, Vol. 12, 12–19 to 12–24, 1977.
- [16] Jeng, V., Kasai, K. and Maison, B. F., "A Spectral Difference Method to Estimate Building Separation to Avoid Pounding," *Earthquake Spectra*, Vol. 8, No. 2, 201–223, 1992.
- [17] Jing, H.-S. and Young, M., "Random Response of a Single-Degree-of-Freedom Vibro-Impact System with Clearance," *Earthquake Engineering and Structural Dynamics*, Vol. 19, 789–798, 1990.
- [18] Jing, H.-S. and Young, M., "Impact Interactions Between Two Vibration Systems Under Random Excitation," *Earthquake Engineering and Structural Dynamics*, Vol. 20, 667–681, 1991.
- [19] Kasai, K., Maison, B. F., and Patel, D. J., "An Earthquake Analysis of Buildings Subjected to a Type of Pounding," *Proceedings, Fourth National Conference on Earthquake Engineering*, Palm Springs, CA, 1990.
- [20] Kasai, K., Jeng Van and Maison, B. F., "The Significant Effects of Pounding – Induced Accelerations on Building Appurtenances," *Proc. ATC – 29 Seminar: Seismic Design and Performance of Equipment and Nonstructural Elements in Buildings and Industrial Structures*, Oct. 3–4, 1990.
- [21] Kobrinskii, A. E., *Dynamics of Mechanisms with Elastic Connections and Impact Systems*, ILIFFE Books, Ltd., London.
- [22] Lee, T. W. and Wang, A. C., "On the Dynamics of Intermittent-Motion Mechanisms, Part I: Dynamic Model and Response," *ASME*, Paper No. 82, DET-64, 1982.
- [23] Mahin, S. A., Bertero, V. V., Chopra, A. K., and Collins, R. G., "Response of the Olive View Hospital Main Building During the San Fernando Earthquake," Report No. EERC 76-22, Earthquake Engineering Research Center, University of California, Berkeley, 1976.
- [24] Maison, B. F., and Kasai, K., "Analysis for Type of Structural Pounding," *Journal of Structural Engineering*, Vol. 116, 957–977, 1990.

- [25] Maison, B. F., and Kasai, K., "Dynamics of Pounding When Two Buildings Collide," *Earthquake Engineering and Structural Dynamics*, Vol. 21, 771–786, 1992.
- [26] Masri, S. F. and Ibrahim, A. M., "Stochastic Excitation of Simple System with Impact Damper," *Earthquake Engineering and Structural Dynamics*, Vol. 1, 337–346, 1973.
- [27] Miller, R. K., and Felszeghy, S. F., "Engineering Features of the Santa Barbara Earthquake of August 13, 1978," Report No. UCSB-ME-78-2, Earthquake Engineering Research Institute, Berkeley, California, 1978.
- [28] Miller, R. K., "Steady Vibroimpact at a Seismic Joint Between Adjacent Structures," *Proc., 8th World Conf. on Earthquake Engineering*, Istanbul, Turkey, Vol. 6, 57–64, 1980.
- [29] Newmark, N. M. and Rosenblueth, E., Fundamentals of Earthquake Engineering, Prentice-Hall, Inc., Englewood Cliffs, NJ, 1971.
- [30] Nguyen, D. T., Noah, S. T., and Kettleborough, C. F., "Impact Behavior of an Oscillator with Limiting Stops, Part I: A Parametric Study and Part II: Dimensionless Design Parameters," *Journal of Sound and Vibration*, Vol. 109, 309–325, 1986.
- [31] Noah, S. T., Kettleborough, C. F., and Griffin, R. B., "Dynamics and Wear of Mechanical Systems with Clearances," *Proceedings of the Society of Manufacturing Engineers, Eleventh Conference on Production Research and Technology*, Pittsburgh, PA, 1984.
- [32] Parmelee, A., Perelman, D. S. and Lee, S.-L., "Seismic Response of Multiple-Story Structures on Flexible Foundations," *Bulletin of the Seismological Society of America*, Vol. 59, 1061–1070, 1969.
- [33] Paz, M., Structural Dynamics, Von Nostrand Reinhold Company, Inc., New York, NY, 1985.
- [34] Popplewell, N., Bapat, C. N., and McLachlan, K., "Stable Periodic Vibroimpacts of an Oscillator," *Journal of Sound and Vibration*, Vol. 87, 41–59, 1983.
- [35] Rohanimanesh, M. S. and Singh, M. P., "A Study of Structural Pounding During Strong Earthquake," NSF Technical Report VPI-E-92-1, January 1992.
- [36] Rosenblueth, E., and Esteva, L., "Folleto Complementario: Diseno Sismico de Edificios, Proyecto de Reglamento de las Constucciones en el Distrito Federal," Ediciones Ingenieria, Mexico, 1962.
- [37] "The Central Greece Earthquake of February–March, 1981," *Reconnaissance and Engineering Report*, Earthquake Engineering Research Institute, 1982.
- [38] "Thessaloniki, Greece, Earthquake – June 20, 1978," *Reconnaissance Report*, Earthquake Engineering Research Institute, 1978.

- [39] Thompson, J. M. T., and Ghaffari, R., "Chaos After Period Doubling Bifurcations in the Resonance of an Impact Oscillator," *Physics Letters*, 91A, 5–8, 1982.
- [40] Velusami, M. A., Crossley, F. R. E. and Horvay, G., "Multiple Impacts of a Ball Between Two Plates, Part 1 and Part 2: Mathematical Modeling," *Journal of Engineering for Industry*, Vol. 97, 828–835, 1975.
- [41] Wada, A., Shinozaki, Y. and Nakamura, N., "Collapse of Building with Expansion Joints through Collision Caused by Earthquake Motion," *Proc., 8th World Conference on Earthquake Engineering*, San Francisco, Vol. IV, 855–862, 1984.
- [42] Westermo, B. D., "The Dynamics of Interstructural Connection to Prevent Pounding," *Earthquake Engineering and Structural Dynamics*, Vol. 18, 687–699, 1989.
- [43] Whitman, R. V., Protonotarios, J. N., and Nelson, M. F., "Case Study of Dynamic Soil-Structure Interaction," *Journal of the Soil Mechanics and Foundation Division*, Vol. 99, 997–1009, 1973.
- [44] Winfrey, R. C., Anderson, R. V. and Ghilka, C. W., "Analysis of Elastic Machinery with Clearances," *Journal of Engineering for Industry*, Vol. 95, 695–703, 1973.
- [45] Wolf, J. P., and Skrikerud, P. E., "Mutual Pounding of Adjacent Structures During Earthquakes," *Transactions, 5th International Conference on Structural Mechanics in Reactor Technology*, Berlin, Paper K8/9, 1979.
- [46] Wolf, J. P. and Skrikerud, P. E., "Mutual Pounding of Adjacent Structures During Earthquakes," *Nuclear Engineering and Design*, Vol. 57, 253–275, 1980.

Appendix A

MATRICES

Influence vectors, first introduced in equations 6.38 - 6.41, are defined as follows:

$$\mathbf{r}_{gfp}^T = [\overbrace{1, 0, 0, 1, 0, 0, \dots, 1, 0, 0}^{3(n-\frac{m}{2})}]$$

$$\mathbf{r}_{gcp}^T = [\overbrace{1, 0, 0, 1, 0, 0, \dots, 1, 0, 0}^{3\frac{m}{2}}]$$

$$\mathbf{r}_{\theta fp}^T = [\overbrace{h_{q+1}, -b/2, -1, \dots, h_p, -b/2, -1, h_1, b/2, -1, \dots, h_p, b/2, -1}^{3(n-\frac{m}{2})}]$$

$$\mathbf{r}_{\theta cp}^T = [\overbrace{h_1, -b/2, -1, \dots, h_q, -b/2, -1}^{3\frac{m}{2}}]$$

$$\mathbf{r}_{gfq}^T = [\overbrace{1, 0, 0, 1, 0, 0, \dots, 1, 0, 0}^{3\frac{m}{2}}]$$

$$\mathbf{r}_{gcq}^T = [\overbrace{1, 0, 0, 1, 0, 0, \dots, 1, 0, 0}^{3\frac{m}{2}}]$$

$$\mathbf{r}_{\theta fq}^T = [\overbrace{h_1, -b/2, -1, \dots, h_q, -b/2, -1}^{3\frac{m}{2}}]$$

$$\mathbf{r}_{\theta cq}^T = [\overbrace{h_1, b/2, -1, \dots, h_q, b/2, -1}^{3\frac{m}{2}}]$$

The combined mass, damping and stiffness matrices and forcing function vector appearing in equation 6.50 are defined as:

Mass Matrix:

$$\mathbf{M} = \begin{bmatrix} \mathbf{M}_{11p} & \mathbf{M}_{12p} & 0 & 0 & 0 & 0 & 0 \\ \mathbf{M}_{21p} & \mathbf{M}_{22p} + \mathbf{M}_{22q} & \mathbf{M}_{21q} & 0 & 0 & 0 & 0 \\ 0 & \mathbf{M}_{12q} & \mathbf{M}_{11q} & 0 & 0 & 0 & 0 \\ 0 & 0 & 0 & m_{bp} & 0 & 0 & 0 \\ 0 & 0 & 0 & 0 & I_{bp} & 0 & 0 \\ 0 & 0 & 0 & 0 & 0 & m_{bq} & 0 \\ 0 & 0 & 0 & 0 & 0 & 0 & I_{bq} \end{bmatrix}$$

Damping Matrix:

$$\mathbf{C} = \begin{bmatrix} c_{11} & c_{12} & \dots & c_{17} \\ c_{21} & c_{22} & \dots & c_{27} \\ \vdots & \vdots & \ddots & \vdots \\ c_{71} & c_{72} & \dots & c_{77} \end{bmatrix}$$

where

$$c_{11} = \mathbf{C}_{11p}$$

$$c_{12} = \mathbf{C}_{12p}$$

$$c_{13} = 0$$

$$c_{14} = -(\mathbf{C}_{11p}\mathbf{r}_{gfp} + \mathbf{C}_{12p}\mathbf{r}_{gcp})$$

$$c_{15} = -(\mathbf{C}_{11p}\mathbf{r}_{\theta fp} + \mathbf{C}_{12p}\mathbf{r}_{\theta cp})$$

$$c_{16} = 0$$

$$c_{17} = 0$$

$$c_{21} = \mathbf{C}_{21p}$$

$$c_{22} = \mathbf{C}_{22p} + \mathbf{C}_{22q}$$

$$c_{23} = \mathbf{C}_{21q}$$

$$c_{24} = -(\mathbf{C}_{21p}\mathbf{r}_{gfp} + \mathbf{C}_{22p}\mathbf{r}_{gcp})$$

$$c_{25} = -(\mathbf{C}_{21p}\mathbf{r}_{\theta fp} + \mathbf{C}_{22p}\mathbf{r}_{\theta cp})$$

$$c_{26} = -(\mathbf{C}_{21q}\mathbf{r}_{gfq} + \mathbf{C}_{22q}\mathbf{r}_{gcq})$$

$$c_{27} = -(\mathbf{C}_{21q}\mathbf{r}_{\theta fq} + \mathbf{C}_{22q}\mathbf{r}_{\theta cq})$$

$$c_{31} = 0$$

$$c_{32} = \mathbf{C}_{12q}$$

$$c_{33} = \mathbf{C}_{11q}$$

$$c_{34} = 0$$

$$c_{35} = 0$$

$$c_{36} = -(\mathbf{C}_{11q}\mathbf{r}_{gfq} + \mathbf{C}_{12q}\mathbf{r}_{gcq})$$

$$c_{37} = -(\mathbf{C}_{11q}\mathbf{r}_{\theta fq} + \mathbf{C}_{12q}\mathbf{r}_{\theta cq})$$

$$c_{41} = -(\mathbf{r}_{gfp}^T \mathbf{C}_{11p} + \mathbf{r}_{gcp}^T \mathbf{C}_{21p})$$

$$c_{42} = -(\mathbf{r}_{gfp}^T \mathbf{C}_{12p} + \mathbf{r}_{gcp}^T \mathbf{C}_{22p})$$

$$c_{43} = 0$$

$$c_{44} = \mathbf{r}_{gfp}^T \mathbf{C}_{11p} \mathbf{r}_{gfp} + \mathbf{r}_{gfp}^T \mathbf{C}_{12p} \mathbf{r}_{gcp} + \mathbf{r}_{gcp}^T \mathbf{C}_{21p} \mathbf{r}_{gfp} + \mathbf{r}_{gcp}^T \mathbf{C}_{22p} \mathbf{r}_{gcp} + c_x$$

$$c_{45} = \mathbf{r}_{gfp}^T \mathbf{C}_{11p} \mathbf{r}_{\theta fp} + \mathbf{r}_{gfp}^T \mathbf{C}_{12p} \mathbf{r}_{\theta cp} + \mathbf{r}_{gcp}^T \mathbf{C}_{21p} \mathbf{r}_{\theta fp} + \mathbf{r}_{gcp}^T \mathbf{C}_{22p} \mathbf{r}_{\theta cp}$$

$$c_{46} = 0$$

$$c_{47} = 0$$

$$c_{51} = -(\mathbf{r}_{\theta fp}^T \mathbf{C}_{11p} + \mathbf{r}_{\theta cp}^T \mathbf{C}_{21p})$$

$$c_{52} = -(\mathbf{r}_{\theta fp}^T \mathbf{C}_{12p} + \mathbf{r}_{\theta cp}^T \mathbf{C}_{22p})$$

$$c_{53} = 0$$

$$c_{54} = \mathbf{r}_{gfp}^T \mathbf{C}_{11p} \mathbf{r}_{\theta fp} + \mathbf{r}_{gfp}^T \mathbf{C}_{12p} \mathbf{r}_{\theta cp} + \mathbf{r}_{gcp}^T \mathbf{C}_{21p} \mathbf{r}_{\theta fp} + \mathbf{r}_{gcp}^T \mathbf{C}_{22p} \mathbf{r}_{\theta cp}$$

$$c_{55} = \mathbf{r}_{\theta fp}^T \mathbf{C}_{11p} \mathbf{r}_{\theta fp} + \mathbf{r}_{\theta fp}^T \mathbf{C}_{12p} \mathbf{r}_{\theta cp} + \mathbf{r}_{\theta cp}^T \mathbf{C}_{21p} \mathbf{r}_{\theta fp} + \mathbf{r}_{\theta cp}^T \mathbf{C}_{22p} \mathbf{r}_{\theta cp} + c_{\theta}$$

$$c_{56} = 0$$

$$c_{57} = 0$$

$$c_{61} = 0$$

$$c_{62} = -(\mathbf{r}_{gfq}^T \mathbf{C}_{12q} + \mathbf{r}_{gcq}^T \mathbf{C}_{22q})$$

$$c_{63} = -(\mathbf{r}_{gfq}^T \mathbf{C}_{11q} + \mathbf{r}_{gcq}^T \mathbf{C}_{21q})$$

$$c_{64} = 0$$

$$c_{65} = 0$$

$$c_{66} = \mathbf{r}_{gfq}^T \mathbf{C}_{11q} \mathbf{r}_{gfq} + \mathbf{r}_{gfq}^T \mathbf{C}_{12q} \mathbf{r}_{gcq} + \mathbf{r}_{gcq}^T \mathbf{C}_{21q} \mathbf{r}_{gfq} + \mathbf{r}_{gcq}^T \mathbf{C}_{22q} \mathbf{r}_{gcq} + c_x$$

$$c_{67} = \mathbf{r}_{gfq}^T \mathbf{C}_{11q} \mathbf{r}_{\theta fq} + \mathbf{r}_{gfq}^T \mathbf{C}_{12q} \mathbf{r}_{\theta cq} + \mathbf{r}_{gcq}^T \mathbf{C}_{21q} \mathbf{r}_{\theta fq} + \mathbf{r}_{gcq}^T \mathbf{C}_{22q} \mathbf{r}_{\theta cq}$$

$$c_{71} = 0$$

$$c_{72} = -(\mathbf{r}_{\theta fq}^T \mathbf{C}_{12q} + \mathbf{r}_{\theta cq}^T \mathbf{C}_{22q})$$

$$c_{73} = -(\mathbf{r}_{\theta fq}^T \mathbf{C}_{11q} + \mathbf{r}_{\theta cq}^T \mathbf{C}_{21q})$$

$$c_{74} = 0$$

$$c_{75} = 0$$

$$c_{76} = \mathbf{r}_{gfq}^T \mathbf{C}_{11q} \mathbf{r}_{\theta fq} + \mathbf{r}_{gfq}^T \mathbf{C}_{12q} \mathbf{r}_{\theta cq} + \mathbf{r}_{gcq}^T \mathbf{C}_{21q} \mathbf{r}_{\theta fq} + \mathbf{r}_{gcq}^T \mathbf{C}_{22q} \mathbf{r}_{\theta cq}$$

$$c_{77} = \mathbf{r}_{\theta fq}^T \mathbf{C}_{11q} \mathbf{r}_{\theta fq} + \mathbf{r}_{\theta fq}^T \mathbf{C}_{12q} \mathbf{r}_{\theta cq} + \mathbf{r}_{\theta cq}^T \mathbf{C}_{21q} \mathbf{r}_{\theta fq} + \mathbf{r}_{\theta cq}^T \mathbf{C}_{22q} \mathbf{r}_{\theta cq} + c_{\theta}$$

Stiffness Matrix:

$$\mathbf{K} = \begin{bmatrix} k_{11} & k_{12} & \dots & k_{17} \\ k_{21} & k_{22} & \dots & k_{27} \\ \vdots & \vdots & \ddots & \vdots \\ k_{71} & k_{72} & \dots & k_{77} \end{bmatrix}$$

where

$$k_{11} = \mathbf{K}_{11p}$$

$$k_{12} = \mathbf{K}_{12p}$$

$$k_{13} = 0$$

$$k_{14} = -(\mathbf{K}_{11p}\mathbf{r}_{gfp} + \mathbf{K}_{12p}\mathbf{r}_{gcp})$$

$$k_{15} = -(\mathbf{K}_{11p}\mathbf{r}_{\theta fp} + \mathbf{K}_{12p}\mathbf{r}_{\theta cp})$$

$$k_{16} = 0$$

$$k_{17} = 0$$

$$k_{21} = \mathbf{K}_{21p}$$

$$k_{22} = \mathbf{K}_{22p} + \mathbf{K}_{22q}$$

$$k_{23} = \mathbf{K}_{21q}$$

$$k_{24} = -(\mathbf{K}_{21p}\mathbf{r}_{gfp} + \mathbf{K}_{22p}\mathbf{r}_{gcp})$$

$$k_{25} = -(\mathbf{K}_{21p}\mathbf{r}_{\theta fp} + \mathbf{K}_{22p}\mathbf{r}_{\theta cp})$$

$$k_{26} = -(\mathbf{K}_{21q}\mathbf{r}_{gfq} + \mathbf{K}_{22q}\mathbf{r}_{gcq})$$

$$k_{27} = -(\mathbf{K}_{21q}\mathbf{r}_{\theta fq} + \mathbf{K}_{22q}\mathbf{r}_{\theta cq})$$

$$k_{31} = 0$$

$$k_{32} = \mathbf{K}_{12q}$$

$$k_{33} = \mathbf{K}_{11q}$$

$$k_{34} = 0$$

$$k_{35} = 0$$

$$k_{36} = -(\mathbf{K}_{11q}\mathbf{r}_{gfq} + \mathbf{K}_{12q}\mathbf{r}_{gcq})$$

$$k_{37} = -(\mathbf{K}_{11q}\mathbf{r}_{\theta fq} + \mathbf{K}_{12q}\mathbf{r}_{\theta cq})$$

$$k_{41} = -(\mathbf{r}_{gfp}^T \mathbf{K}_{11p} + \mathbf{r}_{gcp}^T \mathbf{K}_{21p})$$

$$k_{42} = -(\mathbf{r}_{gfp}^T \mathbf{K}_{12p} + \mathbf{r}_{gcp}^T \mathbf{K}_{22p})$$

$$k_{43} = 0$$

$$k_{44} = \mathbf{r}_{gfp}^T \mathbf{K}_{11p} \mathbf{r}_{gfp} + \mathbf{r}_{gfp}^T \mathbf{K}_{12p} \mathbf{r}_{gcp} + \mathbf{r}_{gcp}^T \mathbf{K}_{21p} \mathbf{r}_{gfp} + \mathbf{r}_{gcp}^T \mathbf{K}_{22p} \mathbf{r}_{gcp} + k_x$$

$$k_{45} = \mathbf{r}_{gfp}^T \mathbf{K}_{11p} \mathbf{r}_{\theta fp} + \mathbf{r}_{gfp}^T \mathbf{K}_{12p} \mathbf{r}_{\theta cp} + \mathbf{r}_{gcp}^T \mathbf{K}_{21p} \mathbf{r}_{\theta fp} + \mathbf{r}_{gcp}^T \mathbf{K}_{22p} \mathbf{r}_{\theta cp}$$

$$k_{46} = 0$$

$$k_{47} = 0$$

$$k_{51} = -(\mathbf{r}_{\theta fp}^T \mathbf{K}_{11p} + \mathbf{r}_{\theta cp}^T \mathbf{K}_{21p})$$

$$k_{52} = -(\mathbf{r}_{\theta fp}^T \mathbf{K}_{12p} + \mathbf{r}_{\theta cp}^T \mathbf{K}_{22p})$$

$$k_{53} = 0$$

$$k_{54} = \mathbf{r}_{\theta fp}^T \mathbf{K}_{11p} \mathbf{r}_{\theta fp} + \mathbf{r}_{\theta fp}^T \mathbf{K}_{12p} \mathbf{r}_{\theta cp} + \mathbf{r}_{\theta cp}^T \mathbf{K}_{21p} \mathbf{r}_{\theta fp} + \mathbf{r}_{\theta cp}^T \mathbf{K}_{22p} \mathbf{r}_{\theta cp}$$

$$k_{55} = \mathbf{r}_{\theta fp}^T \mathbf{K}_{11p} \mathbf{r}_{\theta fp} + \mathbf{r}_{\theta fp}^T \mathbf{K}_{12p} \mathbf{r}_{\theta cp} + \mathbf{r}_{\theta cp}^T \mathbf{K}_{21p} \mathbf{r}_{\theta fp} + \mathbf{r}_{\theta cp}^T \mathbf{K}_{22p} \mathbf{r}_{\theta cp} + k_\theta$$

$$k_{56} = 0$$

$$k_{57} = 0$$

$$k_{61} = 0$$

$$k_{62} = -(\mathbf{r}_{gfq}^T \mathbf{K}_{12q} + \mathbf{r}_{gcp}^T \mathbf{K}_{22q})$$

$$k_{63} = -(\mathbf{r}_{gfq}^T \mathbf{K}_{11q} + \mathbf{r}_{gcp}^T \mathbf{K}_{21q})$$

$$k_{64} = 0$$

$$k_{65} = 0$$

$$k_{66} = \mathbf{r}_{gffq}^T \mathbf{K}_{11q} \mathbf{r}_{gffq} + \mathbf{r}_{gffq}^T \mathbf{K}_{12q} \mathbf{r}_{gfcq} + \mathbf{r}_{gfcq}^T \mathbf{K}_{21q} \mathbf{r}_{gffq} + \mathbf{r}_{gfcq}^T \mathbf{K}_{22q} \mathbf{r}_{gfcq} + k_x$$

$$k_{67} = \mathbf{r}_{gffq}^T \mathbf{K}_{11q} \mathbf{r}_{\theta ffq} + \mathbf{r}_{gffq}^T \mathbf{K}_{12q} \mathbf{r}_{\theta fcq} + \mathbf{r}_{gfcq}^T \mathbf{K}_{21q} \mathbf{r}_{\theta ffq} + \mathbf{r}_{gfcq}^T \mathbf{K}_{22q} \mathbf{r}_{\theta fcq}$$

$$k_{71} = 0$$

$$k_{72} = -(\mathbf{r}_{\theta ffq}^T \mathbf{K}_{12q} + \mathbf{r}_{\theta fcq}^T \mathbf{K}_{22q})$$

$$k_{73} = -(\mathbf{r}_{\theta ffq}^T \mathbf{K}_{11q} + \mathbf{r}_{\theta fcq}^T \mathbf{K}_{21q})$$

$$k_{74} = 0$$

$$k_{75} = 0$$

$$k_{76} = \mathbf{r}_{gffq}^T \mathbf{K}_{11q} \mathbf{r}_{\theta ffq} + \mathbf{r}_{gffq}^T \mathbf{K}_{12q} \mathbf{r}_{\theta fcq} + \mathbf{r}_{gfcq}^T \mathbf{K}_{21q} \mathbf{r}_{\theta ffq} + \mathbf{r}_{gfcq}^T \mathbf{K}_{22q} \mathbf{r}_{\theta fcq}$$

$$k_{77} = \mathbf{r}_{\theta ffq}^T \mathbf{K}_{11q} \mathbf{r}_{\theta ffq} + \mathbf{r}_{\theta ffq}^T \mathbf{K}_{12q} \mathbf{r}_{\theta fcq} + \mathbf{r}_{\theta fcq}^T \mathbf{K}_{21q} \mathbf{r}_{\theta ffq} + \mathbf{r}_{\theta fcq}^T \mathbf{K}_{22q} \mathbf{r}_{\theta fcq} + k_\theta$$

Forcing Function Vector:

$$\mathbf{f} = \begin{Bmatrix} f_1 \\ f_2 \\ \vdots \\ f_7 \end{Bmatrix}$$

where

$$f_1 = (\mathbf{C}_{11p} \mathbf{r}_{gffp} + \mathbf{C}_{12p} \mathbf{r}_{gfcq}) \dot{x}_g + (\mathbf{K}_{11p} \mathbf{r}_{gffp} + \mathbf{K}_{12p} \mathbf{r}_{gfcq}) x_g$$

$$f_2 = (\mathbf{C}_{21p} \mathbf{r}_{gffp} + \mathbf{C}_{22p} \mathbf{r}_{gfcq} + \mathbf{C}_{21q} \mathbf{r}_{gffq} + \mathbf{C}_{22q} \mathbf{r}_{gfcq}) \dot{x}_g + (\mathbf{K}_{21p} \mathbf{r}_{gffp} + \mathbf{K}_{22p} \mathbf{r}_{gfcq} + \mathbf{K}_{21q} \mathbf{r}_{gffq} + \mathbf{K}_{22q} \mathbf{r}_{gfcq}) x_g$$

$$f_3 = (\mathbf{C}_{11q} \mathbf{r}_{gffq} + \mathbf{C}_{12q} \mathbf{r}_{gfcq}) \dot{x}_g + (\mathbf{K}_{11q} \mathbf{r}_{gffq} + \mathbf{K}_{12q} \mathbf{r}_{gfcq}) x_g$$

$$\begin{aligned}
f_4 = & -m_{bp}\ddot{x}_g - (\mathbf{r}_{gfp}^T \mathbf{C}_{11p} \mathbf{r}_{gfp} + \mathbf{r}_{gfp}^T \mathbf{C}_{12p} \mathbf{r}_{gcp} + \mathbf{r}_{gcp}^T \mathbf{C}_{21p} \mathbf{r}_{gfp} + \\
& \mathbf{r}_{gcp}^T \mathbf{C}_{22p} \mathbf{r}_{gcp}) \dot{x}_g - (\mathbf{r}_{gfp}^T \mathbf{K}_{11p} \mathbf{r}_{gfp} + \mathbf{r}_{gfp}^T \mathbf{K}_{12p} \mathbf{r}_{gcp} + \\
& \mathbf{r}_{gcp}^T \mathbf{K}_{21p} \mathbf{r}_{gfp} + \mathbf{r}_{gcp}^T \mathbf{K}_{22p} \mathbf{r}_{gcp}) x_g
\end{aligned}$$

$$\begin{aligned}
f_5 = & -(\mathbf{r}_{gfp}^T \mathbf{C}_{11p} \mathbf{r}_{\theta fp} + \mathbf{r}_{gfp}^T \mathbf{C}_{12p} \mathbf{r}_{\theta cp} + \mathbf{r}_{gcp}^T \mathbf{C}_{21p} \mathbf{r}_{\theta fp} + \mathbf{r}_{gcp}^T \mathbf{C}_{22p} \mathbf{r}_{\theta cp}) \dot{x}_g - \\
& (\mathbf{r}_{gfp}^T \mathbf{K}_{11p} \mathbf{r}_{\theta fp} + \mathbf{r}_{gfp}^T \mathbf{K}_{12p} \mathbf{r}_{\theta cp} + \mathbf{r}_{gcp}^T \mathbf{K}_{21p} \mathbf{r}_{\theta fp} + \mathbf{r}_{gcp}^T \mathbf{K}_{22p} \mathbf{r}_{\theta cp}) x_g
\end{aligned}$$

$$\begin{aligned}
f_6 = & -m_{bq}\ddot{x}_g - (\mathbf{r}_{gfq}^T \mathbf{C}_{11q} \mathbf{r}_{gfq} + \mathbf{r}_{gfq}^T \mathbf{C}_{12q} \mathbf{r}_{gcq} + \mathbf{r}_{gcq}^T \mathbf{C}_{21q} \mathbf{r}_{gfq} + \\
& \mathbf{r}_{gcq}^T \mathbf{C}_{22q} \mathbf{r}_{gcq}) \dot{x}_g - (\mathbf{r}_{gfq}^T \mathbf{K}_{11q} \mathbf{r}_{gfq} + \mathbf{r}_{gfq}^T \mathbf{K}_{12q} \mathbf{r}_{gcq} + \\
& \mathbf{r}_{gcq}^T \mathbf{K}_{21q} \mathbf{r}_{gfq} + \mathbf{r}_{gcq}^T \mathbf{K}_{22q} \mathbf{r}_{gcq}) x_g
\end{aligned}$$

$$\begin{aligned}
f_7 = & -(\mathbf{r}_{gfq}^T \mathbf{C}_{11q} \mathbf{r}_{\theta fq} + \mathbf{r}_{gfq}^T \mathbf{C}_{12q} \mathbf{r}_{\theta cq} + \mathbf{r}_{gcq}^T \mathbf{C}_{21q} \mathbf{r}_{\theta fq} + \mathbf{r}_{gcq}^T \mathbf{C}_{22q} \mathbf{r}_{\theta cq}) \dot{x}_g - \\
& (\mathbf{r}_{gfq}^T \mathbf{K}_{11q} \mathbf{r}_{\theta fq} + \mathbf{r}_{gfq}^T \mathbf{K}_{12q} \mathbf{r}_{\theta cq} + \mathbf{r}_{gcq}^T \mathbf{K}_{21q} \mathbf{r}_{\theta fq} + \mathbf{r}_{gcq}^T \mathbf{K}_{22q} \mathbf{r}_{\theta cq}) x_g
\end{aligned}$$

VITA

Mohammad S. Rohanimanesh was born in Bandar Anzali, Iran, on February 6, 1956, the son of Mr. Mohammad T. Rohanimanesh and Mrs. Madineh Rastjou Herfeh. He graduated from Kharazmi High School in 1974. He then came to the USA for his college education at the University of the District of Columbia, Washington D. C. in January 1979. He received his Bachelor of Science degree in Civil Engineering in July 1982. He joined the Engineering Science and Mechanics Department at Virginia Polytechnic Institute and State University, Blacksburg in September 1982. He received his Master of Science in Engineering Mechanics in July 1984. He completed his Doctor of Philosophy degree in April 1994. His major area of concentration is Random Vibrations and Earthquake Engineering. He has accepted a faculty position at the Mechanical Engineering Department, Shiraz University, Iran.



5/2/94